

DX 237372

University Library



Author/Filing Title WAN MOHAMED, W.

Class Mark T

Please note that fines are charged on ALL
overdue items.

FOR REFERENCE ONLY

0403271487



ANALYSIS OF SURFACE TEXTURE AND ITS AFFECT ON PRESSURE BALANCES

by

WAN ABD MALIK WAN MOHAMED


B.Sc (Electrical Engineering), Seoul National University, Korea

**A Doctoral Thesis submitted in partial fulfilment of the
requirements for the award of
Doctor of Philosophy
of
LOUGHBOROUGH UNIVERSITY**

WOLFSON SCHOOL OF MECHANICAL AND MANUFACTURING ENGINEERING

July 2006

© by Wan Abd Malik Wan Mohamed (2006)

 Loughborough University Pilkington Library
Date JAN 2007
Class T
Acc No. 0403271487

DEDICATED TO:

my lovely parents Khadijah and Wan Mohamed (Allahyarham)

my lovely wife Salwani

my sons Wan Muhammad (Faris, Shahmi, Adib, Amir and Naqib)

my brothers and sisters

ABSTRACT

There are two primary methods to derive pressure from the base units of mass, length and time, i.e. a liquid manometer and a pressure balance. The key problem associated with pressure measurement using a pressure balance is centred on the determination of the effective area of the piston-cylinder assembly (PCA) under the appropriate operating conditions. Dimensional measurements alone cannot provide formally recognised traceability to the SI unit, the pascal (Pa), without extreme levels of data and mathematical modelling, supported with extensive comparison histories with other instruments of proven performance. Intercomparisons have demonstrated that the uncertainty of measurements using pressure balances, have reached a plateau of approximately 5 to 10 ppm due to unexplained phenomena.

The aim of this research is to identify any evidence of pressure dependency as a function of surface texture applied onto the piston of 35 mm diameter PCA, using a gas-operated (gas-lubricated) pressure balance. This has been achieved via a number of research objectives; understanding and documentation of the PCA manufacturing techniques, design and manufacture of a pair of pressure balances, investigation of the influence of rotational speed (RS) and rotational direction (RD), investigation of the influence of a range of PCAs with different surface textures, and calibration directly to the UK Primary Pressure Standard.

The novel results of the research demonstrated the quality of the pressure balance build and stability, and the performance of the PCAs. Experimental investigation has identified that RS (0.5 to 1 Hz) and RD (clockwise or counter clockwise) do not affect the determination of the effective area. The work has further concluded that the limited range of surface texture applied to the PCAs, generally does not influence the determined effective area with respect to the uncertainty budget of the pressure balance (16.4 ppm at $k = 2$). However, very smooth PCAs consistently produce the lowest value of effective area.

ACKNOWLEDGMENTS

Firstly, I would like to express my highest gratitude to my supervisor Dr. Jon Petzing for his helpful discussions, guidance, support, encouragement, comments, patience, time and his continuous great excitement and interest concerning my research topic during my time as a research student at Loughborough University. I am also very grateful to extend my sincere thanks to Mr. Jagpal Singh, Mr. Derrick Hurrell, Mr. Bob Ludlam and Mr. Andy Sandaver for their rewarding discussions and unselfish support. Many thanks to other staff and colleagues, within the Wolfson School of Mechanical and Manufacturing Engineering for their friendship.

It is my pleasure to acknowledge SIRIM Berhad and the Ministry of Science, Technology and Innovation (Malaysia) for their sponsorship. My special thanks go to Mr. Ken Nishibata (ex-JICA expert), my great guru, who has contributed significantly to my learning of pressure metrology; NPL (UK), Mettler-Toledo (Switzerland), DH-Budenberg (UK) and Druck (UK) for their support.

Lastly, I would like to express my highest appreciation to my lovely parents for their guidance and support throughout my upbringing, and my lovely wife Salwani Abdullah and sons Wan Muhammad Faris, Wan Muhammad Shahmi, Wan Muhammad Adib, Wan Muhammad Amir and Wan Muhammad Naqib; my brothers and sisters for their unconditional understanding, patience and support throughout my studies. I love you all.

TABLE OF CONTENTS

Abstract.....	i
Acknowledgements.....	ii
Table of Contents	iii
List of Abbreviations	x
List of Terminologies	xii
List of Symbols	xxi
List of Figures.....	xxx
List of Tables	xxxv
 1. Introduction.....	 1
1.1 Background and Motivation	1
1.2 Rationale of the Research.....	3
1.3 Aims and Objectives of the Research.....	4
1.4 Overview of the Thesis.....	6
 2. Introduction to Pressure and Surface Metrology	 8
2.1 Background of Pressure and Surface Metrology	8
2.2 The Measurement of Pressure	10
2.2.1 What is Pressure?.....	10
2.2.2 The International System of Units (SI).....	11
2.2.3 The Definitions of the SI Units.....	11
2.2.4 Pressure as a Derived Unit.....	12
2.2.5 Pressure Modes	13
2.2.6 The Role of the Primary Pressure Standards in the Measurement System.....	15
2.2.7 Comparison Between the Two Primary Pressure Standards.....	17
2.3 The Measurement of Surface Texture	21
2.3.1 What is Surface Texture?.....	21

2.3.2	The Importance of Surface Texture	21
2.3.3	Concepts, Terms and Definitions of Surface Texture.....	22
2.3.4	The Nature of Surface Texture	23
2.3.5	Orders of Geometrical Irregularities	23
2.3.6	Surface Texture Instrumentation.....	28
2.3.7	Surface Texture Parameters	30
2.3.8	Amplitude Parameter	30
2.4	Summary.....	33
3.	The Pressure Balance.....	34
3.1	Early History of the Pressure Balance	34
3.2	Physical Principles of the Pressure Balance	37
3.3	Basic Types of Piston-Cylinder Assembly (PCA).....	38
3.3.1	Simple Type.....	38
3.3.2	Controlled-clearance Type.....	38
3.3.3	Re-entrance Type	39
3.3.4	Differential Type.....	39
3.4	Pressure Conversation Equation.....	41
3.4.1	Mass and Buoyancy	42
3.4.2	Local Acceleration Due to Gravity	44
3.4.3	Surface Tension	45
3.4.4	Temperature Correction.....	46
3.4.5	Elastic Pressure Distortion Coefficient.....	46
3.4.6	Effective Area	47
3.5	Theory of the Piston-Cylinder Assembly (PCA)	48
3.6	Summary.....	53
4.	Review of the Gas-Operated Pressure Balance.....	55
4.1	The 1940s	56
4.2	The 1950s	56
4.3	The 1960s	57
4.4	The 1970s	58
4.5	The 1980s	62

4.6	The 1990s	65
4.7	Recent Research (2000 - 2006).....	72
4.8	Summary.....	74
5.	Manufacturing Process.....	76
5.1	Selection of Materials.....	77
5.1.1	Materials for the Pressure Balance	77
5.1.2	Materials of the Piston-Cylinder Assembly (PCA).....	78
5.2	Manufacturing of the Pressure Balance	80
5.3	Manufacturing of the Piston-Cylinder Assembly (PCA).....	85
5.3.1	Manufacturing of the PCA's Blank.....	85
5.3.2	Manufacturing of the 316 Stainless Steel PCA	91
5.3.2.1	Aluminium Curved-Shell	96
5.3.2.2	Expandable Slotted-End PVC Tube.....	97
5.3.2.3	Piston's Blank Secured on a Mandrel.....	98
5.3.2.4	Expandable Mild-Steel Mandrel	98
5.3.2.5	Honing Tool	99
5.3.2.6	Lapping Tool.....	101
5.3.2.7	Matching Work of 316 Stainless Steel PCAs	104
5.4	Trimming and Matching Techniques of the Tungsten Carbide Piston- Cylinder Assembly (PCA).....	108
5.4.1	Grade of the Selected Tungsten Carbide.....	108
5.4.2	Piston and Cylinder Blank	109
5.4.3	Clamping/Securing Method.....	110
5.4.4	Design of the Lapping Tools.....	111
5.4.5	Lap Contraction/Expansion	112
5.4.6	Lap Fit.....	113
5.4.7	Lap Materials	114
5.4.8	Abrasives	115
5.4.9	Lubricating Fluid	115
5.4.10	Reciprocation Method.....	115
5.4.11	Polishing Method.....	116
5.5	Summary.....	117

6. Cross-floating Method and Its Uncertainty Budget	119
6.1 Practical Aspects of Use of the Pressure Balance in the Cross-floating Method.....	120
6.1.1 Environmental Conditions	120
6.1.2 Location of the Experimental Pressure System	122
6.1.3 Pressure Fittings.....	123
6.1.4 Leveling	124
6.1.5 Handling.....	126
6.1.6 Cleanliness of the PCA.....	126
6.2 Cross-floating Method.....	129
6.2.1 General Cross-floating Method	129
6.2.2 Cross-floating Method Used in this Research Work	131
6.2.3 Speed and Temperature Measurement.....	134
6.3 Uncertainty of Measurement	135
6.3.1 Uncertainty of Measurement in the Cross-floating Method of Gas-operated Pressure Balance	139
6.4 Summary.....	143
7. Investigation of the Effects of Rotational Speed and Rotational Direction on the Determined Effective Area.....	145
7.1 Rationale.....	145
7.2 Investigation Approach.....	146
7.2.1 Comparison Procedure.....	147
7.2.2 Cycle of Measurement	148
7.3 Measurement Results.....	149
7.3.1 Results of Experiment E: P_4C_2 vs. P_2C_3	150
7.3.2 Results of Experiment F: P_4C_4 vs. P_2C_3	156
7.4 Uncertainty Analysis.....	161
7.5 Summary and Discussions.....	165
8. Investigation on the Effects of Surface Texture on the Determined Effective Area	167
8.1 Rationale.....	168

8.2	Investigation Approach.....	168
8.2.1	Comparison Procedure.....	172
8.2.2	Cycle of Measurement	172
8.3	Measurement Results.....	172
8.3.1	Results of the Surface Texture Characterisations	173
8.3.1.1	Surface Characterisation Results of Piston 1	174
8.3.1.2	Surface Characterisation Results of Piston 2	175
8.3.1.3	Surface Characterisation Results of Piston 3	176
8.3.1.4	Surface Characterisation Results of Piston 4	177
8.3.1.5	Surface Characterisation Results of Piston 5	178
8.3.1.6	Surface Characterisation Results of Piston 6	179
8.3.1.7	Surface Characterisation Results of Piston 7	180
8.3.2	Comparison of Surface Profiles Between Seven Pistons.....	181
8.3.3	Results of the Effective Area Determinations	183
8.3.3.1	Experiment A: P_1C_2 vs. P_2C_3	183
8.3.3.2	Experiment B: P_1C_4 vs. P_2C_3	185
8.3.3.3	Experiment C: P_3C_2 vs. P_2C_3	186
8.3.3.4	Experiment D: P_3C_4 vs. P_2C_3	187
8.3.3.5	Experiment G: P_5C_2 vs. P_2C_3	188
8.3.3.6	Experiment H: P_5C_4 vs. P_2C_3	190
8.3.3.7	Experiment I: P_6C_2 vs. P_2C_3	191
8.3.3.8	Experiment J: P_6C_4 vs. P_2C_3	193
8.3.3.9	Experiment K: P_7C_2 vs. P_2C_3	194
8.3.3.10	Experiment L: P_7C_4 vs. P_2C_3	195
8.3.3.11	Experiment m: P_7C_4 vs. P_3C_2	196
8.3.3.12	Experiment n: P_7C_2 vs. P_3C_4	197
8.3.3.13	Experiment o: P_6C_2 vs. P_3C_4	198
8.3.3.14	Experiment p: P_7C_4 vs. P_4C_2	199
8.3.3.15	Experiment q: P_2C_2 vs. P_4C_4	200
8.3.3.16	Experiment r: P_3C_3 vs. P_4C_4	201
8.3.3.17	Experiment s: P_6C_2 vs. P_4C_4	202
8.3.3.18	Experiment t: P_7C_2 vs. P_4C_4	203

8.3.3.19	Experiment u: P_7C_4 vs. P_6C_2	204
8.3.3.20	Experiment v: P_6C_4 vs. P_7C_2	205
8.3.3.21	Experiment w: P_2C_2 vs. P_7C_4	206
8.3.3.22	Experiment x: P_3C_3 vs. P_2C_2	207
8.4	Comparison of Effective Area Determinations Through Different Routes	210
8.4.1	Effective Area of the P_2C_2 ($A_{(P2C2)}$)	210
8.4.2	Effective Area of the P_3C_3 ($A_{(P3C3)}$)	211
8.4.3	Effective Area of the P_6C_2 ($A_{(P6C2)}$)	211
8.4.4	Effective Area of the P_6C_4 ($A_{(P6C4)}$)	211
8.4.5	Effective Area of the P_7C_2 ($A_{(P7C2)}$)	212
8.4.6	Effective Area of the P_7C_4 ($A_{(P7C4)}$)	212
8.5	Summary and Discussion	213
9.	Calibration/Verification Against the UK's National Primary Pressure Standard	216
9.1	Rationale	217
9.2	Calibration/Verification Approach	217
9.3	Calibration Plans	218
9.4	Calibrations and Their Results	218
9.4.1	Initial Calibrations	218
9.4.2	Calibration Y1: P_2C_3 vs. PCA-602	221
9.4.3	Calibration Y2: P_3C_4 vs. PCA-602	223
9.4.4	Calibration Y3: P_4C_2 vs. PCA-602	224
9.4.5	Calibration Y4: P_4C_4 vs. PCA-602	225
9.5	Verification Process	225
9.5.1	Deviation Check	226
9.5.2	Normalised Errors, E_n	227
9.6	Thermal Stability Comparisons	228
9.6.1	Lufbra 1 vs. Ruska 2465	230
9.6.2	Lufbra 1 vs. DHI PG7601	231
9.7	Summary and Discussions	233

10. Conclusions.....	235
10.1 Research Objectives Summary.....	235
10.2 Engineering and Scientific Contribution.....	238
10.3 Future Work.....	240
10.3.1 Existing Facilities.....	240
10.3.2 New PCAs and Modified Pressure Balance.....	241
10.4 Disseminations.....	242
References.....	244

LIST OF ABBREVIATIONS

Abbreviation	Description
ppm	Parts per million
rpm	Rotation per minute
BIPM	International Bureau of Weights and Measures
BSI	British Standards Institute
CCM	Consultative Committee for Mass and Related Quantities
CCW	Counter-clockwise
CIPM	International Committee for Weights and Measures
CMI	Czech Institute of Metrology
CW	Clockwise
CGPM	General Conference on Weights and Measures
CNC	Computer Numerical Controls
CYL	Cycle of measurement
GTM	Gas Thermometer Manometer
HSS	High speed steel
IMGC	Istituto di Metrologia "Gustavo Colonnetti", Italy
IMC	The Institute of Measurement and Control, UK
ISO	International Organization for Standardization
LNE	Laboratoire National d'Essais, France
LU	Loughborough University
NBS	National Bureau of Standards, former name of the NIST
NIST	National Institute of Standards and Technology (formerly NBS), USA.
NMI	National Measurement Institute

List of Abbreviations

NMS	National Measurement System (Department of Trade and Industry, UK)
NPL	National Physical Laboratory, UK
NPLi	National Physical Laboratory, India
OIML	International Organization of Legal Metrology
PCA	Piston-cylinder assembly
PTB	Physikalische-Technische Bundesanstalt, Germany
PVC	Polyvinyl chloride (polychloroethene), is a widely-used plastic.
RC	Rotational combination
RD	Rotational direction
RMS	Root mean square
RS	Rotational speed
RSS	Root-sum-of square
SEQ	Sequence of measurement
SI	The International System of Units
UIM	Ultrasonic Interferometer Manometer
UK	United Kingdom
USA	United States of America
VNIIFTRI	All-Russian Research Institute for Physical, Technical and Radio-Technical Measurements, USSR

LIST OF TERMINOLOGIES

Terminology	Definition/Explanation
Adjustment (of a measuring instrument)	Operation of bringing a measuring instrument into a state of performance suitable for its use [PD6461-1 1995].
Areal	Two dimensional measurement of area. Sometimes called 3-dimensional measurement [Whitehouse 1994].
Average	The sum of values divided by the number of values [ISO/TAG 4 1993].
Base unit (of measurement)	Unit of measurement of a base quantity in a given system of quantities [PD6461-1 1995].
Base quantity	One of the quantities that, in a system of quantities, are conventionally accepted as functionally independent of one another [PD6461-1 1995].
Blank	A workpiece that has not been cut into its specific shape.
Brinell hardness test (HB)	The typical test uses a 10 mm diameter steel ball as an indenter with a 3,000 kgf (29 kN) force. For softer materials, a smaller force is used; for harder materials, a tungsten carbide ball is substituted for the steel ball [Wikipedia 2006].
Calibration	A set of operations that establish, under specified conditions, the relationship between the values of quantities indicated by a measuring instrument or measuring system, and the corresponding values realised by standards [NPL 2006].
Check standard	A predetermined test standard that act as a checking mechanism in a verification process.
Calibration chain	The chain of calibration from international to workshop standard [Whitehouse 1994].
Coefficient of friction	The dimensionless ratios of the friction force (F) between two bodies, to the normal force (N) pressing these bodies together [Bushan 2001].
Coherent system of unit (of measurement)	System of unit of measurement in which all of the derived units are coherent [PD6461-1 1995].

Coherent (derived) unit (of measurement)	Derived unit of measurement that may be expressed as a product of powers of base units with the proportionality factor one [PD6461-1 1995].
Conventional mass	For a weight taken at 20°C, the conventional mass is the mass of a reference weight of a density of 8000 kgm ⁻³ which it balances in air of a density of 1.2 kgm ⁻³ .
Conventional true value (of a quantity)	Value attributed to particular quantity and accepted, sometimes by convention, as having an uncertainty appropriate for a given purpose [PD6461-1 1995].
Conversion equation	An equation that relates the generated pressure and the mass of the weights loaded, taking into account the other input quantities.
Coverage factor	Numerical factor used as a multiplier of the combined standard uncertainty in order to obtain an expanded uncertainty [PD6461-4 2004].
Cutting speed	Is the speed difference between the cutting tool and the surface of the workpiece it is operating on.
Degree of freedom	In general, the number of terms in a sum minus the number of constraints on the terms of the sum [ISO/TAG 4 1993].
Derived unit (of measurement)	Unit of measurement of a derived quantity in a given system of quantities [PD6461-1 1995].
Diametral	Variations across diameters in roundness measurement [Whitehouse 1994].
Dilatometer	An instrument to determine the linear thermal expansion coefficient of material.
Dimension of a quantity	Expression that represents a quantity of a system of quantities as the product of powers of factors that represent the base quantities of the system [PD6461-1 1995].
Discrimination (equilibrium)	The smallest change in mass (weight) that can influence the equilibrium condition of the cross-floating experiment.

Dynamometer (digital pressure balance)	A device used to measure force based on electromagnetic force compensation that utilise the electrodynamic conversion principle.
Effective area (A_e)	The area of a piston and cylinder combination determined for a particular instrument by comparison with a reference pressure balance or liquid manometer for the specified temperature and pressures prevailing during the calibration process. This value is used in the conversion equation for the calculation of the measured pressure. The area is neither that of the piston nor cylinder, but has a value somewhere in between them.
Errors (dimension)	Deviation from intended shape or size [Whitehouse 1994].
Error (of measurement)	Results of a measurement minus a true value of the measurand [PD6461-1 1995].
Expanded uncertainty	Quality defining an interval about the result of a measurement that may be expected to encompass a large fraction of the distribution of values that could reasonably be attributed to the measurand [ISO/TAG 4 1993].
Fall rate	Rate of fall of the piston at a specific pressure value, while it is floating and rotating conditions, and is measured in mms^{-1} .
Feed rate	Is the distance a cutting tool advances per revolution. Its metric units are millimeters per revolution.
Form / Profile	Form/profile is the overall shape of the object and it is on the dividing line in size scale between geometric errors and finish errors.
Friction	The resisting force tangible to the common boundary between two bodies when, under the action of an external force, one body moves or tends to move relative to the surface of the other [Bushan 2001].
Function	The application of a workpiece [Whitehouse 1994].
Galling	Is a severe form of adhesive wear which occurs when two metallic components slide against each other at relative low speed [Magee 1996].

Gauge (pressure mode)	The value of pressure measured with respect to atmospheric pressure [NPL 2006].
Generatrix	Measurement points used in the straightness and parallelism characterisations of an object (piston or cylinder), based on angular separation of x° with y mm with respect to the x-axis, or circle traces [PTB 2006].
Goniometer	An instrument used in declination angle measurement, or commonly used as a direction finder that determines the angular direction of incoming radio signals.
Hardness	The resistance of a material to plastic deformation (usually by indentation) [Budiski and Budiski 1999].
Lapping	A surface finishing process involving motion against a fine abrasive embedded in a soft metal [Bushan 2001].
Influence quantity	Quantity that is not the measurand but that affects the result of the measurement [PD6461-1 1995].
International System of Units, SI	The coherent system of units adopted and recommended by the General Conference on Weights and Measures (CGPM) [PD6461-1 1995].
Lay	Predominant directional striations across a surface, as a result of a particular production method and geometry used.
Lobing	Undulations on a nominally round workpiece produced usually by clamping or chatter [Whitehouse 1994].
Lubrication	The reduction of frictional resistance and wear, or other forms of surface deterioration, between two load-bearing surfaces by the application of a lubricant [Bushan 2001].
Magnetic susceptibility	Degree of magnetization of a material in response to an applied magnetic field [Wikipedia 2006].
Mandrel	An object used to shape machined work; a tool component that grips or clamps materials to be machined; or a tool component that can be used to grip other moving tool components [Wikipedia 2006].
Measurand	Particular quantity subject to measurement [ISO/TAG 4 1993].

Measurement	Set of operations having the object of determining a value of a quantity [ISO/TAG 4 1993].
Metrology	The science of measurement [PD6461-1 1995].
Modulus of elasticity	The ratio of stress to strain in a material loaded within its elastic range; a measure of rigidity [Budiski and Budiski 1999].
Noise floor	The measure of the signal created from the sum of all the noise sources and unwanted signals within a measurement system [Wikipedia 2006].
Packing (valve)	A material that is designed to prevent or prohibit leakage.
Parallelism	The tolerance zone is limited in the measuring plane by two straight lines a distance t apart and parallel to the datum [Mahr 2006b].
Peak	Maximum extent of the profile between two adjacent valleys [Whitehouse 1994].
Piston-cylinder assembly (PCA)	An assembly where weights are loaded on top of it, and it consists of a circular vertical piston that is free to slide in a cylinder with a very fine clearance. It is rotated during operation to eliminate friction between piston and cylinder.
Polishing	A surface finishing process utilising successive grades of abrasive [Bushan 2001].
Pressure balance	An instrument consisting of a finely machined piston mounted vertically in a close-fitting cylinder used for maintaining a calculable pressure; also known as a piston gauge. When fitted with a means of pressure control, additional pressure ports, masses etc, the complete system is commonly known as a dead-weight tester [NPL 2006].
Primary (standard)	Standard that is designated or widely acknowledged as having the highest metrological quality and whose value is accepted without reference to other standards of the same quantity [NPL 2006].
Profile (surface)	The tolerance zone is limited by two surfaces enveloping spheres of diameter t , the centres of which are situated on a surface having the true geometrical form [Mahr 2006b].

Reference (standard)	Standard, generally having the highest metrological quality available at a given location or in a given organisation, from which measurements made are derived. The reference standard itself must be periodically calibrated [NPL 2006].
Reference conditions	Reference conditions apply to the effective area of the piston and cylinder with respect to temperature and pressure. The standard conditions are taken as 20°C and atmospheric pressure.
Reference level	The vertical level with respect to a clearly defined part of the support column or the base of a pressure balance, to which a measured pressure is referred to when the piston is at a specific operating level. Normally it lies in the horizontal plane, which passes through the base of the piston.
Relative uncertainty	Uncertainty expressed as a proportion or percentage of the measurement result [PD6461-4 2004].
Repeatability (of results of measurements)	Closeness of the agreement between the results of successive measurements of the pressure carried out under the same conditions of measurement. Conditions include: same procedure, observer, instrument, conditions, location; and carried out over a short period of time [PD6461-1 1995].
Reproducibility (of results of measurements)	Closeness of the agreement between the results of measurements of the pressure carried out under changed conditions of measurement. Includes changing some of those conditions which are held constant for 'repeatability', and may refer to measurements carried out over a long period of time [PD6461-4 2004].
Resolution (of a displaying device)	Smallest difference between indications of a displaying device that can be meaningfully distinguished. Note that it is important not to confuse the resolution of a display alone with the resolution of a pressure measuring system which incorporates a display; the system will have less (poorer) resolution than the display alone [PD6461-1 1995].
Roughness	Process marks or witness marks produced by the action of the cutting tool or machining process, but may include other factors such as the structure of the material [Taylor Hobson 2006].

Roundness	The tolerance zone is limited in the measuring plane perpendicular to the axis by two concentric circles a distance t apart [Mahr 2006b].
Straightness	The tolerance zone is limited in the measuring plane by two parallel straight lines a distance t apart [Mahr 2006b].
True value	Value consistent with the definition of a given particular quantity [ISO/TAG 4 1993].
Type K thermocouple	The general purpose thermocouple. It is low cost, and owing to its popularity; made of Chromyl (Ni-Cr alloy) / Alumel (Ni-Al alloy) [Wikipedia 2006b].
Spinning time	Time taken for a piston to stop from spinning, once it is spun at a specific initial speed of rotation (at a specific pressure value), and is measured in min.
Standard deviation	A mathematical quantity used to characterise the dispersion of results [NPL 2006].
Standard uncertainty	Uncertainty of the result of a measurement expressed as a standard deviation [NPL 2006].
Stylus	Mechanical implement used to contact workpiece and to communicate displacement to transducer [Whitehouse 1994].
Surface	A surface is a boundary that separates an object from another object or substance and it can be divided into two types. Anisotropic surface - a surface with a visible directional lay on its roughness. Isotropic surface - a surface having no obvious directional lay on its roughness [Whitehouse 1994].
Surface texture	The geometry imparted [Whitehouse 1994].
Thermocouple	Is a widely used type of temperature sensor, and can also be used as a means to convert thermal potential difference into electric potential difference. It measures the temperature difference between two points, not absolute temperature [Wikipedia 2006].

Traceability	Property of the result of a measurement or the value of a standard whereby it can be related to stated references, usually national or international standards, through an unbroken chain of comparisons all having stated uncertainties [NPL 2006].
Transducer	Device that provides an output quantity having a determined relationship to the pressure. Commonly used in pressure measurement to refer to pressure transducers with voltage outputs [NPL 2006].
Transfer standard	Standard used as an intermediary to compare standards [NPL 2006].
Tribology	The science and technology of interacting surfaces in relative motion and of the practices related thereto [Bushan 2001].
Trimming (cross-floating)	A balancing process using a set of standard weights in order to get an equilibrium condition.
Trimming (lapping)	Final work (lapping and superfinishing) to match a piston into a cylinder, so that any observable geometrical imperfections are refined.
True value (of a quantity)	Value consistent with the definition of a given particular quantity [PD6461-1 1995].
Type A uncertainty	Method of evaluation of uncertainty by the statistical analysis of a series of observations [PD6461-4 2004].
Type B uncertainty	Method of evaluation of uncertainty by means other than the statistical analysis of a series of observations [PD6461-4 2004].
Uncertainty of measurement	Parameter, associated with the result of a measurement, that characterised the dispersion of the values that could reasonably be attributed to the measurand [ISO/TAG 4 1993].
Uncertainty budget	A calculation detailing the component terms contributing to the uncertainty of a measurement, their statistical distribution, mathematical manipulation and summation [NPL 2006].
Valley	Minimum extent of the profile of a surface [Whitehouse 1994].

List of Terminologies

Vickers hardness test (HV)	A pyramid-shaped indenter made of diamond is used. It is based on the principle that impressions made by this indenter are geometrically similar regardless of load [Wikipedia 2006].
Waviness	This is usually produced by instabilities in the machining process, such as an imbalance in a grinding wheel, or by deliberate actions in the machining process. Waviness has a longer wavelength than roughness which is superimposed on the waviness [Taylor Hobson 2006].
Wringing	Sticking of smooth surfaces in contact. Presence of fluid film necessary [Whitehouse 1994].

LIST OF SYMBOLS

Symbols are arranged in alphabetical order based on chapters. Some symbols may differ from chapter to chapter.

Chapter 2

Symbol	Description
A	Area (m^2)
F	Force in newton (N)
g	Acceleration due to gravity (ms^{-2})
h	Height of mercury column (m)
l	Assessment length of profile, containing few sampling length (μm)
l_i	i^{th} sampling length (μm)
p	Pressure in pascal (Pa)
R_a	Arithmetic mean of the absolute magnitude of the roughness profile (μm)
R_{ku}	Kurtosis – is a measure of the sharpness of the surface profile (μm)
R_p	Maximum height of the profile above the mean line (μm)
R_q	RMS parameter corresponding to R_a (μm)
R_{sk}	Skewness – is the measure of the symmetry of the profile about the mean line (μm)
R_t	Maximum peak to valley height of the profile (μm)
R_v	Maximum depth of the profile below the mean line (μm)
$z(x)$	Vertical characteristics of the surface profile variation (μm)
ρ	Density of mercury (kgm^{-3})

Chapter 3

Symbol	Description
A_0	Effective area of the PCA at a reference temperature t , and atmospheric pressure (m^2)
A_1	Effective area of a larger piston (differential PCA) (m^2)
A_2	Effective area of a smaller piston (differential PCA) (m^2)

List of Symbol

A_e	Differential effective area (m^2)
C	Circumference of the piston at the level where it emerges from pressure transmitting fluid (m)
C_T	Temperature correction factor, due to linear thermal expansion coefficients of piston and cylinder
D_{rel}	Relative different in mass, between true mass (m) and conventional mass (m_c) (kg)
E_c	Young's modulus of elasticity of the cylinder (Pa)
E_p	Young's modulus of elasticity of the piston (Pa)
F	Force detected by the weighing instrument (N), but displayed in mass unit (kg)
F_a	Weight force of the displaced air (N)
F_f	Frictional force exerted on the vertical flanks of the piston by the pressure transmitting fluid (N)
F_m	Actual gravitational force generated by the mass, m (N)
g_L	Local acceleration due to gravity (ms^{-2})
$g_L(0,0)$	Gravity value at the equator and at sea level, which is equal to $9.7803184 ms^{-2}$
$g_L(\varphi, H)$	Gravity value calculated for latitude φ and height H meters above sea level (ms^{-2})
h	Difference in heights between the piston base and a selected reference level (m)
H	Height above sea level (m)
h_c	Radial separation between the piston and cylinder (m)
h_o	Radial separation between the piston and cylinder at $x = 0$ (m)
l	Engagement length of a piston in a cylinder (m)
m	Mass of the weighing sample (kg)
m_c	Conventional mass (kg)
m_i	Individual true mass value of each weight (including all floating elements e.g. piston and ball-bearing) applied on the piston (kg)
p	Gauge pressure measured at the reference level (Pa)
p_1	Fluid pressure being measured at the base of the piston (Pa)
p_2	Fluid pressure being measured at the level where it emerges from pressure transmitting fluid and exposed to the ambient pressure (Pa)

p_j	Operating jacket pressure of the controlled-clearance PCA (Pa)
p_o	Atmospheric pressure (Pa)
r	Outer radius of the piston (m)
R	Inner radius of the cylinder (m)
\hat{r}	Radius of the neutral surface (m)
R_c	Average outer radius of the cylinder (m)
r_c	Average inner radius of the cylinder (m)
r_o	Piston radius at the position $x = 0$ (m)
t	Measured temperature of the PCA at the moment measurement taken/pressure is generated ($^{\circ}\text{C}$)
t_{ref}	Reference temperature at which A_o is measured, normally 20°C
u	Piston deviations from the ideal reference radius (m)
U	Cylinder deviations from the ideal reference radius (m)
W	Gravitational force due to applied masses (N)
w	Gravitational force acting on the column of fluid of annular cross-section contained between the surface of the piston and the neutral surface (N)
W'	True value of the corrected gravitational force due to applied mass (N)
w'	Corrected gravitational force acting on the column of fluid of annular cross-section contained between the surface of the piston and the neutral surface (N)
α	Angle of a tilting PCA
α_c	Linear thermal expansion coefficient of the cylinder ($^{\circ}\text{C}^{-1}$)
α_p	Linear thermal expansion coefficient of the piston ($^{\circ}\text{C}^{-1}$)
β_1	A constant, which is equal to 0.0053024
β_2	A constant, which is equal to 0.0000059
Γ	Surface tension of the pressure transmitting fluid used (Nm^{-1})
ϵ	Ratio between the radial separation, h_c and the radius of the piston, r
φ	Latitude, where the gravity value is calculated (arc degree)
λ	Elastic pressure distortion coefficient of the PCA (Pa^{-1})
ν_c	Poisson coefficient of the cylinder
ν_p	Poisson coefficient of the piston
ρ_a	Density of ambient air (kgm^{-3})

List of Symbol

ρ_{ac}	Conventional value of air density (1.2 kgm^{-3})
ρ_f	Density of the pressure-transmitting fluid (kgm^{-3})
ρ_m	Density of mass, m (kgm^{-3})
ρ_{mc}	Conventional density of weighing sample (8000 kgm^{-3})
ρ_{mi}	Density of i^{th} weight (kgm^{-3})

Chapter 4

Symbol	Description
1σ	Approximately 68.3% level of confidence, or $k = 1$
2σ	Approximately 95.5% level of confidence, or $k = 2$
^3He	Helium-3
3σ	Approximately 99.7% level of confidence, or $k = 3$
^4He	Helium-4
Ar	Argon
CO_2	Carbon dioxide
H_2	Hydrogen
He	Helium
Kr	Krypton
N_2	Nitrogen
p_j	Jacket pressure (Pa)
P_z	Stall jacket pressure, i.e. the value of jacket pressure, p_j at which the clearance between the piston and cylinder is zero (Pa)
SF_6	Sulfur hexafluoride
$u(A_e)/A_e$	Relative standard uncertainty of the determined effective area (ppm)
ΔP	A method introduced to eliminate effects such as surface tension, mass or density of piston in the determination of the effective area

Chapter 5

Symbol	Description
Al_2O_3	Aluminium oxide
Co	Cobalt
Cr_3C_2	Chromium carbide
k	Coverage factor
P_2C_3	Reference PCA
P_XC_Y	Combination of a Piston X with a Cylinder Y , where $X = 1$ to 7 and $Y = 2$ to 4
R_a	The arithmetic mean of the absolute magnitude of the roughness profile (μm)
SiC	Silicon carbide
TaC	Tantalum carbide
Ti	Titanium
WC	Cemented tungsten carbide
ZrO_2	Toughened zirconia
χ	Magnetic susceptibility
\varnothing	Diameter (mm)

Chapters 6, 7, 8, 9 and 10

Symbol	Description
a	Pressure distortion coefficient determined by the NPL (ppm/MPa)
A_0	Effective area determined by the NPL (mm^2)
A_{r0}	Simplified symbol for $A_{r(p,20^\circ\text{C})}$ (mm^2)
$A_{r(p,20^\circ\text{C})}$	Effective area of the reference PCA at pressure p and reference temperature 20°C (mm^2)
$A_{r(\text{P2C3})}$	Effective area of the reference PCA, assigned to be equal to 981.45955 (mm^2)
A_t	Simplified symbol for $A_{t(p,20^\circ\text{C})}$ (mm^2)
$A_{t(p,20^\circ\text{C})}$	Effective area of the test PCA at pressure p and reference temperature 20°C (mm^2)

List of Symbol

A_{PXC_Y}	Calculated effective areas of the test PCA ($P_X C_Y$) from individual determination (mm^2)
$A_{i(PXC_Y)}$	Adjusted values of the check standards based on $A_{i(P_2 C_Y)NPL}$ (mm^2)
$A_{i(PXC_Y)}$	General symbol for the determined effective area of the test PCA ($P_X C_Y$) (mm^2)
$A_{i(PXC_Y)Z}$	Average effective area of the test PCA ($P_X C_Y$) determined via Experiment Z ($Z = A$ to L and m to x) (mm^2)
$A_{i(PXC_Y)}^{Zabc}$	Determined effective area of the test PCA ($P_X C_Y$) through calibration routes "Z-a-b-c" (mm^2)
$A_{(PXC_Y)NPL}$	Effective area of the test PCA ($P_X C_Y$) determined by the NPL using the UK Primary Pressure Standard (mm^2)
c_i	Sensitivity coefficient, describes how the output estimate y varies with changes in the values of the input estimates x_i
E_i	Error due to spirit level indication (div)
E_n	Normalised errors
$E_{n(PXC_Y)}$	Normalised error of the $P_X C_Y$ combination
E_v	Error due to piston verticality (div)
f	A functional relationship that relates the output quantity dependency to the input quantities
g_L	Local acceleration due to gravity (ms^{-2})
H	Head correction due to height difference in the reference level of the two pressure balances (Pa)
h_r	Relative humidity (%RH)
k	Coverage factor
k_p	Coverage factor of probability, p
m_{dis}	Discrimination weight that produced a detectable pressure change (kg)
m_{pr}	Mass of the reference piston (kg)
m_{pt}	Mass of the test piston (kg)
m_{wr}	Total mass of weights, including piston and any other floating elements loaded on the reference pressure balance (kg)
m_{wt}	Total mass of weights, including piston and any other floating elements loaded on the test pressure balance (kg)
n	Number of series of measurement
$P_2 C_3$	Reference PCA in the calibration chain

List of Symbol

p_a	Atmospheric pressure at equilibrium condition/measurement taken (Pa)
p_{ar}	Ambient pressure at the reference level of the reference pressure balance (Pa)
p_{at}	Ambient pressure at the reference level of test pressure balance (Pa)
p_{N_2}	Pressure value of the pressure transmitting fluid (N_2)
p_r	Gauge pressure at the reference level of the reference pressure balance (Pa)
p_t	Gauge pressure at the reference level of the test pressure balance (Pa)
$P_X C_Y$	A combination of a Piston X and Cylinder Y , where $X = 1$ to 7 and $Y = 2$ to 3
R	Repeatability of measurement
R_a	Profile statistic of the arithmetic mean of the absolute magnitude of the roughness profile (μm)
R_p	Ratio of the effective areas between the test and reference PCAs, based on the ratio of the equilibrium loads
R_q	Profile statistic of the RMS parameter corresponding to R_a (μm)
R_t	Profile statistic of the maximum peak to valley height of the profile (μm)
R_{ti}	R_t of i^{th} piston (μm), where $i = 1$ to 7
R_{qi}	R_q of i^{th} piston (μm), where $i = 1$ to 7
R_{ai}	R_a of i^{th} piston (μm), where $i = 1$ to 7
s_l	Estimated standard deviation
s_l^2	Estimated variance
t_a	Ambient temperature ($^{\circ}C$)
t_{N_2}	Temperature of the pressure transmitting fluid (N_2)
t_p	Student- t distribution
t_r	Temperature of the reference PCA ($^{\circ}C$)
t_t	Temperature of the test PCA ($^{\circ}C$)
$u(A_t)$	Standard uncertainty of the effective area of the test PCA (mm^2)
$U(x)$	Expanded uncertainty of the measurand
$u(x_i)$	Individual standard uncertainty of the input parameter x_i
$u_A(x)$	Standard uncertainty of Type A
$u_A(\bar{x})$	Estimated standard deviation of arithmetic mean (ESDM) of input estimates of Type A uncertainty

List of Symbol

$u_B(x)$	Standard uncertainty of Type B
$u_c(y)$	Combined standard uncertainty
$U_k(x)$	Expanded uncertainty obtained from available knowledge or scientific judgment
U_p	Expanded uncertainty of probability, p
V1	Ball-valve 1
V2	Ball-valve 2
V3	Ball-valve 3
W	Total downward gravitational force acting on the piston (N)
W'	Effective downward gravitational force acting on the piston (N)
W_r	Effective loads applied on the reference (N)
W_t	Effective loads applied on the test (N)
\bar{x}	Arithmetic mean of input estimates
x_i	i^{th} input estimate
X_N	N^{th} other input quantities
x_N	N^{th} input estimate
x_s	Indication of a precision spirit level bar before 180° turn (div)
Y	Measurand
y	An estimate of measurand
y_s	Indication of a precision spirit level bar after 180° turn (div)
λ_r	Pressure distortion coefficient of the effective area of the reference PCA (Pa ⁻¹)
$\partial f / \partial x_i$	Partial derivative of input estimate, x_i ; known as sensitivity coefficient
α_{cr}	Linear thermal expansion coefficients of the reference cylinder (°C ⁻¹)
α_{ct}	Linear thermal expansion coefficients of the test cylinder (°C ⁻¹)
α_{pr}	Linear thermal expansion coefficients of the reference piston (°C ⁻¹)
α_{pt}	Linear thermal expansion coefficients of the test piston (°C ⁻¹)
Δh	Height difference between two reference levels (m)
Δ_{PXC_Y}	Difference in determined effective area (LU - NPL) for the $P_X C_Y$ combination (mm ²)
ρ_a	Air density of the ambient air (kgm ⁻³)

List of Symbol

ρ_f	Density of pressure transmitting fluid (kgm^{-3})
$\rho_{N_2(t,p)}$	Density of the pressure transmitting fluid used (purified nitrogen), at temperature t in $^{\circ}\text{C}$ and pressure p in Pa (kgm^{-3})
ρ_{pr}	Density of the reference piston (kgm^{-3})
ρ_{pt}	Density of the test piston (kgm^{-3})
ρ_{wr}	Density of the weights loaded on the reference pressure balance (kgm^{-3})
ρ_{wt}	Density of the weights loaded on the test pressure balance (kgm^{-3})
θ	Inclination of piston angle to the vertical (radians)
ν_{eff}	Effective degree of freedom
ν_i	Degree of freedom

LIST OF FIGURES

2.1	Pressure range in various natural phenomena and technologies [Nishibata 1997].....	14
2.2	Mode of pressure measurement [IMC 1998]	16
2.3	Pressure reference configurations [Colijn 1983].....	16
2.4	Simple type liquid columns.....	18
2.5	BIPM laser interferometric mercury manobarmeter [BIPM 2006c].....	19
2.6	Pressure balance with simple type piston-cylinder assembly	20
2.7	Macroscopic illustration of a nominally flat surface representing profile and waviness.....	25
2.8	Microscopic illustration of a nominally flat surface and its order of geometrical irregularities	26
2.9	Surface characteristics and their terminology [BS1134-1 1988]	27
2.10	Influence of direction of measurement on the effective spacing of profile crests [BS1134-2 1990]	27
2.11	Typical roughness values obtainable by different finishing processes [BS1134-2 1990].....	28
2.12	Typical profile graph of amplitude parameters, represented by $z = f(x)$	32
2.13	Numerical values of amplitude parameters.....	32
3.1	Four basic types of piston-cylinder assembly	40
3.2	An ideal simple type piston-cylinder assembly	50
3.3	A generalised non-ideal simple type piston-cylinder assembly [Dadson 1982].....	52
5.1	A schematic diagram (not to scale) of a pressure balance	81
5.2	Two pressure balance units before connection	82
5.3	Calibration chain made up of test PCAs linked directly to a reference PCA	86
5.4	The initial design of a 35 mm piston-cylinder assembly	88
5.5	Four types of initial piston design.....	89
5.6	Final design of the 316 stainless steel piston blank (Design D)	90

5.7	Geometrical imperfections of the cylinder caused by machining processes [Fischer 1986].....	94
5.8	Mandrel used in the early stages of trimming and matching of the piston.....	95
5.9	Expandable mandrels used in the early stages of trimming and matching of the cylinder.....	96
5.10	External lapping tool used in trimming and matching of a piston blank.....	102
5.11	Internal lapping tool used in trimming and matching of a cylinder blank.....	103
5.12	Damaged PCA after release with force due to seizing.....	105
5.13	A summary of the manufacturing processes of the 316 stainless steel piston-cylinder assemblies (PCAs).....	107
5.14	Abrasive wear, caused by either unintentionally introduced abrasives or debris (originated from fractured initial asperities or lips) that produces piling up of asperities on highly polished 316 stainless steel	108
5.15	The DF6 tungsten carbide piston-cylinder assembly (PCA).....	110
5.16	External and internal lapping tools used in trimming and matching of the piston and cylinder blanks.....	112
5.17	Manufactured tungsten carbide pistons and cylinders	117
6.1	A schematic diagram of an experimental cross-floating set-up.....	131
6.2	A picture of an experimental cross-floating arrangement.....	132
7.1	Variation of the overall effective areas of the P_4C_2 at 100 kPa and 20°C ($A_{P_4C_2}$) with respect to the RSs of the reference and the test PCAs	153
7.2	Variation of the $A_{P_4C_2}$ based on the RS (regardless of RD) of the individual PCA.....	153
7.3	Variations of $A_{P_4C_2}$ with SEQs based on four individual RCs. The overall results (regardless of the RCs) are represented by a shifted trend line, plotted for comparison purposes.....	155

7.4	Variation of the overall effective areas of the P_4C_4 at 100 kPa and 20°C ($A_{P_4C_4}$) with respect to the RSs of the reference and the test PCAs.....	158
7.5	Variation of the $A_{P_4C_4}$ based on the RS (regardless of RD) of the individual PCA.....	159
7.6	Variations of $A_{P_4C_4}$ with SEQs based on four individual RCs. The overall results (regardless of the RCs) are represented by a shifted trend line, plotted for comparison purposes.....	160
8.1	A schematic diagram of the calibration chain that relates the test PCAs to the reference PCA through direct and indirect cross-floating experiments	171
8.2	Typical images of Piston 1	174
8.3	Typical images of Piston 2	175
8.4	Typical images of Piston 3	176
8.5	Typical images of Piston 4	177
8.6	Typical images of Piston 5	178
8.7	Typical images of Piston 6	179
8.8	Typical images of Piston 7	180
8.9	The trend lines of surface parameters of the seven pistons.....	181
8.10	A summary of the manufacturing processes of the DF6 Dymet tungsten carbide PCAs	182
8.11	Experiment A: variation of $A_{P_1C_2}$ with the SEQ.....	184
8.12	Experiment B: variation of $A_{P_1C_4}$ with the SEQ.....	185
8.13	Experiment C: variation of $A_{P_3C_2}$ with the SEQ.....	186
8.14	Experiment D: variation of $A_{P_3C_4}$ with the SEQ.....	187
8.15	Experiment G: variation of $A_{P_5C_2}$ with the SEQ.....	188
8.16	Experiment H: variation of $A_{P_5C_4}$ with the SEQ.....	190
8.17	Experiment I: variation of $A_{P_6C_2}$ with the SEQ	191
8.18	Experiment J: variation of $A_{P_6C_4}$ with the SEQ.....	193
8.19	Experiment K: variation of $A_{P_7C_2}$ with the SEQ.....	194
8.20	Experiment L: variation of $A_{P_7C_4}$ with the SEQ	195

8.21	Experiment m: variation of A_{P7C4} with the SEQ.....	196
8.22	Experiment n: variation of A_{P7C2} with the SEQ.....	197
8.23	Experiment o: variation of A_{P6C2} with the SEQ.....	198
8.24	Experiment p: variation of A_{P7C4} with the SEQ.....	199
8.25	Experiment q: variation of A_{P2C2} with the SEQ.....	200
8.26	Experiment r: variation of A_{P3C3} with the SEQ	201
8.27	Experiment s: variation of A_{P6C2} with the SEQ	202
8.28	Experiment t: variation of A_{P7C2} with the SEQ.....	203
8.29	Experiment u: variation of A_{P7C4} with the SEQ.....	204
8.30	Experiment v: variation of A_{P6C4} with the SEQ.....	205
8.31	Experiment w: variation of A_{P2C2} with the SEQ.....	206
8.32	Experiment x: variation of A_{P3C3} with the SEQ.....	207
8.33	Trend lines of all the determined effective area through direct comparisons	209
8.34	Trend lines of all the determined effective area through indirect comparisons	209
9.1	A complete unbroken calibration chain, with the source of traceability from the NPL. P_3C_4 , P_4C_2 and P_4C_4 act as the check standards in the verification process	219
9.2	The first initial calibration results, which shows unsatisfactory repeatability at 300 and 400 kPa	220
9.3	The second initial calibration results, which shows a deterioration of performance.....	220
9.4	Cross floating experiment against the UK's Primary Pressure Standard.....	222
9.5	The results obtained from Calibration Y1, which shows excellent performance of the LU PCA and pressure balance	222
9.6	The results obtained from the Calibration Y2, which shows very good repeatability.....	224
9.7	The results obtained from the Calibration Y3, which shows very good repeatability.....	224

9.8	The results obtained from the Calibration Y4, which shows very good repeatability.....	225
9.9	Temperature variations of the room with time, Ruska 2465 and Lufbra 1	231
9.10	Temperature variations of the room with time, DHI PG7601 and Lufbra 1	231

LIST OF TABLES

5.1	Materials which have been considered for the PCAs [Budinski and Budinski 1999]	79
5.2	A set of weight belonging to each pressure balances.....	82
5.3	Operation plan to manufacture a piston blank	92
5.4	Operation plan to manufacture a cylinder blank	93
5.5	Measurement results after using aluminium curved-shells.....	97
5.6	Measurement results after using an expandable slotted-end PVC tube	97
5.7	Measurement results after using a blank piston secured on mandrel.....	98
5.8	Measurement results after application of a tapered-expandable mild-steel mandrel.....	99
5.9	Measurement results after application of an improved mandrel, i.e. a parallel-expandable mild-steel mandrel	99
5.10	Measurement results after application of a honing tool	100
5.11	Measurement results after an initial lapping process	104
5.12	Material properties of the Dymet DF6 tungsten carbide [Corewire 2004]	109
6.1	Disturbance factors in high-precision pressure measurement via cross-floating experimentation.....	121
6.2	Other disturbance factors in high-precision pressure measurement	123
6.3	Commonly used probability distribution in uncertainty calculation, and its devisor	137
6.4	Level of confidence and its coverage factor	139
7.1	A simplified version of the excel spreadsheet used in the effective area calculations	149
7.2	A_{P4C2} tabulated in accordance to their cycles and measurement sequences.....	151
7.3	A_{P4C2} (mm^2), tabulated in accordance to the four rotational combinations	154
7.4	Measurement results of the P_4C_4 , tabulated in accordance to their sequences.....	157

7.5	A_{P4C4} (mm ²), tabulated in accordance to their four rotational combinations	160
7.6	Estimated values of the relative expanded uncertainties of input parameters	162
7.7	Relative uncertainty calculation of the determined effective area, $A_{t(P4C2)E}$	163
7.8	Relative uncertainty calculation of the determined effective area, $A_{t(P4C4)F}$	164
8.1	Summarised results of the surface profile characterisations for Piston 1	174
8.2	Summarised results of the surface profile characterisations for Piston 2	175
8.3	Summarised results of the surface profile characterisations for Piston 3	176
8.4	Summarised results of the surface profile characterisations for Piston 4	177
8.5	Summarised results of the surface profile characterisations for Piston 5	178
8.6	Summarised results of the surface profile characterisations for Piston 6	179
8.7	Summarised results of the surface profile characterisations for Piston 7	180
8.8	Overall results of the surface profile characterisations for the seven pistons	181
8.9	A list of experiments for the effective area determinations	183
8.10	Experiment A: A_{P1C2} tabulated in accordance to its cycles and measurement sequences	184
8.11	Experiment B: A_{P1C4} tabulated in accordance to its cycles and measurement sequences	185
8.12	Experiment C: A_{P3C2} tabulated in accordance to its cycles and measurement sequences	186

8.13	Experiment D: A_{P3C4} tabulated in accordance to its cycles and measurement sequences	187
8.14	Experiment G: A_{P5C2} tabulated in accordance to its cycles and measurement sequences	189
8.15	Experiment H: A_{P5C4} tabulated in accordance to its cycles and measurement sequences	190
8.16	Experiment I: A_{P6C2} tabulated in accordance to its cycles and measurement sequences	192
8.17	Experiment J: A_{P6C4} tabulated in accordance to its cycles and measurement sequences	193
8.18	Experiment K: A_{P7C2} tabulated in accordance to its cycles and measurement sequences	194
8.19	Experiment L: A_{P7C4} tabulated in accordance to its cycles and measurement sequences	195
8.20	Experiment m: A_{P7C4} tabulated in accordance to its cycles and measurement sequences	196
8.21	Experiment n: A_{P7C2} tabulated in accordance to its cycles and measurement sequences	197
8.22	Experiment o: A_{P6C2} tabulated in accordance to its cycles and measurement sequences	198
8.23	Experiment p: A_{P7C4} tabulated in accordance to its cycles and measurement sequences	199
8.24	Experiment q: A_{P2C2} tabulated in accordance to its cycles and measurement sequences	200
8.25	Experiment r: A_{P3C3} tabulated in accordance to its cycles and measurement sequences	201
8.26	Experiment s: A_{P6C2} tabulated in accordance to its cycles and measurement sequences	202
8.27	Experiment t: A_{P7C2} tabulated in accordance to its cycles and measurement sequences	203

List of Tables

8.28	Experiment u: A_{P7C4} tabulated in accordance to its cycles and measurement sequences	204
8.29	Experiment v: A_{P6C4} tabulated in accordance to its cycles and measurement sequences	205
8.30	Experiment w: A_{P2C2} tabulated in accordance to its cycles and measurement sequences	206
8.31	Experiment x: A_{P3C3} tabulated in accordance to its cycles and measurement sequences	207
8.32	Summary of the results of the determined effective areas	208
8.33	Comparison of $A_{I(P2C2)}$ values, determined from different calibration routes	210
8.34	Comparison of $A_{I(P3C3)}$ values, determined from different calibration routes	211
8.35	Comparison of $A_{I(P6C2)}$ values, determined from different calibration routes	211
8.36	Comparison of $A_{I(P6C4)}$ values, determined from different calibration routes	212
8.37	Comparison of $A_{I(P7C2)}$ values, determined from different calibration routes	212
8.38	Comparison of $A_{I(P7C4)}$ values, determined from different calibration routes	212
9.1	Effective areas of the check standards determined by the NPL	226
9.2	Effective areas of the check standards determined at LU, traceable to $A_{(P2C3)NPL}$	226
9.3	Uncertainty calculation of the effective area of P_4C_2 , $A_{I0(P4C2)}$	229
9.4	Temperatures of the room, Ruska 2465 and Lufbra 1, extracted from the first initial calibration	230
9.5	Temperatures of the room, DHI PG7601 and Lufbra 1, extracted from the Y1 Calibration	232

CHAPTER 1

INTRODUCTION

1.1 BACKGROUND AND MOTIVATION

One of the metrology instruments that provides a primary method to derive pressure from the base units of mass, length and time is a pressure balance. The pressure balance derives pressure through a piston-cylinder assembly (PCA), when weights of known mass values are applied onto the piston which is orientated vertically in the earth's gravitational force. The PCA is the heart of the pressure balance consisting of a finely lapped and polished (super-finished) piston, fitting into a matching cylinder of similar surface characteristics with a clearance of typically 1 μm or less (gas-operated PCAs). Correct determination of the effective area of the PCA becomes the core issue related to the pressure balances hence, research into PCAs appears to be very buoyant topic among pressure community in order to improve uncertainty of measurement.

Historically, the first practical gas-operated pressure balance for metrological applications were developed in the mid-1900s [Ehrlich 1994]. Since then, the requirements for improved uncertainty in a wider measuring range (than those measured by the liquid-column manometers) have increased, attracting the attention of metrologists and scientists to explore the critical parameters in a variety of approaches. This has become one of the main factors towards the rapid technological improvements of the gas-operated pressure balance used nowadays, besides the development of high-quality air-bearing technologies which have further stimulated its advancement.

One of the first literature references related to a modern gas-operated pressure balance was published by Brubach [1947]. Developments continued until Dadson and Greig

[1964] presented their seminal paper concentrating on the gas-operated pressure balance which has become one of the most important sources of reference for gas-operated pressure measurement. Effects of non-uniformities in diameter, tilt of the piston and the transition to molecular flow in the annular gap between piston and cylinder at very low pressures were addressed.

One year later Dadson et al. [1965] published a paper on the development of an accurate high-pressure measurement, which concentrated on the elastic distortion caused by the applied pressure. This work was the initial investigation into the possible use of gas-operated pressure balance as a primary pressure standard, competing with the liquid manometer [Ehrlich 1994]. Lack of information on the suitability of a pressure balance at high levels of accuracy have caused detailed investigations to be undertaken, thus research work has continued to improve the uncertainty of pressure measurement using gas-operated pressure balance, with various technological approaches being introduced.

Establishing accurately the effective area of the PCA is the first step towards allowing a greater understanding of other issues related to the pressure measurement using pressure balances. Unfortunately, the effective area determination of PCAs, especially aiming at the state-of-the-art level of uncertainty, is one of the most challenging tasks faced by National Measurement Institutes (NMIs) all over the world. This is due to the nature of the pressure quantity that has no sources of defined reference points, i.e. there are no intrinsic reference points to support the pressure traceability system, and it is entirely dependent on derived standards [Bair 2002]. In other words, pressure quantities cannot be extended through additive techniques like other standards, where larger amounts can simply be obtained from addition of smaller amounts of known values, e.g. mass and length. However, it appears to have reached uncertainty levels of 5 to 10 ppm level but there are still many effects that are not fully understood [Ehrlich 1994].

There are numbers of manufacturers around the world who produce pressure balances and pressure related instruments from kPa to GPa range, to suit the industrial and research requirements. They are DH-Budenberg (France); DH Instruments (United

States of America, USA); Ruska (USA), Druck (United Kingdom, UK) and Pressurements (USA) (now under GE Sensing, USA); Furness Controls (UK); Nagano Keiki (Japan); Harwood Engineering (USA) etc. However, there are only three well-known manufactures who produce high quality gas-operated pressure balances, of 35 mm diameter PCAs. These pressure balances measure/generate pressures up to 1 MPa using 35 mm PCAs, and they are commonly used as primary pressure standards among the NMIs. These manufacturers are DH-Budenberg who produce models APX50 and 5111; DH Instruments who produce model PG7601; and Ruska Instruments who produce model 2466. An approximate cost for a complete set of these pressure balances (one platform/base, a set of weights and a set of PCA) ranges from £60,000 to £100,000, depending on manufacturer and associated accessories; and a 35 mm PCA may reach £10,000 per unit.

1.2 RATIONALE OF THE RESEARCH

This thesis describes the novel experimental investigations which have been completed over the past three years to improve further the knowledge on effective area determination with respect to the influence of surface texture. The rationale behind this investigation is with respect to the three following issues:

- **Manufacturing** – Whatever manufacturing methods are used to generate polished surfaces, there will always be some inseparable form of surface texture associated with them [Miller 1962]. Manipulation of the surface texture is the manufacturing parameter that is fully utilised by the manufacturers to produce an excellent working PCA, ending with final lapping and polishing processes, once geometrical dimensions have been satisfied.
- **Surface Metrology** – Surface metrology ensures that all aspects of surface geometry are known and are preferably controlled. If the shape and texture of the work piece is correct, then it will be able to move at the speeds, loads and temperatures specified in the design, thus ensuring the dynamic characteristics have been satisfied [Whitehouse 1994].

- **Tribology** – Friction and wear can be kept low if the contact interface is well-lubricated [Kato and Adachi 2001]. In a gas-operated gas-lubricated pressure balance, the PCA is lubricated by the pressure transmitting fluid which separates the opposing surfaces by a fluid film, hence the friction between the two sliding surfaces is almost negligible (ideal PCA). In order to manifest this situation, at least one surface (normally both surfaces) must be sufficiently rough (microscopically) so that the surface valleys will act as pockets to retain lubricating fluid, hence continuous lubrication remains during operation. This phenomenon is supported by Grassam and Powell [1964], who clearly stated that:

“The rotor and thrust plate would ‘lock’ after a fraction of a revolution showing the phenomenon of ‘wringing’ and presumably adding about 14 lb./in.² (≈ 100 kPa) to the bearing load. It was found possible to break this effect either by impairing the surface finish of one of the bearing members by taking it back by powder blast, etching or lapping, or by misshaping a face by crowning or convexity”

1.3 AIMS AND OBJECTIVES OF THE RESEARCH

The aim of this research is to reveal any evidence of pressure dependency on the surface texture applied onto the surface of a 35 mm piston (forming part of a PCA), using a gas operated pressure balance. In order to accomplish this primary aim, several objectives are outlined:

- Manufacture of two identical pressure balance units for cross-floating experiments, that can accept very-large PCAs, and be capable of measuring pressure at very demanding uncertainty specifications.
- Manufacture of identical pistons (of various surface texture specifications) and identical cylinders, which are interchangeable. Both of these elements are novel and have not been reported in literature.

- Identify an approach (calibration chain) to investigate pressure dependency on the surface texture applied onto the pistons.
- Identify the best method in determining the equilibrium conditions in cross-floating experiments, using interchangeable pistons and cylinders.
- Identify the effects of rotational speeds (RSs) and rotational directions (RDs) on the pressure generated.
- Identify the most practical method of measurement in quantifying the surface texture applied onto pistons.
- Identify the effects of the surface texture on the pressure generated as a function of the effective area.
- Complete calibrations with respect to working and primary pressure standards.

With any findings obtained, they will enable the understanding of the mechanisms controlling pressure generated, making pressure generated more predictable, hence higher level of accuracy can be achieved.

The novel aspects of this work can therefore be identified as:

- Unique design of a pressure balance.
- Quantification of PCA manufacturing process.
- Production of PCA's with bespoke surface texture.
- Production of fully functional interchangeable pistons and cylinders.
- Linking effective area calculation variations to piston surface texture specifications.

1.4 OVERVIEW OF THE THESIS

This thesis is presented in ten chapters. This chapter presents a brief introduction of the topic to be investigated, identifying the motivations which have led to this research. The aims of the research and its objectives are outlined with a clear identification of the novel content of the research.

Chapters 2, 3 and 4 provide the context for the research, detailing aspects of literature and theory. Chapter 2 provides an introduction to pressure and surface metrology which cover background, definitions and roles. Chapter 3 concentrates on the pressure balance. It starts by describing the history of the pressure balance, followed with its physical principles and types of PCA which are commonly used. Further detailed information on the pressure balance is discussed in the pressure conversion equation and the simple theory of the PCA. Chapter 4 completes the background context by providing a review of the gas-operated pressure balance, which extends from the mid 1940's to the present.

The second half of the thesis is concerned with the manufacture of the pressure balance and PCAs, and the cross-floating experimentation. Chapter 5 discusses the manufacturing processes used for the pressure balances and PCAs. It begins with the selection of materials and considers a range of manufacturing processes, including turning, honing, lapping and polishing. Chapter 6 describes the techniques used in the determination of the effective area, known as the cross-floating method. It covers the practical aspects of use, detailed descriptions about cross-floating experiments and the evaluation of the uncertainty of measurement through this method. Chapter 7 concentrates on two cross-floating experiments that aimed at finding evidence of pressure dependency due to the RSs and RDs. This has been completed as an experimental verification of the overall performance envelope of the pressure balances.

Chapter 8 presents the measurements used in characterising the surface of the manufactured pistons. It also reveals the results obtained from twenty two cross-floating experiments carried out, complete with comparisons of the determined effective areas via various of the possible routes available on six PCA combinations. This is then put

into context by the calibration of the pressure balances providing an absolute fix of the pressure experimentation. Chapter 9 highlights the calibration/verification against the UK's primary pressure standard, where four PCA combinations were calibrated by the National Physical Laboratory (NPL) at its facilities. Comparisons are also identified between the pressure balances against two commercial and traceable pressure balances in terms of the thermal stability.

Finally, Chapter 10 concludes the thesis by summarising the achievements based on the objectives outlined. The novel and unique engineering and scientific contributions which have been delivered through this research are presented. The future work that might be carried out is proposed, based on the experiences and lessons learned in this research.

CHAPTER 2

INTRODUCTION TO PRESSURE AND SURFACE METROLOGY

This chapter introduces pressure and surface metrology which are the core subjects in this thesis. The chapter is organised as follows: Section 2.1 begins with describing the background of pressure and surface metrology, and explains how they are inter-related. Section 2.2 provides a brief introduction to the measurement of pressure, detailing the pressure definition, International System of Units (SI), pressure modes, the role of the primary pressure standards in the measurement systems, and also includes the comparison between the two primary pressure standards in deriving pressure from base units. Section 2.3 introduces surface metrology which covers basic concepts, the importance of surface texture, terms and definitions, the nature of surface texture, the orders of surface irregularities and instrumentations used in surface metrology. Finally, Section 2.4 presents a summary of this chapter.

2.1 BACKGROUND OF PRESSURE AND SURFACE METROLOGY

Pressure measurement plays a very important role in our daily life. During the industrial revolution, pressure measurement was largely used in transforming water into steam, whereas in our modern world it is applied over wider ranges such as to measure those found in inter-planetary space, to those found at the bottom of the deepest ocean trench [NMS 2002]. Pressure measurement is common in our society and its applications are commonly found in industries such as power, gas, optical, aerospace, defence, meteorological, automotive, medical, safety etc. Most pressure-related measurements are made for commercial purposes, as part of research and development activities, and production engineering to ensure product quality, reliability and safety [IMC 1998].

In the medical sector, pressure measurements are commonly used in life support machines, anaesthetic delivery and sphygmomanometers (blood pressure measuring instrument). The National Measurement System [NMS 2002] reported that:

“There is evidence that significant metrological problems exist in using the mercury-based sphygmomanometer where some estimates indicate that more than 10% display erroneous readings. A recent study indicates that of 24,000 women diagnosed as hypertensive, 7,000 may be receiving incorrect treatment due to calibration errors”

This is one of the critical reasons why the primary pressure standard at barometric pressure should be well maintained, as well as it being the main source of the traceability for the whole spectrum of pressure measuring range [Legras 1994a, Legras et al. 1999a].

One of the instruments that provides a primary method to derive pressure from the base units of mass, length and time is the pressure balance. The pressure balance derives pressure through a PCA, where weights of known mass values are applied onto the piston that is orientated vertically in the earth's gravitational force, i.e. some means of applying pressure to the piston so that the pressure applied across the effective area of the PCA exactly balances the downward gravitational force. Meanwhile a PCA is the heart of the pressure balance where it consists of a finely lapped and polished (super-finished) piston, fitting into a matching cylinder of similar surface characteristic. Therefore, correct determination of the effective area of the PCA becomes the core issue related to the pressure balances. Hence research on PCAs appears to be a very buoyant topic among the pressure community, in order to improve uncertainty of measurement.

From a manufacturing point of view, whatever methods are employed to generate polished/super-finished surface, there will always be some inseparable form of texture associated with them [Miller 1962]. Unfortunately, research on how surface texture affects the pressure generated by the pressure balance has never been considered by the pressure community in their research work, even-though various research approaches have been conducted so far. In metrology, surface texture measurement occupies a

somewhat anomalous position since the property of the surface texture is essentially qualitative. Its quantitative index can only be assigned indirectly by reference to the instrumentation operating in accordance with geometric parameters, while other parameters such as dimensions, shapes and metallurgical structures of engineering can be unambiguously specified in terms of length or mass [Thomas 1974]. Surface metrology is a subject related to the measurement and characterisation of the topographical features of surfaces. These topographical features comprise of minute peaks and valleys which recur at regular or irregular intervals, that may vary both in height and spacing, and consequently form a kind of pattern or texture [Scarr 1967].

2.2 THE MEASUREMENT OF PRESSURE

Introduction to the measurement of pressure is covered within seven sections, which are as follows:

2.2.1 What is Pressure?

Pressure is generally the result of molecules, within a gas or liquid, impacting on a surface in a direction perpendicular to that surface, and it is defined as the normal force exerted over a defined unit area [IMC 1998]. Pressure is transmitted to solid boundaries or across arbitrary sections of fluid normal to these boundaries or sections at every point [Wikipedia 2006a]. Pressure gradient is force density, where it is considered as a scalar quantity when the pressure mediums are gaseous [Molinar 1992]. The International System of Units (known as the SI system) for pressure is the pascal (Pa), in honour of the philosopher and scientist Blaise Pascal (1623-1662), where 1 Pa is equivalent to 1 newton per square meter (N/m²). The relationship between pressure (p), force (F) and area (A) is mathematically given by:

$$p = \frac{F}{A} \quad (2.1)$$

It applies whether the pressure is very small or very large, thus referring to the entire range of 'force per unit area', inclusive of vacuum measurement.

2.2.2 The International System of Units (SI)

Formal definitions of all SI base units are approved by The General Conference on Weights and Measures (CGPM), which is made up of representatives of the governments of the Member States, and observers from the Associates of the CGPM [BIPM 2006a]. To support a continuous need of increased accuracy in measurement, the measurement methods keep evolving, hence providing more accurate realisations of the base units. These evolving methods have made all definitions subject to modifications from time to time, where the first such definition was approved in 1889 and the most recent in 1983. This means that the SI is not static, but evolves accordingly to suit the corresponding need for improvements.

Seven well-defined SI base units (which by convention are regarded as dimensionally independent) that relate the base quantity to the unit name and symbol are as follows:

- *Length* in metre (m).
- *Mass* in kilogram (kg).
- *Time* in second (s).
- *Electric current* in ampere (A).
- *Thermodynamic temperature* in kelvin (K).
- *Amount of substance* in mole (mol).
- *Luminous intensity* in candela (cd).

2.2.3 The Definitions of the SI Units

The definitions of the SI Units as laid down by CGPM are as follows [BIPM 2006b]:

- **The metre** is the length of the path travelled by light in vacuum during a time interval of $1/299,792,458$ of a second.
- **The kilogram** is the unit of mass; it is equal to the mass of the international prototype of the kilogram.

- **The second** is the duration of 9,192,631,770 periods of the radiation corresponding to the transition between the two hyperfine levels of the ground state of the caesium 133 atom.
- **The ampere** is that constant current which, if maintained in two straight parallel conductors of infinite length, of negligible circular cross-section, and placed 1 metre apart in vacuum, would produce between these conductors a force equal to 2×10^{-7} newton per metre of length.
- **The kelvin**, unit of thermodynamic temperature, is the fraction $1/273.16$ of the thermodynamic temperature of the triple point of water.
- **The mole** is the amount of substance of a system which contains as many elementary entities as there are atoms in 0.012 kilogram of carbon 12.
- **The candela** is the luminous intensity, in a given direction, of a source that emits monochromatic radiation of frequency 540×10^{12} hertz and that has a radiant intensity in that direction of $1/683$ watt per steradian.

However some of these base units may be considered less fundamental than the others as they are dependent to other units in their definitions, e.g. the metre that relies on the definition of the second. On the other hand, the definition of the kilogram (the only base unit that is derived from a physical object) is somewhat unusual since it contains the recommended prefix (*kilo*) which is used to denote multiples of unit. From these seven base units, one can derive other units (known as derived units) to describe any quantity which can be measured, e.g. the pressure that relies on kilogram, metre and second thus formed a special name, pascal; with a symbol, Pa.

2.2.4 Pressure as a Derived Unit

There are two primary methods to derive pressure from fundamental units of mass (kilogram), length (meter) and time (second). They are the liquid manometer and the pressure balance. The liquid manometer is based on the discovery by Evangelista

Torricelli (1608-1647), where the height of mercury in an inverted tube is used to measure atmospheric pressure [Molinar 1992]. The operation of the liquid manometer is based on the following equation:

$$p = \rho \cdot g \cdot h \quad (2.2)$$

where p is the pressure, ρ is the density of mercury, g is the acceleration due to gravity, and h is the height of the mercury column. Whereas a pressure balance derives pressure through a PCA when weights of known mass values are applied onto the piston. The operation of a pressure balance is based on the Equation (2.1).

Measuring methods for pressure can generally be divided into two categories. The first category involves the direct measurement of pressure by fundamental methods, which are classified as “direct-principle” pressure standards (one of the requirements to become a primary pressure standard). The second method makes use of the direct measurement of the physical properties or behaviour of materials under the application of the pressure, which are classified as “indirect-principle” pressure standards, and they are generally classified as secondary pressure standards [IMC 1998].

In the universe, the highest pressure will exist at the centre of neutron stars and the lowest in the space between the galaxies, as shown in Figure 2.1. The equipment and techniques to realise the scale and the accuracy of the measurement vary greatly over this range. The accuracy of measurement is highest around atmospheric pressure, where an accuracy of a few parts per million (ppm) is achieved using a Laser Interferometric Liquid Manobarometer [BIPM 2006c]. However, the pressure balance is mostly used because its prominent features such as portability, robustness and the ability to measure pressure over a wide range [Delajoud and Girard 1988, Delajoud et al. 1999, Dargent and Poirier 1999].

2.2.5 Pressure Modes

There are three types of pressure measurement that are commonly used in pressure measurements. They are as follows [IMC 1998, Molinar 1992]:

- **Absolute mode** - When zero value (theoretically perfect vacuum) is used as a reference point in a measurement, it is referred to as an absolute pressure measurement (e.g. kPa abs.). Laser Interferometric Liquid Manobarometers and vacuum gauges are examples of absolute mode pressure measuring instruments.

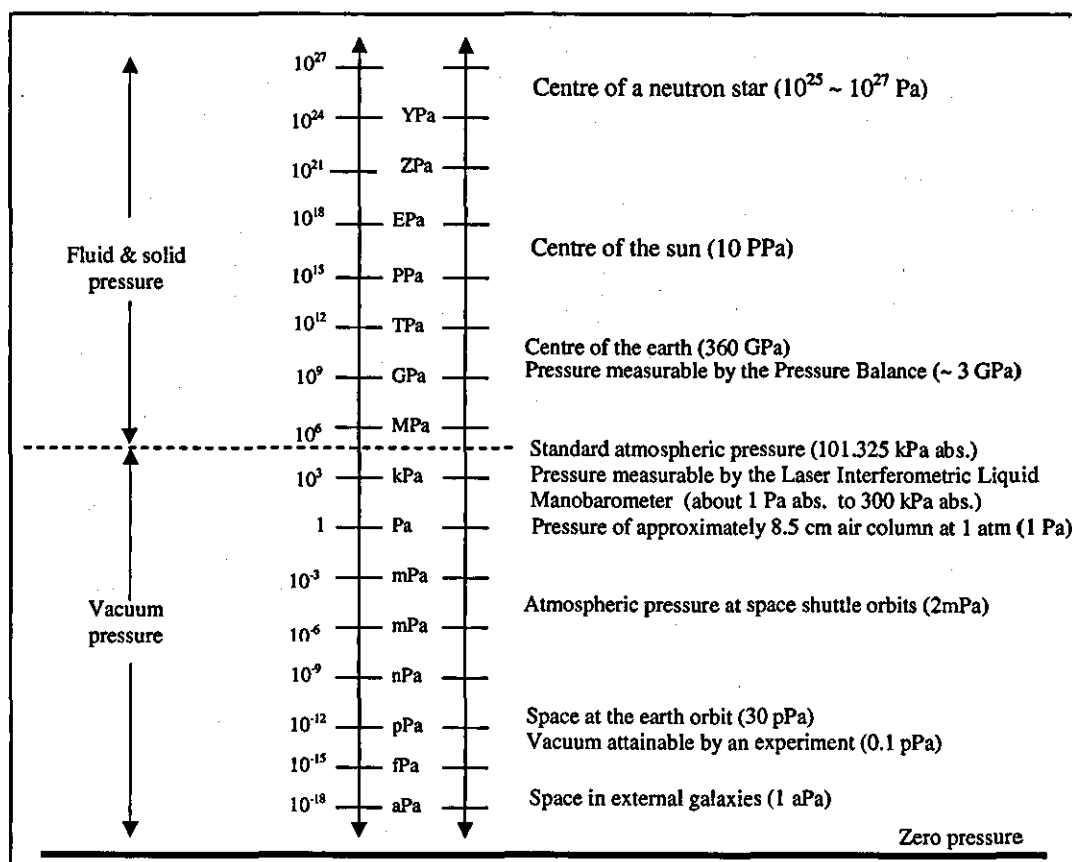


FIGURE 2.1 Pressure range in various natural phenomena and technologies [Nishibata 1997]

- **Differential mode** - When the difference between two unknown pressure points is essential (the reference pressure may be any value that is compatible with the types and working ranges), these types of measurement are known as differential pressure measurement. A typical example for this mode is a diaphragm pressure gauge used in flow measurement, where the flow of gas along a pipeline depends on the pressure difference between the ends of the pipe.

- **Gauge mode** - This mode is actually a part of differential mode where it is the commonest measurement in pressure metrology, with atmospheric pressure is used as a reference point. An example of this mode is the air pressure in a car tyre, which might be said to be “210 kPa”, but actually 210 kPa above atmospheric pressure. Since the atmospheric pressure is fluctuating approximately 100 kPa (absolute), the absolute pressure in the tyre is therefore about 310 kPa. The relationship between absolute pressure and gauge pressure is as follows:

$$\text{Absolute pressure} = \text{gauge pressure} + \text{atmospheric pressure}$$

Figure 2.2 clearly illustrates the three modes that are commonly used in pressure measurements and Figure 2.3 shows their configurations.

2.2.6 The Role of the Primary Pressure Standards in the Measurement System

The most fundamental role of primary pressure standards in the measurement system is to derive pressure metrologically in a completely independent way from the base units of the SI system. This should provide accurate and traceable pressure values, thus assuring that the definition of pressure will be coherent with the other SI system and the value used throughout the world [Molinar 1992]. Since the pressure dimension is $p = [\text{ML}^{-1}\text{T}^{-2}]$, a primary pressure standard should thus involve the measurement of mass, length and time only.

Primary pressure standards are the tools used by most of the NMIs such as National Physical Laboratory (NPL), United Kingdom (UK); Physikalische-Technische Bundesanstalt (PTB), Germany; Laboratoire National d'Essais (LNE), France; National Institute of Standards and Technology (NIST), United States of America (USA); Istituto di Metrologia “Gustavo Colonetti” (IMGC), Italy; Institute for National Measurement Standards (INMS), Canada etc., to accomplish their role in maintaining reference values for pressure at their national level and then disseminate those values to the rest of their National Measurement System (NMS).

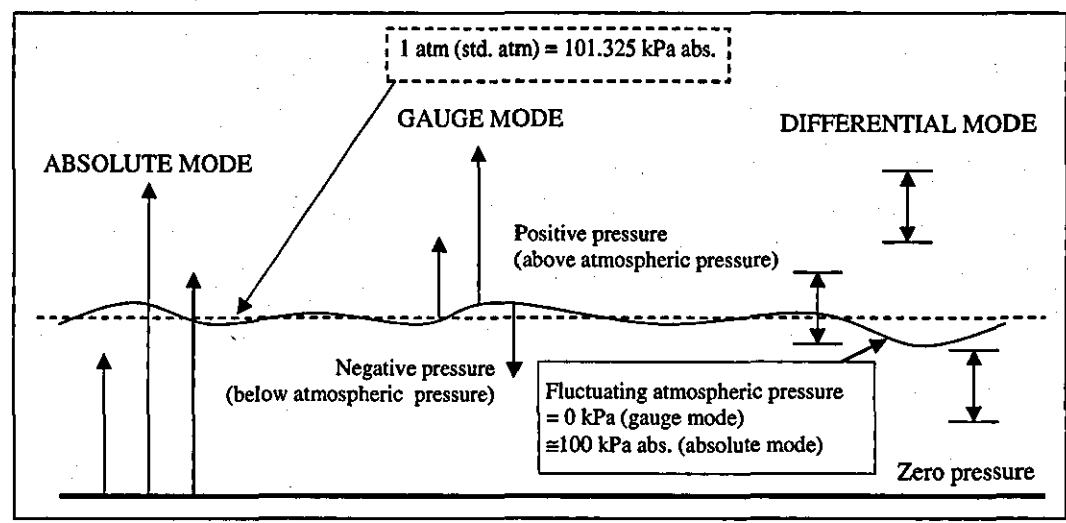


FIGURE 2.2 Mode of pressure measurement [IMC 1998]

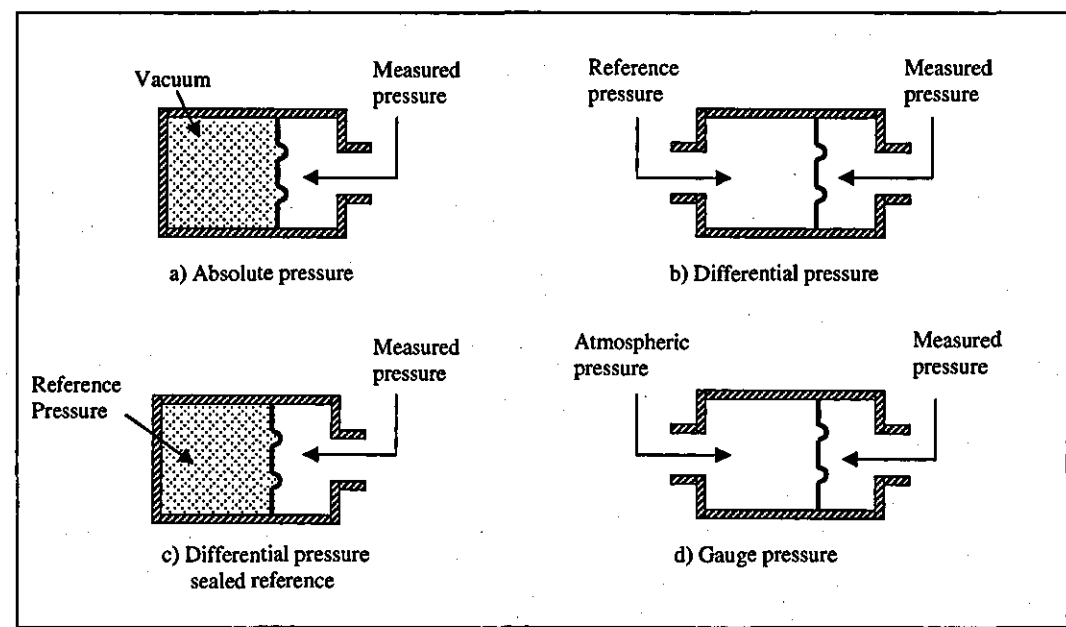


FIGURE 2.3 Pressure reference configurations [Colljn 1983]

2.2.7 Comparison Between the Two Primary Pressure Standards

A simple type of liquid column (mercury barometer and liquid manometer) shown in Figure 2.4, derives pressure through a column of fluid where the pressure at the bottom of a fluid column is calculated by multiplying together the density of the fluid, the acceleration due to gravity and the height of the column; (Equation 2.2). It has dimensions of $(\text{mass} / \text{length}^3) \times (\text{length} / \text{time}^2) \times \text{length}$ which simplifies to $\text{mass} / (\text{length} \times \text{time}^2)$ or $\text{M.L}^{-1}.\text{T}^{-2}$. Figure 2.5 shows the International Bureau of Weights and Measures (BIPM) Laser Interferometric Mercury Manobarometer, which uses the same principle to derive pressure around atmospheric pressure.

On the other hand, the pressure balance as shown in Figure 2.6 derives pressure through the PCA when weights of known mass values are applied onto the piston. Pressure is defined as force per unit area; (Equation 2.1). It has dimensions of $\text{mass} \times (\text{length}/\text{time}^2) / \text{length}^2$ which simplifies to $\text{mass} / (\text{length} \times \text{time}^2)$ or $\text{M.L}^{-1}.\text{T}^{-2}$.

There are several advantages in using a pressure balance over a liquid manometer. The advantages are as follows [Delajoud and Girard 1988, Dargent and Poirier 1999]:

- Sources of uncertainty are fewer and easier to measure and monitor. There is no need for complicated temperature regulation/monitoring system, i.e. no meniscus and parallax problems and is less affected by environmental conditions etc.
- No usage of dangerous liquid such as mercury.
- Operation is faster and easier.
- Measuring principle is fully coherent with pressure standards used for measuring higher pressure up to the full spectrum of pressures e.g. up to 2.5 GPa, whereas the highest measuring range for liquid manometer is limited to around 300 kPa only.
- Smaller in size and is portable.
- Lower purchasing cost.
- Lower maintenance cost.

- Requires smaller space/room.
- Much easier to further improve the uncertainty calculation in measurement.

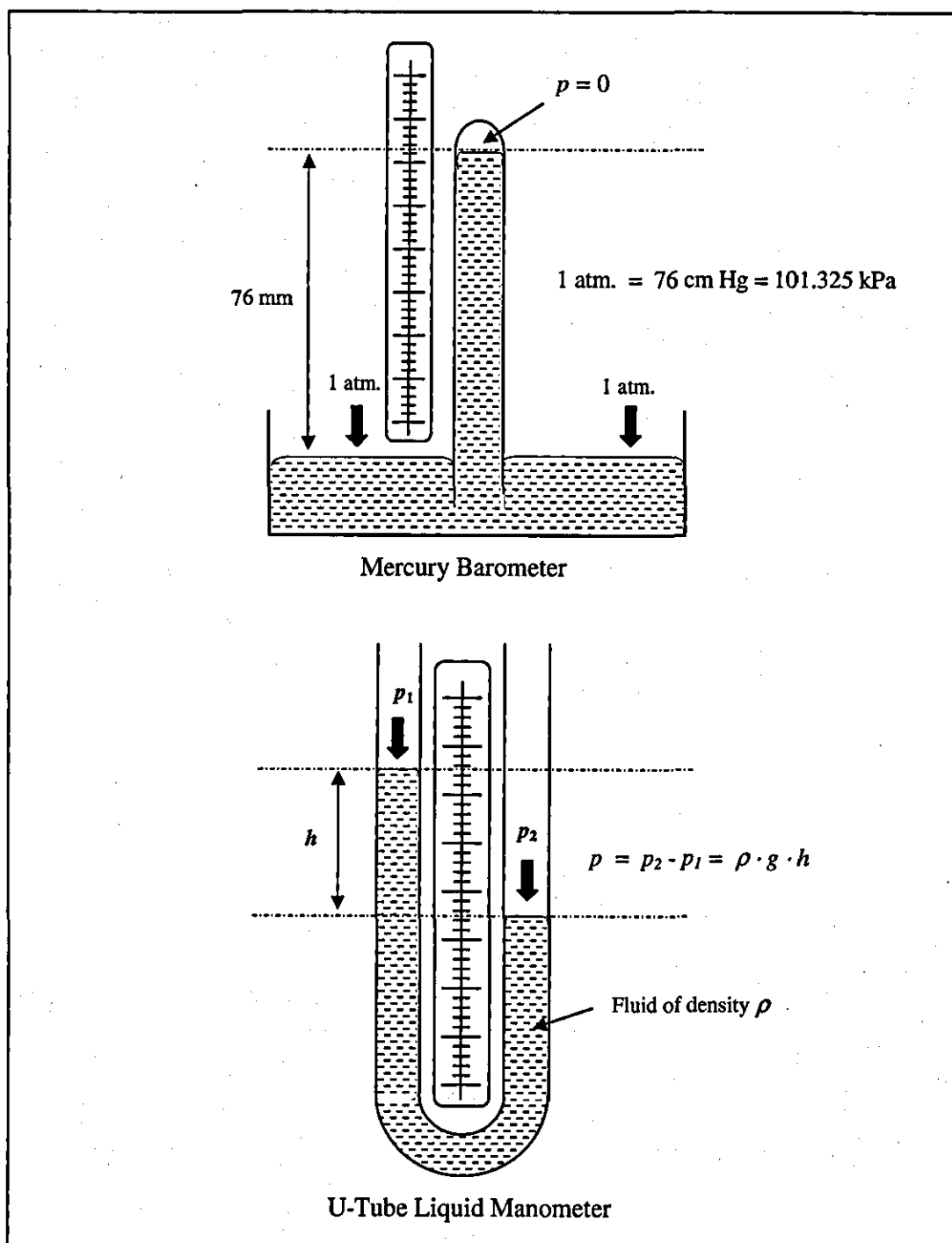


FIGURE 2.4 Simple type liquid columns

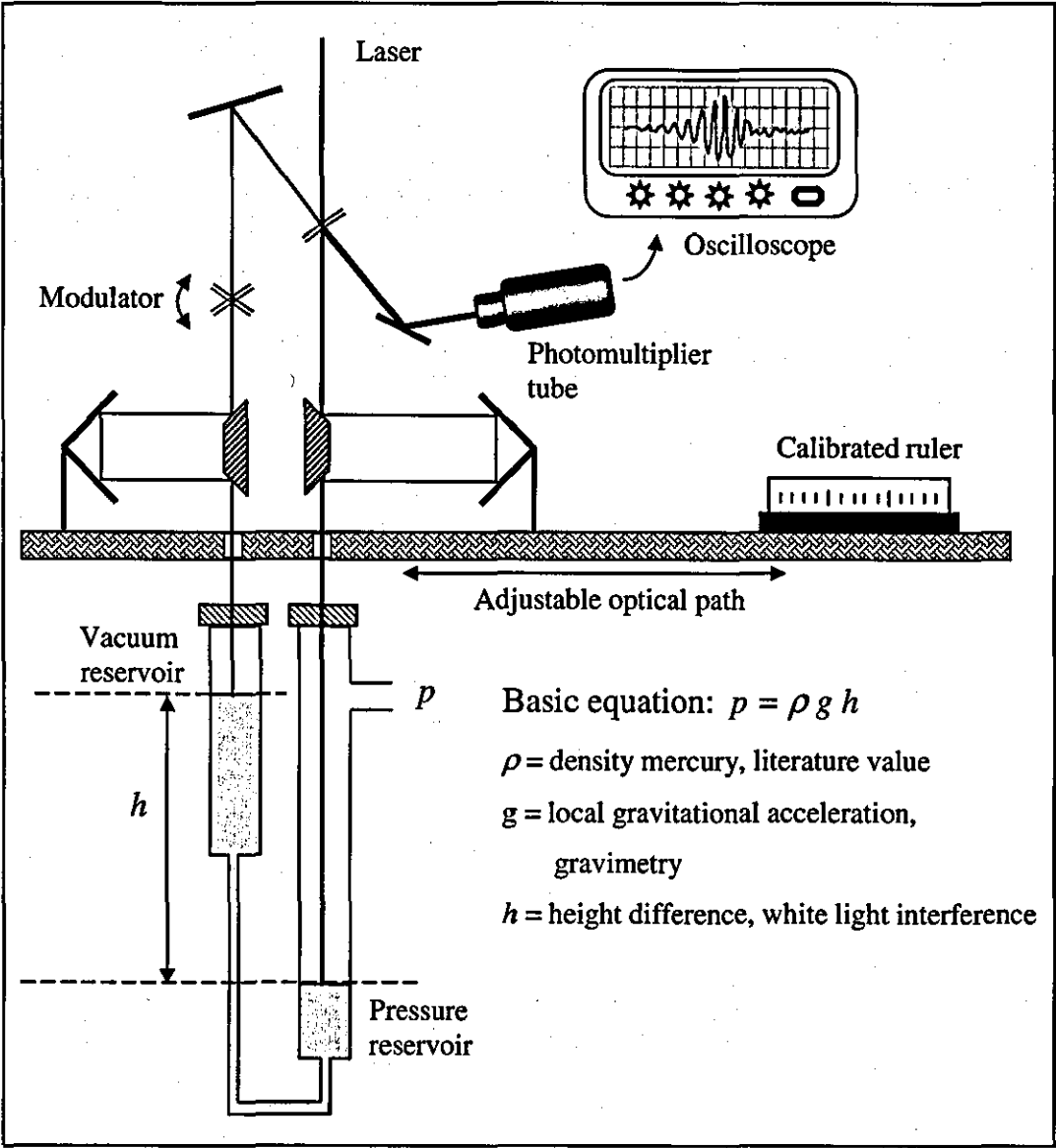


FIGURE 2.5 BIPM laser interferometric mercury manobarometer [BIPM 2006c]

While the performance of pressure measuring instrumentation has improved radically with regards to the ever increasing demands for higher accuracy, the measurement uncertainty of primary pressure standards at national level NMI must also be improved proportionally. The pressure balance is the best primary pressure measuring instrument to be investigated [Delajoud and Girard 1988, Delajoud et al. 1999, Dargent and Poirier 1999, Bair 2002].

However within the pressure balance, the PCA is the focal point to be investigated. It is due to its role as a heart of the pressure balance where the pressure quantity is derived from. Small departures from its ideal dimensions will directly affect the pressure generated, hence affecting the uncertainty of measurement. Surface texture associated with any manufactured PCA is one of the factors that contributes to the imperfection of the PCA, not only due to the cutting actions during the manufacturing process but also due to the microstructure of the material. Clearly, it is useful to have a basic understanding about surface texture so that the characterisation work carried out is meaningful and appropriate. The next section briefly describes the measurement of surface texture and its related topics applicable to this research work.

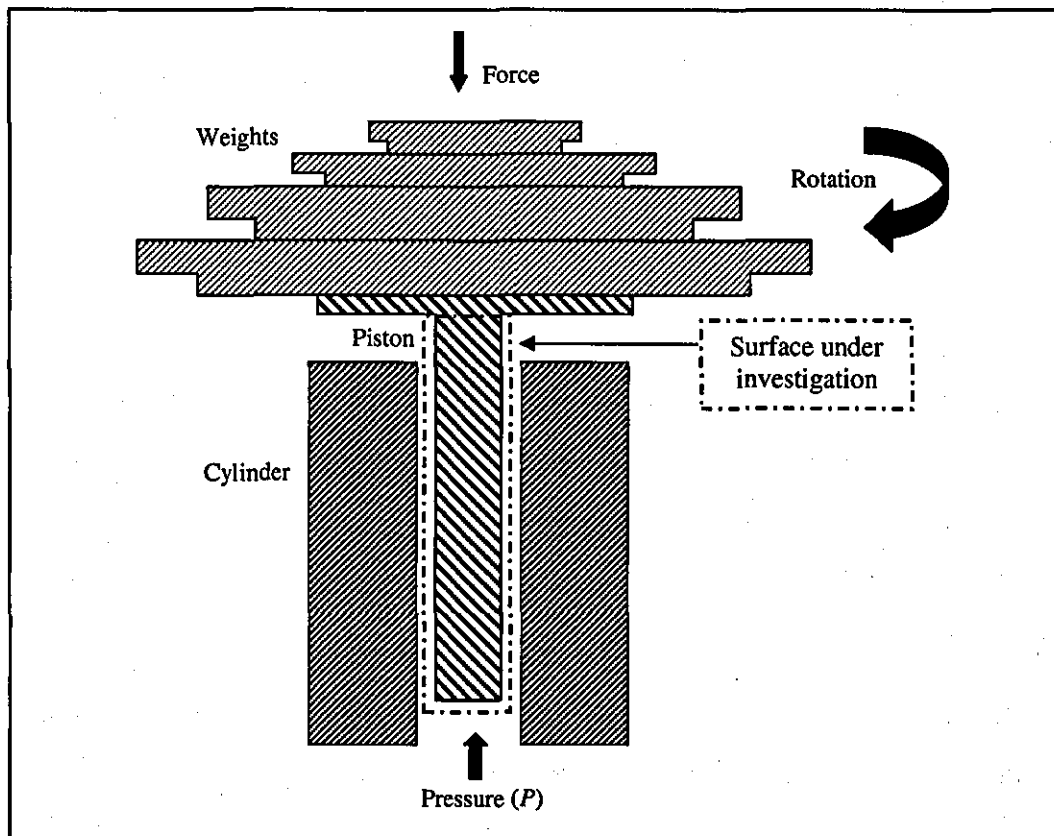


FIGURE 2.6 Pressure balance with simple type piston-cylinder assembly

2.3 THE MEASUREMENT OF SURFACE TEXTURE

Introduction to the measurement of surface texture is covered within eight sections, which are as follows:

2.3.1 What is Surface Texture?

A surface is a boundary that separates an object from another object or substance and its technology is widely used in various disciplines such as in metrology, metallurgy, tribology, chemistry, physics, material science etc. [Precision Devices 2006, Taylor Hobson 2006]. In metrology, surface texture measurement occupies a somewhat anomalous position since the property of the surface texture is essentially qualitative. Its quantitative index can only be assigned indirectly by reference to instrumentation operating in accordance with geometric parameters while other parameters such as dimensions, shapes and metallurgical structures of engineering can be unambiguously specified in terms of length or mass [Thomas 1974]. Surface metrology is a subject related to the measurement and characterisation of the topographical features of surfaces.

2.3.2 The Importance of Surface Texture

There are reasons why designers specify surface texture in their specifications. In general, the reason is because the surface that they have specified will come into contact with some other surface that may demonstrate different performance if a different type of surface texture is applied. In order to achieve a good performance, they have to control the surface texture applied onto their products [Thomas 1974]. However there are also many cases where non-contacting situations may happen, in which surface texture is important e.g. when it is concerned with the influence on corrosion, specular reflection in optical measurement, relative motion of PCA in pressure measurement etc. In other words, it is because the designers have strong beliefs that the surface texture will affect the performance of their product through the controlling of the nature of static and dynamic contact between solids.

In real situations controlling the surface texture in a product will potentially give longer service life, better fatigue resistance, better efficiency and more consistent functional interchangeability including some other advantages such as reduction of power consumption and vibration if the right surface textures are chosen [Thomas 1974, Whitehouse 2001]. There are many other properties that are essentially dependent on surface texture such as wear, friction, hydraulic resistance, corrosion, strength of pressed joints etc. Surface texture can be important in controlling the manufacture (the means of how to transform raw material into a work piece having the desired form, size and surface texture quality) and also the way in which the surface texture can influence how well a work piece will function (mainly covered under tribology study) [Whitehouse 1994].

Therefore, it is vital to quantitatively evaluate and classify them into unambiguous manner in order to improve the quality of our products. A functionally sound method whereby the surface texture may be quantified numerically so as the numerical value bears some relationship to the functional characteristics of the surface texture, where the measurement of each and every departure from the ideal surface plus the effect of the combined texture should be carried out [Whitehouse 2001].

2.3.3 Concepts, Terms and Definitions of Surface Texture

The features to be measured in surface metrology encompass texture, roundness, straightness, flatness, cylindricity and so on [Whitehouse 2001]. It plays a very important role especially in engineering metrology to ensure that the work-piece works in accordance to the designer's aim. With the increase in the understanding of the influence of surface texture on certain functions, the designer tends to specify surface finish more strictly in order to achieve a certain level of functioning [Whitehouse 1994].

Function is a term used in relating surface textures to their performance.

Measurements are carried out in order to quantify the deviations of a work-piece from its intended shape [Whitehouse 1994]. These topographical features are comprised of minute peaks and valleys which recur at regular or irregular intervals that may vary both

in height and spacing, and consequently form a kind of pattern or texture [Scarr 1967]. Texture is the combination of relatively short wavelength (high and medium frequency) deviations of a surface from the nominal surface comprising of roughness and waviness [Precision Devices 2006].

2.3.4 The Nature of Surface Texture

In general, surface texture is a combination of various kinds and magnitudes of irregularities due to some particular cause (e.g. tool geometry, cutting speed, feed rate tool's cutting action, imbalance in a grinding wheel etc.), which are superimposed each other to form a complex surface condition. Every surface produced by chip-removal process departs from its ideal form (intended shape by the designer) through a variety of causes and tendencies, which are interrelated each other. These could cause roundness error, straightness errors, parallelism errors, squareness errors, conicity errors or even form errors. Their geometrical irregularities can be categorised into four principal orders [Miller 1962, Smith 2001, Whitehouse 2001]:

- **First order** - inaccuracies in the machine tool, lack of straightness in the slide ways, insecure clamping, uneven wear in machining equipment, deformation of the work piece due to cutting forces, effect of the weight of the material itself etc.
- **Second order** - vibration of any kind, e.g. chatter marks.
- **Third order** - the inherent action/characteristic of the particular production process or material condition, which would be present even if the machine were perfect and completely free from vibrations.
- **Fourth order** - rupture of the material during chip removal process.

2.3.5 Orders of Geometrical Irregularities

All the four orders of geometrical irregularity cause may be broken out into three main categories. They are surface roughness, surface waviness and surface profile [Thomas 1974, Smith 2001, Whitehouse 2001] as described below:

- **Surface roughness** - Comprising of the finest irregularities that occur in short-frequency components that constitute of micro-geometrical departure from the ideal surface. They are often the result from manufacturing processes such as the inherent action of the cutting tool geometry on the material, or by some other disturbances e.g. friction, corrosion, wear, wheel grit, etc. Irregularities of this kind include the third and fourth orders causes.
- **Surface waviness** - Comprising of more widely spaced irregularities that occur in medium-frequency components of a periodic character upon which surface roughness is superimposed. It constitutes of macro-geometrical departure from the ideal surface. They are caused by improper manufacturing factors such as mechanical disturbances in the generating set-up, heat treatment, vibrations, chatter, material strain and extraneous effects. Irregularities of this kind include the first and second order causes.
- **Surface profile** - comprising the overall form of the surface that occurs in long-frequency components, ignoring the relatively small variations due to roughness and waviness. It is located on the dividing line between geometric errors and finish errors. The irregularities are caused by errors in machine tool slide ways, in thermal distortion or in rotating members of the machine, which are from the first order causes.

Macroscopic and microscopic illustrations representing profile, waviness and roughness on a nominally flat surface are depicted in Figure 2.7 and Figure 2.8 respectively. Figure 2.9 shows the surface characteristics and their terminology, and Figure 2.10 presents an influence of direction of measurement on the effective spacing of profile crests. Figure 2.11 shows a typical roughness obtainable by different finishing processes.

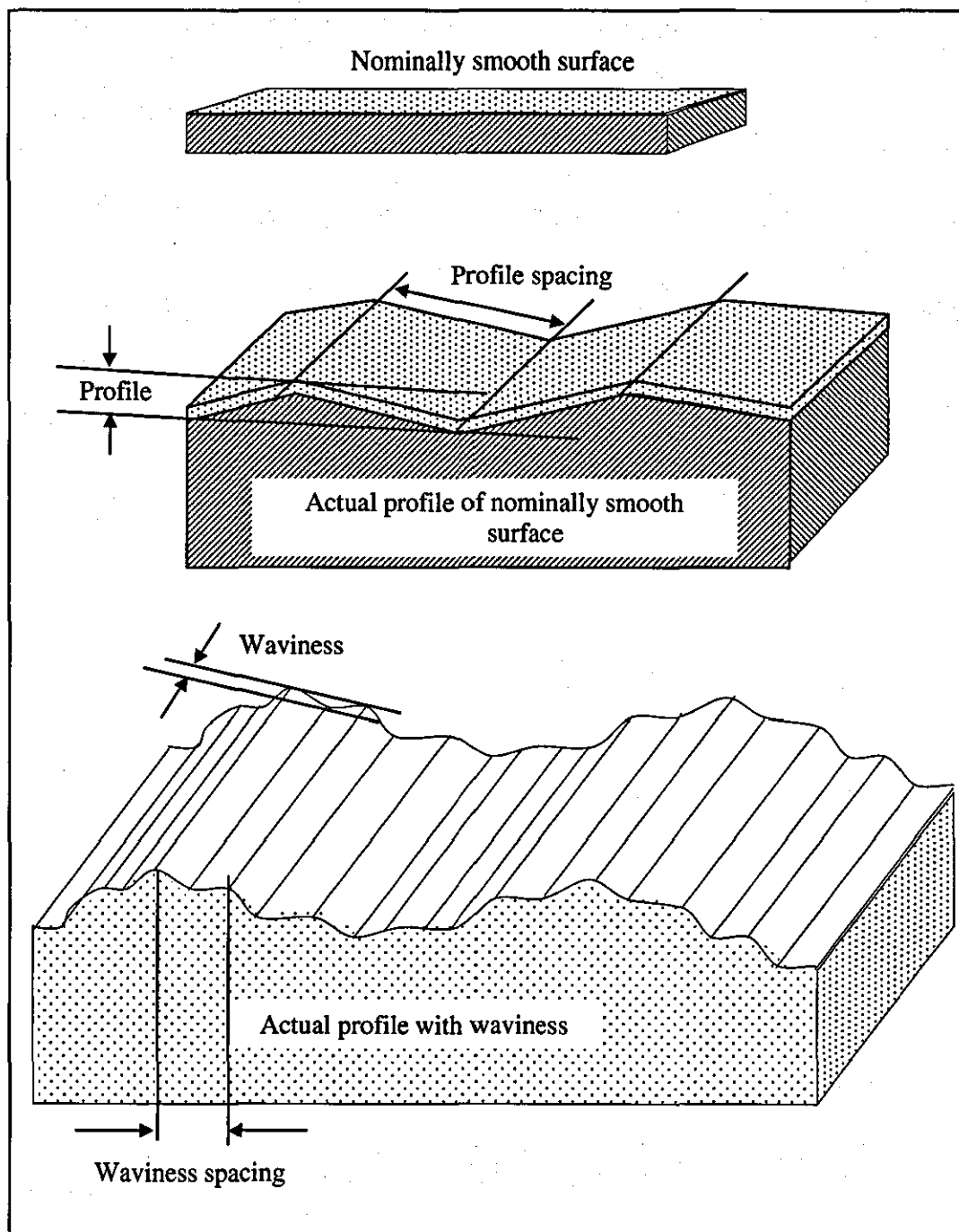


FIGURE 2.7 Macroscopic illustration of a nominally flat surface representing profile and waviness

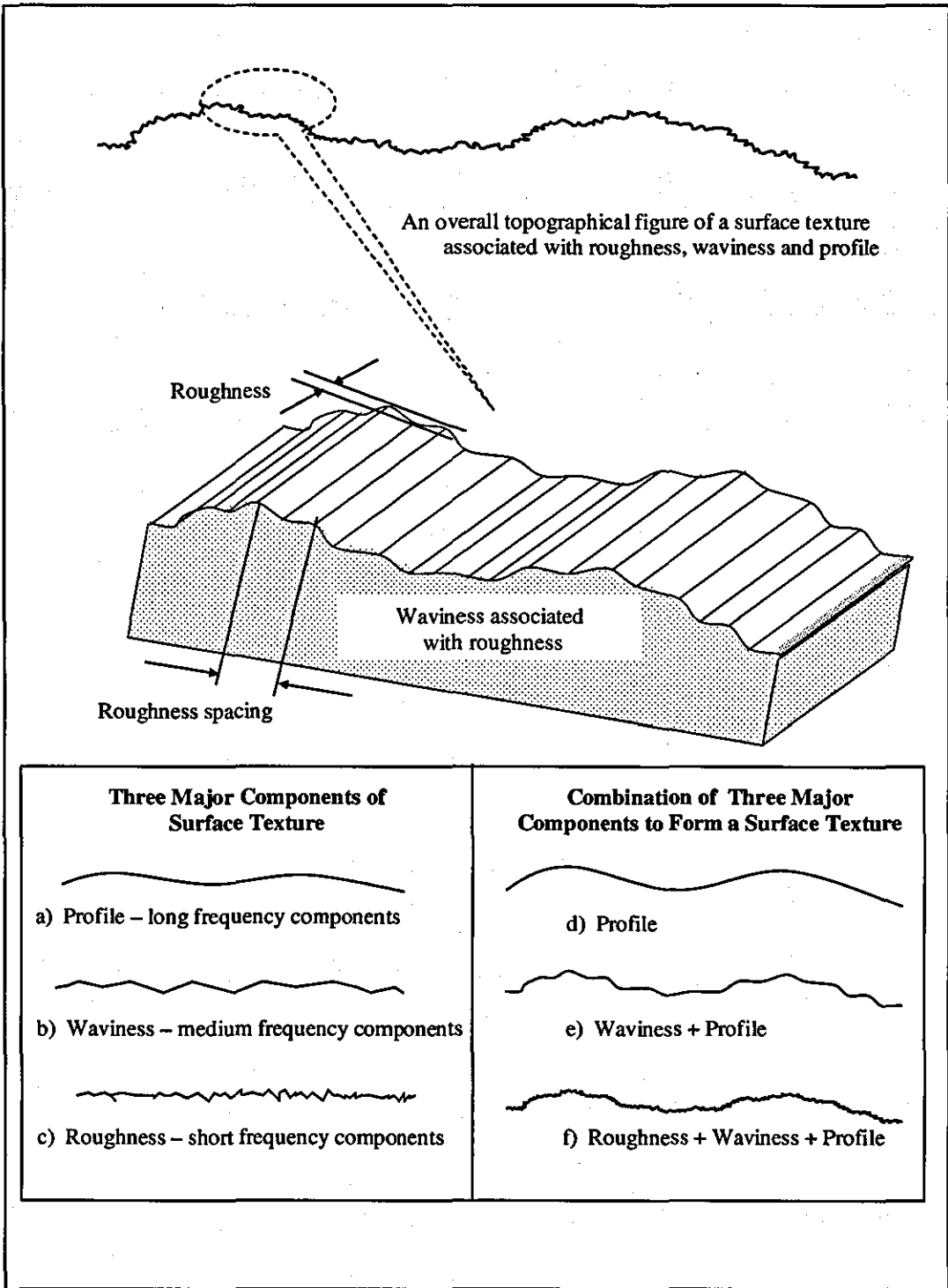


FIGURE 2.8 Microscopic illustration of a nominally flat surface and its order of geometrical irregularities

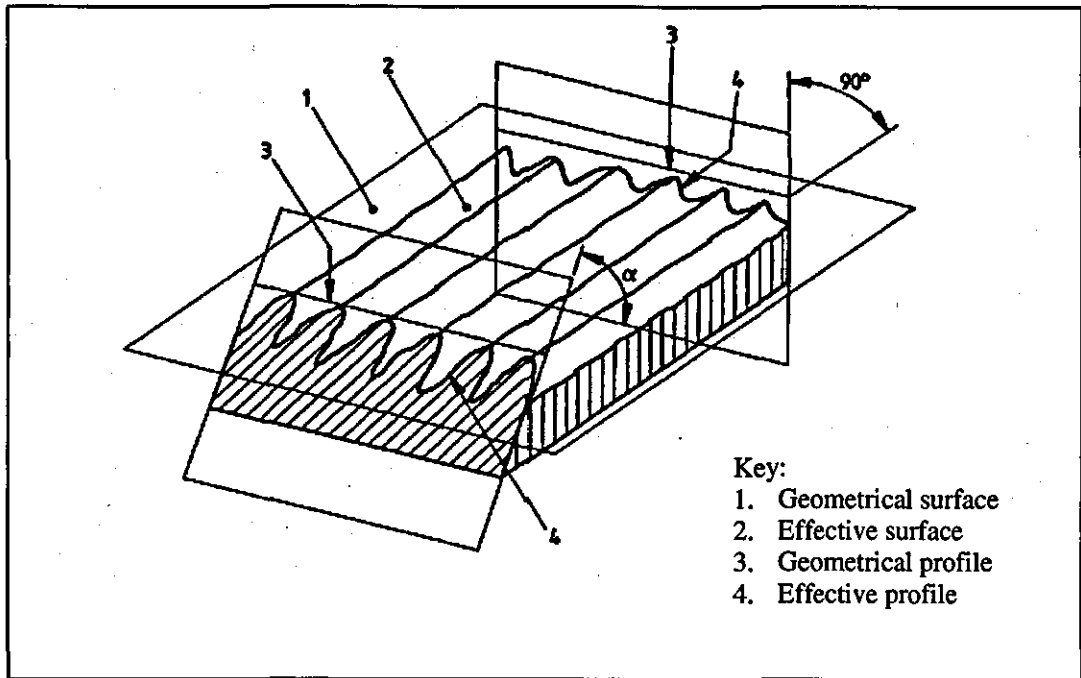


FIGURE 2.9 Surface characteristics and their terminology [BS1134-1 1988]

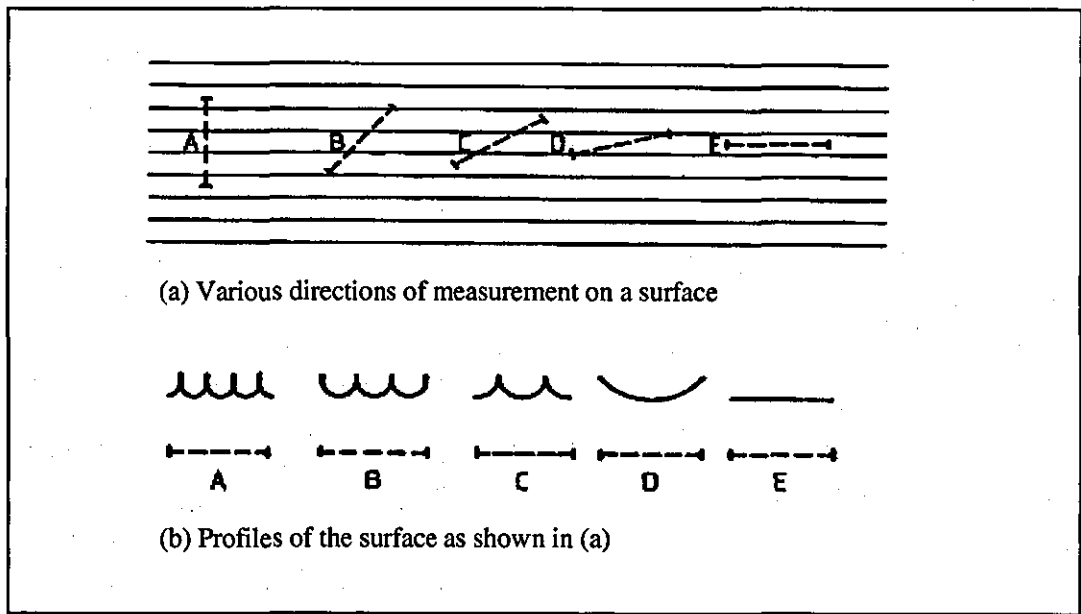


FIGURE 2.10 Influence of direction of measurement on the effective spacing of profile crests [BS1134-2 1990]

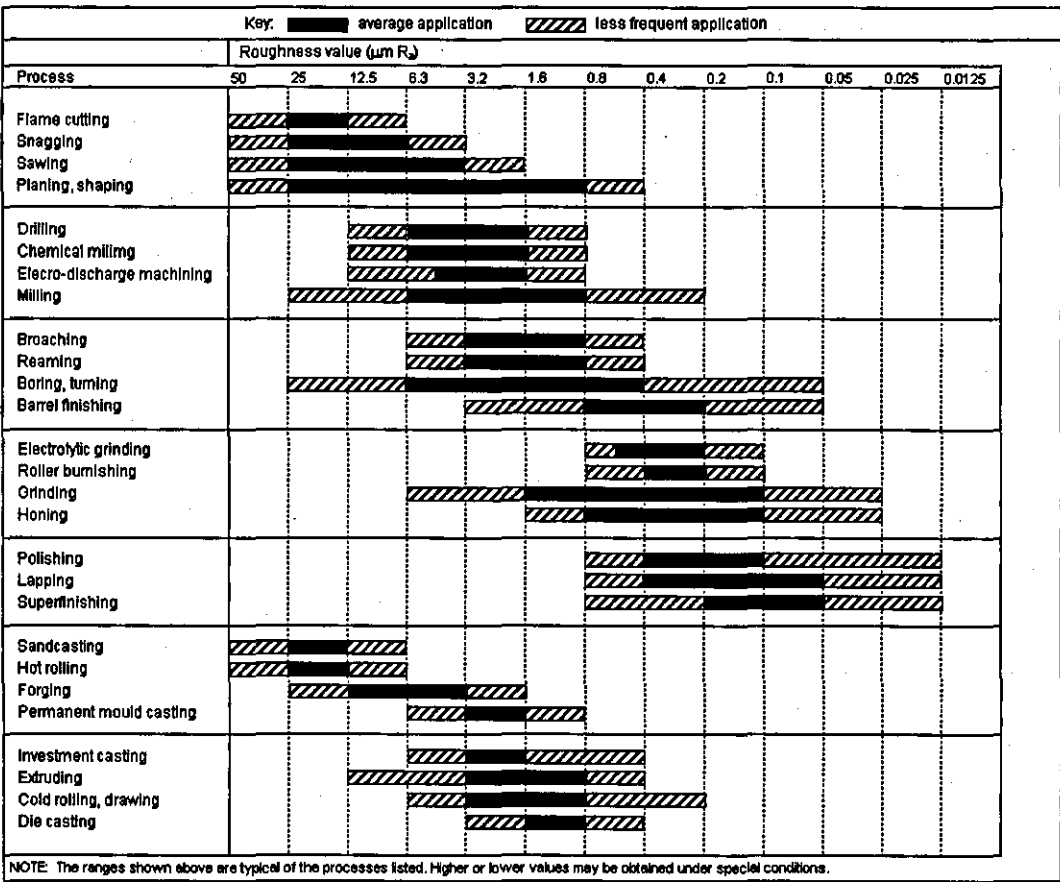


FIGURE 2.11 Typical roughness values obtainable by different finishing processes [BS1134-2 1990]

2.3.6 Surface Texture Instrumentation

There are three existing topography measurement techniques which are commercially available and commonly used in science, engineering and industry [Stout and Blunt 2000, Whitehouse 2001]:

- **Stylus-based profilometric system** – These have been in use for forty years in surface texture measurement, and are the most widely used in industries. This type of instrument basically consists of a contact probe; transducer and reference; amplifier; filter or processor; and recorder such as a meter or computer [Taylor Hobson 2006, Mitutoyo 2006, Mahr 2006a, Precision Devices 2006].

- **Optical-based system** – The application of this type of instrument is increasing where its three-dimensional (3-Dimensional) surface topography measurement is progressively being accepted in academia and industries. This is due to its significant advantages as a non-contact instrument, and it has higher vertical resolution than stylus-based systems [Veeco Instruments 2006]. However, the measuring range is generally smaller than equivalent stylus based instruments.

In this research work, a Zygo New View 5000 instrument [Zygo Corporation 2006] which is based on a scanning white light interferometer (SWLI) was used for characterisation of surface texture applied onto PCA pistons. This instrument was chosen due to its suitability to fit the purpose, where nanometer surface resolution is required on very large pistons in an accurate and repeatable manner. As the measuring beam scans the surface, it identifies surface asperities by measuring the phase shift between a reference beam and a measuring beam that is reflected from the surface. Consequently the phase shift is recorded by an image detector array, where the interference pattern can be viewed on the monitor. Quantitative measurement of specimen surface height is carried out by manipulating the interference patterns, and then implementing appropriate algorithms.

- **Scanning microscope** – Is the ultimate vertical resolution surface measurement instrument currently available [Cross 2003]. Examples of these types of instruments are scanning tunnelling microscopes (STM), atomic force microscopes (AFM) and scanning electron microscopes (SEM) where they are effectively used in material and biological science investigations. Besides having very high vertical resolution, they also have very high horizontal resolution. However, they typically have very small vertical and horizontal ranges, making them suitable in measuring small specimens that require high-precision measurement with resolution down to atomic-scale structures of surface.

2.3.7 Surface Texture Parameters

It is well known that the surface topography of surfaces greatly influence the mechanical and physical properties of contacting parts. The characteristics in terms of amplitude, spatial distribution and pattern of the surface texture dominates the functional application in the fields of friction, wear, bearing surfaces, lubrication, optical properties, etc. [Stout and Blunt 2000]. Therefore it is necessary to quantify the surface characteristics either in two-dimensional (2-Dimensional) or 3-Dimensional measurement, so that the behaviour of manufactured components' are predictable to a greater extent, and manufacturing processes are more controllable. Quantifying processes are achieved using surface texture parameters, these are categorised into three basic types [Taylor Hobson 2002, Zygo Corporation Corporation 2005]:

- **Amplitude parameters** – are measures of the vertical characteristic of the surface which are inherent in the production process. They are also known as known as roughness parameters (*R* parameters).
- **Spacing parameters** – are measures of the horizontal or lateral characteristics of the surface deviations.
- **Hybrid parameters** – are the combinations of spacing and amplitude parameters.

However, surface measurements carried out in this work are based on amplitude parameters, which are described in the next section.

2.3.8 Amplitude Parameter

Amplitude parameters based on 2-Dimensional calculation were used in this research work to characterise the surface texture applied onto the test pistons. Illustrations of the surface texture being measured are depicted in Figures 2.12 and 2.13. The parameters used were [Taylor Hobson 2002, Zygo Corporation 2005, Precision Devices 2006, Veeco Instruments 2006]:

- **R_a** – The arithmetic mean of the absolute magnitude of the roughness profile, $z(x)$ that deviates from its mean line over one sampling length, l . It is universally

recognised, and mostly used as an international parameter of roughness, typically to describe the roughness of machined surfaces. It is useful in indicating overall profile height characteristics and for monitoring process in manufacturing work. The mathematical derivation of R_a is given by:

$$R_a = \int_0^l |z(x)| dx \quad (2.2)$$

- R_t – Is the vertical distance between the profile peak height above the mean line (R_p) to the maximum profile valley depth below the mean line (R_v) which are taken over the evaluation length. R_p provides information about friction and wear characteristics on a part, whereas R_v gives information about how a part might characteristically retain a lubricant within valleys or pockets. Thus R_t provides the overall roughness of a surface, with its mathematical equation corresponding to R_p and R_v as follows:

$$R_t = R_p + R_v \quad (2.3)$$

- R_q – Is the root mean square (RMS) of the arithmetic mean of the roughness profile which is taken over the entire measured length, l that deviates from its mean line. In other word, it represents the standard deviation of the profile heights. Since it corresponds to the RMS of R_a , it is more easily related to functional performance of the surface, hence gradually superseding R_a [Whitehouse 2001]. It reflects the optical performance of the surface being measured in a more accurate manner, and is used in computation of skewness (R_{sk}) and kurtosis (R_{ku}) parameters. R_{sk} and R_{ku} are a measure of the asymmetry of the profile about the mean line, and a measure of the distribution of spikes above and below the mean line, respectively.

$$R_q = \sqrt{\frac{1}{l} \int_0^l z^2(x) dx} \quad (2.4)$$

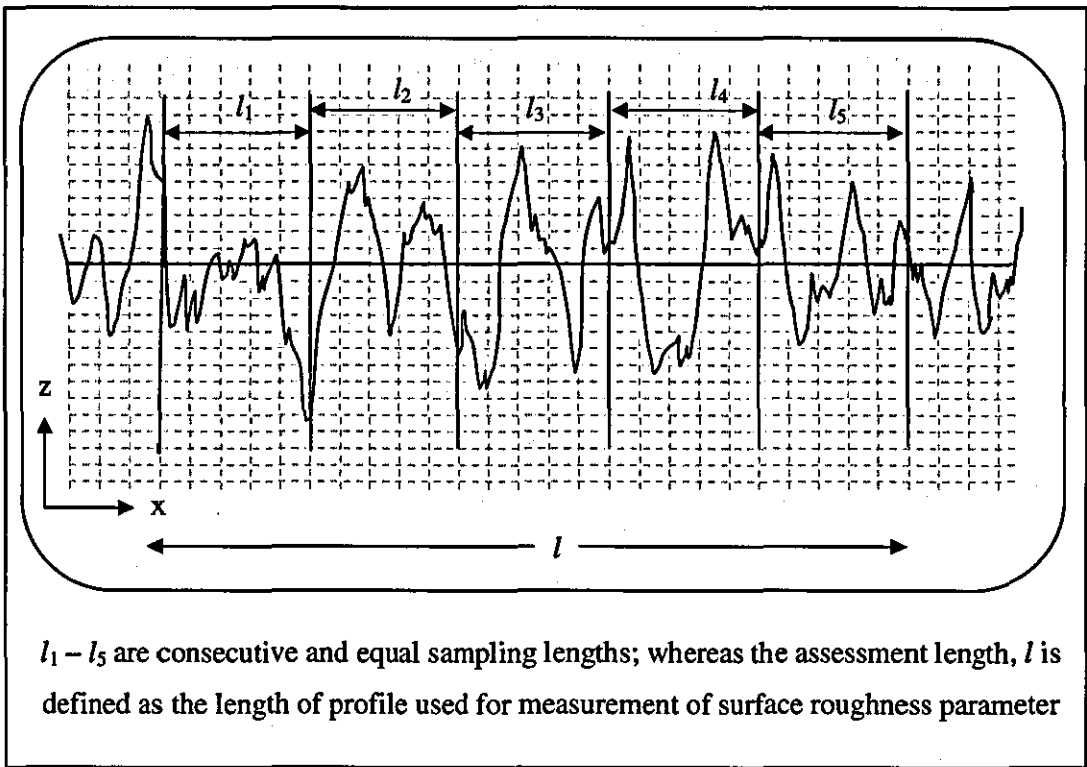


FIGURE 2.12 Typical profile graph of amplitude parameters, represented by $z = f(x)$

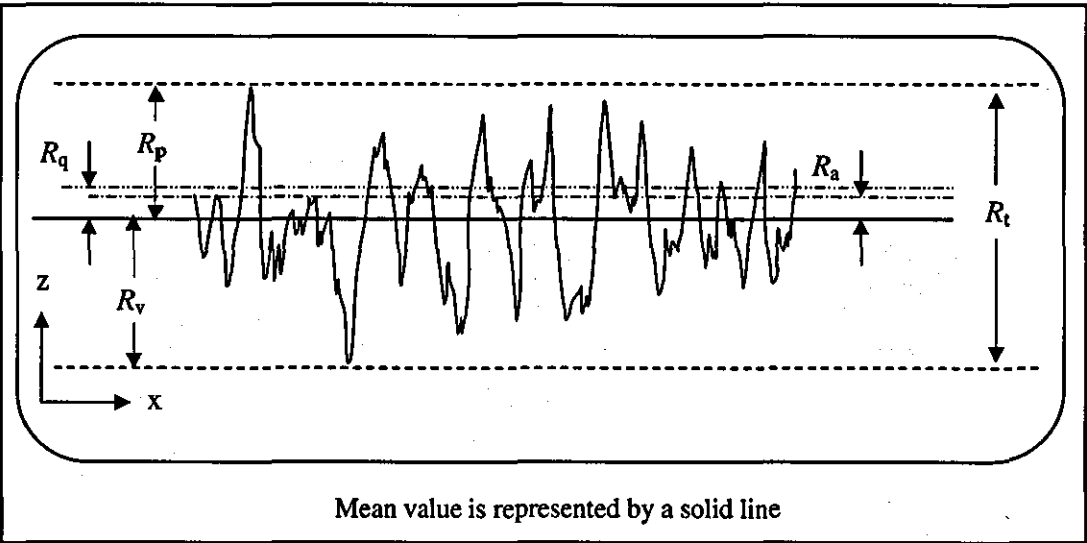


FIGURE 2.13 Numerical values of amplitude parameters

2.4 SUMMARY

This chapter has introduced the background of pressure and surface metrology, and also explains how they are related to each other in pressure balance application. Pressure is a derived unit that can be broken down into three modes; absolute, differential and gauge modes. There are two instruments that can derive pressure metrologically in a completely independent way from the base units, i.e. the liquid column manometer and the pressure balance. However the pressure balance is more preferable compared to the liquid column manometer due to its prominent features such as faster and easier in operation, larger measuring range, lower maintenance and purchasing costs etc.

Surface metrology plays very important role when surface geometry/texture are a necessity, as required in manufacturing of the PCA. Surface geometrical irregularities can be divided into three categories; roughness, waviness and profile, depending on the frequency of irregularities which recur at regular or irregular intervals. These topographical irregularities can be measured using instruments which are either stylus-based, optical-based or scanning microscope-based systems. Before embarking upon surface characterisation, basic knowledge about surface metrology is important since selecting the most appropriate measurement parameter to be used is a difficult task due to the lack of real information about the surface, and each parameter is normally suitable/useful in certain applications. Furthermore, one parameter alone is not sufficient to describe the roughness of the part being measured, thus a combination of parameters gives better information to describe its functional characteristics such as friction and wear, load carrying capacity, porosity, bearing property etc.

CHAPTER 3

THE PRESSURE BALANCE

This chapter provides general information about the pressure balance which is used in this research work. It is organised as follows: Section 3.1 reveals a brief history of the pressure balance, which is traced back at least 150 years. Section 3.2 explains about the physical principles employed in the pressure balance. Section 3.3 describes the four commonly available types of the PCA used in pressure balances, as well as some unusual configurations. Section 3.4 explains about the pressure conversion equation that is used in gauge-mode pressure measurement, detailing other parameters which influence the pressure generated. Section 3.5 describes the theory of effective area calculation of the PCA, from the ideal type to the generalised non-ideal type. Finally, Section 3.6 summarises all of the topics discussed in this chapter.

3.1 EARLY HISTORY OF THE PRESSURE BALANCE

In the late 18th century, studies of fluid compressibility stimulated demands for accurate high pressure measurement, especially when James Watt (1764) began to measure the properties of steam, for his foundation of the Steam Tables. This stimulation was further enhanced with associated possibilities of power generation and other important consequences [Heydemann and Welch 1975, Dadson et al. 1982, Dadson 1983]. Mercury manometers which were invented by Torricelli (1644) were the only pressure measuring instrument during that time, however their measuring ranges were very limited. The requirement for high pressure measurement became crucial after the first high pressure steam engine was built around 1800. Steam pressure gauges started to be used in 1848 on locomotives, based on the bourdon tube principle. However the exact time of emergence of the pressure balance as a precise pressure measuring instrument is

not clear, although it can be traced back approximately 150 years. A time table of historical developments of the pressure balance in chronological order is presented as follows [Heydemann and Welch 1975, Dadson et al. 1982, Dadson 1983, Molinar 1992]:

- 1826 Perkin, was a pioneer in this field through his writing in 1826. He developed a pressure balance that could generate pressure up to 200 MPa. His pressure balance comprised of a simple PCA in which the load was applied to the piston via a lever system.
- 1833 Parrot and Lenz, developed a pressure balance of a similar type as Perkin, but covered a pressure measuring range up to 10 MPa.
- 1846 Galy-Cazalat described a novel pressure balance which measured pressure up to 2 MPa, made use of a mercury manometer and a hydraulic piston multiplier. Two pistons of significantly different diameters were mechanically coupled, so that the high pressure which acted on the small piston (via a rubber diaphragm) transmitted force to a larger diameter that was connected to the mercury manometer. A piston-area ratio was utilised to determine the system pressure, based on the indicated value by the mercury manometer.
- 1869 Seyss described a less conventional design which was made using two pistons of two different diameters, mounted coaxially within one cylinder, inbuilt with automatic loading device. It is believed that this is the predecessor of the modern dual-range PCAs, which are widely used in industrial calibrations in the present-day.
- 1871 Desgoffe (designer) and Pelletier (manufacturer) produced a pressure balance of 100 MPa measuring range, which was based on similar principles to Galy-Cazalat. Packing (sealing material) was used with the high pressure piston, whereas a rubber membrane was used at the lower piston for sealing purposes.
- 1880 Cailletet described a pressure balance of 150 MPa measuring range with an uncertainty of 0.5%, using a PCA which had a radial gap of approximately 5 μm .

- 1883 Ruchholz reported on a directly loaded pressure balance that utilised a circular table, which was rigidly attached to the top of the piston. His idea seemed to be very simple, made use of a rotating piston, which is not much different to a present-day pressure balance.
- 1893 Amagat described a notable pressure balance that departed from the normally used pressure balance during that time, which could measure up to 300 MPa. He used a similar instrument as Desgoffe, without using packing material and rubber diaphragm. A free-rotation piston was introduced that relieved friction between the piston and the cylinder, thus improved the sensitivity. This pressure balance was used by Amagat for extensive studies of gas compressibility.
- 1893 Stückrath reported on a 50 MPa pressure balance with a beam loading facility, but it had no provision for rotation of the packed piston. He claimed that a typical sensitivity for such pressure balance reached the order of 0.04% at 25 MPa, proved that this arrangement was convenient to use, and also demonstrated that manufacturing technology of the cylindrical component had improved.
- 1908 Bridgman described a generator for pressure to about 700 MPa in which a controlled-clearance PCA was introduced to reduce the excessive fluid leakage through the PCA.
- 1911 Bridgman introduced a new idea in the construction of the PCA after he abandoned his controlled-clearance design. A re-entrance type of PCA was introduced, and successfully used.
- 1953 Newhall refined and adapted the controlled-clearance principle to his pressure balance, where accurate pressure measurement with liquid medium was possible up to approximately 1.4 GPa.

3.2 PHYSICAL PRINCIPLES OF THE PRESSURE BALANCE

The pressure balance is a very reliable instrument used to generate and measure pressure, using hydraulic or gas pressure transmitting fluid with a reproducibility in the order of a few parts per million (ppm) [Delajoud et al. 1999, Legras 1994a]. Its fundamental operating principle and excellent long term stability have made it an indispensable tool in high accuracy pressure metrology. It is one of the primary pressure measuring instruments that can metrologically derive pressure units in a complete and independent manner with reference to the basic units of the International System of Units (SI) i.e. mass (kg), length (m) and time (s). It derives pressure directly in terms of force which is exerted on a surface of a piston-cylinder assembly (PCA) of known effective area, i.e. when weights of known mass values are applied onto the piston, so as the pressure applied across the effective area of the PCA by the pressure transmitting fluid exactly balances the downward gravitational force.

It consists of an accurately manufactured circular vertical piston that fits into a matched hollow coaxial cylinder with a very fine clearance (typically around 1 μm for 35 mm diameter of piston) and it is free to slide in the cylinder. It is rotated during operation to reduce the influence of friction between piston and cylinder. An ideal PCA is made of carefully chosen materials, and it fulfils the following requirements [Molinar 1992]:

- Capable of withstanding high compressive load under elastic conditions
- Have very small thermal expansion coefficients
- Maintain a highly-polished surface finish (sub-micrometer surface roughness values)
- Extremely accurate in geometry (roundness, straightness and parallelism) along the entire engagement length
- Have a very small and uniform clearance between piston and cylinder
- Ideally experience no friction between piston and cylinder
- Demonstrate a small fall rate with very high reproducibility

- Exhibit no unpredictable distortion due to sealing works
- Accessible for a contact precision temperature measurement

The effective area of the PCA is neither the area of the piston nor the cylinder, but has a value somewhere in between them. Under reference conditions (with respect to pressure and temperature), its value is denoted by the symbol A_0 , (normally expressed in m^2 or mm^2) and is used in the conversion equation for the calculation of the measured pressure.

3.3 BASIC TYPES OF PISTON-CYLINDER ASSEMBLY (PCA)

Generally the PCA can be categorised into four basic types, depending on their construction that are designed to serve their particular needs, and/or the manner in which it is attached to the body of the pressure balance [Dadson et al. 1982, Molinar 1992 and Newhall et al. 2003]. A summary of the main variants between each type are described below:

3.3.1 Simple Type

This is the simplest and most widely adopted design of PCA to realise pressure in terms of force per unit area. It is commonly used in oil and gas-operated pressure balances. The force is applied to the head of the piston, whereas the pressure to be measured, p , is applied to the base of piston as shown in Figure 3.1(a). The piston and cylinder are stressed only by the pressure inside the clearance between piston and cylinder, hence they are subjected to free elastic deformations on their geometries, which depend on the value of pressure applied. This type of PCA is also known as a free-deformation type and it is normally used up to 600 MPa, due to limitations of rapid leaking beyond this point [Molinar 1992].

3.3.2 Controlled-clearance Type

The controlled-clearance configuration that is shown in Figure 3.1(b) can cover a very wide range of pressure using a single PCA. However it is designed mostly for operations

at very high pressure, up to few GPa [Molinar 1992, Lewis and Peggs 1992]. An independent controllable pressure system, known as jacket pressure, p_j , is applied to the external surface of the cylinder, hence providing control of the clearance between piston and cylinder (at the same time controlling the leakage past the clearance) at the operator's will [Newhall et al. 2003]. So, the clearance is a function of the geometry of the system, jacket pressure (p_j) and pressure being measured (p).

3.3.3 Re-entrance Type

This type of PCA is designed to minimise the excessive leakage flow through its clearance at high pressures. Figure 3.1(c) shows this configuration where force is applied to the head of the piston, whereas the pressure to be measured, p , is applied to the base of the piston. When the pressure p is applied, it will act simultaneously on a well-defined external part as well as on the internal part of the cylinder, thus introducing a differential pressure between the pressure, p , and the pressure distribution in the clearance. This situation makes the clearance between piston and cylinder contract proportional to the differential pressure between them. This type of configuration is commonly used in high pressure measurement, up to 700 MPa.

3.3.4 Differential Type

The configuration of the differential type PCA is shown in Figure 3.1(d) aiming at avoiding the use of pistons of very small cross-sections. It allows one to use large diameter pistons, but requires relatively small loads. The effective area of the PCA is the difference in area of the large and small piston-cylinder pairs, i.e. $A_e = A_1 - A_2$, thus it can be very small. However, since the accuracy of pressure measurement using a simple type PCA (of the same effective area) is greater than a differential type, the differential type remains unpopular at present.

However there are some unusual configurations that have been used such as:

- **Spherical piston** - Known as floating-ball pressure balance, e.g. ceramic ball which combines a ball to receive the load and a hemisphere base to support the ball. These types of configurations reduce the viscous drag on the piston thus

allowing operation in gauge mode at low pressures [Heydemann and Welch 1975, Dadson et al. 1982].

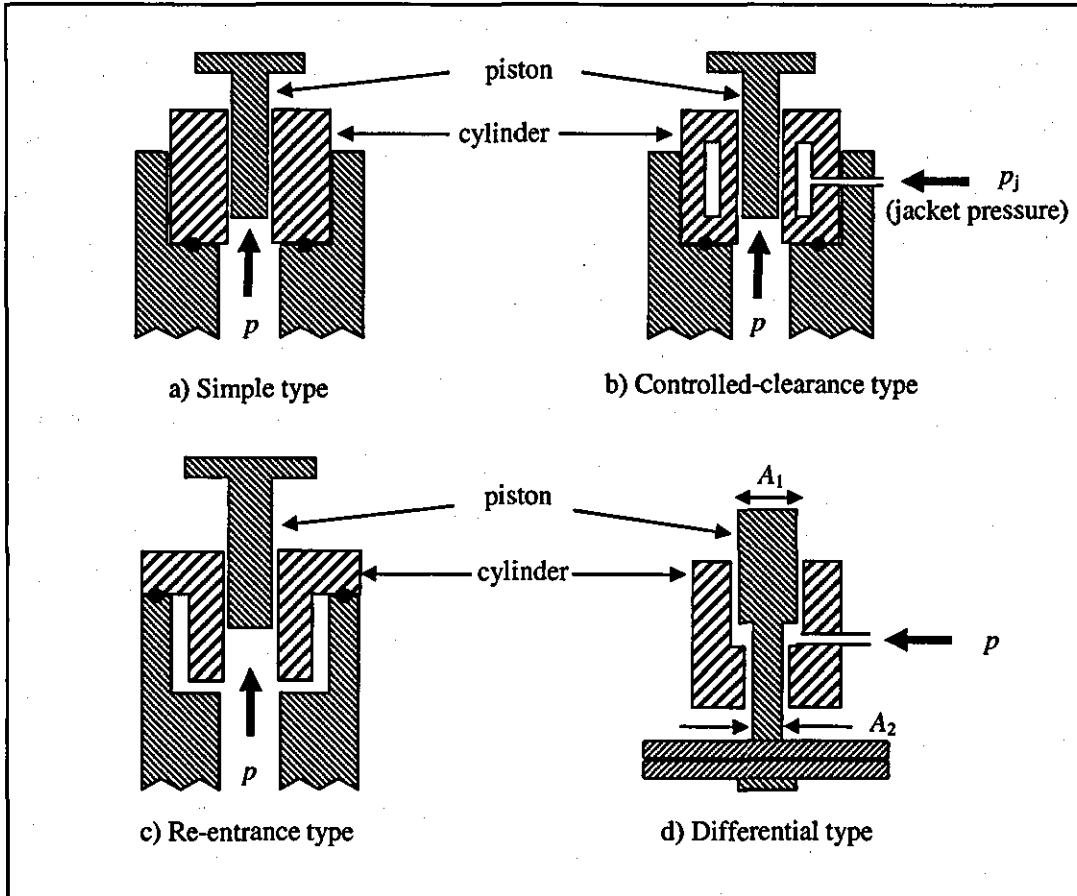


FIGURE 3.1 Four basic types of piston-cylinder assembly

- **Grooved piston** - In order to reduce substantially the deceleration rate of the pistons whilst improving the sensitivity of pressure measurement. This is due to very low friction between piston and cylinder [Heydemann and Welch 1975, Dadson et al. 1982].
- **Hybrid-PCA** - A mixed configuration of simple and re-entrance types where a simple type design (bottom part) and a re-entrance type design (middle part) portions of the cylinder are used to derive pressure at lower and higher pressures respectively [Nishibata 1997].

- **Dual-range PCA** - A high piston is fitted into a matched low piston, concurrently acting as a cylinder for the high piston. At the same time, the low piston is fitted into a matched cylinder hence providing two ranges of pressure measurements. They work in similar manner like a simple-type PCA but each range is treated separately [Dadson et al. 1982, Lewis and Peggs 1992].
- **Tilting PCAs** - used in lower pressure ranges where in these ranges the limitation is due to the weight of the piston itself. By tilting the piston of weight Mg to a tilting angle α , the effective weight acting downwards becomes $Mg \sin \alpha$ [Heydemann and Welch 1975, Dadson et al. 1982].

3.4 PRESSURE CONVERSION EQUATION

The pressure conversion equation is an equation that relates the pressure generated/measured by a pressure balance to the mass of weights (loaded onto the piston) while taking into account other input quantities. The pressure p is computed at its reference level h by analysing the different components of the forces acting on a piston of known cross sectional area. For a simple type pressure balance which is working in gauge-mode, the pressure p can be expressed by the following conversion equation [Nishibata 1997]:

$$p = \frac{\sum_i m_i g_L (1 - \rho_a / \rho_{mi}) + \Gamma C}{A_0 (1 + \lambda p) [1 + (\alpha_p + \alpha_c)(t - t_{ref})]} \pm \rho_f g_L h \quad (3.1)$$

where the symbols have the following meanings:

- p is the gauge pressure measured at the reference level (Pa)
 m_i is the individual true mass value of each weight (including all floating elements e.g. piston and ball-bearing) applied on the piston (kg)
 g_L is the local acceleration due to gravity (ms^{-2})
 ρ_a is the density of ambient air (kgm^{-3})
 ρ_{mi} is the density of i^{th} weight (kgm^{-3})

- A_0 is the effective area of the PCA at a reference temperature t , and atmospheric pressure (m^2)
- Γ is the surface tension of the pressure transmitting fluid used (Nm^{-1})
- C is the circumference of the piston at the level where it emerges from pressure transmitting fluid (m)
- λ is the elastic pressure distortion coefficient of the PCA (Pa^{-1})
- α_p is the linear thermal expansion coefficient of the piston ($^{\circ}\text{C}^{-1}$)
- α_c is the linear thermal expansion coefficient of the cylinder ($^{\circ}\text{C}^{-1}$)
- t is the measured temperature of the PCA at the moment measurement taken/pressure is generated ($^{\circ}\text{C}$)
- t_{ref} is the reference temperature at which A_0 was measured, normally 20°C
- ρ_t is the density of the pressure-transmitting fluid (kgm^{-3})
- h is the difference in the heights between the piston base and a selected reference level (m)

Equation (3.1) is divided into two pressure components; the first component expresses the pressure generated at the base of the piston, and the second component calculates the head correction due to the difference in two levels. Subsequently, the first component is divided into a few terms. The term $(1 - \rho_a / \rho_{\text{ml}})$ is the air buoyancy correction for i^{th} weight. The term ΓC is an additional force exerted on the piston due to surface tension of the pressure transmitting fluid. The term $(1 + \lambda p)$ calculates the change of the effective area with pressure due to the pressure distortion coefficient. The term $[1 + (\alpha_p + \alpha_c)(t - t_{\text{ref}})]$ is the correction factor of the effective area due to temperature deviation from its reference temperature. Lastly, the term $\rho_f g_L h$ in the second pressure component represents the head correction, as a result of the density of the pressure transmitting fluid associated with its height difference.

3.4.1 Mass and Buoyancy

In practice, the weighing instruments used in mass determination only react to the total gravitational force that exerts the weighing pan. Since the weighing process is carried

out in ambient air, the actual gravitational force, F_m generated by the mass, m , is reduced by the weight force of the displaced air, F_a , (known as buoyancy). Consequently this force is detected by the weighing instrument as F , which represents the mass of the weighing sample. This phenomenon is in accordance to the Archimedes' principle, and the three forces relationship can be expressed as follows [Debler 2000]:

$$F = F_m - F_a \quad (3.2)$$

From Equation (3.2), the resultant gravitational force F of the weighing sample in relation to its mass, m ; its density, ρ_m ; density of ambient air, ρ_a ; and the local gravitational acceleration, g_L can be simplified as follows:

$$F = m(1 - \rho_a / \rho_m)g_L \quad (3.3)$$

The term $(1 - \rho_a / \rho_m)$ is known as the air buoyancy correction factor.

The problem regarding to different weight force generated by the same mass of weighing sample (of different density) has been rectified through the introduction of conventional mass, m_c [OIML R111-1 2004]. A convention which is widely adopted, where:

- The weighing sample is assigned to the conventional density, ρ_{mc} of 8000 kgm^{-3}
- The air density is assigned to its conventional density ρ_{ac} , of 1.2 kgm^{-3}

Therefore all weighing instruments are adjusted to the above conditions, hence all the indicated values are automatically corrected to the conventional values even though the density of the weighing sample deviates from ρ_{mc} . The relationship between true mass, m and conventional mass, m_c in equilibrium condition at $\rho_a = \rho_{ac}$ is as follows:

$$m(1 - \rho_a / \rho_m)g_L = m_c(1 - \rho_a / \rho_{mc})g_L \quad (3.4)$$

Rearranging Equation (3.4), the conventional mass value can be related to the true mass value by the following equation:

$$m_c = m \frac{(1 - \rho_a / \rho_m)}{(1 - \rho_a / \rho_{mc})} \quad (3.5)$$

where the Equation (3.5) can also be represented by the following form:

$$m = m_c \left[1 + \rho_a \left(\frac{1}{\rho_m} - \frac{1}{\rho_{mc}} \right) \right] \quad (3.6)$$

From Equation (3.5), the difference in numerical values between m and m_c is as follows:

$$m - m_c = m \left[1 - \frac{(1 - \rho_a / \rho_m)}{(1 - \rho_a / \rho_{mc})} \right] \quad (3.7)$$

Therefore, the relative difference, D_{rel} between m and m_c in their numerical value is given by:

$$D_{rel} = \frac{(m - m_c)}{m} = 1 - \frac{(1 - \rho_a / \rho_m)}{(1 - \rho_a / \rho_{mc})} \quad (3.8)$$

By simplifying Equation (3.8), an approximation of D_{rel} is given by:

$$D_{rel} \approx \rho_a \left[\frac{1}{\rho_m} - \frac{1}{\rho_{mc}} \right] \quad (3.9)$$

Equation (3.9) demonstrates that if the density of weight deviates by 2.5% (i.e. $\pm 200 \text{ kgm}^{-3}$) from its conventional mass value which is calculated at air density $\rho_a = 1.2 \text{ kgm}^{-3}$, the relative difference is approximately 4 ppm. Furthermore, the actual air density during measurement is rarely equal to its conventional value, but always differs to a certain level of deviation hence influencing the effective downward force. Therefore when the highest level of accuracy in pressure measurement is required, calculation using true mass values is necessary, especially when they are used in absolute mode. However in order to avoid any confusion and mistakes in pressure computation, the use of true mass value in high accuracy pressure measurement in gauge mode is also highly recommended [Nishibata 1997]. Therefore a good knowledge of density of all floating components involved is essential.

3.4.2 Local Acceleration Due to Gravity

The local acceleration due to gravity, g_L shall be measured at the site for high accuracy pressure measurement since its value will be proportionally affecting the calculated pressure. Direct measurement to the accuracy of 0.1 ppm is possible with residual standard deviation of 0.02 ppm [Molinar 1992]. However there is an acceptable formula that is recommended by the International Association of Geodesy which in general gives a value better than 50 ppm in accuracy [Lewis and Peggs 1992]:

$$g_{L(\varphi,H)} = g_{L(0,0)} (1 + \beta_1 \sin^2 \varphi - \beta_2 \sin^2 2\varphi) - 3.086e^{-6} H \quad (3.10)$$

where

$g_{L(\varphi,H)}$ is a gravity value in ms^{-2} , calculated for latitude φ and height H metres above sea level (ms^{-2})

$g_{L(0,0)}$ is a gravity value at the equator and at sea level, which is equal to $9.7803184 \text{ ms}^{-2}$

β_1 is a constant, which is equal to 0.0053024

β_2 is a constant, which is equal to 0.0000059

Equation (3.10) above shows that the rate of gravity change per metre altitude is approximately 0.3 ppm/metre which means that height difference cannot be ignored in high accuracy pressure measurement, i.e. when “gravity-independent” pressure measuring instruments (using mechanical deformation sensing elements) are calibrated against pressure balance. However, in the cross-floating experiments, gravitational effects on both pressure balances cancel each other out, hence the knowledge of its value is not important.

3.4.3 Surface Tension

Surface tension is a relatively small additional downward force correction that affects the pressure measurement. It is formed by the surface layer of the pressure transmitting fluid that behaves like an elastic sheet. At the surface of the fluid, the molecules are pulled inwards by other molecules deeper inside the fluid, hence creating an imbalanced

condition. This condition is balanced by a surface tension that is a resistance to compression at the surface layer of the pressure transmitting fluid. Its effect is only appreciable when measurement is carried out at low and moderate pressure using oil-operated and gas-operated oil-lubricated pressure balances. However it is negligible for a gas-operated gas-lubricated pressure balance [Dadson 1983]. This force is equal to γC that occurs at the level where piston emerges from the pressure transmitting fluid.

3.4.4 Temperature Correction

The coefficient of thermal expansion is a subject related to the expansion and contraction of solids in response to heating and cooling respectively. The linear thermal expansion coefficient relates the change in a material's linear dimensions to its temperature change. The area coefficient of the PCA is the sum of linear thermal expansion coefficients of piston and cylinder, symbolised by α_p and α_c respectively, where the temperature correction factor, C_T is given by:

$$C_T = 1 + (\alpha_p + \alpha_c)(t - t_{ref}) \quad (3.11)$$

For a high accuracy pressure measurement, α_p and α_c must be determined with an uncertainty of the order of a few percent, which can be characterised independently using dilatometric techniques (thermo-mechanical analysis) and a specific cross-floating experiment [Molinar 1992]. Its typical value extracted from the Tables of Physical Constants is not accurate enough since it commonly leads to an error of approximately 10% to 20%.

3.4.5 Elastic Pressure Distortion Coefficient

The correction factor for an elastic pressure distortion coefficient is represented by the term $(1 + \lambda p)$, which shows a linear change of its value with pressure. When pressure is applied to the system, the piston and cylinder undergo variation in their dimensions which is due to elastic properties of the material. At high pressure measurements, this phenomenon contributes the biggest source of error, thus an accurate value is essential if high pressure measurement is to be realised [Dadson et al. 1982]. However, it is extremely difficult to measure this coefficient directly since its value is very small, and

enclosed within a high pressure environment. The determination of this coefficient becomes more complicated for pressures ranging from 1 to 5 MPa, however the influence of this distortion coefficient uncertainty is reduced if tungsten carbide is used instead of hardened steel [Molinar 1992], because the modulus of elasticity of tungsten carbide is approximately three time higher than hardened steel.

For a simple type PCA that measures pressure below 0.5 MPa, an advisable formula in computing the elastic pressure distortion coefficient by Molinar [1992] is as follows:

$$\lambda = \frac{3\nu_p - 1}{2E_p} + \frac{1}{2E_c} \left(\frac{R_c^2 + r_c^2}{R_c^2 - r_c^2} + \nu_c \right) \quad (3.12)$$

where

- ν_p is the Poisson coefficient of the piston
- ν_c is the Poisson coefficient of the cylinder
- E_p is the Young's modulus of elasticity of the piston (Pa)
- E_c is the Young's modulus of elasticity of the cylinder (Pa)
- R_c is the outer radius of the cylinder (m)
- r_c is the inner radius of the cylinder (m)

3.4.6 Effective Area

The effective area of the PCA at its reference temperature, t_{ref} and atmospheric pressure, p_0 can be determined through one of the three following approaches [Dadson et al. 1982, Molinar 1992]:

- Calculation based on direct dimensional measurement
- Cross-floating against liquid column manometer
- Cross-floating against a reference pressure balance

The advantage of the first approach is being an absolute and independent method, that fulfils one of the requirements to become the primary pressure standard. Unfortunately

this method is very costly due to its requirement for the state-of-the-art equipment [Neugebauer 1998], long time measurement process and highly skilled personnel.

Besides these disadvantages, one should bear in mind that the results determined using direct calculation from measured dimensions, may introduce discrepancies (ppm level) compared to the results obtained from cross-floating against a liquid column manometer or other pressure balance. Therefore, dimensional measurements alone cannot provide formally recognised traceability to the SI pascal, without extreme levels of data and mathematical modelling, supported with extensive comparison histories with other instruments of proven performance [NPL 2006]. This is due to the following reasons:

- Dimensional based measurement and cross-floating based measurement are carried out in totally different manners, i.e. in static and dynamic conditions respectively.
- The interaction effect between the piston and cylinder during operation may introduce other sources of error which do not appear in the static condition, i.e. dimensional measurement. These effects are immeasurable using direct dimensional measurement.
- Errors introduced by the software in determining the mean effective area. This is due to the complexity of surface textures on the piston and cylinder, plus other sources of errors in roundness, straightness and parallelism which lead towards a very complicated characterisation of effective area.

3.5 THEORY OF THE PISTON-CYLINDER ASSEMBLY (PCA)

An ideal PCA is assumed to be highly polished and perfect in geometries such as straightness, parallelism and roundness with constant radii respectively (thus having perfectly circular cross sections and their axes are coaxial and vertical) and assuming the normal law of viscous flow in the inter-space [Dadson et al. 1965, Dadson et al. 1982, Lewis and Peggs 1992]. Firstly, these assumptions should be considered in order to

derive the effective area of the PCA, which is a function of the dimensions of both piston and cylinder. This ideal system is shown in Figure 3.2 for the simplest geometrical case, where r , R and h_c are the radii of the piston and cylinder bore, and the radial separation between them respectively. Radial separation which is normally called the clearance, is simply obtained by:

$$h_c = R - r \quad (3.13)$$

The fluid pressure, p_1 being measured is applied to the base of the piston, while the top of the piston is exposed to the ambient pressure, p_2 [Dadson et al. 1982]. At the equilibrium condition, the upward vertical force due to the pressure difference $(p_1 - p_2)$, is balanced against a known gravitational force W , that is applied to the piston. However, the total upwards force acting on the piston is due to the actual pressure acting on the bottom level of the piston i.e. $\pi r^2(p_1 - p_2)$, and a very small frictional force, F_f , exerted on the vertical flanks of the piston by the fluid which is being forced to move upwards under the influence of the pressure gradient. Therefore when the piston is in equilibrium, those forces are balanced by the true gravitational force, W' as follows:

$$W' = \pi r^2(p_1 - p_2) + F_f \quad (3.14)$$

If the normal laws of viscous flow are maintained and plane-parallel surfaces are assumed, the bounding surface which is known as the "neutral surface" of radius \hat{r} is located precisely in the middle of the two boundaries [Dadson 1983]. At this surface (depicted in broken lines), the frictional force between adjacent layers of fluid due to fluid motion will be zero. The total downwards force acting on the column of fluid between neutral surface and piston surface are a sum of frictional force, F_f , exerted on the vertical flanks of the piston by the fluid and the downward gravitational force, w' due to its mass. Hence the following equation is obtained:

$$w' + F_f = \pi(\hat{r}^2 - r^2)(p_1 - p_2) \quad (3.15)$$

Therefore, combining Equations (3.14) and (3.15) and simplifying them, we have

$$p_1 - p_2 = \frac{W' + w'}{\pi \hat{r}^2} \quad (3.16)$$

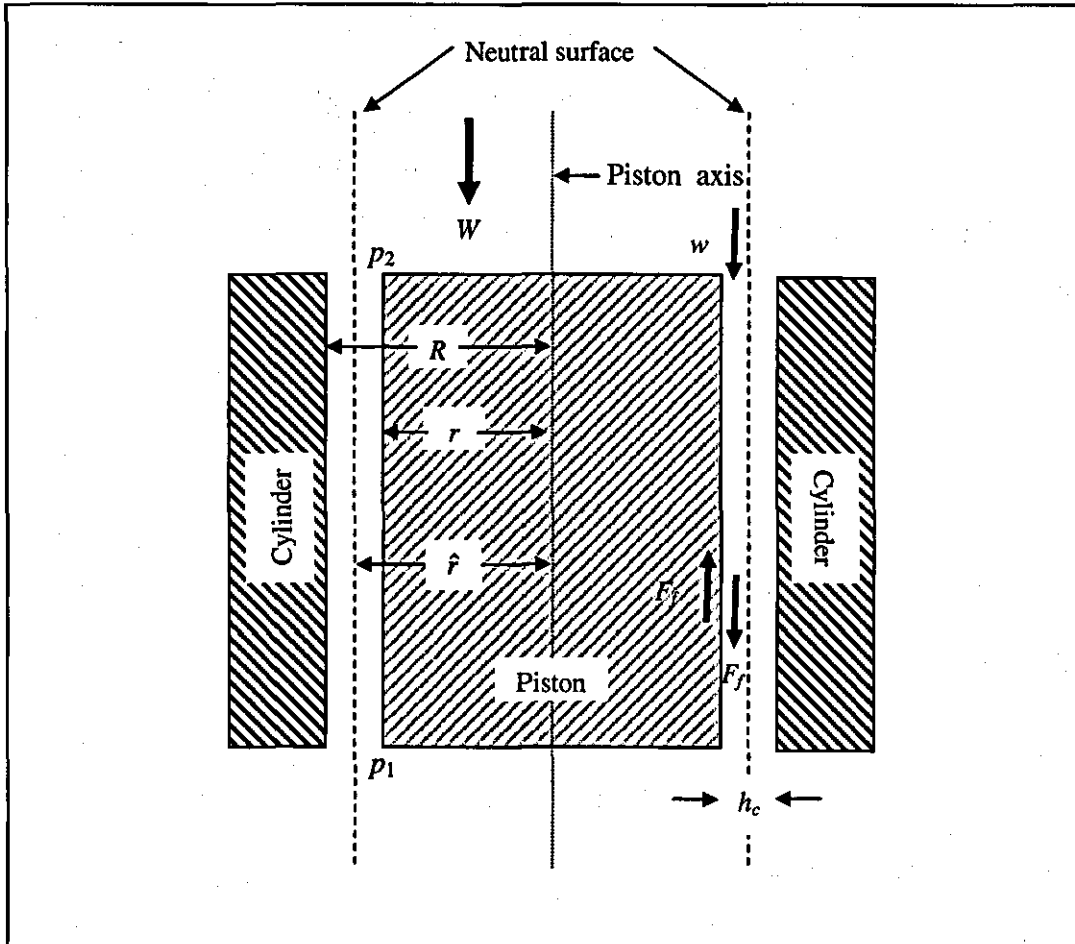


FIGURE 3.2 An ideal simple type piston-cylinder assembly

Rearranging Equation (3.16) above, the effective area, A_0 of radius \hat{r} will be given by:

$$A_0 = \frac{W' + w'}{(p_1 - p_2)} = \pi \hat{r}^2 \quad (3.17)$$

The effective area, A_0 above is the quantity that is used in the conversion equation for the calculation of the measured pressure where the applied force must be divided into.

An adequate approximation average of the radius of the neutral surface, \hat{r} , that is adopted by Dadson et al. [1982] in their monograph is $\hat{r}^2 = r^2(1+\epsilon)$, where ϵ is not likely to be greater than 10^{-3} . Consequently for an ideal model of the PCA, Equation (3.17) can be reduced to:

$$A_0 = \pi^2 \left(1 + \frac{h_c}{r} \right) = \pi^2 (1 + \epsilon) \quad (3.18)$$

However if the highest level of accuracy is required, the following approximation is advisable:

$$A_0 = \pi^2 \left(1 + \epsilon + \frac{\epsilon^2}{6} \right) \quad (3.19)$$

Equations (3.18) and (3.19) represent the effective areas when there is no vertical movement of the piston taken place, i.e. at zero fall rate. However this does not happen in reality with the piston typically dropping at a very slow rate, in order to compensate for volume losses of pressure transmitting fluid, which leaks through the clearance. In the situation where the piston drops at its natural fall rate, the effective radius is given by:

$$\hat{r} = r \left\{ 1 + \frac{h_c}{2r} + \frac{1}{6} \left(\frac{h_c}{r} \right)^2 \right\} \quad (3.20)$$

Hence the effective area of an ideal PCA which drops at its fall rate is represented by the following equation:

$$A_0 = \pi^2 \left\{ 1 + \epsilon + \frac{7}{12} \epsilon^2 \right\} \quad (3.21)$$

Unfortunately, in real situations pistons and cylinders are not perfect, having geometric irregularities or tapering along their generatrices that might reach a few micrometres [Molinar 1992, PTB 2006]. A more generalised (non-ideal) simple type PCA is depicted in Figure 3.3. The radii of piston and cylinder may vary with their axial position where u and U represent the deviations from their ideal reference radius respectively; whereas h_o

and r_o are the radial separation between the piston and cylinder, and piston radius at $x = 0$.

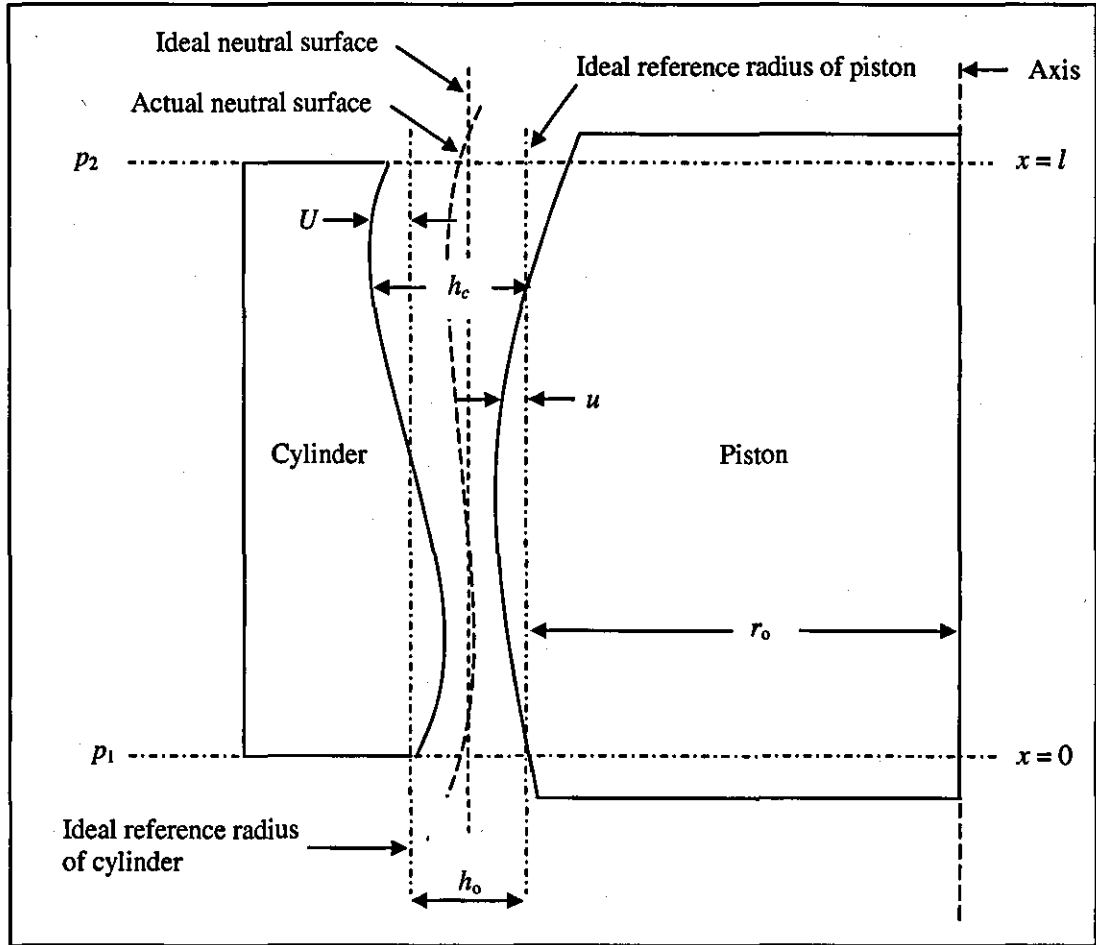


FIGURE 3.3 A generalised non-ideal simple type piston-cylinder assembly [Dadson 1982]

The effective area of a generalised non-ideal PCA can be derived by the following equation [Peggs 1977 and Dadson et al. 1982]:

$$A_0 = \pi r_o^2 \left\{ 1 + \frac{h_o}{r_o} - \frac{1}{r_o(p_1 - p_2)} \int_0^l (u + U) \frac{dp}{dx} dx \right\} \quad (3.22)$$

3.6 SUMMARY

The exact time of emergence of the pressure balance as a precise pressure measuring instrument is not clear, however it emerged approximately 150 years ago when the requirement for high pressure measurement became important after the first high pressure steam engine was built around 1800. After undergoing refinement processes for more than 150 years, the pressure balance has become a very reliable instrument used to generate and measure pressure with a reproducibility in the order of a few parts per million (ppm) and demonstrates an excellent long term stability. It fulfills the requirement as one of the primary pressure measuring instruments that can metrologically derive pressure units in a complete and independent manner with reference to the basic units of the International System of Units (SI).

The heart of the pressure balance is a PCA, consisting of an accurately made circular vertical piston that fits into a matched hollow coaxial cylinder with a very fine clearance. There are four basic types of PCA that are commonly available, as well as a few other unusual configurations. The pressure generated/measured by a pressure balance can be related to the mass of weights, local acceleration due to gravity, effective area, temperature, pressure distortion coefficient and other quantities using a pressure conversion equation. The level of accuracy of each parameter involved shall be measured/determined to some extent suitable to the accuracy of the pressure to be determined. The effective area of the actual PCA used in practice, is definitely not ideal in term surface roughness, roundness, straightness and parallelism, can be calculated using an equation recommended by Peggs [1977] and Dadson et al. [1982], that is still valid and accepted by the pressure community.

The results obtained from direct calculation of measured dimensions may introduce some discrepancies (ppm level) compared to the results obtained from cross-floating methods. This may be due to the difference in measurement nature between the two methods, interaction effects which are immeasurable using direct dimensional method, and errors introduced by the software in manipulating data which are obtained from dimensional measurements.

The next chapter will provide a review on the development of the gas-operated pressure balance and the scale of discrepancies in pressure measurement results when different techniques and approaches are applied.

CHAPTER 4

REVIEW OF THE GAS-OPERATED PRESSURE BALANCE

The development of hydraulic pressure balances started during the mid-1800s [Heydemann and Welch 1975, Dadson et al 1982, Molinar 1992], but gas-operated pressure balances started almost a hundred years later. Lack of knowledge, material and machining technology to fabricate the PCA with an acceptable radial gap between pistons and cylinder became the main reason for this delay [Ehrlich 1994].

Since the initial development of the pressure balance, the requirements to scale down measurement uncertainty in a wider measuring range (than those measured by the liquid-column manometers) have increased. Therefore the gas-operated pressure balances have attracted the attention of the metrologist and scientist to explore the critical parameters in a wide variety of approaches. This became one of the main factors towards the rapid technological improvements of the pressure balance, besides the development of high-quality air-bearing technologies during that period, which further stimulated its advancement. In this instance, the requirement for excellent geometric dimensions and tolerances, such as roundness, straightness and parallelism, were vital to minimising the gap dimensions, thus uncertainties.

The emphasis of this chapter is to review the research and developments of the gas-operated pressure balances which were carried out in the past, are currently in progress, and potential future development. The review is based on literature which starts from the earliest development, to its present situation (based on the year of publication). It is presented in each decade as follows:

4.1 The 1940s

One of the first publications related to a gas-operated pressure balance was published by Brubach [1947], who conducted research to measure the back-leak through various types of mask valves, which were used in oxygen breathing equipment. He devised a simple measuring apparatus, resembling a gas-operated pressure balance using a dry hypodermic syringe to produce a low friction gas sealed bearing. An ordinary clean and dry medical hypodermic syringe was utilised, where the plunger of the syringe was spun within the barrel. While spinning, the syringe centred itself within the barrel by the air film which acted as a bearing surface. This apparatus was used in accurate measurements of gas volume of very low pressure heads, and also gas pressures of low pressure heads i.e. as low as $0.6 \text{ dynes per cm}^2$ (0.06 Pa)

4.2 The 1950s

Brubach's experiments in 1947 encouraged Hutton [1959] to construct a tilting air-lubricated pressure balance at the National Bureau of Standards, NBS (former name for the National Institute of Standards and Technology (NIST, USA)) for ranges of differential pressures up to 0.5 inHg (1.7 kPa). Without resorting to weight changing, but with use of the toolmaker's sine bar method of angle measurement, a resolution of better than 10 ppm of full scale was achieved. Comparative tests against manometers demonstrated that this instrument agreed within 0.025% (250 ppm).

Ehrlich [1994] reported that at this time, the first commercial gas-operated pressure balance of absolute and gauge modes had already become available, which measured an approximate range of 2 to 35 kPa . Later, a gas-operated pressure balance of controlled-clearance design was constructed at the NBS in 1958. Its measuring range was approximately 2 to 4000 kPa , with the measurement uncertainty achieved being 20 ppm (2σ). The controlled clearance pressure balance then became commercially available, with the National Physical Laboratory, India (NPLi) successfully using it with an uncertainty of measurement of approximately 50 ppm (2σ).

4.3 The 1960s

Ehrlich [1994] also reported that the gas-operated tilting pressure balance first became available on the market in 1963, and by the mid-1960s, the gas-operated pressure balance had become fully established as a legitimate metrological and industrial instrument.

Dadson and Greig [1964] presented their seminal paper concentrating on the gas-operated pressure balance. This has become one of the most important sources of reference for gas-operated pressure measurement, and it is still relevant to this day. This work was the initial investigation into the possible use of the gas-operated pressure balance as a primary pressure standard, competitive with the liquid manometer. This paper covered topics on the determination of the effective area of a PCA, the effect of non-uniformities in diameter, the effect of tilt of the piston, and the effect of transition to molecular flow in the annular gap, between the piston and cylinder at very low pressures.

One year later, Dadson et al [1965] published a paper on the development of accurate high-pressure measurement, which concentrated on the elastic distortion caused by the applied pressure. Two methods were introduced to investigate the variations of the effective area due the elastic distortion. The first method (known as the similarity method) where the principle of similarity was applied to two PCAs of the same general dimensions but constructed from materials of substantially different elastic moduli. In the second method, use was made of the flow characteristics of the pressure transmitting fluid applied to two PCAs having a known difference of diameter. They reported that the distortion factor could be represented as a linear function of the pressure, where the final accuracy of its determinations was approximately $\pm 2\%$, which corresponded to approximately 10 ppm (at 100 MPa)

The principles used by Hutton in 1959 attracted Douslin and Osborn [1965] to develop an inclined pressure balance that was needed in thermochemical research, which required accurate vapour-pressure measurements in the low and intermediate pressure

range (1.3 – 4000 Pa). They introduced a unique oscillatory method to reduce residual friction between the piston and the cylinder, hence allowed full sensitivity of the gauge to be realised. On the other hand, a goniometer of readability 1 arcsec (0.0003°) was utilised in declination angle measurement that was to adjust the weight to area ratio, where the accuracy in a range of 0.1 to 1.6 Pa from lower to upper pressure range was claimed.

4.4 The 1970s

Bass and Green [1972] published one of the first papers to compare the effective area calculated using two different methods:

- From dimensional measurements combined with Dadson's model [Dadson et al. 1965] for pressure dependence.
- From measurements obtained via cross-floating against a mercury manometer.

They revealed that the differences between these two methods at 100 kPa (in absolute and gauge modes) were less than 10 ppm.

In order to improve the performance in cross-floating experiments using gas-operated pressure balance, Markus [1972] introduced a constant volume valve which minimises the volume change in the gas system during valve operations. He claimed that the volume change was less than 0.15 mm^3 between the open and closed positions, with the leak rate less than $5 \times 10^{-5} \text{ mole/sec}$ at 100 kPa differential pressure. The valve was designed to withstand the full differential pressure of 140 MPa.

Heydemann and Welch [1975] discussed the basic equations used in calculating pressure generated by the pressure balances (involving basic laws of thermodynamics) and the elastic distortion coefficient, which became the largest source of error (contributing to the change of the effective area with pressure) besides temperature effects, air buoyancy and head corrections. They also discussed various designs of PCA, (including irregular

designs such as ball gauges and grooved pistons), calibration of pressure balances and the use of pressure balances.

A method of computing the effective area of a pressure balance from diametral measurement was published in a NPL report by Peggs [1977]. He described a computer program that enabled the effective area to be determined, either in a compressible or a non-compressible pressure transmitting fluid.

Peggs and Lewis [1977] reported their work on the NPL primary pressure balance standard, in order for realisation and maintenance in accordance with the SI pressure unit (Pa). Three main issues were discussed:

- Dimensional measurement of the pistons and cylinders.
- Comparisons with a precision mercury column via a transfer standard.
- The three different methods of providing information on the relative dimensions of the pistons and cylinders.

Thorough analysis on the uncertainty budgets were presented, where Peggs and Lewis [1977] estimated that the overall uncertainty of the pressure measurement (1 to 4 MPa) was no more than 20 ppm at 99.7% (3σ) level of confidence, with 1 ppm contributed by the random uncertainties.

Continuous efforts have been carried out to improve the uncertainty of measurements using pressure balances from various perspectives. Prowse and Hatt [1977] are believed to be the first who published their investigations on the rotational effects into the performance of a gas-operated pressure balance. They experimented on three PCAs of different sizes, but detailed measurements have been made on only one PCA, which was 81 mm^2 (measuring range of 11 to 300 kPa). Experimentation was carried out with the rotational frequency ranging from less than 30 to 1000 rpm. They found that the usual relative rotation of the piston and cylinder with added masses, could produce a pressure effect up to ten times greater than the accuracy of measurements relative to vacuum. The

magnitude of this pressure effect depended on the rotational frequency and whether a bell-jar was in place or not. They also found that the gas-operated pressure balance was insensitive to rotation at about 100 rpm.

Bass [1978] published concerning the analysis of the contribution of the radial deformation and viscous effect to the effective area of the PCA, using varied experimental techniques at 40, 80, 120 and 160 kPa, for different PCA geometries and materials of construction. Lack of information on the suitability of the pressure balance at high levels of accuracy, and relatively low pressures motivated Bass to carry out this investigation. This work identified a significant correlation between the theoretical model and experimental data, and suggested that the pressure balance could be used to replace a mercury manometer without serious degradation in the overall absolute accuracy, at a low gauge pressure ranging from 10 – 160 kPa.

Similar studies as Prowse and Hatt [1977] were carried out by Sutton [1979] using the same model of pressure balance, in order to report in a more accurate manner regarding the variation of pressure with rotational frequency. He found that at low rotational frequencies (180 to 600 rpm), the generated pressure increased with the square of the frequency, and that the extrapolated pressure for zero frequency (aerodynamic forces are zero) corresponded to the calculated pressure. Furthermore, his work demonstrated that at low frequencies, the force due to the rotation acting on the pressure balance was almost independent of load applied, and the force due to rotation of the PCA was independent of its effective area. Both studies [Prowse and Hatt 1977, and Sutton 1979] discovered that differences corresponding to hundreds of ppm in relative pressure value might be observed at high speeds of rotation, under certain gauge-mode operating conditions.

Research on a modified version of a gas-operated (gas-lubricated) pressure balance was carried out in the late 1970s when the manufacturer of pressure balances (Desgranges et Huot Company, France) introduced a gas-operated oil-lubricated pressure balance. This type of design was intended for high pressure applications where the test medium was of

any type of non-corrosive gas [DH-Budenberg n.d. c]. The main advantages of this type of pressure balance were:

- Fall rate of the piston was much lower especially at high pressure compared to the gas-operated gas-lubricated pressure balance, hence gas pressure measurement could be accurately measured up to 100 MPa.
- Eliminates the needs of oil/gas interfaces or separators that supplement other sources of uncertainty in the system.

However, the performance of this type of standard was not comparable to the gas-operated gas lubricated pressure balance due to lack of sensitivity in measurement as a result of oil-lubrication, and the contamination in the clearance between piston and cylinder became a potential problem [Ehrlich 1994].

Lewis and Peggs published a book in 1979, republished in 1992 [Lewis and Peggs 1992] as a practical guide on how to use the pressure balance. It covers the theory of the pressure balance, practical aspects of use including balancing procedures (cross-floating method) of the gas-operated pressure balance, evaluation of pressure generated, evaluation of effective area from pressure balance comparisons, and estimation of measurement uncertainties.

In order to ensure the degree of equivalence, which led towards increased technical confidence to the values attributed to the NPL and the PTB standards, an intercomparison between these two institutes was carried out [Peggs et al. 1978]. Measurements were completed at 100 kPa in absolute mode, and in the range of 20 to 100 kPa in gauge mode. The uncertainties quoted by the NPL were 19 and 18 ppm in absolute and gauge modes respectively, whereas PTB were 40 and 34 ppm, both NMIs at 99.7% (3σ) level of confidence respectively. The results of the experiments carried out indicated that both pressure balances performed well in the pressure range 100 kPa (absolute mode), and from 40 to 100 kPa (gauge mode) with the maximum mean fractional difference being 14.4 ppm and 1.9 ppm respectively.

As a consequence of the research and development within this decade, gas-operated pressure balances became common within the NMIs by the late 1970s, leading to more theoretical and experimental investigations. More results were then published demonstrating various effects that were commonly encountered during the measurement processes in the next decades.

4.5 The 1980s

Aerodynamic effects encountered in the experiments carried out by Prowse and Hatt [1977] and Sutton [1979] resulted in Sutton [1980] producing another paper devoted to an improved mechanism for spinning the floating element of a gas-operated pressure balance. He utilised a continuous rubber belt to impart a torque to the floating element at rotational frequencies up to approximately 1000 rpm, in either direction (clockwise or counter clockwise). The floating element was freely rotated to eliminate contact, hence friction between the piston and the cylinder. Besides the free rotating mechanism, the motor was mounted in such a way that it did not significantly affect the thermal stability of the PCA.

More intercomparisons of gas-operated pressure balance were completed during 1980s, when the Laboratoire National d'Essais (LNE) and NBS (now NIST) conducted a bilateral intercomparison over the range of pressure of 0.4 to 3.9 MPa. Two pressure balances of different principles and operating mediums were intercompared. LNE used an oil-operated pressure balance of a simple type PCA, calibrated against a standard whose effective area was the average of the measured area. The NBS used its primary gas-operated pressure balance of a controlled clearance type PCA, with the effective area derived from the measurement of the piston only. A coaxial capacitor gas/oil separator was used to connect both these pressure balances. The agreement between these two NMIs was within 6.4 ppm based on calculated effective area, and 3.3 ppm based on the pressure generated, thus demonstrating the two different methods employed were well verified at this pressure range.

Dadson et al [1982] published a book containing discussion and thorough review of the pressure balances. It covers the introductory discussion of history, basic concepts, terminology etc., followed by a thorough description of the fundamentals of the pressure balance, such as the hydrodynamic theory of the instrument, effects of elastic distortion, methods of deriving effective areas of the PCA from the first principles etc. More specialised developments and applications are also discussed in depth, and it finishes with detailed elaborations on a number of small departures from ideal behaviour, which are likely to be of particular concern to the specialists who are dealing with state-of-the-art uncertainties.

Verification on the effective area determined via the direct dimensional measurement method against the cross-floating (pressure generated) method continued. This occurred through a bilateral intercomparison between the IMGC and the NBS, where a primary gas-operated pressure standard of the IMGC was compared against two pressure balances of the NBS. Intercomparisons were made using the pressure generated method i.e. by a "transfer" gas-operated pressure standard (PG23) of NBS, and a primary gas-operated pressure standard (PG24) of NBS. The effective areas of both primary pressure standards were determined by direct dimensional measurements, whereas a transfer pressure standard was determined by intercomparison with another pressure balance or liquid manometer. The agreement between the average pressure generated by the IMGC primary pressure standard and the NBS transfer pressure standard was within 7 ppm (over the range 0.75 to 5.0 MPa), and the agreement between the IMGC primary pressure standard and the NBS primary pressure standard was within 6 ppm (over the range 0.5 to 1.5 MPa). The agreements were well within the estimated uncertainties of the pressure balances involved.

Very large PCAs were developed at LNE, France in the mid-1980s, which were significantly larger than the ordinary PCA at that time. PCAs with 35 mm piston diameter, specially fabricated with the piston-cylinder clearance in the order of 1 μm , roundness within 0.1 μm and straightness within 0.15 μm , began to be used as the primary pressure standard for France [Legras 1994a]. The diameter of the pistons and

cylinders were determined through dimensional measurements, which made the effective areas directly traceable to the primary length standard (i.e. the metre).

Delajoud and Girard [1981] published on the development of a digital read-out pressure standard which provided much greater convenience compared to the traditional method of achieving equilibrium using ordinary pressure balance (especially in the cross-floating method). It consisted of a PCA and a dynamometer which was well coupled so that the piston was free to slide within the cylinder and their axes were coaxial and vertical. The dynamometer was directly adjusted by the weights, hence ensuring the derived pressure were from mass, length and time. Similar topics have been discussed by Dargent [1994]. However, parasitic perturbations due to the piston's rotation became a problem in the measurements, although it was shown to be within a few parts in 10^5 when used as a transfer standard during intercomparisons [Legras 1994b]. Its status to be categorised as a primary pressure standard is still a controversial issue.

Detailed investigations on two primary gas-operated pressure standards of 2 and 5 MPa measuring ranges were completed by Maghenzani et al. [1987] in gauge mode operations. The performance of each pressure balance was evaluated as regards to fall rate reproducibility, rotational frequency reproducibility, and the possibility of the influence of the gas species N_2 (nitrogen), He (helium) and CO_2 (carbon dioxide). These investigations revealed that no significant differences were observed when different gas species were used. Helium was found to be a very satisfactory fluid alternative to N_2 , but CO_2 was recommended to be avoided in primary pressure applications due to poor reproducibility. The overall uncertainty in the gauge mode pressure measurements with the two pressure balances in the range of 0.1 to 5 MPa was consistently better than 14 ppm.

Assessment of the suitability of several gas species as a working pressure transmitting fluid was carried out by Sharma et al. [1988]. They characterised a controlled clearance pressure balance up to 5 MPa, by measuring the fall rate of the piston as a function of the jacket pressure, P_j . The pressure transmitting fluids investigated were Ar (argon), N_2 ,

He and H₂ (hydrogen). They found that a relatively better reproducibility in the stall jacket pressure, P_z (the value of the jacket pressure at which the clearance between the piston and the cylinder is zero) was obtained for He and H₂ compared to Ar and N₂. Therefore, Helium was confirmed to be suitable to be used in addition to N₂, but a higher value of P_j was required to get a good floating condition.

4.6 The 1990s

After undergoing refinement processes for more than forty years, gas-operated pressure balances have become the common primary pressure standards around atmospheric pressure, because they have several advantages over the mercury manometer such as; higher measuring capacity, lower thermal expansion coefficient and portability [Legras 1994a, Legras 1994b]. However, the suitability of the gas-operated pressure balances as a primary pressure standard, i.e. as an alternative to the mercury manometer, becomes an issue for debate. More recent intercomparisons between gas-operated pressure balances and primary standard manometers have shown that there are some significant unexplained differences between them.

Schmidt et al. [1994] identified that a number of researchers had reported that the gas species used may cause significant difference, whereas the mode of operations (absolute and gauge mode) may cause up to 25 ppm differences. This prompted them to investigate the mode (absolute and gauge modes) and gas species affecting the effective area of the PCA using He, H₂, N₂ and SF₆ (sulfurhexafluoride), which demonstrated significant differences in the rotational dissipation between the four gas species. Through these studies, a mathematical model to relate effective area with gas species was developed, but with this limited theory it indicated a change of less than 2 ppm in the effective area when the mode was changed.

Further effects were observed on the pressure generated, when the same pressure balance was operated in two different modes. Significant differences in the rotational dissipation were observed between the four species of gas especially between He and

other gas species, and even larger differences were observed (especially with the same gas species) between the two operational modes (gauge and absolute). Consequently, the measured results were transferred into a basic model (for the momentum transfer function) that was used to interpret the rotational dissipation, which depended on the pressure profile due to the gas species in the clearance between piston and cylinder. Good agreements were obtained between the measured and modeled results for all four gas species.

Similar experiments have been carried out by Meyer and Reilly [1994] using H_2 , 3He (helium-3), 4He (helium-4), N_2 , CO_2 and SF_6 . They found that the effective area differences ranged from 26 ppm (at 1.4 kPa) to 4 ppm (at 45 kPa). However, the maximum differences were constant at 6 to 7 ppm from 100 kPa to 162 kPa. These findings supported the claims that the effective area is gas-species dependent, especially at the lowest pressure (1.38 kPa). Meyer and Reilly [1994] noted that effects are "instrument-dependent" for the highest accuracy pressure measurement.

Extended research on the effect of gas species and the mode of operation (absolute, gauge and intermediate modes) affecting the effective area of the PCA using He and N_2 have been carried out at NIST. This research has included the vertical and rotational effects into considerations, aimed at providing further evidence that these two effects were under controlled conditions. Through these studies, a mathematical model to relate effective area with gas species was developed [Schmidt et al. 1994], and predicted that the effective area should increase monotonically by about 6 ppm of the geometric piston area. However, the mode effects remained cannot be predicted.

Legras [1994a] published work entitled 'Stability of Piston-Cylinder Assemblies from an Experience of Fifteen Years', which emphasised the possibility to construct pressure balances for use as primary pressure standards with a reproducibility of less than 1 ppm. He demonstrated that it was possible to characterise them in the SI system with the uncertainty of measurement of approximately 5 ppm. This work also presented methods used at the LNE to check the stability of the PCAs and to improve knowledge of the

effective area determinations, and at the same time described the results obtained over a period of more than fifteen years. The methods presented were known as:

- The “ Δp Method”, which was introduced (implemented in 1975) to eliminate effects such as surface tension, and mass or density of the piston in the determination of the effective area.
- Calculate the ratios of the effective values “two by two”, i.e. when the materials of the two PCAs and the set of masses were the same, and when the dimensions of two PCAs and the altitude of the two reference levels were the same.

Other efforts to bring the uncertainty of measurement to the lowest possible level have been carried out through studies of other factors that may contribute to the effects, such as surface finish treatment of masses, magnetic and electrostatic forces, method of rotation, interface between weights and piston, cleaning technique of the PCA, torque applied in mounting the cylinder etc. [Ehrlich 1994]. As an example, the effective area of the test PCA of a nominal area of 98 mm^2 , determined by an ordinary cross-floating method, showed a small increase with increasing torque, where the effective area of the PCA was measured using three different values for the mounting torque. It was found that the maximum increase in the effective area was approximately 2 ppm at a torque value of 8 Nm [Rantanen 1994]. Furthermore, it was mentioned that in order to achieve the maximum accuracy, the PCA should be calibrated with its own balance body, hence indicating that the advantages of the inter-changeability features were lost.

Intercomparison is one of the approaches to allow standards to progress continuously and it is the best tool to evaluate the quality of standards and to validate the uncertainties estimated. Intercomparisons allow the detection of any possible systematic errors, experimental errors, missing contributing factors in uncertainty budget, or mistakes in calculations [Legras 1994b]. Intercomparisons in the whole range of pressure measurement have been carried out since 1975 with more structured activities taking place after the establishment of the Consultative Committee for Mass and Related Quantities (CCM) in 1980 [BIPM 2006d].

One of the intercomparisons was the comparison of a mercury manometer in the 10 kPa to 140 kPa range (absolute and/or gauge mode), which made use of a gas-operated pressure balance as a transfer standard, and participation from thirteen laboratories. The progress was reported by Stuart [1994], documenting that the transfer standard had shown good repeatability and long-term stability. However, the results demonstrated significant difference for several participants which were believed to be due to the transfer standard behaving differently in the two modes.

Significant differences (unsatisfactory results) were also seen through a bilateral intercomparison between a pressure balance of the LNE and a mercury manometer of the All-Russian Research Institute for Physical, Technical and Radio-Technical Measurements (VNIIFTRI) in the range of 30 to 110 kPa [Astrov et al. 1994] using N₂ and He as a pressure transmitting fluids. A relative difference of 12.2 ppm was considered significant as the comparison was estimated at 8.4 ppm (2σ), with unexplainable phenomenon.

Similar degrees of disagreement were found in a bilateral comparison between LNE and PTB, with relative differences of up to 11.6 ppm [Klingenberg and Legras 1994]. The differences in effective area determination were due to the differences in the dimensional data obtained by the two NMIs (insufficient accuracy), even though these values were reproducible in dimensional measurements within 1.6 ppm. They also highlighted that the difficulty in finding the correct reference position became the probable reason in the differences encountered, and noted that cross-floating intercomparisons using pressure balances were possible at ppm levels.

Jain et al. [1993] published concerning the intercomparison of the effective areas of a gas-operated pressure balance of 1 MPa capacity determined by different techniques. The intercomparison involved four PCAs of 35 mm diameter as the test units, aimed at investigating the consistency in their effective areas obtained by one or more of the following methods:

- Calibration against a pressure balance standard (1.4 MPa capacity), that had a traceability chain to the NIST Gas Thermometer Manometer (GTM) of 0.1 MPa capacity via another pressure balance (0.3 MPa capacity).
- Cross-floating intercomparisons between the test PCAs.
- Direct geometrical measurements.
- Calibration of one of the test PCAs against a controlled-clearance pressure balance (7 MPa capacity).

They found that the overall level of agreement between the three different techniques used was within 10 ppm, i.e. within the estimated total uncertainties of the individual techniques.

Jain et al. [1993] suggested that further investigation should be carried out to understand better the effects of factors such as the molecule-surface interaction, the pressure profile and the flow of gas through the clearance between piston and cylinder in order to get increased confidence in the effective area values derived through the direct geometrical measurement. The work also concluded that there was the possibility of a simple type PCA of larger-diameter to be used as a primary pressure standard (with higher degree of confidence based on direct geometrical measurement), once a good understanding of these effects was obtained and with improved accuracy of geometrical measurement.

The development of PTB's new state-of-the-art Abbe-type length comparator for measurement of the diameter and form has contributed significantly to the effective area determination, especially for very large PCAs. This comparator, which uses contact probe techniques, was utilised to calibrate 35 mm diameter PCA. This PCA has served as a transfer standard in the CCM 1 MPa pressure intercomparison between NIST, LNE, IMGC and PTB [Neugebauer 1998]. The PCA was also calibrated with another Abbe-type comparator, which agreed within the ranges of uncertainty quoted. The expanded uncertainty obtained using this new comparator was 11 nm ($k = 2$) which is the smallest ever achieved for a 35 mm diameter PCA.

To compare the effective area results determined from the dimensional measurement against its determination through direct pressure measurement, the Czech Institute of Metrology (CMI) carried out an international pressure comparison with the PTB, ranging from 0.07 MPa to 0.4 MPa, in absolute and gauge modes [Tesar et al. 1999]. The transfer standard used was a gas-operated pressure balance with a 35 mm diameter PCA (ceramic piston and tungsten carbide cylinder). The reference pressure standards were a primary pressure balance with 1 MPa capacity, used in gauge mode comparison, and a primary standard mercury manometer of 0.2 MPa range, used in absolute and gauge mode comparison. The reports showed that there were very small differences in effective area values determined from dimensional data and measured pressure (3.4 ppm), and also noted that the change in effective areas were very small between measurement in gauge and absolute mode (1.5 ppm).

Under the auspices of the CCM of the International Committee for Weights and Measures (CIPM), a key comparison was conducted. It was divided into two phases, i.e. Phase A1 and A2. In the Phase A1 key comparison, all participants were required to determine the effective areas from dimensional measurement on two PCAs of 35 mm diameter (in the pressure range from 0.05 MPa to 1 MPa). The main difference between the two PCAs that were used as transfer standards was the piston material, where one was tungsten carbide and the other one was ceramic, while both cylinders were tungsten carbide.

The participants (IMGC, Italy; LNE, France; NIST, USA; NPL, UK and PTB, Germany) were required to perform diameter, straightness and roundness measurements on each piston and cylinder, and calculate the effective area of each PCA using their own method. Molinar et al. [1999] reported that the effective areas determined by participants from dimensional data agreed within two standard uncertainties with the reference values, and their deviations with the reference values were reproducible within 5 ppm for both transfer standards. However, twenty-six out of eighty diameters were found to differ from their respective reference values, hence Molinar et al. [1999] highlighted the

need for harmonisation of diametric measurements between national metrology laboratories.

In Phase A2, the same PCAs that were used in phase A1 (associated with their own balance bases) were circulated to the same participants (as in phase A1) for effective area determination from pressure measurement, i.e. by comparison with respective laboratory pressure balance standard. The objective of the second phase was the comparison of pressure standards at the lowest uncertainty, where the observation of the behaviour of both PCAs made from different material (from two manufacturers) was also considered [Legras et al. 1999b]. Findings from this intercomparison were:

- Comparison results were considered as fully satisfactory, with very few laboratory differences from the average value being greater than 5 ppm.
- There was no significant difference observed in the behaviour, particularly for the standard deviations and deviations from linearity between two of the transfer standards.
- Both standards have shown a repeatability expressed in relative standard uncertainty of less than 1 ppm over a large pressure range.
- This work demonstrated that there is a possibility in the future to achieve 1 ppm level comparisons of national standards.

Other developments in gas-operated pressure balances can be seen when Delajoud et al. [1999] published on the development and characterisation of a 50 mm diameter gas-operated pressure balance, as the primary standard in atmospheric range, aimed at less than 5 ppm level of relative combined standard uncertainty. Pistons and cylinders were made from ceramic, where they were designed as controlled-clearance types with the cylinders as the rotating parts. All pistons and cylinders were then characterised dimensionally at NIST, with subsequent calculation of the effective areas and associated uncertainties. The performance of these pressure balances was examined by comparing them, where the mode of operation and gas-species dependence of the effective areas

were also investigated. This work provided preliminary support to the proposal that by sufficiently reducing the piston-cylinder clearance to radius ratio, the relative influences of operating mode and gas species will be reduced to less than 2 ppm. Ceramic/ceramic combination of the PCA has demonstrated practical difficulties associated with static charging at low starting pressure. As a consequence, tungsten carbide/tungsten carbide PCAs were considered preferable for the primary standard since better quality of surface finish and higher Young's modulus with tungsten carbide were beneficial to the dimensional characterisation process.

A model for drag forces in the clearance of the gas-operated PCAs in the viscous-flow and molecular-flow regimes was presented by Schmidt et al [1999]. The effects due to the operational mode (gauge and absolute) and gas species at low-pressure (up to 130 kPa) were their prime concern, to quantify the possible differences in geometrical effective area and mode of operation effects. Data was obtained from six different gas species i.e. He, Ne, N₂, Ar, Kr (krypton), CO₂. The behaviour of the gas-operated pressure balance became predictable, with respect to the viscosity and molecular weight of the pressurising pressure transmitting fluid, but not the magnitude of the shift in effective area between two modes. Due to this unexplained possible shift, NIST has included 6 ppm (1 σ) in their uncertainty budget since their primary pressure standard was a mercury manometer, of absolute mode. Model results were compared with published measurements of the effective area of several pressure balances, in which relative changes as large as 30 ppm were observed when different pressurising gases were used.

4.7 RECENT RESEARCH (2000 – 2006)

Schmidt et al. [2000] reported that two techniques used at the NIST, to realise pressure up to 1 MPa, using controlled-clearance pressure balances and mercury manometer, demonstrated drawbacks. These were due to its dependence upon a linearised model and extrapolation procedure that limits the minimum uncertainty, in the first case. Whereas

in the second case, problems were due to the limitation of coverage (pressure range) that introduced larger uncertainty at higher pressure.

Recent development and advancement in the technology of fabrication of high-quality large-diameter (35 mm) PCA with excellent geometry and very small clearance, with the ability to characterise them to very high accuracy (few tens of nanometer), have allowed the effective area determination to reach a relative standard uncertainty $u(A_e)/A_e$ of approximately 1.4 ppm (1σ). This value has been supported with close agreement within 2.5 ppm compared to the value obtained via NIST's Ultrasonic Interferometer Manometer (UIM), and agreed within 1 ppm compared to previous measurements carried out some years ago (even though new measurements yielded substantially reduced uncertainty) [Jain et al. 2003]. These achievements have allowed the NIST pressure balance to generate pressures that approach total relative uncertainties previously obtained only by manometers, hence improving the international acceptance of dimensionally characterised pressure balances as a primary pressure standard, as an alternative to manometers.

A future candidate of a primary pressure standard was highlighted by Schmidt et al. [2005] when they presented on a progress of a primary pressure standard at NIST, which uses a totally different methods compared to a manometer or pressure balance. This new instrument realised pressure based on the dielectric permittivity of helium. They have targeted a development of a new primary pressure standard that could measure with a relative standard uncertainty of 6 ppm in the range of 0.4 to 7 MPa.

In general, the current research trends at leading NMIs (NPL, PTB, LNE, NIST, IMGC etc.) on the gas-operated pressure balance are as follows:

- Further investigation on traceability systems that are based on the pressure balance as a primary pressure standard, where the entire national pressure scales are traceable to one source of reference i.e. dimensionally characterised pressure balance through stepping-up and stepping down procedures.

- Establishment of sub-micrometric dimensional measurement system for effective area characterization of large diameter PCA.
- Use of a simple type tungsten carbide PCA instead of control-clearance type.
- Research on non-rotary digital piston manometer.
- Research on the elastic distortion coefficient of the PCA, especially on high pressure system.

4.8 SUMMARY

The technology and theoretical advancement of gas-operated pressure balances can be seen over the last forty years, where the improvement in materials and manufacturing technologies have resulted in instruments of simpler design with superior performance over broader operating pressure ranges. This advancement is further stimulated with various types of investigation that have been carried out, such as investigation on the effects of the rotational speed, gas species, mode of operation, rotational drag, direct dimensional measurement etc.; including the incorporation of computers and advanced electronics into commercial pressure balances. Intercomparisons conducted have become the best tool in evaluating the quality of standards produced by the participating NMIs, and at the same time validate their uncertainty budget, so that the values disseminated by each NMI are coherent with the internationally recognised SI unit for pressure, the pascal (Pa).

However, intercomparisons have shown disagreements between NMIs which are unexplained. Therefore, Ehrlich [1994] suggested that in order to get a better understanding of such unexplained effects, the requirements for better physical and mathematical models of the pressure balances system are necessary. Furthermore, it should start with the most fundamental definition of the effective area, i.e. the full air buoyancy corrected weight of the piston and masses, divided by the gauge pressure at the specific reference level under balance conditions, followed by other effects that should be explicitly accounted for at microscopic levels. Molinar [1992] stressed that the

pressure balance could approach the accuracy of the mercury manometer only if parameters such as gas species, mode of operation, possible hydrodynamic effect of weights, frequency of rotation, electrostatic charges, surface magnetisation etc., are fully understood and minimised.

This literature review has clearly shown that no investigation related to surface texture (on the PCA) has been carried out or published, except by Wan Mohamed and Petzing [2005]. Surface texture on the PCA is believed to be one of the factors that contributes to these unexplained effects.

CHAPTER 5

MANUFACTURING PROCESS

A proper pressure balance design, and appropriate method of trimming and matching of the PCA have been used to assist in characterising the issues associated with the effect of surface texture against the pressure. The manufacture of pressure balances and PCAs involves a number of manufacturing processes, in order to control the geometric and pressure tolerances of the working system. Precise control over the processes, especially those involved in the manufacturing of PCAs, has provided the ability to accurately develop various surface textures on the pistons. The final process involved in developing PCAs were lapping and polishing, simply a two-motion action (rotation and reciprocation), low pressure and abrasive machining process which are used whenever there is a requirement for highly accurate sizing and tolerances. With the correct manufactured PCAs and pressure balances, characterization work carried out is anticipated to demonstrate the relationship between pressure generated and surface texture applied.

The material presented in this chapter describes the overall manufacturing processes, for the pressure balances and the PCAs. Section 5.1 describes selection of materials for the PCA and the pressure balance. Section 5.2 provides information on manufacturing of the pressure balance, where its design and construction are highlighted. Next, Section 5.3 elaborates about the manufacturing of PCAs which begins with initial PCAs made of scrap materials, subsequently the manufacturing of 316 stainless steel PCAs, which ended with unsuccessful results. Section 5.4 provides a detailed account of the trimming and matching techniques for the tungsten carbide PCAs, which have been successfully manufactured, and finally used in the experimental work. Lastly, Section 5.5 summarises all of the information discussed in this chapter.

5.1 SELECTION OF MATERIALS

The selection of materials is governed by many factors, so appropriate materials must be identified before manufacturing processes begin. This was due to the functionality of the parts in the system (to ensure their reliability and performance), which is highly dependant on the material used. The most critical parts which have needed to be carefully considered, are the PCA and the weights of the pressure balance, however their criteria are different. Therefore, the selection of materials has been divided into two groups, i.e. material for the pressure balance and material for the PCA.

5.1.1 Materials for the Pressure Balance

The main specifications of the material for the pressure balance (especially the weights) are in accordance to the specifications of standard weights, which are commonly available in literature and as standards documents. From the International Organisation of Legal Metrology (OIML) and Mettler-Toledo GmbH, the specifications are as follows [OIML R111-1 2004, OIML R110 1994, Mettler-Toledo 1991]:

- The weights shall be of corrosion resistant material, against the active constituent of the atmosphere such as ozone, ammonia and water vapour.
- The hardness of the weights' material and their resistance to wear shall be similar, or better than austenitic stainless steel (Vickers hardness, $HV \geq 260$ or Brinell hardness, $HB \geq 160$). The quality of the material shall be such that the change in the mass/surface of weights due to physical actions in relation to the maximum permissible error are negligible under normal conditions of use and the purpose for which they are being used.
- The material of weights and the body of the pressure balance shall be practically non-magnetic (preferably magnetic susceptibility, $\chi \leq 0.2$).
- The behaviour of the surface resistance on electrostatic charging for weights and the body of pressure balance shall at a minimum level, hence most of the metals are acceptable.

- The material of the weights shall be able to be ground or polished so that their surfaces have no rough spots or porous sites visible to the naked eye.

Stainless-steel 316 has been identified as a candidate for all parts involved in the construction of the pressure balance since it complies with all of the specifications above, as well as its cost-effectiveness and machinability factors. However, aluminium alloy of Grade 6082 T6 has been chosen for the base of the pressure balance since it is cheaper, and supported with the fact that the base only needs to be non-magnetic and has excellent resistance to electrostatic charging.

5.1.2 Materials of the Piston-Cylinder Assembly (PCA)

A great number of materials can be used for gas-lubricated PCAs, however its suitability in application must be considered. Gas-lubricated PCAs require more demanding specifications and tolerances than the components of oil-lubricated PCAs. Furthermore, the materials (and their combinations) must be compatible friction-wise without the aid of any additional liquid lubricants, except the compressed pressure transmitting gas which is used in measurement. These two criteria made the selection work more difficult and limited the options, thus a compromise had to be made. These difficulties and limitations were made worse by there being very little information about the performance of various combinations of materials within the literature. The specifications of materials to be chosen are quite similar to those required for gas bearing materials, which are as follows [Grassam and Powell 1964, Molinar 1992]:

- **Machinability** – the materials shall be able to be machined to the high quality bearing surfaces (highly polished to sub-micron level) and demanding exceptional dimensional tolerances with a uniform clearance (better than 2 μm) between two surfaces. Hard materials are preferable when these two conditions become a requirement.
- **Stability** – the material shall be highly stable physically and metallurgically, so, once excellent geometrical and surface finish is achieved, they are not subject to unpredictable distortions, which can be permanent or temporary.

- Strength and elasticity – mechanically, the material shall be able to withstand high compressive loads under elastic conditions.
- Thermal expansion – self generated and external heating can lead to uneven temperature distribution and deformation of the PCAs, hence the materials with low thermal expansion are preferable.

Table 5.1 shows the materials which have been considered:

TABLE 5.1 Materials which have been considered for the PCAs [Budinski and Budinski 1999]

Material	Hardness (HV)	Modulus of Elasticity (GPa)	Density (kgm ⁻³)	Thermal conductivity (W/m °K)	Thermal Exp.Coeff. (10 ⁻⁶ m/m/°K)
	Mechanical Property		Physical Property		
Aluminium Oxide, Al ₂ O ₃	1900	360	3920	34	7.4
Silicon Nitride, Si ₃ N ₄	1750	310	3200	33	3.1
Silicon Carbide, SiC	2550	405	3200	60	4.5
Toughened Zirconia, ZrO ₂	1300	204	6000	6	8.5
Cemented Tungsten Carbide WC / 6%Co	1600	612	17200	86	7.4
Stainless Steel 303	260	193	7800	16	17.3
Stainless Steel 304	260	193	7800	16	17.3
Stainless Steel 316	260	193	7800	16	16
Be Copper (C17200)	410	131	8250	107	17.8
Titanium Ti-6Al-4V	360	114	4500	7.2	9.5

316 stainless steel was chosen based on its excellent performance as standard weights, supported with the fact that its detailed material properties (physical, mechanical and chemical) can easily be identified in literature (if required). Its softness (compared to

other selected materials in Table 5.1) also became one of the reasons why it was chosen, with the assumption that “the softer, the easier manufacturing process will be”.

5.2 MANUFACTURING OF THE PRESSURE BALANCE

Two identical gas-operated pressure balances were designed and manufactured (at Loughborough University, LU) for measuring pressures at a very demanding relative uncertainty budget (approximately 10 ppm, at $k = 2$), as detailed in the schematic diagram of Figure 5.1. Figure 5.2 shows the manufactured pressure balances before being inter-connected in a common pressure circuit. Manufacturing processes for the pressure balances were workshop based and straight forward, however particular attention was paid to their design and construction, so that the highest level of accuracy in pressure measurements was achievable.

The base of the pressure balance is triangular in shape [Nagano Keiki n.d.], manufactured from a solid aluminum plate of 25 mm thickness with 340 mm cross-section, and supported with 3 adjustable leveling feet. The mounting post which is directly attached to the base plate is made from 316 stainless steel of 90 mm diameter and 214 mm height. A large weight loading bell (102 mm inner diameter) associated with the weights was designed in order to accept very large PCAs, i.e. 35 mm diameter (and 50 mm diameter PCAs, intended for future work). These dimensions were chosen to accommodate the design, towards comfortable handling and capable of measuring pressures up to 400 kPa using 35 mm diameter PCAs.

Each pressure balance has been manufactured with a set of 36 kg weights as a combination of disk weights and ring weights. The weights can be combined in any order to the nearest 100 g over the full range (400 kPa). The combination of the weights is shown in Table 5.2.

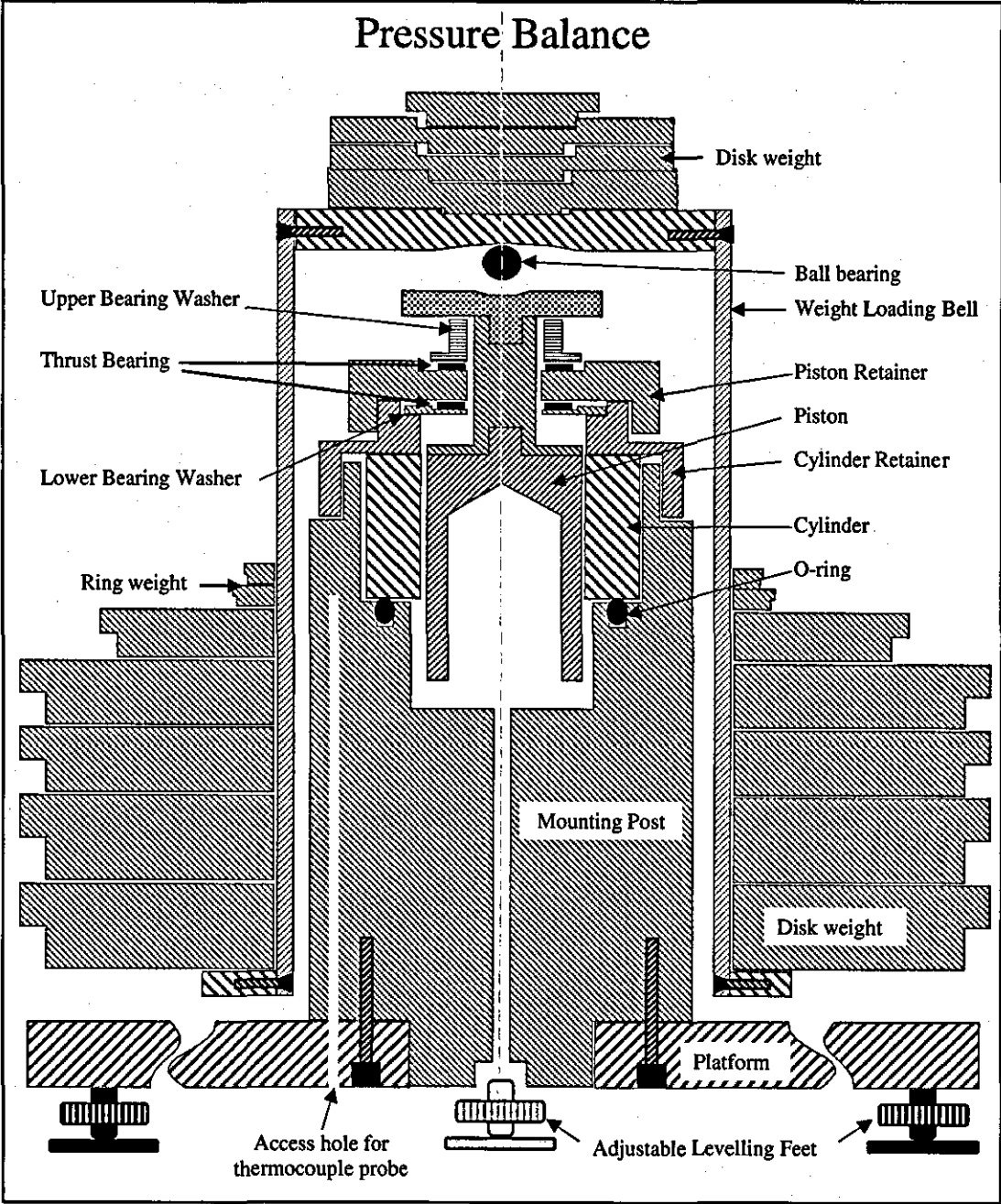


FIGURE 5.1 A schematic diagram (not to scale) of a pressure balance

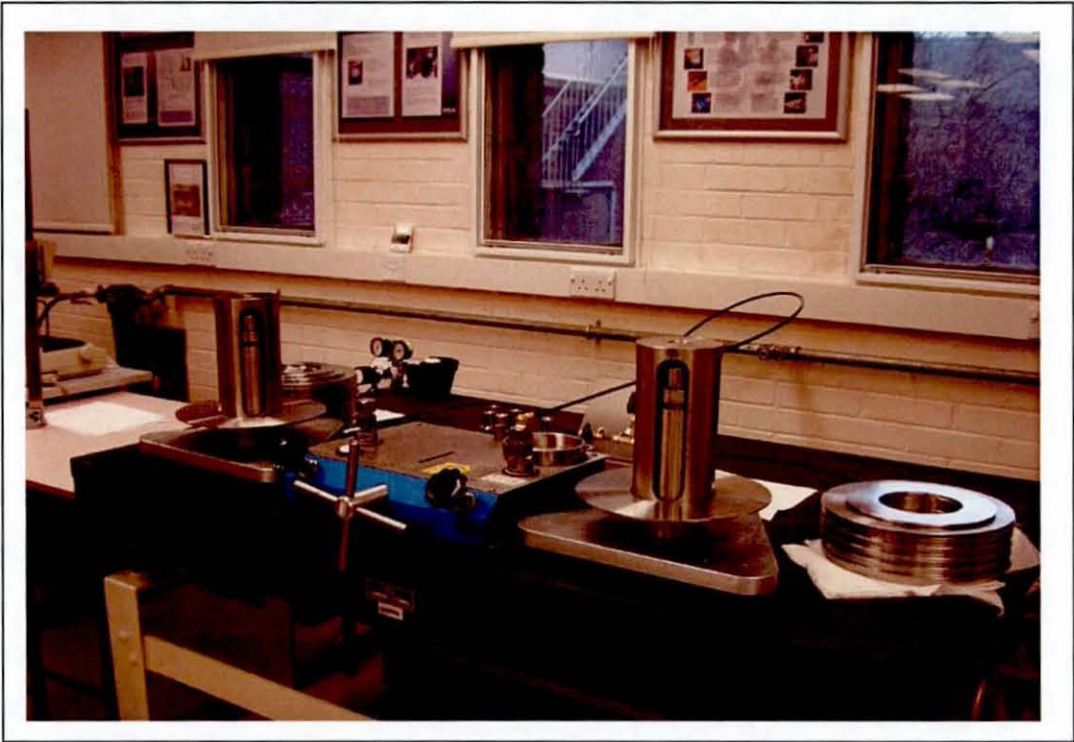


FIGURE 5.2 Two pressure balance units before connection

TABLE 5.2 A set of weight belonging to each pressure balances

No.	Nominal Value	Type	No. of pieces	Total value
1.	5 kg	Disk	6	30 kg
2.	2 kg	Disk	2	4 kg
3.	1 kg	Disk	1	1 kg
4.	500 g	Ring	1	500 g
5.	200 g	Ring	2	400 g
6.	100 g	Ring	1	100 g

The cylinder is seated vertically on top of an o-ring, which is located in a groove inside the mounting post. It is secured using a 316 stainless steel cylinder retainer for pressure sealing purposes, consequently forming a free-deformation type of assembly [Nagano Keiki n.d., Nishibata 1997]. The piston is secured by a 316 stainless steel piston retainer, which acts as a “stopper” when the pressure increases beyond the equilibrium point. A

piston-retainer coupled with a 316 stainless steel upper-bearing washer acts as a supporting mechanism when pressure decreases below the lower equilibrium point, thus avoiding damage to the piston base. This mechanism enables piston and associated weights to rotate on the thrust bearing while the piston is fully seated.

Since the pressure balance performance may be affected by the PCA verticality and weight loading concentricity, a 316 stainless steel ball bearing is used as a non-rigid load interface mechanism between the piston and the overhang-type weight loading bell. Weights are stacked at the lower end of the weight loading bell, lowering their center of gravity relative to the PCA, hence improving the stability of the rotating piston. Consequently loaded weights are free to pivot, while maintaining the weights' centre of gravity coincident with the piston's axis. This design should eliminate non-vertical (side loading) forces that may occur due to slight misalignment of loaded components [Ruska 2000].

The design provides a large contact area between the PCA and the rest of the pressure balance, which is exposed to the ambient temperature. Moreover, the base plate is sitting on 3 adjustable leveling feet (approximately 25 mm gap from table top) that gives room for air circulation underneath the pressure balance. These criteria provide this design with an in-built "temperature stabiliser" that delays the rate of change in the PCA's temperature.

A windowed-type weight loading bell with 4 windows [Nagano Keiki n.d.], of 210 mm long and 40 mm width was designed for the following reasons:

- To avoid escaping gases (through PCA's clearance) from introducing any additional source of error in equilibrium, that is immeasurable.
- To ensure that retainers and mounting post are always exposed directly to the ambient temperature.
- To reduce the mass value, hence reducing the starting pressure point.

Besides having 4 large windows, a large gap between the bottom surface of the loaded weights and the top surface of the base plate (approximately 55 mm gap at mid-float position) helps to smooth the circulation of air currents flowing along side the mounting post and retainers (when their temperature differ from surroundings). This large gap has helped to improve the equilibrium condition and thermal stability of the mounting post and retainers, thus PCA during operation.

The stability of the PCA's temperature has been proven to be excellent throughout operations as demonstrated in cross-floating work carried out within the Metrology Laboratory, where the PCA's temperature has changed almost linearly within $0.2\text{ }^{\circ}\text{C}$ of the room air temperature, which fluctuated within $20\text{ }^{\circ}\text{C} \pm 0.5\text{ }^{\circ}\text{C}$ over 8 hours. This performance claim is further supported with evidence produced during calibration experiments at the National Physical Laboratory (NPL) against the Primary Pressure Standard. At the NPL, the room temperature fluctuated randomly between 20.02 to $20.49\text{ }^{\circ}\text{C}$ (minimum to maximum) for a period of 4.5 hours, with a standard deviation of $0.13\text{ }^{\circ}\text{C}$. Meanwhile the PCA's working temperature with this pressure balance gave readings that changed almost linearly, between 20.03 to $20.10\text{ }^{\circ}\text{C}$ (minimum to maximum) with $0.02\text{ }^{\circ}\text{C}$ standard deviation. A pressure balance that can keep its PCA's temperature stable, is vital in high precision pressure measurement, since the error due to the thermal expansion coefficient of the PCA is reduced.

Furthermore, the piston and loaded weights are rotated manually during operation, which demonstrated a better temperature control compared to any motor-driven pressure balance. Besides having a highly stable temperature control, all weights are constructed from single piece 316 stainless steel. This ensures that weights are always free from any contamination associated with joining parts, which is advantageous especially in the stability of the mass value. The temperatures of the PCAs were measured using a dual-channel digital thermometer, with 2 thermo-couples (Type K). The thermocouple was inserted into an access hole, which runs from the bottom of the mounting post to a point that is close to the cylinder (approximately 5 mm), thus enabling accurate temperature measurement of the PCA.

5.3 MANUFACTURING OF THE PISTON-CYLINDER ASSEMBLY (PCA)

The intention of the research was to complete multiple cross-floating experiments, with pistons exhibiting different extents of surface texture, as shown in the example in Figure 5.3. This could then be linked into an overall calibration chain. In order to realise this approach, a complete system, consisting of two pressure balances associated with a group of test PCAs and a reference PCA required development so that the ratio-based cross-floating experiments could be conducted.

Unfortunately, even though thousands of PCAs have been manufactured by various manufactures all over the world, there is no publication concerning manufacturing techniques publicly available. This work is believed to be the first attempt to demonstrate step by step procedures on how to manufacture PCAs from a piece of selected material. It covers from the machining processes of the bar stock, to the trimming and matching processes.

5.3.1 Manufacturing of the PCA's Blank

Manufacturing of the gas-lubricated PCA is very challenging work since it requires exceptional dimensional tolerances (see Section 5.3.2), hence comprehensive studies (on specific manufacturing techniques and tooling) and special techniques to fabricate them were crucial.

As a starting point, PCAs were fabricated from scrapped/discarded materials for the purpose of gaining hands-on experience in all aspects of PCA's manufacturing processes, especially machining processes using manual and Computer Numerical Controls (CNC) machining. The processes involved were turning, drilling, boring, honing, lapping and finally polishing of PCAs.

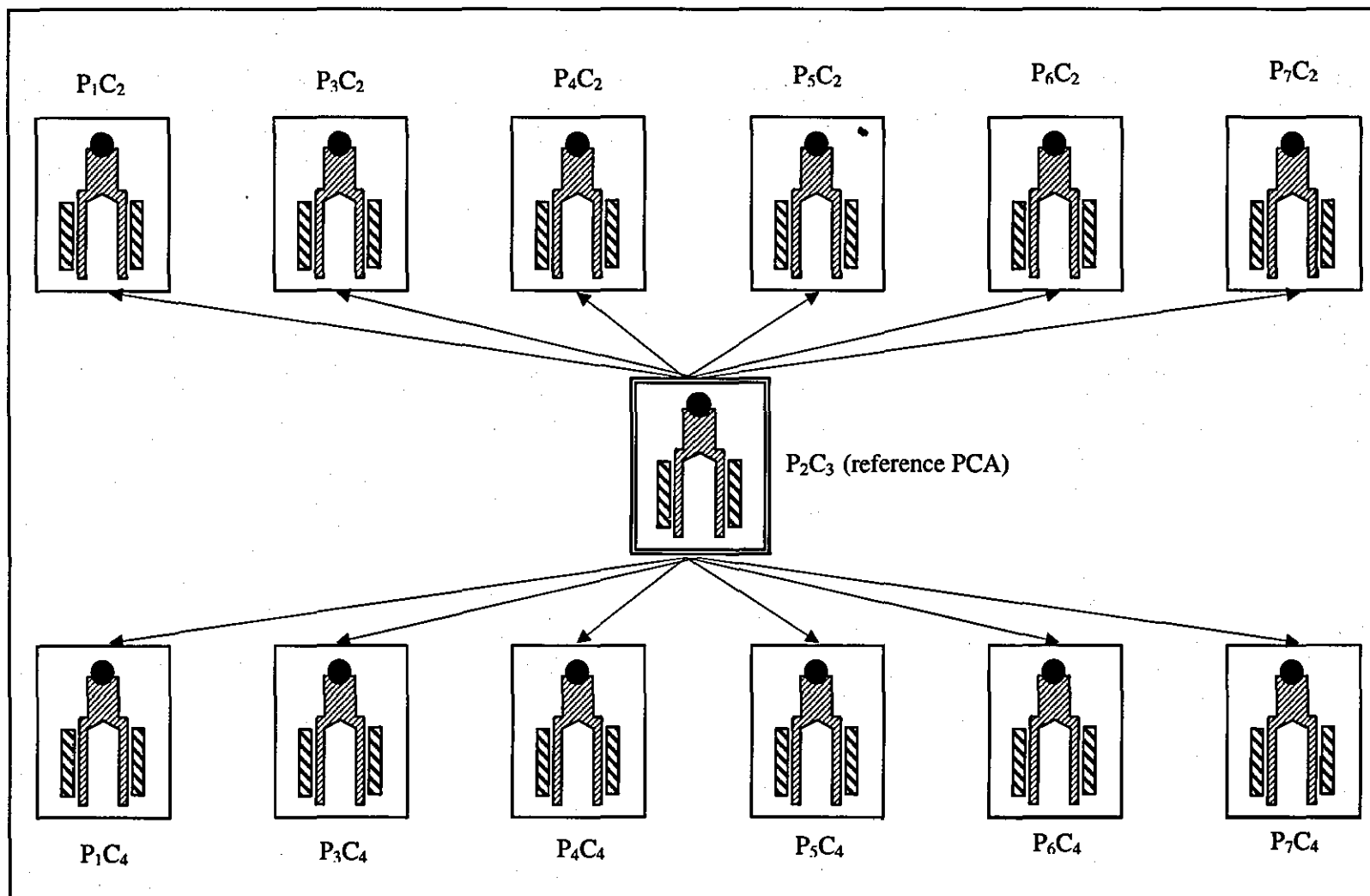


FIGURE 5.3 Calibration chain made up of test PCAs linked directly to a reference PCA

Pistons were machined into four types of design, aiming at establishing the most suitable shape to be used. It was important that the selected design was accomplishable and practically easy in further material removal processes, particularly in the matching process (which involves lapping and polishing work). Figure 5.4 shows the initial design of the PCA in the earliest stages of the research, meanwhile Figure 5.5 shows all four types of piston design that were considered.

Initial results were obtained using aluminum alloy, bronze, brass and mild steel, even though they are clearly unacceptable due to their material softness. Through this trial work, it was realised that the softness of the materials actually made trimming work very difficult and unsuccessful. However, continual improvements were seen in surface roughness, roundness and clearance between piston and cylinder after completing a great number of PCAs (approximately 20 pistons and 10 cylinders). Each improvement enabled the spinning/floating time of the pistons to be gradually increased, nevertheless observable in very limited periods. In this case, spinning/floating time was the ability of the piston to rotate and float freely within cylinder (without additional load) after being spun to a certain initial rotation rate, until it stopped or fully seated/sunk, whichever occurred first. The range of the spinning and floating times was approximately from 1 to 3 seconds.

The CNC and manual lathe machines used were as follows:

- Name: 2 Axis CNC Lathe Machine (associated with Acramatic A1200 Computer Control)
Manufacture: Cincinnati Milacron
Model No.: Hawk 150
- Name: Centre Lathe Machine
Manufacture: Harrison
Model No.: M400

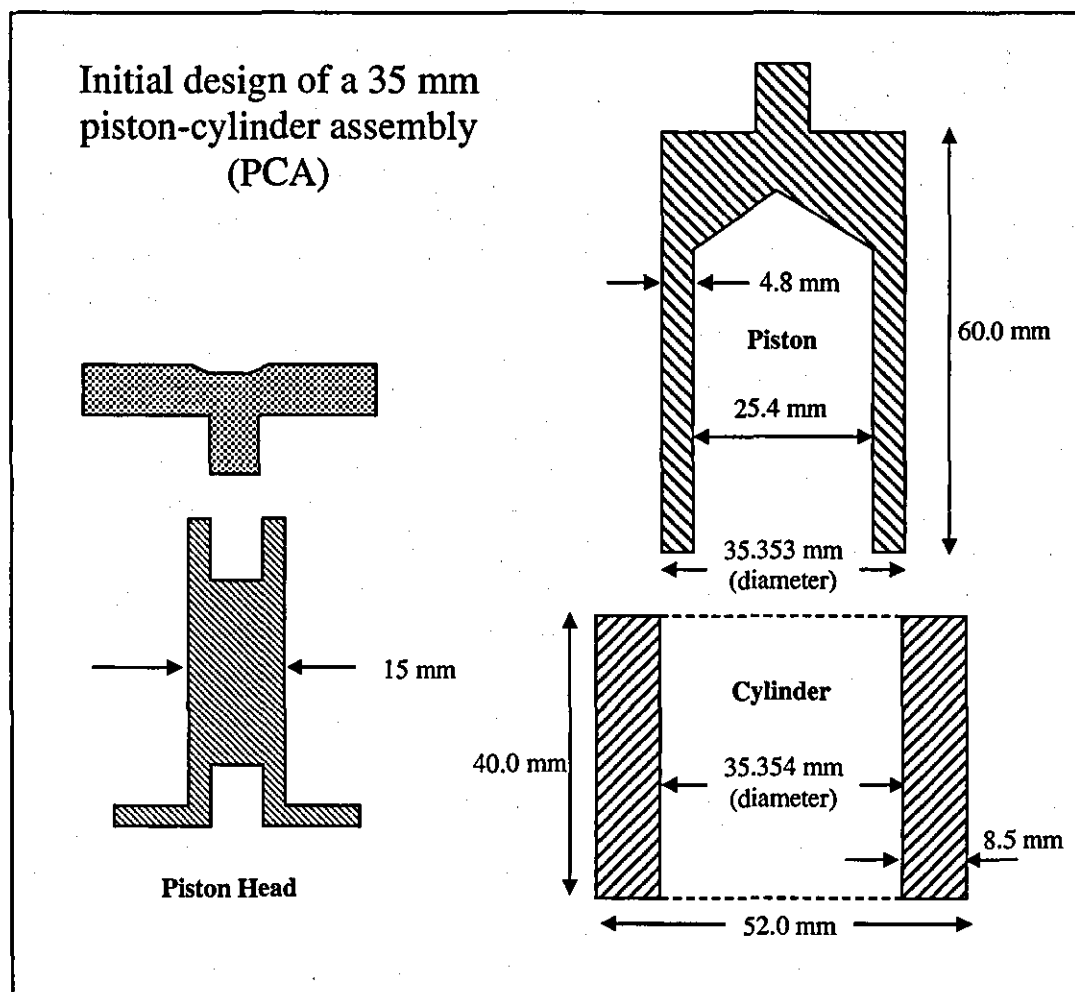


FIGURE 5.4 The initial design of a 35 mm piston-cylinder assembly

Comparison on the dimensions and tolerances of the manufactured piston blanks using each machine was carried out, where close examination at each stage revealed the imperfections of the turning process such as turning marks and lobing effects. Subsequently the same manufacturing processes were repeated on cylinders using both machines. The results showed that both of the machines produced a very similar quality of dimensions and tolerances (approximately $0.5\ \mu\text{m}$ in surface roughness, R_a ; and $10\ \mu\text{m}$ in roundness and straightness). As a result, a manual lathe machine has been continuously used for the rest of the process due to its simplicity, ease of use and finally the most important reason was due to its convenience of accessibility to the work-piece

for measurements/inspections at any time where necessary (crucial requirement in the lapping and polishing processes).

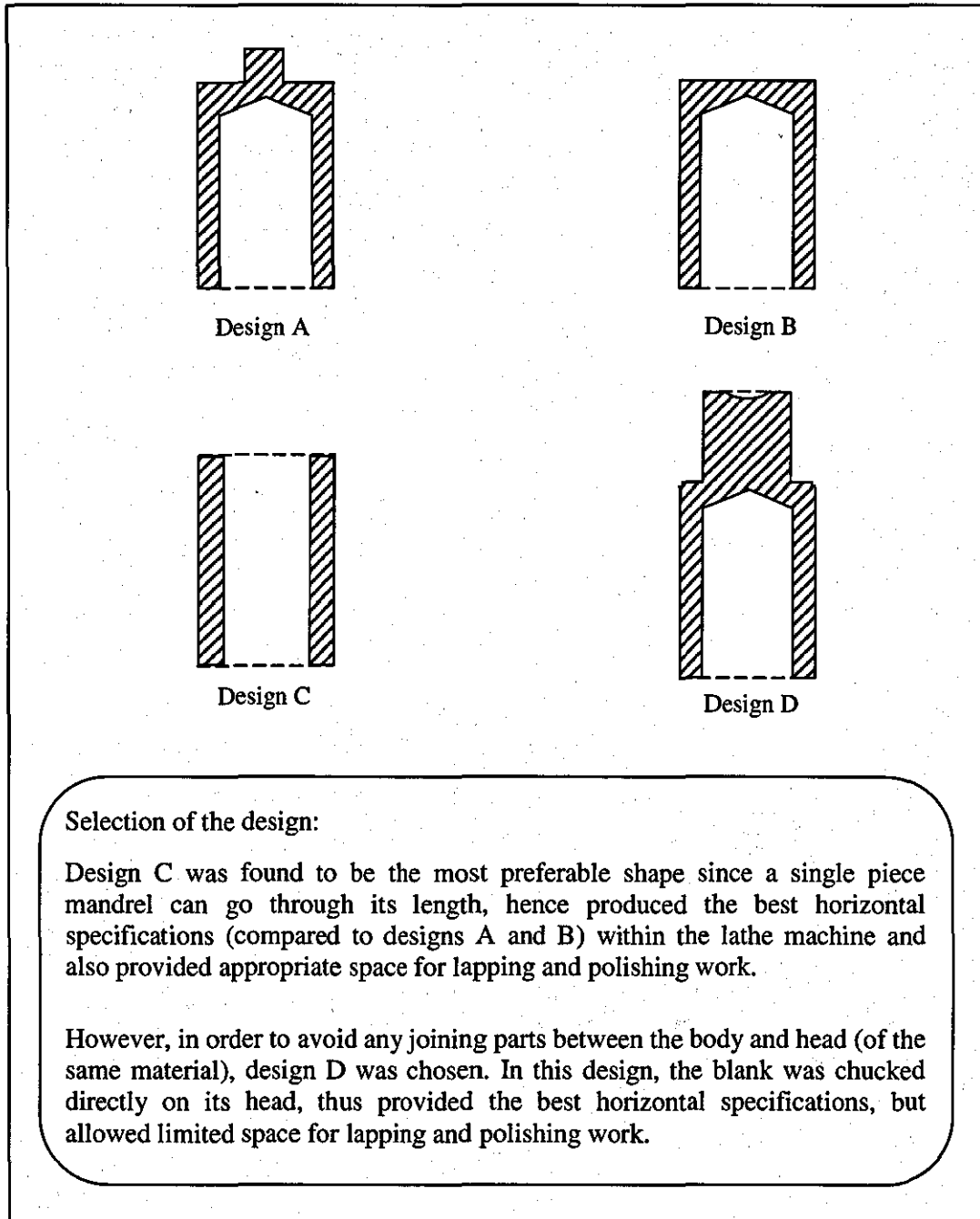


FIGURE 5.5 Four types of initial piston design

After completion of the first series of learning processes using soft materials of different hardness, it was identified that the PCA manufacturing process of a harder material was easier than a softer one, if high level dimensional of tolerances were to be achieved. At the same time, this learning process managed to identify the route towards the best method and design to manufacture an acceptable good working PCA. Therefore a harder material than mild steel was required for the next fabrication stages. The piston and cylinder were subsequently manufactured out of 316 stainless steel, where the final design of the piston blank is shown in Figure 5.6. The piston blank has been cylindrically ground on its outside surface, whilst the cylinder has to be cylindrically ground on its inside surface.

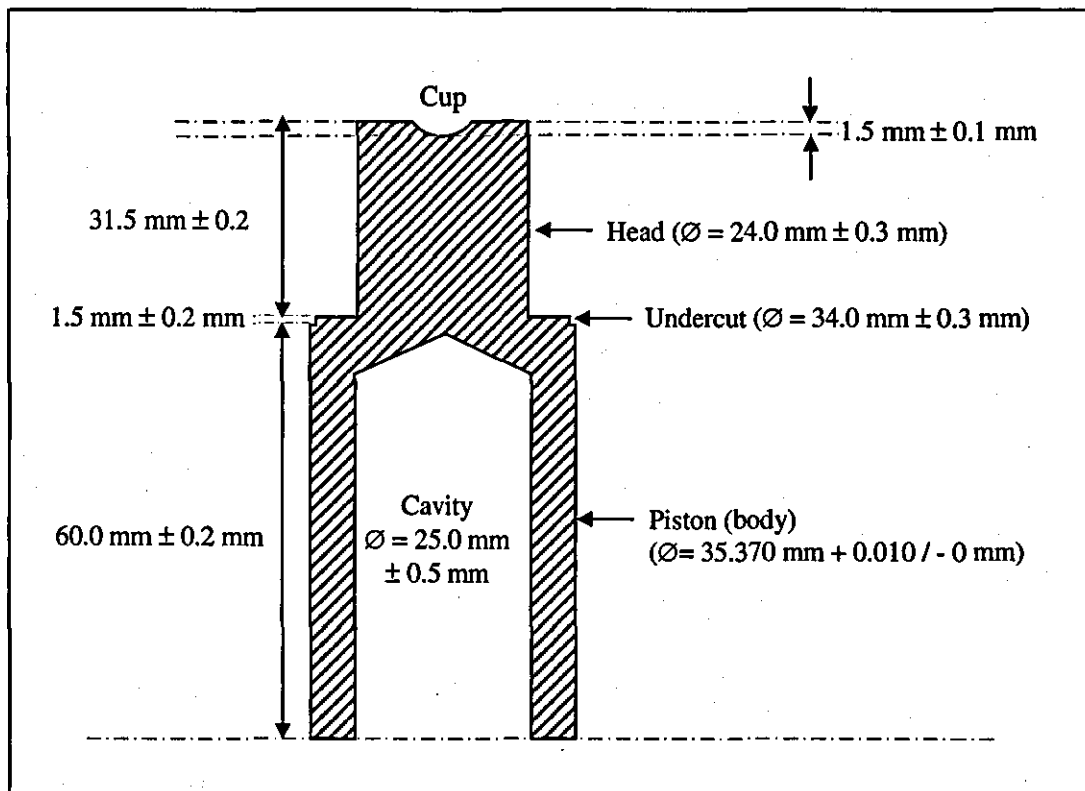


FIGURE 5.6 Final design of the 316 stainless steel piston blank (Design D)

5.3.2 Manufacturing of the 316 Stainless Steel PCA

The initial experimentations provided a good foundation for efficient manufacture of the 316 stainless steel PCA components, with appropriate measuring instruments available to keep monitoring the sizes of the work-piece from time to time, after material removal. Simple operation plans to manufacture piston and cylinder blanks (a workpiece that has not been lapped or polished into its specific tolerances), complete with identified measuring instruments to be used, are shown in Tables 5.3 and 5.4, respectively. Pistons and cylinders were manufactured from 316 stainless steel bar stock, 1½ inch (38.1 mm) and 2¼ inch (57.2 mm) diameter respectively.

The most common geometrical imperfections encountered in the manufacturing processes of the piston and cylinder are [Fischer 1986]:

- Bellmouth
- Barrel
- Taper
- Misalignment
- Rainbow
- Waviness
- Reamer chatter
- Out of round
- Lobing

These geometrical flaws (of the cylinder) are depicted in Figure 5.7.

TABLE 5.3 Operation plan to manufacture a piston blank

No.	Operations	Tools
1.	Securing (chuck) of the blank	3-jaw chuck
2.	Facing of the end	Side tool
3.	Roughing to 36 mm Ø, 94mm length	Roughing tool
4.	Centre drilling	Centre drill bit
5.	Rough drilling to 55mm length (cavity)	Twist drill 10 mm HSS
6.	Re-drilling	Twist drill 18 mm HSS
7.	Re-drilling	Twist drill 24 mm HSS
8.	Inside turning to 25mm Ø (cavity) and chamfering	Boring tool, hand tool
9.	Parting off to 94 mm length	Parting off tool
10.	Undo chuck, rotate work-piece and re-chuck	3-jaw chuck
11.	Roughing and finishing to 24 mm Ø, 32.5 mm length (neck of piston)	Roughing tool, finishing tool
12.	Facing of the end and chamfering	Side tool, hand tool
13.	Centre drilling (cup)	Centre drill, ball nose cutter 10mm HSS
14.	Finishing to 34 mm Ø, 1.5 mm length (undercut) and chamfering	Finishing tool, hand tool
15.	Undo chuck, rotate work-piece and re-chuck	3-jaw chuck
16.	Finishing to 35.380 mm Ø, 60 mm length and chamfering	Finishing tool, hand tool
Measuring instrument used: steel ruler, vernier calliper and micrometer		

Note: HSS = High speed steel

TABLE 5.4 Operation plan to manufacture a cylinder blank

No.	Operations	Tools
1.	Securing of the blank	3-jaw chuck
2.	Facing of the end	Side tool
4.	Centre drilling	Centre drill bit
5.	Rough drilling to 41 mm length	Twist drill 10 mm HSS
6.	Re-drilling	Twist drill 22 mm HSS
7.	Re-drilling	Twist drill 34 mm HSS
8.	Inside turning and finishing to 35.3 mm Ø, and chamfering	Boring tool, hand tool
11.	Outside roughing and finishing to 52 mm Ø, chamfering	Roughing and finishing tool, hand tool
9.	Parting off at 41 mm length	Parting off tool
10.	Undo chuck, rotate work-piece and re-chuck	3-jaw chuck
12.	Facing of the end and chamfering	Side tool, hand tool
Measuring instrument used: steel ruler, vernier calliper, micrometer and inside micrometer		

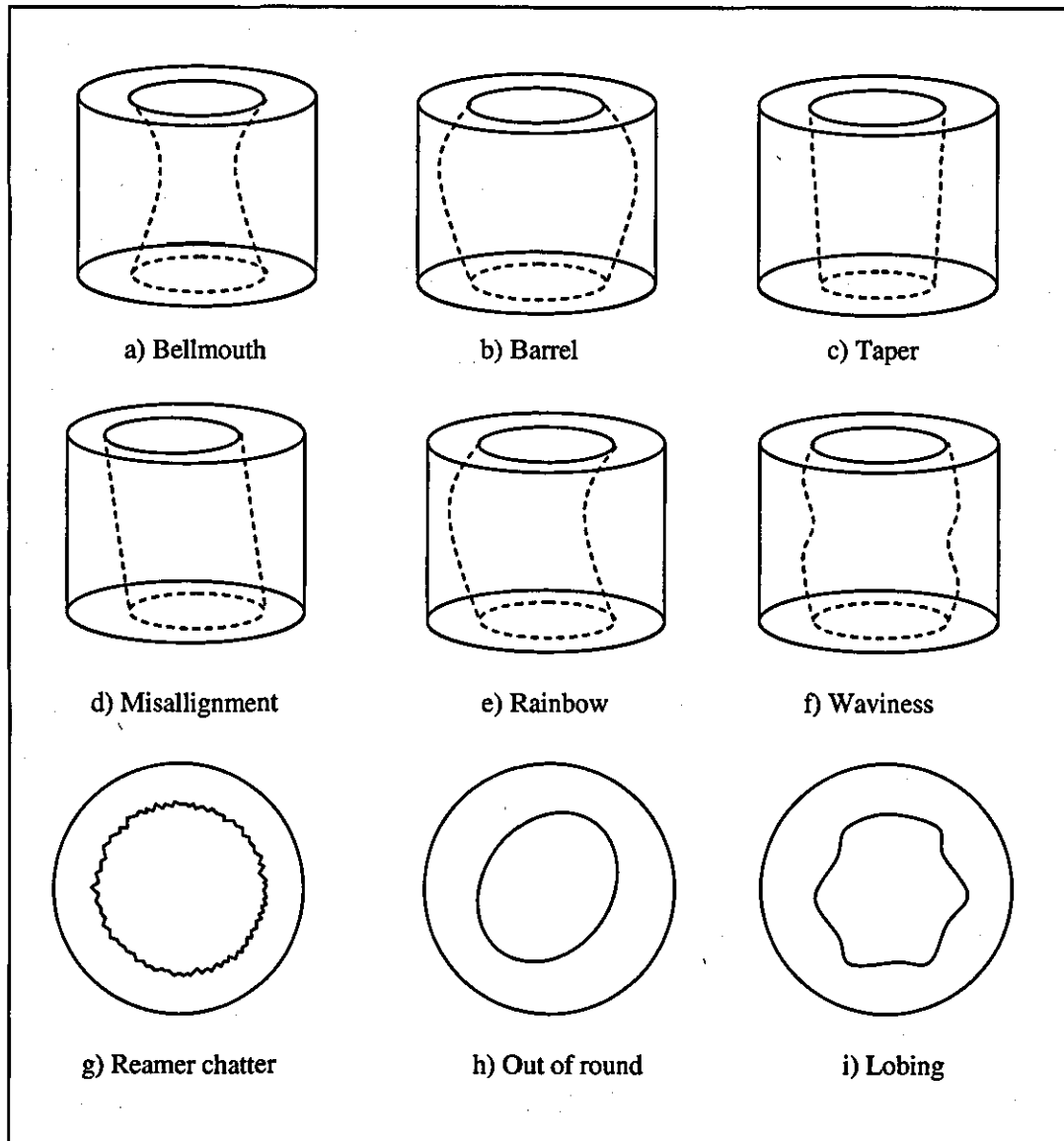


FIGURE 5.7 Geometrical imperfections of the cylinder caused by machining processes
[Fischer 1986]

Specialist tools were designed and produced to facilitate the trimming and matching processes, in order to achieve the very high and demanding PCA specifications especially in roundness, straightness, parallelism and surface finish. The targeted technical specifications of the PCA were as follows [DH-Budenberg n.d.a, DH-Budenberg n.d.b]:

- Roundness: $< 0.3 \mu\text{m}$

- Surface roughness: $< 0.05 \mu\text{m } R_a$
- Straightness: $< 1 \mu\text{m}$
- Parallelism: $< 1 \mu\text{m}$

Figures 5.8 and 5.9 show the tools used in early stages of trimming and matching of the piston and cylinder, after achieving their rough dimensions, i.e. blank. Trimming and matching is the process where the rough machining imperfections are removed, such as turning marks, out-of-round, taper, waviness and oversize for a piston (but undersize for a cylinder). The process then proceeds to achieving a micron or even sub-micron mated clearance between the piston and cylinder.

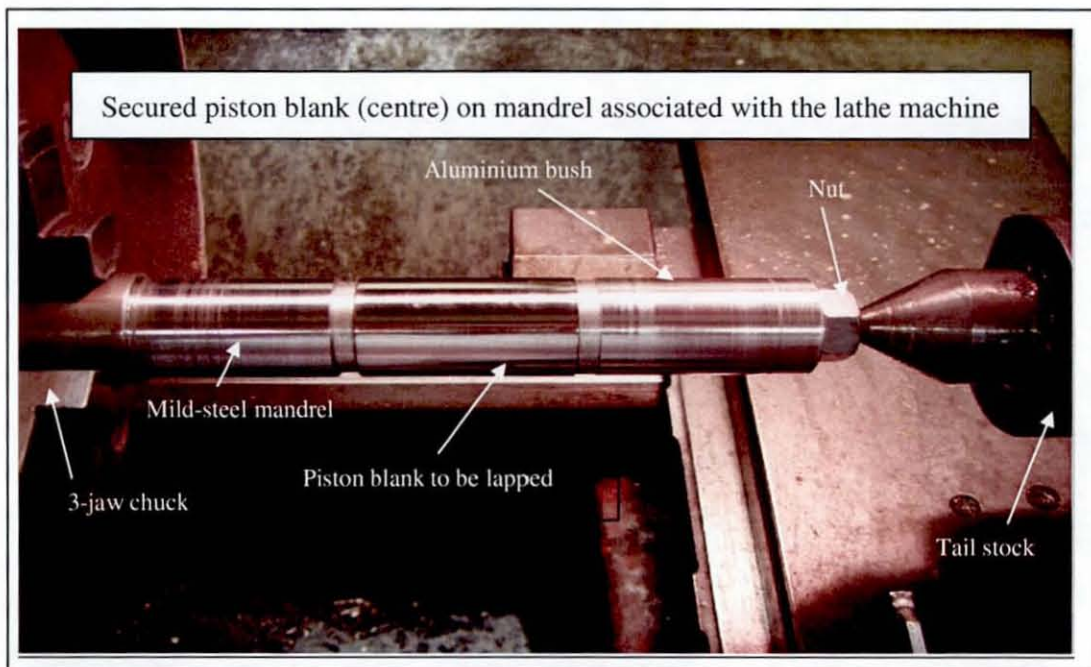


FIGURE 5.8 Mandrel used in the early stages of trimming and matching of the piston

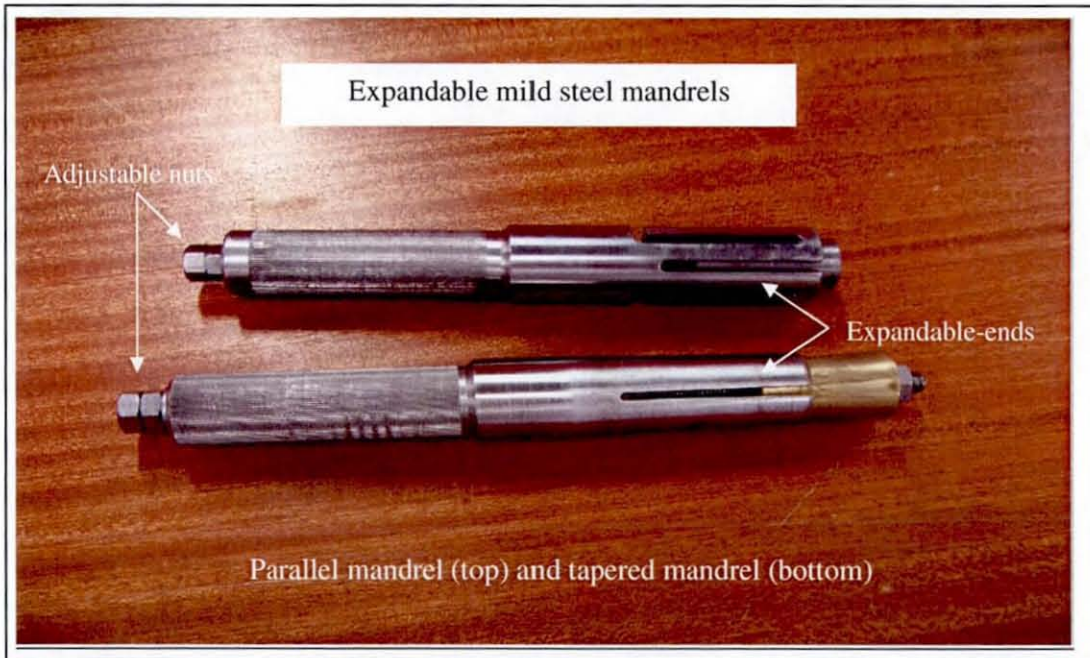


FIGURE 5.9 Expandable mandrels used in the early stages of trimming and matching of the cylinder

Two important parameters i.e. roundness and surface roughness were measured using a Talyrond 50 and a Talysurf 4 respectively. Straightness measurements were only completed once observations with the naked eye had shown satisfactory surface quality. Satisfactory quality was justified when surfaces to be observed were placed obliquely under strip lighting with straight lines showing along both ends of the work piece. Explanations about each procedure used are briefly described in the following sections.

5.3.2.1 Aluminium Curved-Shell

The first trimming operation included manual application of wet and dry emery paper, wrapped around the piston blank, seized between two separate-pieces of aluminium curved-shell, which functioned as padding panels in order to get better and more uniform cutting actions. Half of the blank was held in one hand and simultaneously rotated, meanwhile the other half was seized within the curved-shells where gripping and reciprocating actions took place (fully manual operation, without using mandrel and lathe). The same procedures were repeated a number of times with the orientation of the

piston blank alternately changed. The grit sizes of the wet and dry emery paper used were 400, 600 and 800, applied in sequence from the lower to the higher grit size. A relatively poor straightness was obtained where it can be seen clearly with naked eyes through reflection lines observed, especially on both ends of the blank. Measurement results of roundness and surface roughness are shown in Table 5.5 as follows:

TABLE 5.5 Measurement results after using aluminium curved-shells

No.	Parameter	Measurement Value
1.	Roundness	2 μm
2.	Surface roughness	0.5 μm R_a

5.3.2.2 Expandable Slotted-End PVC Tube

Internal surfaces usually have more accuracy problems rather than external surfaces due to the size limitations of the tool used to fit into the hole. The first trial experiment in correcting the typical imperfections of the cylinder blank were carried out manually through application of wet and dry emery papers (400, 600 and 800 grit sizes), wrapped loosely around an expandable slotted-end of a PVC tube. The PVC tube (which was wrapped with wet and dry emery paper) was held in one hand, and a cylinder blank was held in the other hand while rotating and reciprocating actions of the tube against blank were carried out. This process resulted in stock removal that gradually reduced the imperfection problems. However this method only slightly improved the initial imperfections, since a bellmouth error was seen under normal observation with the naked eye (see Figure 5.7a). Measurement results obtained are shown in Table 5.6, which are quite similar to the previous procedure.

TABLE 5.6 Measurement results after using an expandable slotted-end PVC tube

No.	Parameter	Measurement Value
1.	Roundness	2 μm
2.	Surface roughness	0.5 μm R_a

5.3.2.3 Piston's Blank Secured on a Mandrel

A second trial to reduce piston blank imperfections was completed by manual application of wet and dry emery paper associated with a lathe, as shown in Figure 5.8. However, the types of piston were changed to Design A and Design C (before Design D been used, refer to Figure 5.5) so that they were able to be secured on their own mandrels respectively. The mandrels with secured blanks on them, were secured on the lathe, with handheld wet and dry emery paper taken back and forth over the rotating blank (100 – 800 rpm). The grit sizes used were 400, 600, 800 and 1000, subsequently polished with a 1200 grit size until a semi-mirror finish appearance was observed. However a barrel-shape imperfection was still visible when light pass checking was carried out. Improved measurement results were however obtained for both types of piston blanks, and are shown in Table 5.7 below.

TABLE 5.7 Measurement results after using a blank piston secured on mandrel

No.	Parameter	Measurement Value
1.	Roundness	0.5 μm
2.	Surface roughness	0.05 μm R_a

5.3.2.4 Expandable Mild-Steel Mandrel

The second trial experiments to improve imperfections of the cylinder blank were carried out using a tapered and expandable-end mild steel mandrel (Figure 5.9). It has been designed so that the tapered-end can be spread out to the required size (by setting the adjustable nuts) and then wrapped with a wet and dry emery paper. The cutting process was similar to the PVC tube described above, but the mandrel was mounted directly on the lathe for rotation (60 – 315 rpm), using wet and dry emery paper ranging from 400 to 1200. Improved results compared to the manual process using PVC tube were obtained, however straightness still became a major problem due to the bell-shape error. The measurement results after this process are shown in Table 5.8 below:

TABLE 5.8 Measurement results after application of a tapered-expandable mild-steel mandrel

No.	Parameter	Measurement Value
1.	Roundness	1 μm
2.	Surface roughness	0.08 μm R_a

Next, an improved version of the expandable mild-steel mandrel was designed, where it came with parallel-expandable sleeves, using a similar cutting process as the tapered-expandable mandrel. This new mandrel improved the parallelism problem encountered in the first mandrel's design, hence produced a better result in straightness. Unfortunately the improved straightness was still not acceptable. Measurement results obtained are given in Table 5.9.

TABLE 5.9 Measurement results after application of an improved mandrel, i.e. a parallel-expandable mild-steel mandrel

No.	Parameter	Measurement Value
1.	Roundness	0.5 μm
2.	Surface roughness	0.08 μm R_a

5.3.2.5 Honing Tool

Due to the unsatisfactory results on the manufactured cylinder (especially in straightness), trial experimental work was continued. An old model of honing tool (obsolete model) that was available in the Departmental Workshop was used, with only two sets of roughing honing stones. The equipment is a 4-stone honing tool, where the abrasive makes contact when the stones are expanded inside the bore by turning its feed screw clockwise. Honing processes applies three forces simultaneously to make material removing process happen in effective manner. The three forces are [Fischer 1986]:

- Stone expansion that forces bonded abrasive grains against the wall of the cylinder's blank.
- Low speed rotation of the honing tool that is secured on the lathe machine.

- Back and forth stroking action (reciprocating) of the cylinder blank, associated with rotating honing tool that creates crosshatch pattern on the surface.

Since there were only two sets of roughing honing stones available, they were used only in the first step of the honing process. The honing tool was secured and rotated (40 – 80 rpm) on the lathe, with the cylinder held by hand in a reciprocation action. An adequate flow of suitable coolant was applied to the honing stones to remove heat, increase cutting ability and improve surface quality of the honed surface. This process (rough-honing) only acted as a cleaning-up mechanism, i.e. to correct initial imperfections of the cylinder blank, and hence still produced a relatively poor results.

A “modified honing technique” was attempted where the cylinder blank was honed using a piece of wet and dry emery paper, which was wrapped around the expanded roughing stones. The method started with 400 grit size and continued with 600, 800, 1000 and 1200 grit sizes which were applied in a consecutive manner. This technique improved tremendously the imperfections and surface finish compared to the earlier honing work. Improved results were proven (especially in straightness) when a light pass check showed almost perfect lines through out the honed surface. The quality of the honed cylinder was then measured using Talyrond 50, Talysurf 4 and Talylin 1, where the measurement results obtained are as shown in Table 5.10.

TABLE 5.10 Measurement results after application of a honing tool

No.	Parameter	Measurement Value
1.	Roundness	0.5 μm
2.	Surface roughness	0.05 μm R_a
3.	Straightness	5 μm

These promising results indicated that better results could be achieved if a full set of honing stones (from roughing to finishing stone sets of different grit sizes) were employed. However, further investigation and contact with a honing tool manufacturer

(Delapena Honing Limited) identified that the honing processes would be unable to produce the stringent specifications, and lapping processes would be more appropriate.

5.3.2.6 Lapping Tool

Research on the theory of the lapping process was initiated, to find its capability to satisfy the PCA's technical specifications. Studies conducted identified that internal and external lapping are the only methods to guarantee high precision results whenever there are requirements for accurate sizing, rounding and straightening of bores or/and shafts. This is supported by the comparisons carried out by Westbury [n.d] who found that honing is more practical and useful from a production point of view, but for special operations where specialised equipment is lacking, highly accurate work can be completed by lapping.

Beside geometrical and surface finish improvements, lapping was found to have capability in providing close tolerance accuracy at minimal cost compared to other finishing methods. Cylindrical geometries that had been achieved (by skilled technical staff) with helical laps were around $0.14\text{ }\mu\text{m}$ in roundness, $0.28\text{ }\mu\text{m}$ in straightness and $0.025\text{ }\mu\text{m}$ R_a in surface finish [Kemet n.d., Helical Lap Mfg n.d]. The advantages from these lapping processes such as fast lapping action, perfect roundness, exceptional straightness and superb surface quality, are the prerequisite conditions in matching the PCA piston into the cylinder within a $2\text{ }\mu\text{m}$ tolerance (clearance), convinced the author to apply these methods onto the piston and cylinder .

A new type of piston design (Design D) that could be secured directly on the lathe, was manufactured (refer to Figure 5.5) for this purpose. Twenty piston blanks were manufactured, five of Design A and fifteen of Design D. They were lapped with thick cast iron ring laps (8 mm), slotted right through with a 3 mm gap line at approximately 30° angle. The gap provided a means for the provision of size adjustment. Diamond pastes used in this experiment work were 25, 14, 8, 6, 3 and $1\text{ }\mu\text{m}$ sizes (applied sequentially) where a hose-clip was initially used for contracting the ring lap to the desired size. Lapping work was carried out by rotating the piston blank on the lathe, at

the same time reciprocating the lapping ring manually. Convincing results resulted in the design and manufacture of a proper lapping ring holder, as shown in Figure 5.10 which allowed the work to be more accurate, easier, faster and convenient.

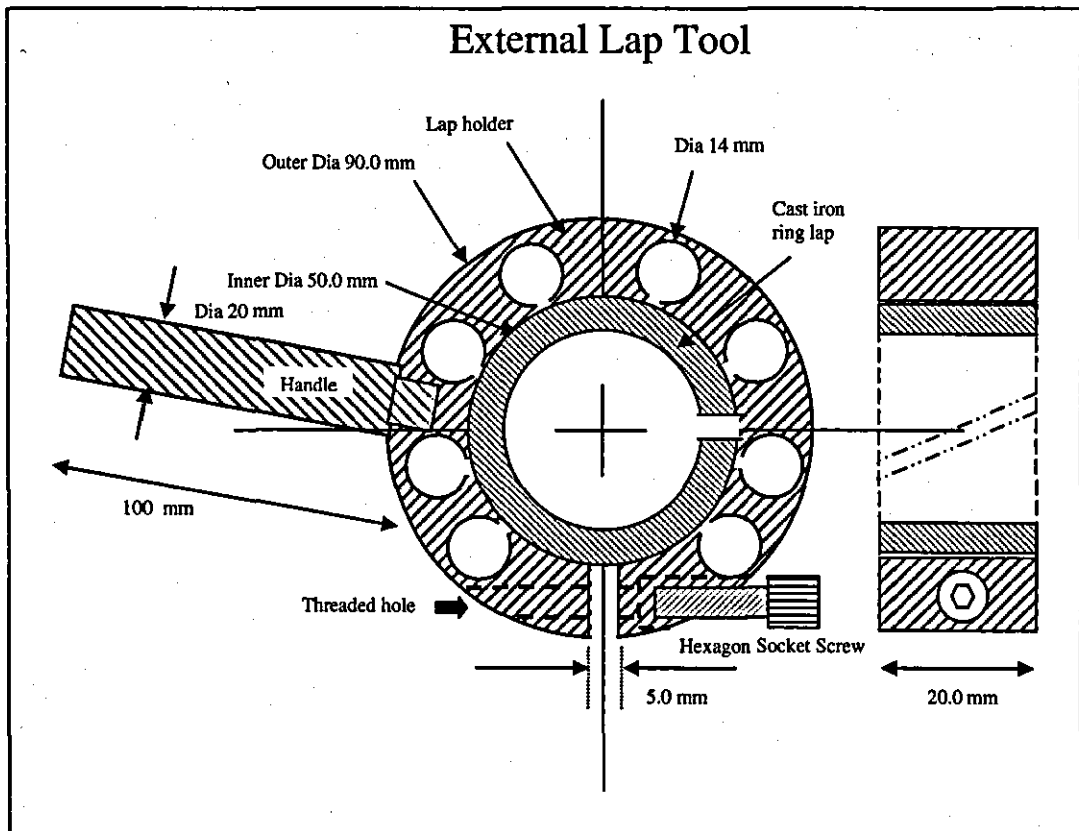


FIGURE 5.10 External lapping tool used in trimming and matching of a piston blank

Eight 316 stainless steel cylinder blanks were manufactured. They were lapped with an internal lap (also known as helical lap) that was slipped over the tapered arbour. The lap was slotted helically right through in a 3 mm gap line, and grooved circumferentially to carry away swarf produced during lapping process (see Figure 5.11). Expansion of the lap to the desired size was achieved when it is tapped gently with a lap expander until the tapered surface of the arbour made contact with internal tapered surface of the lap. These actions allowed a high precision degree of uniform diametrical expansion over the entire outer surface of the lap. A similar method of rotating and reciprocating that had

been applied to the piston blank was used in this work, providing precision stock removal ranging from a fraction of a micron, to a few microns.

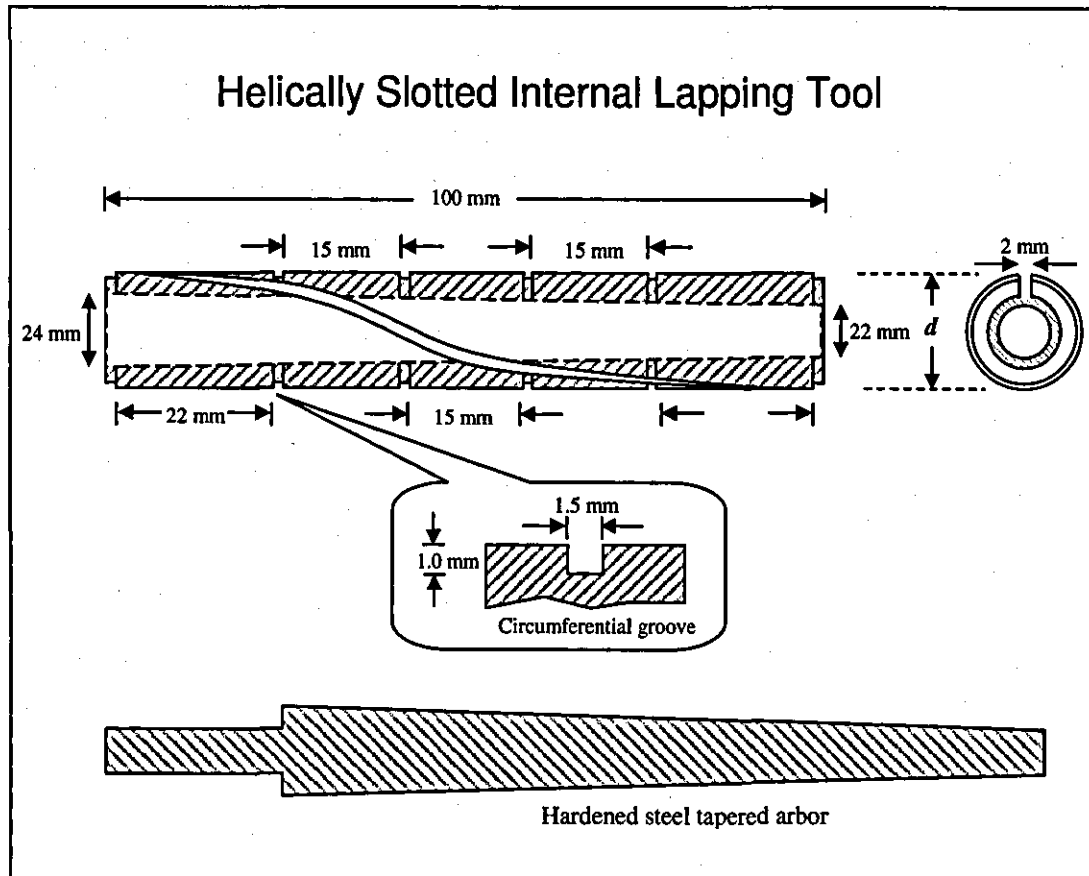


FIGURE 5.11 Internal lapping tool used in trimming and matching of a cylinder blank

Details about the lapping process in trimming and matching work are explained in Section 5.6. It was found that 316 stainless steel could easily get scratched when it was highly polished. Therefore lapping and polishing work became very tedious and difficult. Application of 3 μm diamond pastes in the lapping work made the surface quality worsen than the previous step, hence 6 μm diamond paste was used in the final lapping and polishing work. Measurement results obtained from this initial lapping work on pistons and cylinders are shown in Table 5.11.

TABLE 5.11 Measurement results after an initial lapping process

No.	Parameter	Measurement Value
1.	Roundness	0.3 μm
2.	Surface roughness	0.05 μm R_a
3.	Straightness	1 μm

5.3.2.7 Matching Work of 316 Stainless Steel PCAs

Once pistons and cylinders were lapped and polished to their desired sizes and surface finish, they were then matched. The matching technique was carried out by sliding the piston into the cylinder to check whether the piston was free to slide in cylinder. Those pistons that could slide freely in any selected cylinders then underwent the simple tests by spinning the floating pistons in their matched cylinders. Trapped air within the hollow bottom of pistons and bottom face of the cylinders (which were placed on a flat and smooth surface) caused the pistons to float, thus providing the opportunity to test the performance of the matched PCAs without connecting them to the pressure circuit.

Unfortunately all combinations of the 316 stainless steel pistons and cylinders only worked for the first few spin cycles, before they started to seize. Seized PCAs were released, and both pistons and cylinders were re-polished. Matching work re-continued, however all combinations faced the same problem again, although clearances between pistons and cylinders increased through re-polishing work (and re-lapping process, when necessary). However in the majority of cases, pistons and cylinders welded to each other to the extent that they could only be released with force. Figure 5.12 shows a pair of welded PCA after release.

All the trimming operations of the 316 stainless steel piston and cylinder blanks which were completed are summarised in Figure 5.13.

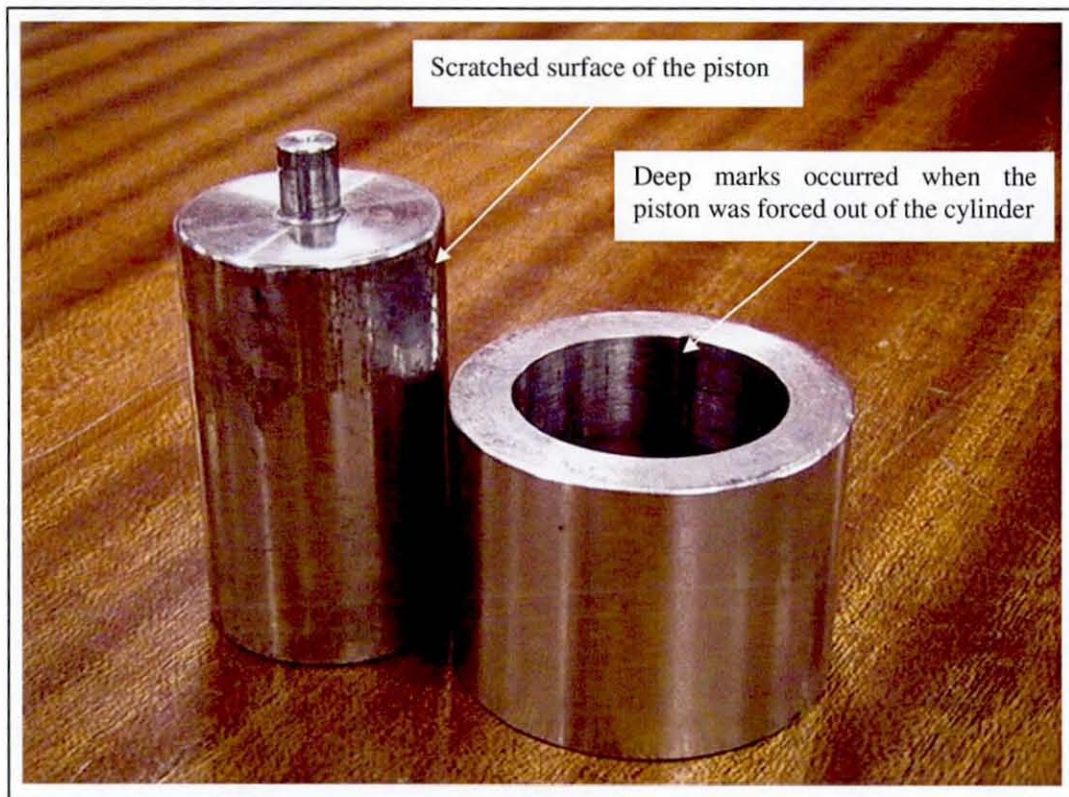


FIGURE 5.12 Damaged PCA after release with force due to seizing

Studies and investigations on the properties of the 316 stainless steel as a bearing material were initiated, aimed at understanding better the reasons behind these problems. From the studies and investigations carried out, it was found that 316 stainless steel is not a suitable candidate for a PCA for the following reasons:

- 316 stainless steel is not hard and tough enough, so manufacturing processes to achieve such a stringent requirement for a gas-lubricated PCA, especially in-term of straightness, roundness and parallelism, is almost impossible [Les Yelland 2004].
- 316 stainless steel does not possess satisfactory galling resistance due to its high ductility, which tend to cause the asperities to be plastically deformed hence smearing and tearing easily; thereby increasing the contact area of mated surfaces and eventually galling occurs [Magee 1996, Drab and Raposo 2002]. This

indicates that 316 stainless steel PCA has poor abrasive wear, hence contributing to poor long term stability.

Surface asperities formed can be seen like a pair of lips, which are separated by valleys in their cross-sections (see Figure 5.14). Initial asperities may cause sliding surfaces to become slightly bonded at the start. Eventually, as sliding continues (with sufficient force due to spinning), the lips are broken away, leaving valleys on one surface. Broken lips become tiny abrasive particles (debris) within PCA's clearance, which contribute to greater destruction of the rubbing surfaces. These processes continue rapidly as the piston keeps rotating, causing high intensity of wear to the sliding surfaces. Finally the piston and cylinder seize together. These situations are get worse if abrasives are unintentionally introduced into the clearance.

In the end, trimming and lapping work of the 316 stainless steel pistons and cylinders discontinued when all combinations seized soon after spinning tests were carried out. However, even though the author failed to produce working condition PCAs using 316 stainless steel, these learning processes contributed invaluable knowledge and skills in all manufacturing aspects of the PCAs. The art of lapping techniques can be simply found in literature, however considerable hands-on training is necessary before one can become proficient. There are certain indescribable experiences such as feeling, touch, sound, motion, refinement, etc., which can only be acquired through a series of repeated practical work [Jones 1915]. Furthermore, the materials required for PCA manufacture have never been publicly documented.

A re-evaluation of the work completed caused the research to select tungsten carbide as the final PCA material. Tungsten carbide is the commonest material used in the manufacture of high precision PCAs [DH-Budenberg n.d.a, DH-Budenberg n.d.b, DH Instrument 1999, Ruska 2000], where their manufacturing processes are explained in detail in the following section.

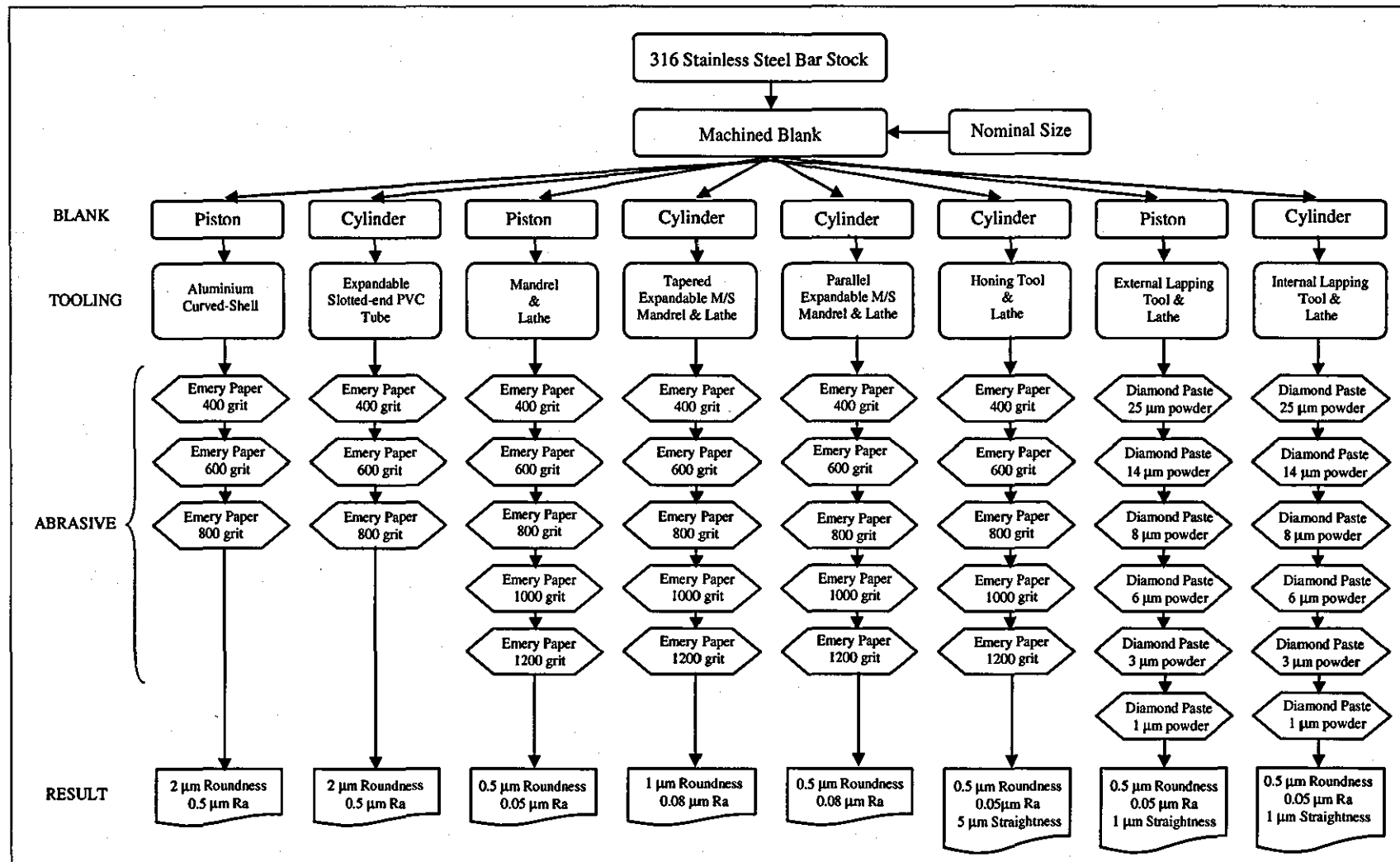


FIGURE 5.13 A summary of the manufacturing processes of the 316 stainless steel piston-cylinder assemblies (PCAs)

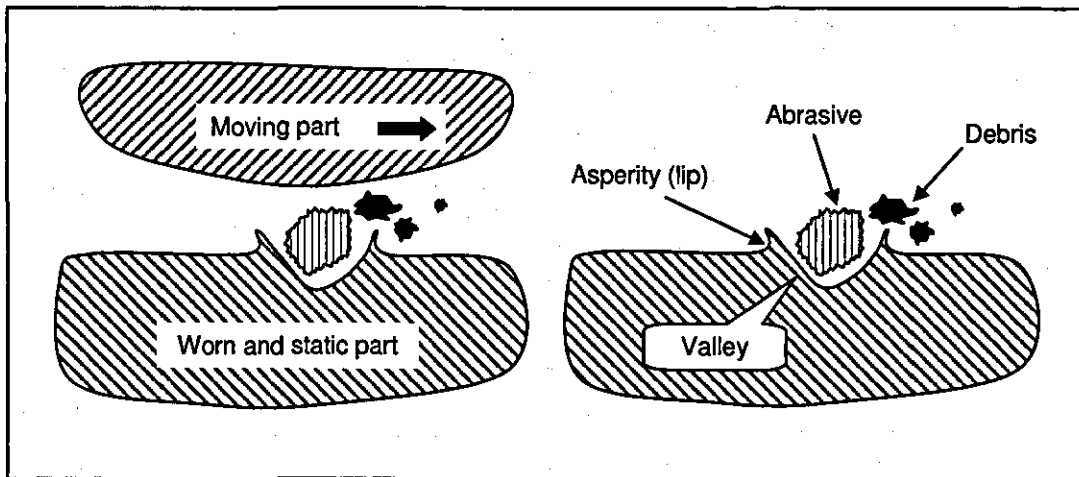


FIGURE 5.14 Abrasive wear, caused by either unintentionally introduced abrasives or debris (originated from fractured initial asperities or lips) that produces piling up of asperities on highly polished 316 stainless steel

5.4 TRIMMING AND MATCHING TECHNIQUES OF THE TUNGSTEN CARBIDE PISTON-CYLINDER ASSEMBLY (PCA)

Lapping was identified in the previous trial experiments as the best process for trimming and matching of the piston into the cylinder. A few considerations were taken into account to make sure that the lapping work carried out was controllable and did not exceed the specified tolerances while cutting processes were in progress. Particular attention was given to the right material and size of the lap used, type of abrasives and lubricant used, degree of fit (pressure to be applied) between the lap and the blank, frequency and reciprocation method implemented, and the spindle speed of the rotating parts. Attention was paid to the correct sequence of abrasives used, and finally the right type of polishing cloth associated with the correct grit size of abrasives used was considered. All the related considerations and sequences applied in the trimming and matching work of the tungsten carbide PCAs are described in the next sections.

5.4.1 Grade of the Selected Tungsten Carbide

Tungsten carbide is a product of powder metallurgy, where it consists of a specific mixture of fine pure tungsten carbide powder with a cobalt-based binder phase(s), that are tailored made for specific applications [Sandvik 2004, Corewire 2004]. The powder grain

size ranges from sub-micron to between 5 to 6 μm , and contributes considerably to the mechanical properties of the tungsten carbide. The powder is compacted through its shrinkage (approximately 50% in volume) during a high-temperature sintering process. During this process, the cobalt melts and fills any remaining voids, which thoroughly bonds the structure. Besides hardness and toughness, tungsten carbide has excellent features to withstand wear, deformation, high pressure and corrosion, and it has very low thermal expansion coefficient. These characteristics made tungsten carbide the best candidate for PCAs' material, but also the most costly.

The grade of the tungsten carbide selected was DF6 (Dymet grade) [Corewire 2004], which is equivalent to K10 (ISO code). Its material properties are shown in Table 5.12.

TABLE 5.12 Material properties of the Dymet DF6 tungsten carbide [Corewire 2004]

Average grain size (μm)	Composition by weight (%)				Transverse Rupture (MN/m^2)	Hardness (HV)	Density (kg/m^3)
	WC	TaC	Cr_3C_2	Co			
1.0	92.7	1.0	0.3	6.0	1800	1750	14900

Note: WC = Tungsten carbide
 TaC = Tantalum carbide
 Cr_3C_2 = Chromium carbide
 Co = Cobalt

5.4.2 Piston and Cylinder Blank

Ready made piston and cylinder blanks (five and three units respectively) of DF6 tungsten carbide were ordered from a supplier, where their dimensions and designs are shown in Figure 5.15. Each piston and cylinder blank was approximately £200.00 and £300.00 respectively. The outer diameter of the piston blanks were specified to be approximately 30 μm larger than final diameter, conversely the inner diameter of the cylinder were specified to be 30 μm smaller than the final diameter. These allowances were required for trimming and matching work through lapping and polishing methods. Design C was chosen for the pistons, where they were bonded with their 316 stainless steel heads using "loctite superglue" to form a complete construction, after the final

lapping processes was completed. A second batch consisting of five pistons of the same material and design, were ordered from the same supplier after the first batch of the piston was successfully trimmed and matched.

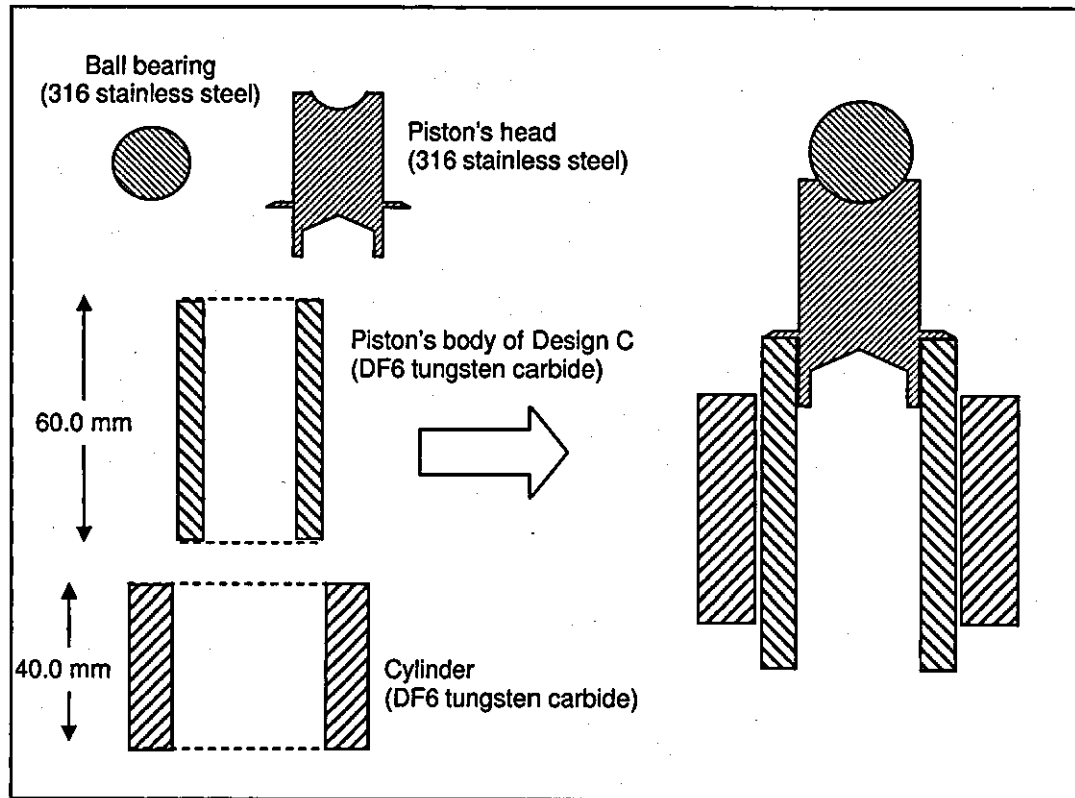


FIGURE 5.15 The DF6 tungsten carbide piston-cylinder assembly (PCA)

5.4.3 Clamping/Securing Method

Fixtures for lapping work were quite simple, however attention was given to ensure that the part to be held was clamped firmly, securely and as close as possible to the three-jaw chuck. This was necessary in order to minimise any source of positioning/aligning problems which would lead to dimensional error of the work-piece. Concurrently, the manner in which the work-piece was being clamped also played a very important role especially when the piston blank was lapped (refer to Figure 5.8). Hollow type piston blanks are end-clamped between a mild-steel mandrel and aluminium bush (softer materials), which is less likely to distort than securing (clamping) directly on its out side

diameter. In contrast, the cylinder blanks were held by hand while lapping and polishing work was in progress. Hence the helical lapping tool needed to be clamped firmly and securely in the three-jaw chuck.

5.4.4 Design of the Lapping Tools

In this research work, two types of laps were used. They were external and internal laps which were made from cast iron [Kemet 2006a, Helical Lap Mfg. 2006, Metals Handbook 1967]. Note that their schematic diagrams were described in Figures 5.10 and 5.11. Details about the laps used are as follows:

- **External lap** - The external lap used consisted of an outer ring that acted as a lap holder, and an inner shell that acted as the lap. The inner shell known as a ring lap, was split right through in a 3 mm gap line at approximately 30° angle and manufactured slightly oversize to allow for clearance. It contracted to the appropriate diameter by tightening an adjusting screw on the lap holder, providing a fast lapping action, excellent piston roundness, exceptional straightness and superb surface finish. The length of the manufactured ring lap was 20 mm i.e. 1/3 of the length of the piston blank, that was shorter than the outer diameter of the piston blank to be lapped, but long enough to provide an appropriate length of stroke. The length of the ring lap was a critical factor in avoiding typical types of geometrical imperfections especially barrel or bell-mouth errors (refer to Figure 5.7). Figure 5.16 shows a picture of the assemblies of an external and internal lapping tools, which were used in the trimming and matching work of the piston and cylinder blanks.
- **Internal lap** - An internal lap consisted of a lap that was slotted helically right through in a 3 mm gap line, and grooved circumferentially to carry away swarf produced during lapping process. It was 100 mm in length, i.e. 2 ½ times longer than cylinder blank to be lapped, which also became a critical factor in avoiding typical types of geometrical imperfections especially barrel or bell-mouth errors. The manufactured size of the lap was slightly undersize to allow for clearance and stock removal process to be realised. The expansion of the lap to the desired size

was achieved when the internally tapered hollow lap was slipped over a matched tapered arbor, and then the lap was tapped gently with a lap expander until the tapered surface of the arbor made contact with internal tapered surface of the lap. These actions therefore allowed a high degree of uniform diametrical expansion over the entire outer surface of the lap. This allowed precision stock removal ranging from a fraction of micron to a few microns.

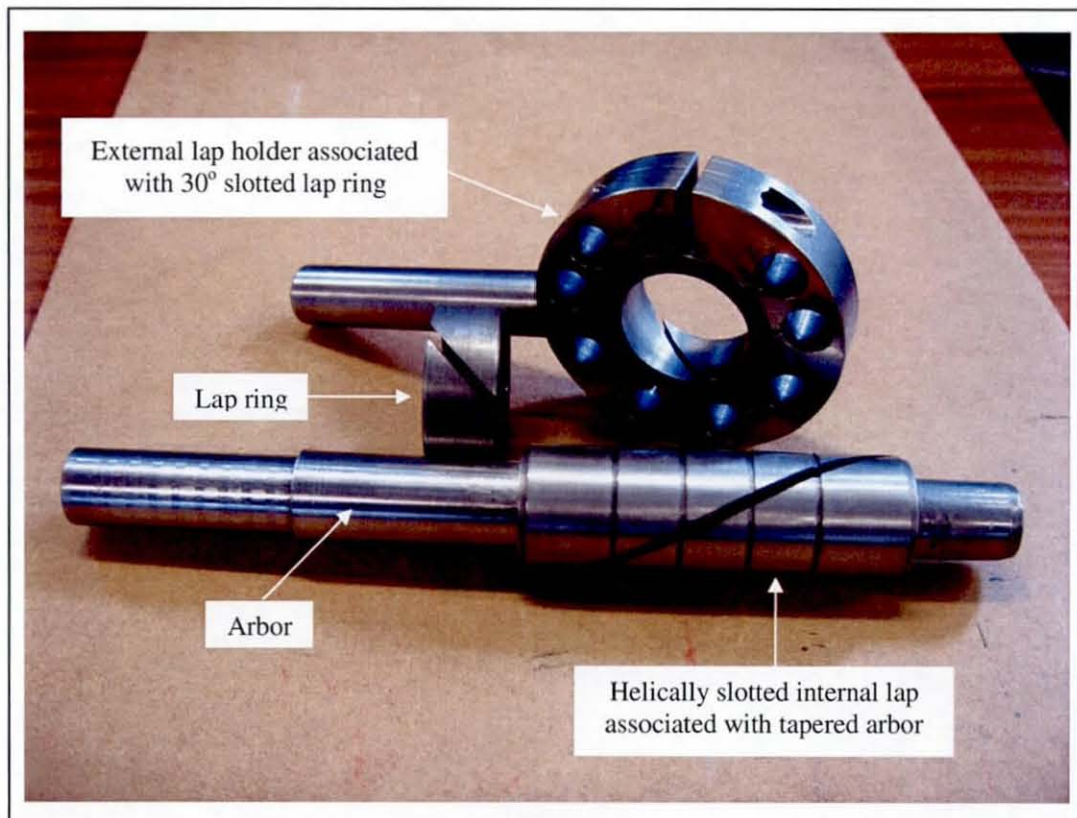


FIGURE 5.16 External and internal lapping tools used in trimming and matching of the piston and cylinder blanks

5.4.5 Lap Contraction/Expansion

The ring lap and helical lap needed to be adjusted so that the contact between lap and blank surfaces fit was appropriate. Methods used in this work for contraction/expansion practices were as follows:

- External lapping tool – initial tightening of the hexagon socket screw stopped the ring lap from slipping out of place. Diamond paste was then applied evenly to the outer surface of the piston blank. The tightening process resumed until the ring lap started to compress the outer surface of the piston blank, and the blank was allowed to rotate in lathe for few cycles in order to improve the evenness of the diamond paste all over the outer surface of the piston blank. Tightening work continued until the ring lap properly fitted the piston blank, however un-tightening was necessary when the ring lap was compressed excessively. The fit was always checked after each successive contraction to avoid any inappropriate fit.
- Internal lapping tool – similar processes as the external lapping tool were carried for internal lapping tool. However the helical lap needed to be expanded to make the contact between lap and inner surface of cylinder blank. This was carried out by gently tapping the lap up the tapered arbour using a mallet and a lap expander until the lap gripped the arbour firmly. The diamond paste was then applied onto the lap, and subsequently the cylinder blank was reciprocated along the rotated lap to improve the evenness of the diamond paste all over the outer surface of the helical lap. Tapping work continued until the helical lap correctly fitted the cylinder blank, with the fit being checked after each successive tap.

5.4.6 Lap Fit

The lap fit is the most difficult part of the lapping process because it is entirely dependent on the judgement of the operator, based on inexpressible sensations i.e. “feeling” [Jones 1915, Hammond 1992]. Furthermore, this “feeling” has a close relationship with the speed of reciprocation and the nature of the lapping motions. In principle, low pressure and rotational speed prevents overheating that might damage the surface. However insufficient pressures applied (loose contact) made the cutting action inefficient (slow and expensive), and generally lead to geometrical flaws such as barrel and bell-mouth shapes. On the other hand, the greater the pressure, the faster the material removal process, but overpressure (too tight contact) may cause surface damage (roughness) to the surface since abrasive grains get caught into valleys, thus deepening them.

Therefore the correct applied pressure (right fit) is crucial in ensuring the dimensional tolerances and surface finish required to be produced. In this work, the right fit was established when the fits between lap and work-piece were as follows:

- Ring lap – the lap holder rotated together with the piston blank at spindle speeds when it was left free, but stopped from rotating when its handle was gripped (by hand) “lightly” assuming that sufficient abrasive had been applied. The gripping force applied was monitored from the beginning of each lapping work, and adjusted accordingly to suit the quality of surface required.
- Helical lap - the cylinder blank rotated together with the helical lap at spindle speeds when it was free, but easily stopped from rotating when the outer surface of the cylinder blank was gripped “firmly” by hand, again assuming that sufficient abrasive had been applied. The gripping force to be applied was monitored and adjusted accordingly as in lapping work of the piston.

Trial and error was used in determining the optimum pressure to be applied in this work, starting with low pressure, and gradually building up, using the lapped blank as an indicator. This process continued until the best conditions were achieved, thus the right fit established.

5.4.7 Lap Materials

The range of the materials of which laps can be made is very wide, and depends on the characteristic of work to be carried out, such as materials to be lapped, tolerances and surface finish to be achieved. Laps are usually made of soft material such as cast iron, copper, brass, lead, polymer, wood etc., and they are “charged” with abrasives which are imbedded stationary into their surfaces, or suspended in a liquid carrier and free to move about. In this work, close-grained cast iron was used as ring laps and helical laps since it is in general, the best material to be used for a higher degree of accuracy in the finished product [Jones 1915]. However, whatever material is used, the lap should be softer than the blank, otherwise the blank will become charged with the abrasives and cut the lap.

5.4.8 Abrasives

The grade or coarseness and type of the abrasive selected, depended upon the surface finish required, material of blank to be lapped and the amount of stock to be removed by the lapping process. Besides the technical specifications, issues of safe use and environmental impact became important factors. The type of the abrasives used were KD diamond compounds produced by Kemet International Limited, that were specially formulated and blended for rapid stock removal, easy cleaning, temperature resistance, lubricity to prevent drying out and superfine surface finish [Kemet 2006b]. They were soluble in both oil and water, and recommended by the manufacturer for precision production applications. The size of the diamond compound used was 25 micron for rapid stock removal process. In the lapping and pre-polishing processes, diamond compounds of sizes 14, 8 and 6 micron were used. In the final polishing work, 6, 3, 1 and ¼ micron of diamond compounds were used, associated with polishing cloths.

5.4.9 Lubricating Fluid

The lubricating fluid used in the lapping and polishing processes is the “vehicle” within which the abrasive grains are suspended. The lighter the vehicle, the faster the cutting process, but this will give the poorest surface qualities. The denser the liquid, the slower the cutting process, but this will produce finer surface qualities [Machinery Publishing n.d]. The OS Type lubricating fluid produced by Kemet International Limited was used in this work. It played a very important role in assisting the diamond compound to cut and polish more effectively. It absorbed frictional heat and diluted the lapping residues that were produced as a result of the cutting action in the lapping process [Kemet 2006c]. Another factor that was considered was its performance in a lubricating role that remained stable even when under high pressure.

5.4.10 Reciprocation Method

In the external lapping process, the piston blank was clamped onto a mandrel which was held in a lathe, and rotated. At the same time, the ring lap which was compressed within a lap holder, was manually stroked back and forth (reciprocated) over the piston blank. The

stroke length was such that the centre point of the ring lap always slightly exceeded both ends of the piston blank. In the internal lapping process, the helical lap which engaged firmly on the tapered arbor was chucked in the lathe, and rotated. Meanwhile, the cylinder blank which was held in one hand was manually reciprocated back and forth over the helical lap. The stroke length was always such that the centre point of the cylinder blank always exceeded both ends of the rotating helical lap.

A characteristic feature of a lapped surface is crosshatching, which makes an excellent lubricant retention and bearing surface [Fischer 1986]. The crosshatch pattern is generated as a function of the reciprocation carried out over the rotating lap/blank. The crosshatch angle obtained on the lapped surface depends on the ratio of the reciprocation speed (stroking speed) to the speed of rotation (spindle speed). In this work, the spindle speed was between 60 to 315 rpm, with a reciprocation speed of between 1 to 10 mms^{-1} , leading to a very small crosshatch angle.

5.4.11 Polishing Method

Polishing improves surface condition either for decorative or functional purposes by removing or smoothing grinding lines, scratches, pits, tool marks, surface defects that adversely affect the appearance or function of a part. It uses abrasives which are firmly attached to a flexible backing such as a polishing cloth, to modify the shape and dimensions of the component being polished. Polishing processes can also be utilised for substantial metal removing purposes, maintaining close tolerances while improving surface conditions [Metals Handbook 1982]. This process causes some plastic working of the surface as metal is removed, hence producing a mirror-finish appearance.

Polishing work started when the final lapping process of piston and cylinder was completed (using 6 μm diamond paste), with approximately 0.5 μm of their diameters left for further removal processes, aimed at improving surface finish and matching the piston into cylinder. Polishing was carried out using Kemet MSF silk-type polishing pads with diamond paste. This self-adhesive synthetic cloth has been developed with a thick and

soft adhesive backing material which was placed underneath a durable woven structure cloth.

The polishing cloth was cut into three rectangular strips, subsequently fixed them (equally-spaced) on the respective laps. The polishing work progressed in the same manner as the lapping process. Different levels of surface roughness produced on each piston were achieved by changing the size of the diamond paste applied in the final lapping process (6 and 8 μm only), and varied appropriately with the pressure applied on the laps. Diversification of the surface roughness has also been done through polishing technique, i.e. changing the grit size of diamond paste applied. Images of the manufactured DF6 tungsten carbide pistons and cylinders are depicted in Figure 5.17.

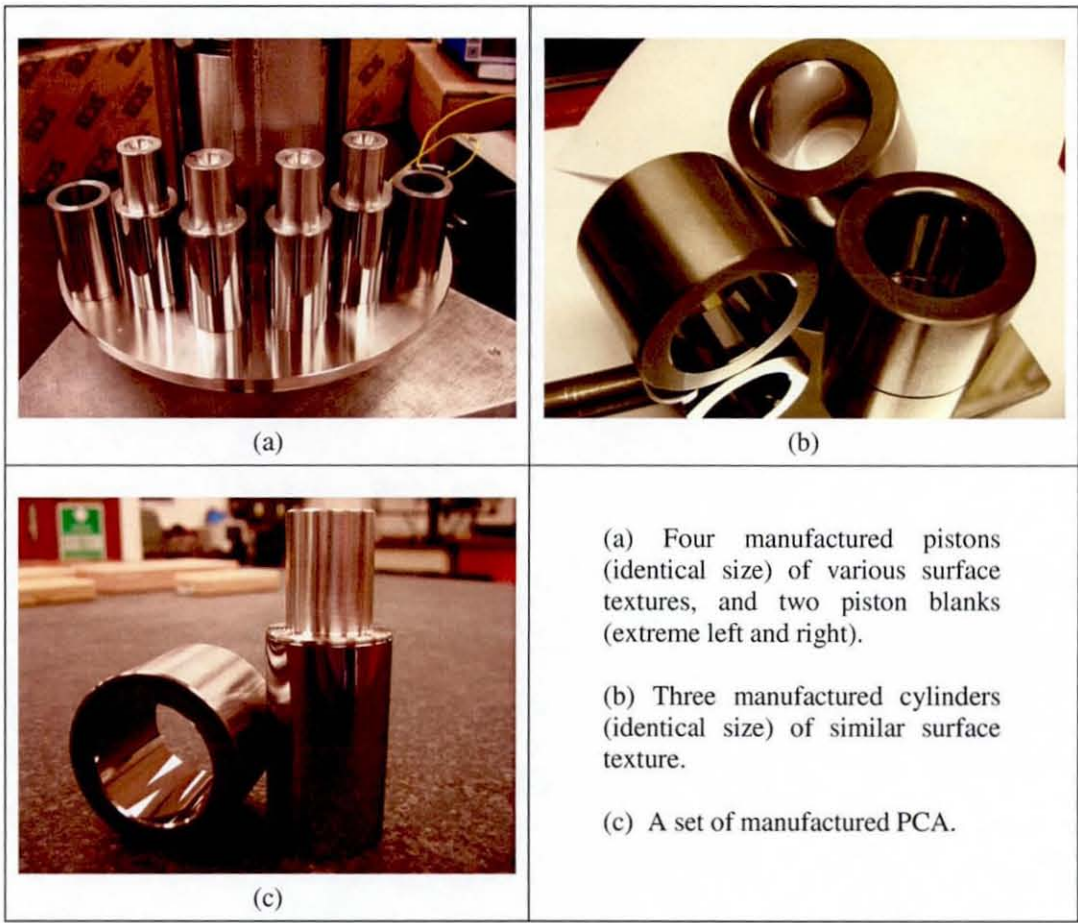


FIGURE 5.17 Manufactured tungsten carbide pistons and cylinders

5.5 SUMMARY

Selection of the right material to be used before the manufacturing process is initiated is very important in order to make sure that the product produced works reliably. 316 stainless steel was chosen for the manufacture of most parts of the pressure balance, complimented with an aluminium base plate. Its design and construction played a very important role in ensuring that its performance was at the top level of accuracy. Meanwhile, manufacturing of PCAs using scrapped soft-materials, followed by the 316 stainless steel provided an excellent foundation of manufacturing knowledge, skill and hands-on experience. A combination of 316 stainless steel has proven to be an unsuitable material for the PCA due to its weakness in adhesive wear resistance, leading to scoring, galling and seizing effects. If demanding tolerances are crucial, harder materials need to be considered, and ironically are easier to manufacture.

Honing processes produced inadequate levels of dimensional accuracy for a gas-operated PCA, hence application of this tool was discontinued. Lapping was identified as the best method to produce PCAs, but is a tedious and expensive process which demands a very skilful operator. Considerable hands-on training was necessary in order to become proficient.

DF6 tungsten carbide was chosen as the final material for the PCA, with lapping and polishing being the best methods for trimming and matching. Correct methods of clamping of the blank, with correct usage of lapping tools, lapping material, abrasives, lubricating fluid, lap fit and reciprocating methods, were the factors which contributed to the successfulness of the lapping process. At the same time, polishing processes were also utilised for metal removing purposes, while maintaining close tolerances and improving surface conditions. Polishing work started when the final lapping process of piston and cylinder was completed, leaving behind approximately $0.5\text{ }\mu\text{m}$ of the diameters for improving surface finish and matching the piston into cylinder. Changing the grit size of the diamond paste and lap fit during the lapping process, followed by variations of grit sizes of diamond paste (applied on the polishing cloth) during polishing process were utilised in manufacture of pistons of various surface textures.

CHAPTER 6

CROSS-FLOATING METHOD AND ITS UNCERTAINTY BUDGET

The emphasis of this chapter is on the fundamental aspect of the cross-floating method and its associated uncertainty budget. It introduces the precautions and general practical aspects related to the cross-floating experiments; discussion of the principles used in the cross-floating experiments; and describes an important element in the measurement result, i.e. the uncertainty of the measurement.

This chapter consists of three sections. Section 6.1 is devoted to the discussion of the practical aspects of use of the pressure balance in the cross-floating method, especially with respect to environmental conditions, location of the workplace, pressure fittings, leveling, handling and cleanliness of the PCA. Section 6.2 elaborates on the cross-floating method itself, concentrating on the two methods of establishing the equilibrium condition, which is crucial in cross-floating experimentation. Section 6.3 presents an explanation of uncertainty of measurement in general, such as types uncertainty, method of combining, sensitivity coefficients, degree of freedom, level of confidence and coverage factor; and also uncertainty of measurement from the cross-floating experiment. Lastly, Section 6.4 provides a summary of this chapter.

6.1 PRACTICAL ASPECTS OF USE OF THE PRESSURE BALANCE IN THE CROSS-FLOATING METHOD

Measurement work can only be carried out when the pressure balances, PCAs, environmental conditions and other related factors are in appropriate condition for such work. The following sections describes the precautions and general practical aspects related to cross-floating experimental work, which needed to be taken care of in order to make sure that the level of relative uncertainties required were achievable.

6.1.1 Environmental Conditions

Acceptable environmental conditions are a pre-requisite in any successful measurement activity. Room temperature, relative humidity and atmospheric pressure were the three main parameters which were continuously monitored during the experimental work. This work was carried out in the Metrology Laboratory, which is dedicated to dimensional metrology related activities, with 24 hour temperature and humidity control, thus environmental conditions were not a problematical issue.

All windows were shielded from direct sunlight, which could introduce temperature gradients within the room. Moreover, the room is equipped with an air-locking system (buffer room), consisting of two doors in series which do not open simultaneously, further helping the stability of the environmental conditions. This controlled-opening of the access door minimised any sudden change of ambient pressure (compression/decompression of air within the calibration room due to door opening/closing) which can disrupt the equilibrium conditions during cross-floating work.

The environmental conditions where the experimental work carried out were as follows:

- Temperature: (19.0 – 21.0) °C, with stability better than 0.5 °C per hour.
- Relative humidity: 40 – 65% RH, with stability better than 10% per hour.
- Atmospheric pressure: as measured.

Table 6.1 tabulates the disturbance factors which are commonly encountered in high-precision cross-floating experiments, where particular attention was given in this work to reduce their effects.

TABLE 6.1 Disturbance factors in high-precision pressure measurement via cross-floating experimentation

No.	Disturbance Factor	Effect on	Effect
1.	Room temperature ($t_r \neq 20^\circ\text{C}$)	<ul style="list-style-type: none"> • Thermal expansion coefficient of the PCA • Floating components • Body of the pressure balance • Air density 	<ul style="list-style-type: none"> • Change in effective area • Change in volume • Thermal stability of the PCA • Change in buoyancy correction
2.	Relative humidity ($h_r \neq 50\%$)	Air density	Change in buoyancy correction
3.	Ambient pressure ($p_r \neq 101.235 \text{ kPa}$)	Air density	Change in buoyancy correction
4.	Air density ($\rho_a \neq 1.2 \text{ kgm}^{-3}$)	Floating components	Change in effective downward force
5.	Sudden change in ambient pressure and air draughts due to rapid door (leaf-type) opening/closing	Equilibrium condition	Random errors
6.	Temperature gradients due to poor temperature distribution or direct sun light	Floating elements	Systematic errors those lead to increase of standard deviation

Other parameters such as room cleanliness, vibration, air draughts and stray magnetic fields were always kept to the appropriate/minimum levels (even though they were not being measured), and they are described in the following section.

6.1.2 Location of the Experimental Pressure System

The best place for installation of the system was chosen, aiming at reducing effects such as vibration, magnetic fields and air draughts due to the air-conditioning system. The laboratory itself is located on the ground floor of a three-story building which should give the lowest vibration levels within the building. Within the laboratory, the location of the work place was chosen near to a corner of the laboratory as it is the most rigid part of the building with the least vibration. This location was situated next to the wall, shared with the next laboratory of the temperature-controlled environment, and it was 3 m from windows. Since the air-conditioning ventilating ports, consisting of four-direction louvers were the main source of draughts, the nearest ventilating port was partially closed. Two louvers that caused air flowing directly towards the workplace were completely closed, while the rest were diverted away from the workplace.

The two pressure balances were placed on a very firm and mechanically stable granite flat table top. The table top itself was placed on an adjustable four-leg stand which stood directly on the floor, without being attached to the wall (simultaneous transmission of vibrations from floor and wall were avoided). The very thick and heavy granite table top ensured that there was no sagging or tilting during operation.

In order to minimise any effects due to magnetic fields, no unrelated ferromagnetic materials were placed on the table top or nearby surroundings. There was no source of strong magnetic fields available around the vicinity such as a transformer or electrical machinery, since balancing errors may arise through magnetic forces which act between floating components and the surroundings. These additional forces (whether attracting or repelling each other) can adversely affect equilibrium conditions, thus a poor reproducibility produced. Cleanliness of the workplace and instruments was taken care of, avoiding dust contamination of all the floating parts. Table 6.2 tabulates other

disturbance factors which could affect pressure measurement results via cross-floating experimentation, where the effects have been minimised in this work.

TABLE 6.2 Other disturbance factors in high-precision pressure measurement

No.	Disturbance Factor	Effect on	Effect
1.	Vibration	Equilibrium condition	Random errors
2.	Magnetic fields	Floating components with high magnetic susceptibility	Systematic errors those lead to great standard deviation and drift
3.	Air draughts due to air-conditioning	Equilibrium condition	Systematic errors those lead to increase of standard deviation
4.	Dust	Floating components	Systematic errors

6.1.3 Pressure Fittings

The most important issue in the gas system pressure circuit plumbing work is safety, since the fluid is highly compressible. Therefore, extreme care was taken in choosing the properly rated and fully compatible type of tubing, sealing components, valves etc. at the maximum pressure envisaged [Heydemann and Welch 1975, Lewis and Peggs 1992]. The pressure circuit was to be kept as short as possible using the largest possible internal diameter tubing, minimising the system volume, and optimising the response time to small changes in pressure (more critical at lower pressure). Proper valve arrangement in the pressure circuit can make cross-floating work more efficient and easier. The use of a constant volume valve is highly recommended especially for an isolation valve, since it can be operated without disturbing the internal pressure of the system [Heydemann and Welch 1975].

In this work, the two pressure balances were connected using 6 mm thermoplastic tubing of 4 mm inner diameter, with associated brass fittings, and a brass ball valve was used for the isolation valve instead of the constant volume valve. All valves and tubing were prior blown with compressed air, followed with nitrogen gas to make sure that the

plumbing system was free from lint, particles of metal or dirt which would introduce erroneous measurements, or damage the PCA. Once plumbing work was completed, leak testing was carried out at the maximum pressure (400 kPa). This was done by applying a soap solution onto all joining parts, where the presence of leaks would be detected through bubbling effects at the offending joint(s).

6.1.4 Leveling

An object is said to be in vertical position if its direction is perpendicularly aligned to the horizon, i.e. the direction of the force of the gravity. If the piston angle is inclined at a small angle of θ radians to the vertical, the total force W acting on the piston will be subjected to a “cosine error” that reduces its value systematically. The effective downward gravitational force, W' acting along the piston axis in this case is given by:

$$W' = W \cos \theta \quad (6.1)$$

The angle θ must be less than 5 arcmin (0.083°) if the error term is to be less than 1 ppm, and must be less than 15 arcmin (0.250°) if the error term is to be less than 10 ppm [Lewis and Peggs 1992]. Since this research was aimed at relative accuracy of less than 10 ppm, leveling became a very important issue to be tackled.

Initially the leveling work was performed by adjusting the three pressure balance leveling feet, with a bull’s eye spirit level placed on top of the piston, while the piston was floating. Adjustment resumed until the spirit level showed an unchanged indication of the air bubble (middle position) throughout 360° of slow-rotation of the piston, which indicated satisfactory vertical orientation. Subsequently, fine adjustment was carried out using a precision spirit level bar of 0.1 mm/m per division or 20 arcsec (0.006°) which permitted a greater degree of leveling accuracy.

Fine adjustment was carried out by placing the weight loading bell directly on top of the piston (without the ball-bearing in place), followed by the subsequent steps:

- The top surface of the weight loading bell and the base of the spirit level bar were cleaned to remove any dirt or dust.

- The spirit level bar was placed in parallel to the two levelling feet, and pressure supplied to let the piston float at its mid-float position.
- Two levelling feet were adjusted until the air bubble settled in the middle of the levelling tube.
- The position of the air bubble was noted as x_s , after the bubble settled (approximately 10 seconds), i.e. $x_s = 0$.
- The weight loading bell was then turned by 180° from its initial position (without touching/moving the spirit level bar). A second reading was noted as y_s , after the air bubble settled.
- Readings were considered +ve values when the air bubble moved towards the left hand side, and -ve value when it moved towards the right hand side (to avoid confusion). When the air bubble remained in its original middle-position after been rotated through 180° , theoretically it indicated that there was no error due to spirit level indication, and the piston was truly vertical.
- However, when there were differences in readings (common case experienced), errors were calculated as follows:

➤ Error due to spirit level indication (in division) is given by:

$$E_l = \frac{(x_s - y_s)}{2} \quad (6.2)$$

➤ Error due to piston verticality (in division) is given by:

$$E_v = \frac{(x_s + y_s)}{2} \quad (6.3)$$

The adjustment process continued until the E_v value approached zero. Once this condition was achieved, adjustment on these two feet was stopped, and they were locked. The weight loading bell was then turned so that the spirit level bar was parallel to the third levelling foot and at a mid point between the first two levelling feet. Similar adjustment was carried out on the third levelling foot (without adjusting the locked feet)

until the E_v value approached zero. Once these two adjustment sequences were completed, theoretically the piston was almost truly vertical, no matter which direction the piston was rotated.

6.1.5 Handling

The PCA, weights and other floating components involved in this experiment demanded great care of handling. Weights were handled with clean gloves to avoid any contamination that could lead to mass errors, and they were covered with laboratory tissue papers or cotton cloths when not in use. A set of trim weights were handled with forceps (synthetic material tips) and were always kept in their wooden box when not in use. Weights and trim weights were cleaned before they were used. Contamination due to light dust deposits were removed using a lens air-blower or clean chamois leather, whereas other contaminations due to finger prints and grease were removed (immediately after being found) using alcohol associated with low-lint paper wipers.

6.1.6 Cleanliness of the PCA

Cleanliness of the PCA was of the utmost importance because any contamination would affect the performance of the pressure balance. Sudden changes in speed of rotation are a normal indication of a contaminated PCA [Lewis and Peggs 1992]. There are two types of contamination that are commonly found in the PCA, i.e. contamination due to particles of matter trapped within the clearance, and contamination due to chemical material such as finger prints [Ruska 1999]. Hard particle contamination may scratch and abrade the highly polished PCA surfaces causing seizure between the two rubbing surfaces, culminating in a damaged PCA. Contamination due to chemical material results in high friction between the two surfaces, thus the piston cannot rotate freely. At the same time this type of contamination may produce a long-term harmful effect to the surfaces, where they may be attacked in a corrosive manner.

A contaminated PCA should be immediately cleaned, but extreme care with the greatest possible skill must be taken. The piston and cylinder are subjected to a degree of risk upon disassembling operation, since both of their surfaces are exposed to the harmful

vicinity such as dirt/particles, corrosive acidic salts of finger prints, and the possibility of accidental events such as contact with other hard materials, or even dropping on the floor/table. Accidental knocking/dropping may result in a chipped piston or cylinder that makes the PCA no longer usable. Besides extreme care, a proper selection of cleaning agent associated with paper wipers (that are not abrasive and low-lint) also plays a very important role to ensure that the PCA is truly clean, simultaneously protecting the PCA from any immediate and long-term harmful effects.

A cleaned work area located near running filtered tap water (in this work, drinking tap water was used) was prepared. The PCA was disassembled by hand which were cleaned and thoroughly dried. If the PCA was found to have too much contamination (e.g. finger prints or grease), the piston and cylinder were initially cleaned using high grade alcohol (e.g. acetone) associated with low-lint wipes (Kimwipes EX-L). They were then rinsed with running tap water while rubbing with another clean kimwipe. Extreme care was taken not to touch (even with cleaned bare hands) the surfaces which had been pre-cleaned.

The next cleaning process was carried out using a gentle liquid hand soap, filtered tap water and kimwipe. A few drops of liquid soap were applied to a folded pre-wetted kimwipe, which was rubbed evenly over the entire inner surface of the cylinder for approximately 20 seconds. Afterwards the cylinder was immediately rinsed with plenty of running tap water, while rubbing its inner surface with another clean kimwipe for a minimum of three times (kimwipe changed), i.e. the overall time taken was approximately 1 minute/rinse/cylinder. Plenty of running tap water was a necessity in ensuring no soap residue was left behind. The cylinder was then wiped with a new clean and dry wipe (soon after the rinsing process) until it was completely dry. The cylinder was then wrapped with clean and dry kimwipes, and was kept in a safe place within the laboratory for thermal stabilisation while waiting for the piston to be cleaned.

The same cleaning procedure was applied to the piston. After the cleaning and drying processes were completed, the piston was also wrapped with clean and dry kimwipes

and kept next to the earlier cleaned cylinder. A minimum period of approximately 15 minutes was given for both the cleaned piston and cylinder to become acclimatised with the laboratory ambient temperature, before they were reassembled. Before reassembling began, the piston and cylinder were wiped with another clean and dry kimwipe then immediately blown with an inert solvent-free gas (RS invertible air duster) to remove any possible lint that may have been attached to the surfaces.

Reassembly was carried out by placing the cylinder upright on a folded kimwipe which was laid on a piece of cleaned smooth plastic laminated material (plastic laminated mouse pad was used in this work). With the piston being held by its head and aligned with the cylinder bore, it was carefully inserted into the top of the cylinder. Without applying any additional force, except the force originated from its own weight, the piston was allowed to sink freely into the cylinder until it touched the kimwipes. No additional force was allowed in this process, to avoid the PCA from scratch/damage. This assembled piston and cylinder, i.e. PCA, was tested for its cleanliness through the following test sequence:

- Once the piston was fully seated on the kimwipe, the piston was lifted upward by approximately 10 mm while maintaining the cylinder seated on the kimwipe.
- With this situation maintained, the assembly was moved aside so that the cylinder base was seated directly on the mouse pad laminated surface.
- The cylinder was lightly pressed downwards to make the trapped air between the hollow-bottom of the piston, cylinder base and the mouse pad surface sealed properly.
- The piston was released accordingly in its floating condition, and the sealing condition was checked by tapping lightly on the piston head (from its top). Satisfactory sealing was indicated by a bouncing piston in the cylinder, from its original position.
- Once satisfactory sealing was achieved, the piston was gently spun either clockwise or counter clockwise to check its free rotation characteristics.

- Satisfactory cleaning process was demonstrated by smooth free rotation of the piston without any sudden change of its speed, and finally stopping in a gradual manner. Perfect cleaning process associated with perfect physical conditions of the two rubbing surfaces (PCA's geometries and their surface finish) resulted in a reversed rotation of the piston (approximately a few arcdegrees) in the last part of its free rotation, just before the final stop.
- Cleaning and testing processes were repeated when a satisfactory performance as described above was not achieved. However, if the performance of the third attempt was still not improved, the PCA was suspected on being damaged, and was not used until further corrective actions/inspections took place.
- The satisfactory PCA was then installed into the pressure balance, and cross-floating experiments were resumed.

6.2 CROSS-FLOATING METHOD

This section is divided into two sections. Section 6.2.1 describes general information about the cross-floating method, and the principles used in determining the equilibrium condition that is commonly practiced in the pressure community. Section 6.2.2 explains the approach used in this research work.

6.2.1 General Cross-floating Method

Cross-floating is one of the methods to determine the effective area and the pressure coefficients of the PCA under test, where the reference and test pressure balances are connected to a common pressure line [Heydemann and Welch 1975, Lewis and Peggs 1992]. Figure 6.1 shows a schematic diagram of a cross-floating set-up used in this work, and Figure 6.2 shows a view of this set up that is sitting on the very stable granite table top. Weights are adjusted onto both pressure balances until the hydrostatic equilibrium is established, with both pistons rotating and floating at their reference levels, simultaneously falling at their natural fall rates.

Once the equilibrium condition is established, the effective area of the test PCA could be calculated based on the ratio between the two loads applied, i.e. the ratio of their effective areas, represented by the ratio of their total loads, as given in the following equations:

$$\frac{A_t}{A_r} = \frac{W_t}{W_r} \quad (6.4)$$

Therefore,

$$A_t = \left(\frac{W_t}{W_r} \right) A_r \quad (6.5)$$

where A_t and A_r are the effective areas of the test and reference PCAs respectively, and W_t and W_r are the effective loads applied onto the test and reference pressure balances. The basis of the cross-floating therefore concentrates on the establishment of the equilibrium condition through load adjustment/trimming. There are two methods which are commonly used in determining the equilibrium condition:

- **Flow-sensing method** – Theoretically, there is “no nett fluid flow” through the connecting pressure line when two PCAs are in equilibrium condition [Lewis and Peggs 1992]. In this method, the fall rates of both pistons being cross-floated are utilised (no differential sensor is required) in giving an indirect indication of the fluid flowing in the pressure line. Each fall rate of the assembly is determined by closing the isolation valve (connecting the two PCAs) and their natural fall-rates are noted. While the isolation valve is opened, the load of one of the pressure balances is precisely adjusted using trim weights until both pistons drop at their natural fall rates. When this condition is achieved, the equilibrium condition is established.
- **Pressure-sensing Methods** – A differential pressure indicator is a necessity if the two systems to be cross-floated use different types of pressure transmitting fluid. This differential pressure indicator may be a null indicator or a differential pressure gauge where their performance contributes the most to the accuracy of the cross-floating experiment. However, a by-passed differential pressure gauge when used as a null indicator with a single type pressure transmitting fluid can

also be utilised in the highest accuracy of cross-floating experiment, as shown in Figure 6.1 [Lewis and Peggs 1992].

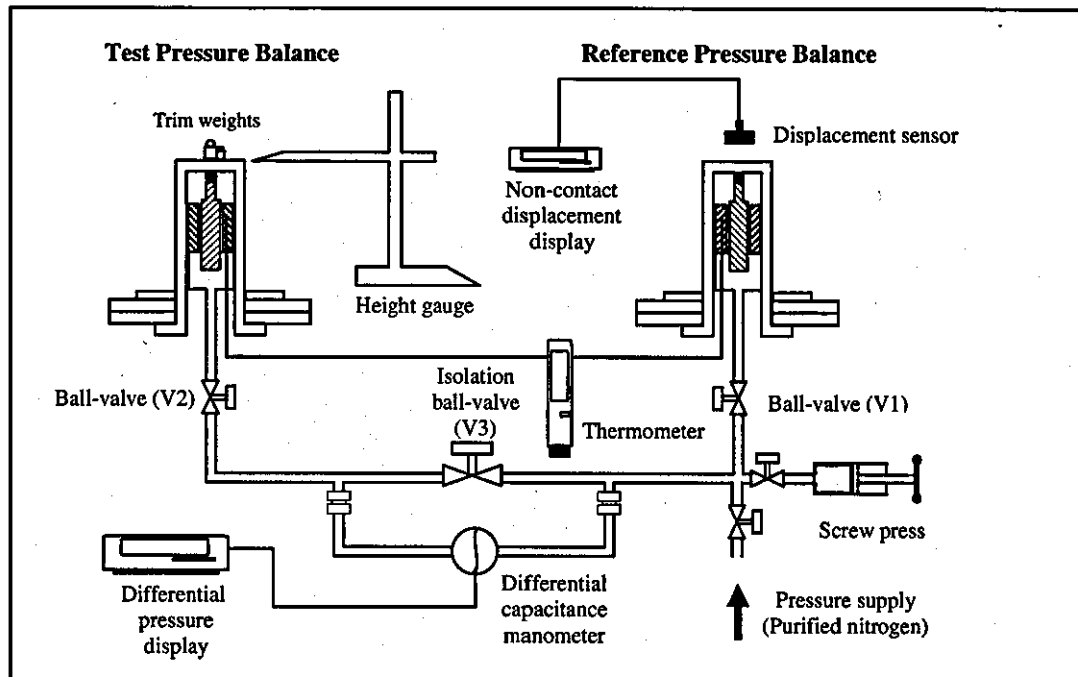


FIGURE 6.1 A schematic diagram of an experimental cross-floating set-up

6.2.2 Cross-floating Method Used in this Research Work

Two types of experiments were carried out in this research via cross-floating methods. The experiments carried out were as follows:

- Investigation on the effect of the rotational speed and rotational direction, on pressure generated, which is discussed in Chapter 7.
- Investigation on the effect of the surface texture on pressure generated, which is discussed in Chapter 8.

A common approach and method which has been used, and is applicable in both experiments (such as cross-floating set-up, measurement point, pressure transmitting

fluid used, method of equilibrium condition determined, temperature and rotational speed measurements carried out) is explained as follows:

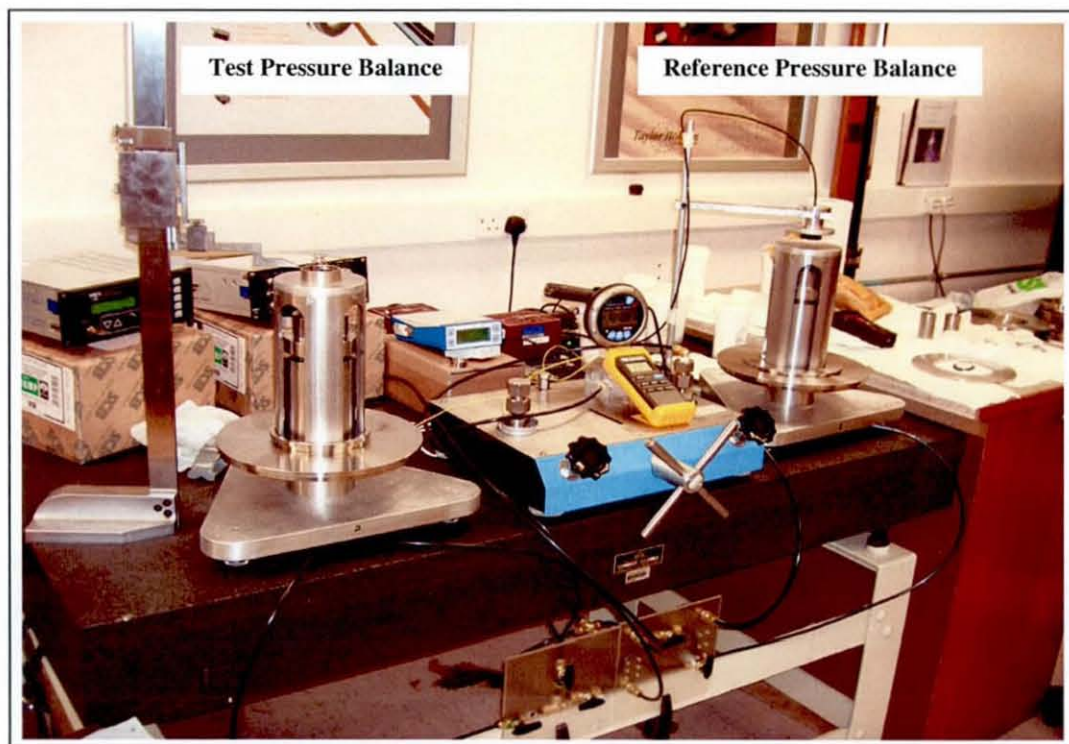


FIGURE 6.2 A picture of an experimental cross-floating arrangement

- Cross-floating Set-up - An arrangement for a traditional cross-floating experiment [Simpson 1994] used in this research work is shown in Figure 6.1 and Figure 6.2. Effective areas of the test PCAs were determined at 100 kPa using purified nitrogen (N_2) of 99.998% purity. A combination of Piston 2 (P_2) and Cylinder 3 (C_3) known as P_2C_3 was used as a reference, whereas the test PCAs were made from the six pistons (P_1 , P_3 , P_4 , P_5 , P_6 and P_7) that were matched with the 2 other cylinders (C_2 and C_4). In order to eliminate the error of the total mass loaded on both pistons, the reference pressure balance was always loaded with a single set of weights throughout the experiment, while the test pressure balance was also loaded with a single set of weights, with variable high

accuracy trim weights added (Mettler-Toledo class F1 weights, ranging from 1 mg up to 100 g), which produced negligible errors for balancing purposes.

- Determination of equilibrium conditions - Initially the natural fall rate of the reference piston was established using a non-contact eddy current displacement transducer (eddyNCDT 3300, manufactured by Micro-Epsilon Messtechnik GmbH) with a resolution of 1 μm . The output was displayed on the controller in the form of displacement units (mm), supplemented with a displacement-bar diagram (displacement/time). The gap between the sensor's front-surface to its target (an aluminium plate that was placed on top of the weight carrying bell) was adjusted, so that the reference level of the reference pressure balance was represented by one assigned gap value. The fall rate value of the reference was established while the piston P_2 was floating and rotating at its mid-float position, while ball valve V1 was closed. The reference level of the test pressure balance was measured and marked using a mechanical height gauge of 0.1 mm readability.
- The actual equilibrium conditions were judged based on the pressure-sensing method. A differential capacitance manometer which acted as a null indicator was used, where it was connected across an isolation ball valve V3. The differential pressure sensor used was a high-accuracy capacitance diaphragm sensor (MKS Type 698A, 1 Torr range). It was set to a 400 msec response time and 0.01 Pa resolutions corresponding to 0.1 ppm at 100 kPa. The sensor was connected to its signal conditioner/display and it was temperature-controlled at 45°C for improved accuracy, hence improved repeatability and stability of its zero reading (crucial as a null indicator). Initial load adjustments were made by adding trim weights onto the test pressure balance, until P_2 's fall rate approached its natural fall rate, while ball valves V1, V2 and V3 were opened.
- Before a final adjustment was made, a reading from the differential pressure sensor was noted, with both pistons in floating and rotating conditions; with valve V3 opened, either one of valves V1 or V2 was closed. In this situation, the differential pressure sensor indicated a reading that represented the zero pressure

difference across the two ports. The final adjustments were achieved by adding or subtracting a trim weight, to/from the test pressure balance, while the ball valves V1, V2 and V3 were opened, i.e. null indicator bypassed [Dadson et al 1982]. The smallest trim weight (discrimination weight) that produced a detectable pressure change (significant effect) in this cross-float was a 2 mg weight, corresponding to 0.2 ppm at 100 kPa. The adjustment process using discrimination weights resumed until the average output of the differential pressure sensor approximately approached the previous value that represented zero pressure difference across the differential sensor.

- The consistency and validity of the cross-floating results produced by the pressure-sensing method were checked by the flow-sensing method. A very similar level of sensitivity in equilibrium (using 2 mg trim weight) was detectable by the displacement sensor, which measured the displacement rate of the reference piston. This displacement rate indirectly indicated the equilibrium condition, was clearly shown by its controller in a real-time bar-diagram. The agreement of the results produced by the differential pressure transducer (pressure-sensing method) and displacement sensor (flow-sensing method) in indicating the equilibrium conditions were very good (within 0.3 ppm). Therefore, the displacement sensor became a backup instrument in making judgement of equilibrium conditions.

6.2.3 Speed and Temperature Measurement

A non-contact laser tachometer of 1 rpm resolution was used to measure the speed of rotation of the pistons. The tachometer emitted a precision laser beam that was aimed at a small piece of a reflective tape, which was affixed to a vertical grooved line on the aluminium plates. Both pressure balances were permanently loaded with identical aluminium plates which were placed on top of the weight loading bells of each pressure balance, to ensure that the external geometry differences between both pressure balances were kept to a minimum. This eliminated systematic errors due to their buoyancy effects, and aerodynamic forces which may arise.

A dual-channel digital thermometer with Type K thermocouples of 0.1°C resolution was to measure the temperature of both PCAs. These thermocouples were inserted into access holes which run through each mounting post (from its bottom surface) to a point, approximately 5 mm distance from the cylinder. Close siting of the thermocouples to each cylinder, associated with very stable thermal stability of the PCAs surrounding, helped the temperature measurement to be carried out in an accurate manner.

6.3 UNCERTAINTY OF MEASUREMENT

The result obtained in any measurement is only an approximation or estimated value, but can be considered as a complete result when it is accompanied with a quantitative statement of uncertainty [ISO/TAG 4 1993, Taylor and Kuyatt 1994, PD6461-4 2004]. Uncertainty is characterised by the dispersion of the values that could reasonably be attributed to the *measurand*, denoted by Y . The measurand (also known as *output quantity*) is determined from N other quantities X_1, X_2, \dots, X_N through a functional relation f :

$$Y = f(X_1, X_2, \dots, X_N) \quad (6.6)$$

Using the equation (6.6) above, an *estimate of the measurand* that is denoted by y can be obtained using *input estimates* (represented by x_1, x_2, \dots, x_N) as follows:

$$y = f(x_1, x_2, \dots, x_N) \quad (6.7)$$

Generally, the uncertainty of the result consists of several components which can be categorised into two groups, i.e. according to the method of estimation that is used in evaluating their numerical values. Those two types are:

- **Type A standard uncertainty** – Evaluated by statistical analysis of a series of observations which is represented by a statistically estimated standard deviation, s_i . It is equal to the positive square root of the statistically estimated variance s_i^2 that is associated with a number of degrees of freedom ν_i . For such a component,

the standard uncertainty is $u_A = s_i$. However, the best experimental standard deviation of a measurement is given by an estimated standard deviation of mean (ESDM), thus the Type A standard uncertainty is given by:

$$u_A(\bar{x}) = \sqrt{\frac{1}{n(n-1)} \sum_{i=1}^n (x_i - \bar{x})^2} \quad (6.8)$$

where n is the number of a series of measurements, x_i is the value of i^{th} input estimates and \bar{x} is the arithmetic mean of input estimates.

- **Type B standard uncertainty** – Evaluated by means other than statistical analysis of a series of observations, which is obtained from previous knowledge or assumed probability (based on belief) distribution from all the available information, usually scientific judgment. Examples of relevant information sources are; previous measurement data, experiences, general knowledge, manufacturer's specifications, calibration reports, handbooks etc. Therefore, Type B standard uncertainty is obtained from the expanded uncertainty, $U_k(x)$ of an available knowledge/scientific judgement at a quoted level of confidence, and divided by its coverage factor k , which is given by:

$$u_B(x) = \frac{U_k(x)}{k} \quad (6.9)$$

Subsequently, a combination of these two standard uncertainties (u_A and u_B) form a combined standard uncertainty of a measurement result y , which is designated by $u_c(y)$. The method used to combine those types of uncertainty is often called the *law of propagation of uncertainty* or the *root-sum-of-square (RSS)*. For uncorrelated input, the $u_c(y)$ is the positive square root of the combined variance $u_c^2(y)$, which is given by:

$$u_c^2(y) = \sum_{i=1}^n \left[\frac{\partial f}{\partial x_i} \right]^2 u^2(x_i) \quad (6.10)$$

where f is a functional relationship that relates the output quantity dependency to the input quantities as given in equation (6.7) and $u(x_i)$ is the individual standard uncertainty arising from type A and/or type B evaluation(s). The partial derivative $\partial f / \partial x_i$, normally

called the *sensitivity coefficient* (denoted with c_i) describes how the output estimate y varies with changes in the values of the input estimates x_i .

In order to eventually sum all the individual input quantities, they must be quoted with the same degree of *level of confidence*. This is carried out by dividing the quantity in question by a *divisor*, which depends on its probability distribution (describes how the results behave). The value of the divisor that can convert the quantity in question to one standard deviation is shown in Table 6.3 below [Davidson et al. 2004]:

TABLE 6.3 Commonly used probability distribution in uncertainty calculation, and its divisor

No.	Distribution	Divisor	Description
1	Normal	1 or 2	Also known as Gaussian distribution where the values are more likely to fall closer to the mean value than further away from it, i.e. resembles a bell
2	Rectangular	$\sqrt{3}$	The results are evenly spread between two limits, and never fall outside these limits
3	Triangular	$\sqrt{6}$	The distribution when two rectangular distributions are added together

Unfortunately, a combined standard uncertainty alone is not sufficient to provide a comprehensive statement of uncertainty. This is due to the lack of information on the interval about the measurement result y within which the value of the measurand Y is confidently believed to lie. Therefore an *expanded uncertainty*, denoted by U_p is used to meet this requirement i.e. by multiplying $u_c(y)$ by *coverage factor*, k_p thus:

$$U_p = k_p u_c(y) \quad (6.11)$$

This high specified coverage probability or level of confidence p confidently gives the quantity of measurand as $y - U_p \leq Y \leq y + U_p$ (commonly written as $Y = y \pm U_p$).

However, the t -distribution in general will not describe the distribution of the variable $(y - Y)/u_c(y)$ if $u_c^2(y)$ is the sum of two or more estimated variance components, i.e.

$u_c^2(y) = c_i^2 u^2(x_i)$. Therefore, an alternative approach may be used where the distribution of that variable may be approximated by a t -distribution through an *effective degree of freedom* v_{eff} . The v_{eff} can be calculated from the Welch-Satterthwaite formula which is as follows [ISO/TAG 4 1993]:

$$v_{eff} = \frac{u_c^4(y)}{\sum_{i=1}^n \frac{u_i^4(y)}{v_i}} \quad (6.12)$$

The degree of freedom, v_i for individual uncertainty contribution of Type A and Type B distribution is usually taken as $(n-1)$ and infinity respectively. For a quantity of normal distribution with infinite degree of freedom, the value of coverage factor k_p that produces a level of confidence p is given in Table 6.4 below:

Finally, once the v_{eff} is calculated, the t -factor can be obtained for the desired level of confidence p from the Student- t Distribution Table. Its value which is denoted by $t_p(v_{eff})$ thus makes the Equation 6.11 become:

$$U_p = k_p u_c(y) = t_p(v_{eff}) u_c(y) \quad (6.13)$$

However, the total calculated uncertainty obtained from equation (6.13) above is commonly written as:

$$U = k u_c(y) \quad (6.14)$$

Meaning that the quantity of measurand confidently lies within $y - U \leq Y \leq y + U$ or $Y = y \pm U$.

TABLE 6.4 Level of confidence and its coverage factor

Level of confidence, p (percentage)	Coverage factor, k_p
68.27	1
90	1.645
95	1.960
95.45	2
99	2.579
99.73	3

6.3.1 Uncertainty of Measurement in the Cross-floating Method of Gas-operated Pressure Balance

Once the equilibrium condition of a cross-floating experiment is established (after the final adjustment of the trim weight), the gauge pressure p_r and p_t at each reference level of the respective reference and test pressure balances are given as follows [Nishibata 1997]:

- Reference pressure balance:

$$p_r - p_{ar} = \frac{m_{pr} g_L (1 - \rho_a / \rho_{pr}) + (m_{wr} - m_{pr}) g_L (1 - \rho_a / \rho_{wr})}{A_{r(p, 20^\circ C)} [1 + \lambda_r (p_r - p_{ar})] [1 + (\alpha_{pr} + \alpha_{cr})(t_r - 20)]} \quad (6.15)$$

- Test pressure balance:

$$p_t - p_{at} = \frac{m_{pt} g_L (1 - \rho_a / \rho_{pt}) + (m_{wt} - m_{pt}) g_L (1 - \rho_a / \rho_{wt})}{A_{t(p, 20^\circ C)} [1 + (\alpha_{pt} + \alpha_{ct})(t_t - 20)]} \quad (6.16)$$

where:

p_r is the gauge pressure at the reference level of the reference pressure balance (Pa)

p_t	is the gauge pressure at the reference level of the test pressure balance (Pa)
p_{ar}	is the atmospheric pressure at equilibrium condition at the reference pressure balance (Pa)
p_{at}	is the atmospheric pressure at equilibrium condition at the test pressure balance (Pa)
m_{pr}	is the mass of the reference piston (kg)
m_{pt}	is the mass of the test piston (kg)
g_L	is the local acceleration due to gravity (ms^{-2})
ρ_a	is the air density of the ambient air (kgm^{-3})
ρ_{pr}	is the density of the reference piston (kgm^{-3})
ρ_{pt}	is the density of the test piston (kgm^{-3})
m_{wr}	is the total mass of weights, including piston and any other floating elements loaded on the reference pressure balance (kg)
m_{wt}	is the total mass of weights, including piston and any other floating elements loaded on the test pressure balance (kg)
ρ_{wr}	is the density of the weights loaded on the reference pressure balance (kgm^{-3})
ρ_{wt}	is the density of the weights loaded on the test pressure balance (kgm^{-3})
$A_{r(p,20^\circ\text{C})}$	is the effective area of the reference PCA at pressure p and reference temperature 20°C (m^2)
$A_{t(p,20^\circ\text{C})}$	is the effective area of the test PCA at pressure p and reference temperature 20°C (m^2)
λ_r	is the pressure distortion coefficient of the effective area of the reference PCA (Pa^{-1})
α_{pr}	is the linear thermal expansion coefficients of the reference piston ($^\circ\text{C}^{-1}$)
α_{pt}	is the linear thermal expansion coefficients of the test piston ($^\circ\text{C}^{-1}$)
α_{cr}	is the linear thermal expansion coefficients of the reference cylinder ($^\circ\text{C}^{-1}$)
α_{ct}	is the linear thermal expansion coefficients of the test cylinder ($^\circ\text{C}^{-1}$)
t_r	is the temperature of the reference PCA ($^\circ\text{C}$)
t_t	is the temperature of the test PCA ($^\circ\text{C}$)

If there is a height difference in the reference level of the two pressure balances, the fluid head correction (H) must be applied. The pressure difference within the system between two levels of Δh apart, at the density of pressure transmitting fluid ρ_f is given by:

$$H = (\rho_f - \rho_a) g_L \Delta h \quad (6.17)$$

However, if the reference level of test piston is Δh higher than the reference piston, the equilibrium condition based on equation 6.15, 6.16 and 6.17 is given by:

$$(p_r - p_{ar}) - (\rho_f - \rho_a) g_L \Delta h = (p_t - p_{at}) \quad (6.18)$$

From equation 6.17, the effective area of test $A_{t(p, 20^\circ\text{C})}$ can be written as follows:

$$A_{t(p, 20^\circ\text{C})} = \frac{m_{pt} g_L (1 - \rho_a / \rho_{pt}) + (m_{wt} - m_{pt}) g_L (1 - \rho_a / \rho_{wt})}{[(p_r - p_{ar}) - (\rho_f - \rho_a) g_L \Delta h] [1 + (\alpha_{pt} + \alpha_{ct})(t_t - 20)]} \quad (6.19)$$

Equation 6.19 can also be expressed as:

$$A_{t(p, 20^\circ\text{C})} = \frac{\frac{m_{pt} g_L (1 - \rho_a / \rho_{pt}) + (m_{wt} - m_{pt}) g_L (1 - \rho_a / \rho_{wt})}{[1 + (\alpha_{pt} + \alpha_{ct})(t_t - 20)]}}{\frac{m_{pr} g_L (1 - \rho_a / \rho_{pr}) + (m_{wr} - m_{pr}) g_L (1 - \rho_a / \rho_{wr})}{A_{r(p, 20^\circ\text{C})} [1 + \lambda_r (p_r - p_{ar})] [1 + (\alpha_{pr} + \alpha_{cr})(t_r - 20)]} - (\rho_f - \rho_a) g_L \Delta h} \quad (6.20)$$

The density of the pressure transmitting fluid used (purified nitrogen), $\rho_{N_2(t,p)}$ at temperature t_{N_2} in $^\circ\text{C}$ and pressure p_{N_2} in Pa is given by [Nishibata 1997]:

$$\rho_{N_2(t,p)} = \frac{\rho_{N_2(20^\circ\text{C}, 101325\text{Pa})}}{[1 + 0.00341(t_{N_2} - 20)]} \left(\frac{p_{N_2}}{101325} \right) \quad (6.21)$$

where the value of $\rho_{N_2(20^\circ\text{C}, 101325\text{Pa})}$ is 1.165 kgm^{-3} . On the other hand, the standard method for determining the air density in kgm^{-3} involves the measurement of

environmental conditions such as temperature t_a in $^{\circ}\text{C}$, pressure p_a in Pa and relative humidity h_r in percent. The following approximate formula may also be used [OIML R111-1 2004]:

$$\rho_a = \frac{0.0034848 p_a - 0.009 h_r e^{0.061 t_a}}{(273.15 + t_a)} \quad (6.22)$$

The standard uncertainty of the effective area of the test PCA $u(A_{t(p, 20^{\circ}\text{C})})$ is obtained by combining the standard uncertainties of input parameters using the law of propagation of uncertainty, where its variance $u^2(A_{t(p, 20^{\circ}\text{C})})$ is given by:

$$u^2(A_{t(p, 20^{\circ}\text{C})}) = \sum_{i=1}^n \left[\frac{\partial A_{t(p, 20^{\circ}\text{C})}}{\partial x_i} \right]^2 u^2(x_i) \quad (6.23)$$

where $u(x_i)$ is the individual standard uncertainty of the input parameter x_i , associated with its partial derivative $\partial A_{t(p, 20^{\circ}\text{C})} / \partial x_i$. The sensitivity coefficient of each input parameter can be calculated based on equations (6.19) and (6.20). In gauge mode operation, the terms $(p_r - p_{ar})$ and $(p_t - p_{at})$ can respectively be replaced with p_r and p_t since $p_{ar} \approx p_a$ and $p_{at} \approx p_a$; and the symbols $A_{r(p, 20^{\circ}\text{C})}$ and $A_{t(p, 20^{\circ}\text{C})}$ can be simplified as A_{r0} and A_t respectively, thus all the individual sensitivity coefficients are given as follows [Nishibata 1997]:

$$\partial A_t / \partial m_{wt} = A_t / m_{wt} \quad (6.24)$$

$$\partial A_t / \partial \rho_a = -A_t / [\rho_{wt}(1 - \rho_a / \rho_{wt})] \quad (6.25)$$

$$\partial A_t / \partial \rho_{wt} = A_t (\rho_a / \rho_{wt}^2) / (1 - \rho_a / \rho_{wt}) \quad (6.26)$$

$$\partial A_t / \partial \alpha_{pt} = -A_t (t_t - 20) \quad (6.27)$$

$$\partial A_t / \partial \alpha_{ct} = -A_t (t_t - 20) \quad (6.28)$$

$$\partial A_t / \partial t_t = -A_t (\alpha_{pt} + \alpha_{ct}) \quad (6.29)$$

$$\partial A_t / \partial p_r \approx -A_t / p_r \quad (6.30)$$

$$\partial A_t / \partial m_{wr} = (\partial A_t / \partial p_r)(\partial p_r / \partial m_{wr}) = -A_t / m_{wr} \quad (6.31)$$

$$\partial A_t / \partial \rho_a = (\partial A_t / \partial p_r)(\partial p_r / \partial \rho_a) = A_t / [\rho_{wr}(1 - \rho_a / \rho_{wr})] \quad (6.32)$$

$$\partial A_t / \partial \rho_{wr} = (\partial A_t / \partial p_r)(\partial p_r / \partial \rho_{wr}) = -A_t(\rho_a / \rho_{wr}^2) / (1 - \rho_a / \rho_{wr}) \quad (6.33)$$

$$\partial A_t / \partial \alpha_{pr} = (\partial A_t / \partial p_r)(\partial p_r / \partial \alpha_{pr}) = A_t(t_r - 20) \quad (6.34)$$

$$\partial A_t / \partial \alpha_{cr} = (\partial A_t / \partial p_r)(\partial p_r / \partial \alpha_{cr}) = A_t(t_r - 20) \quad (6.35)$$

$$\partial A_t / \partial t_r = (\partial A_t / \partial p_r)(\partial p_r / \partial t_r) = -A_t(\alpha_{pr} + \alpha_{cr}) \quad (6.36)$$

$$\partial A_t / \partial A_{r0} = (\partial A_t / \partial p_r)(\partial p_r / \partial A_{r0}) = A_t / A_{r0} \quad (6.37)$$

$$\partial A_t / \partial \lambda_r = (\partial A_t / \partial p_r)(\partial p_r / \partial \lambda_r) \approx A_t p_r \quad (6.38)$$

$$\partial A_t / \partial \rho_f \approx (A_t / p_r) g_L \Delta h \quad (6.39)$$

$$\partial A_t / \partial \rho_a \approx -(A_t / p_r) g_L \Delta h \quad (6.40)$$

$$\partial A_t / \partial \Delta h \approx -(A_t / p_r)(\rho_f - \rho_a) g_L \quad (6.41)$$

All these sensitivity coefficients are subsequently used in the uncertainty budget calculations, which are applied in Tables 7.7, 7.8 and 9.3.

6.4 SUMMARY

This chapter has devoted its discussion to the practical aspects of use of the pressure balance in the cross-floating method, establishment of the equilibrium condition in the cross-floating experiment, and evaluation procedures for measurement uncertainty. Stable environmental conditions (temperature, relative humidity and ambient pressure) within acceptable tolerances are a prerequisite for successful cross-floating work, since these parameters will cause adverse effects on measurement results if they have not been adequately controlled. Other parameters such as room cleanliness, vibration, leveling of the PCA, plumbing procedures, air draughts and stray magnetic fields, must always be kept to the appropriate/minimum levels, to ensure effects will not contribute errors to the measurement results.

In this research, establishment of the equilibrium condition was judged based on the pressure sensing method via a bypassed high-accuracy capacitance differential pressure sensor, which gave a relative uncertainty of 0.2 ppm at 100 kPa. However, its consistency and validity was checked through the flow sensing method, which utilised a non-contact eddy-current displacement sensor. Initial measurement results showed that both methods agreed within 0.3 ppm, thus the flow sensing became a backup method in establishing equilibrium condition.

Any measurement result is only an approximation or estimated value, and it is considered as a complete result if the value quoted is accompanied with an expanded uncertainty associated with its level of confidence. In order to achieve this, a proper approach must be performed in the following sequence; identify all sources and types of uncertainty involved individually, convert them into standard uncertainties, identify the degree of freedom of each component, combine all the Type A and Type B standard uncertainties to become a combined standard uncertainty, determine their individual degree of freedom, compute the effective degree of freedom using Welch-Satterthwaite formula, obtain the t -factor of the desired level of confidence from the Student- t Distribution Table, and finally multiply the obtained t -factor with the computed combined standard uncertainty. These techniques will be used to assess the errors in the experimentations, as described in Chapters 7, 8 and 9.

CHAPTER 7

INVESTIGATION OF THE EFFECTS OF ROTATIONAL SPEED AND ROTATIONAL DIRECTION ON THE DETERMINED EFFECTIVE AREA

It was described earlier in Chapter 6 that the test PCA must be compared against a reference PCA (of known effective area) in order to determine its effective area, through the cross-floating method. This chapter presents a unique investigative approach (consisting of Experiments E and F) on the effects of rotational speed (RS) and rotational direction (RD) on the determination of the effective area. The aim of these experiments was to investigate if there was evidence of pressure dependency on the RS and RD, using the 35 mm PCAs. The approach investigated two combinations of test PCAs, consisting of one test piston, matched with two identical test cylinders.

This chapter is organised as follows: The next section highlights the rationale behind this investigative approach. Section 7.2 describes the approach implemented in these investigations, on top of the general procedures described in Chapter 6. Sections 7.3 and 7.4 discuss the results obtained from these experiments, and is followed with their respective uncertainty analysis. Lastly, Chapter 7.5 summarises this chapter, and concludes the results obtained from the two experiments.

7.1 RATIONALE

Specific research devoted to the investigation of the effects of rotation on gas-operated pressure balances have been carried out by Prowse and Hatt [1977], and Sutton [1979] using a gas-operated pressure balance (Type 6-201, manufactured by CEC, USA), operated at 3 to 10 Hz, mostly using an 81 mm² PCA. Prowse and Hatt identified that

the generated pressure varied with frequency of rotation in gauge mode operation; whereas Sutton discovered that the presence of aerodynamic effects on a rotating floating element increased the generated pressure with its rotational frequency squared, and the extrapolated pressure for zero frequency corresponded to the calculated pressure.

However, the recent development of very large tungsten carbide PCAs, being commonly used as primary pressure standards, operated at relatively low rotational speeds (approximately 0.5 to 1 Hz) has extended significantly beyond the operating parameters of the previous instruments and reported research, and hence the understanding of the effect of RS and RD. There has been no more published research work available on this topic since these two papers, which has prompted the investigation of low, rather than high speed of rotation (to suit the current type of pressure balances) aimed at disclosing any findings obtained. This investigation has been motivated by the need to characterise the pressure balances developed at LU (compatible with existing pressure balances in the market), and simultaneously tackle the RSs and/or RDs issues by novel approaches. The results from this investigation are believed to be more pertinent and relevant to the current applications of the pressure balances in-use today.

7.2 INVESTIGATIVE APPROACH

The scope of this approach was to determine the apparent dependency of the RS and RD on the generated pressure using the 35 mm diameter PCAs in gauge mode operation. Apparent dependencies would be realised with changes of generated pressure, consequently substantiated as variations of calculated effective areas. The effective areas of the very large PCAs were determined through the traditional cross-floating method [Simpson 1993], which was described (in general) in Chapter 6. The reference PCA used was a combinations of Piston 2 and Cylinder 3 (designated as P_2C_3), whereas the test PCAs were the combinations of Piston 4 that was matched with two identical cylinders (Cylinder 2 and Cylinder 4), designated as P_4C_2 and P_4C_4 respectively. Comparisons between P_4C_2 and P_4C_4 , against P_2C_3 , were known as Experiment E and Experiment F respectively. Experiments were carried out at a single nominal pressure i.e. 100 kPa, but

changing the magnitude of RS randomly, from approximately 30 to 90 rpm (0.5 - 1.5 Hz); and the RD either clockwise (CW) or counter-clockwise (CCW) on the reference and/or test pressure balances.

The “true pressure value” (consistent with the definition of the pressure unit) generated by the reference PCA was not important in these investigations. The relative values of the test results (against any assigned reference value) were the prime concern, hence an approximation value of the reference value was sufficient. Therefore, before cross-floating began, a value (effective area) of P_2C_3 was determined simply through dimensional measurements. The outer diameter of the piston and the inner diameter of the cylinder were measured using a length comparator and a bore gauge at three levels (equally-spaced) of each component respectively. Each level consisted of three points, producing nine measurement points for each component. All readings obtained from the instrument were compared directly against a set of block gauges for appropriate corrections. The average of these eighteen corrected readings was used as a reference value, denoted as $A_{r(P_2C_3)}$. It was assigned to be equal to 981.45955 mm^2 at 100 kPa and 20°C . This value was used consistently in these two experiments for the calculation of the effective areas of the test PCAs.

7.2.1 Comparison Procedure

All preparations described in Section 6.2.2 were carried out prior to the experiments. Appropriate single set of weights, which corresponded to the fixed pressure point (100 kPa) were loaded onto both pressure balances, then the system was pressurised until both pressure balances were floating. Trimming work (fine weight adjustment using a set of standard weights or trim weights) was carried out on the test pressure balance until equilibrium condition was established. Once equilibrium was established, the total masses loaded (including trim weights), PCAs’ temperature, RDs and RSs of both pressure balances were noted.

At the same time, the environmental conditions, such as atmospheric pressure, ambient temperature and relative humidity were measured. Due to the very good stability of the

environmental conditions of the laboratory, the averaged value of the air density was believed to be sufficient for the calculations of the air buoyancy correction. These environmental conditions were taken four times, i.e. at the beginning, quarter, three quarter, and end of the measurement process (within the one day experiment). The environmental data were used to calculate the respective air densities, based on Equation (6.22). An average of four calculated air density values was then used as an approximated air density in effective area calculations, i.e. using Equation (6.20).

Once all of the required parameters were keyed into the excel spreadsheet, instantaneous values of each effective area could be obtained. It was important to detect the existence of any systematic or random errors within the system, which needed appropriate and prompt rectification. Comparison of all the results were based on the determined effective areas at 100 kPa and corrected to 20 °C where the calculated effective areas for the combinations of P_4C_2 and P_4C_4 were symbolised by $A_{P_4C_2}$ and $A_{P_4C_4}$ respectively; and their averaged values were denoted by $A_{(P_4C_2)E}$ and $A_{(P_4C_4)F}$ respectively. These symbols have consistently been used in the following data analysis processes.

7.2.2 Cycle of Measurement

A simplified version of the excel spreadsheet that was used for data collection is depicted in Table 7.1. It shows all the parameters that needed to be noted during the experimental work. Eight cycles (CYLs) of comparison, consisting of 32 individual sequences of measurement (SEQs), were applied to both of the experiments. Each CYL consisted of four different pairs (reference-test) of the rotational combination (RC), which were sequentially arranged in RD-RD terms as follows:

- CW-CW
- CW-CCW
- CCW-CCW
- CCW-CW

} Each cycle of measurement process consisted of four pairs of RC, where each RC consisted of a pair of a RD-RD combination. However, RD was always accompanied with its associated RS.

TABLE 7.1 A simplified version of the excel spreadsheet used in the effective area calculations

C Y L	S E Q	Reference PCA: P ₂ C ₃					Test PCA:					
		Pressure (kPa)	Mass (kg)	Temp (t, °C)	RD & RS		Mass (kg)	Temp (t, °C)	RD & RS		Effec. Area (mm ²)	
					CW/CCW	rpm			CW/CCW	rpm	(t, °C)	(20 °C)
1	1	100			CW				CW			
	2	100			CW				CCW			
	3	100			CCW				CW			
	4	100			CCW				CCW			
2	5	100			CW				CW			
	6	100			CW				CCW			
	7	100			CCW				CW			
	8	100			CCW				CCW			
7	25	100			CW				CW			
	26	100			CW				CCW			
	27	100			CCW				CW			
	28	100			CCW				CCW			
8	29	100			CW				CW			
	30	100			CW				CCW			
	31	100			CCW				CW			
	32	100			CCW				CCW			
Environmental Conditions												
No	Temp (°C)		Humidity (%RH)		Atm. Pressure (hPa)		Air Density (kgm ⁻³)		Average Calculated Air Density, ρ_a _____ kgm ⁻³			
1												
2												
3												
4												

Note:

CYL: Cycle of measurement
SEQ: Sequence of measurement

7.3 MEASUREMENT RESULTS

Measurement results obtained in these two experiments are presented in two sections. Section 7.3.1 is dedicated to Experiment E and Section 7.3.2 is for Experiment F. Two non SI units were consistently used in this research, i.e. °C and mm² instead of K and m², since they are commonly used within the pressure community all over the world. However, the results obtained could easily be converted into the SI unit, pascal (Pa) without loosing any accuracy.

7.3.1 Results of Experiment E: P₄C₂ vs. P₂C₃

The overall results obtained from this experiment are tabulated in Table 7.2. The first column shows the CYL, whilst the second column gives the SEQ. This experiment took one and half days, with the first three cycles completed on the first day and the last five cycles completed on the second day. This means that the effective areas were calculated at 100 kPa (and corrected to 20 °C) based on two respective averaged calculated air densities. The calculated effective areas, denoted by $A_{P_4C_2}$ are given in the third and fourth columns in m² and mm² respectively. The RDs of the reference and test are shown in the fifth and seventh columns, while the RSs of the reference and test are shown in the sixth and eighth columns.

The key figures based on a basic statistical analysis are given in the last five rows where the minimum, maximum and average values of the determined effective area were 981.4919 mm², 981.4946 mm² and 981.4934 mm² respectively. The maximum difference between these results was 0.0027 mm² which is equivalent to 2.7 ppm, relative to their averaged value. The measure of how widely these $A_{P_4C_2}$ values dispersed from the averaged value is represented by the standard deviation, where its relative value which is equivalent to 0.75 ppm is shown in the last row. However, to visualise these results clearer, a 3-Dimensional illustration of the $A_{P_4C_2}$ as a function of their RSs (inclusive RDs) for both reference and test PCAs is plotted, as depicted in Figure 7.1.

TABLE 7.2 A_{P4C2} tabulated in accordance to their cycles and measurement sequences

CYL	SEQ	Effective Area of P_4C_2 at 100kPa, 20°C		Rotational Combination (RC)			
		A_{P4C2}		Reference PCA (P_2C_3)		Test PCA (P_4C_2)	
		(m ²)	(mm ²)	RD	RS (rpm)	RD	RS (rpm)
1	1	9.8149320E-04	981.4932	CW	62	CW	65
	2	9.8149222E-04	981.4922	CW	61	CCW	57
	3	9.8149320E-04	981.4932	CCW	73	CCW	68
	4	9.8149286E-04	981.4929	CCW	58	CW	55
2	5	9.8149261E-04	981.4926	CW	57	CW	58
	6	9.8149286E-04	981.4929	CW	62	CCW	66
	7	9.8149192E-04	981.4919	CCW	65	CCW	71
	8	9.8149311E-04	981.4931	CCW	65	CW	57
3	9	9.8149266E-04	981.4927	CW	57	CW	64
	10	9.8149222E-04	981.4922	CW	60	CCW	62
	11	9.8149212E-04	981.4921	CCW	71	CCW	72
	12	9.8149261E-04	981.4926	CCW	52	CW	59
4	13	9.8149320E-04	981.4932	CW	59	CW	65
	14	9.8149384E-04	981.4938	CW	62	CCW	75
	15	9.8149394E-04	981.4939	CCW	73	CCW	72
	16	9.8149271E-04	981.4927	CCW	47	CW	58
5	17	9.8149339E-04	981.4934	CW	56	CW	56
	18	9.8149384E-04	981.4938	CW	59	CCW	65
	19	9.8149364E-04	981.4936	CCW	66	CCW	65
	20	9.8149437E-04	981.4944	CCW	68	CW	62
6	21	9.8149378E-04	981.4938	CW	62	CW	62
	22	9.8149369E-04	981.4937	CW	66	CCW	68
	23	9.8149378E-04	981.4938	CCW	78	CCW	80
	24	9.8149418E-04	981.4942	CCW	64	CW	69
7	25	9.8149413E-04	981.4941	CW	69	CW	67
	26	9.8149457E-04	981.4946	CW	62	CCW	59
	27	9.8149437E-04	981.4944	CCW	58	CCW	48
	28	9.8149408E-04	981.4941	CCW	60	CW	67
8	29	9.8149378E-04	981.4938	CW	67	CW	67
	30	9.8149359E-04	981.4936	CW	56	CCW	52
	31	9.8149428E-04	981.4943	CCW	67	CCW	62
	32	9.8149398E-04	981.4940	CCW	53	CW	63
Minimum Value		981.4919	mm ²	47 rpm		48 rpm	
Maximum Value		981.4946	mm ²	78 rpm		80 rpm	
Average Value ($A_{(P4C2)E}$)		981.4934	mm ²	62 rpm		64 rpm	
Standard Deviation		0.0007	mm ²	7 rpm		7 rpm	
Relative Standard Deviation		0.75	ppm	11 %		11 %	

Figure 7.1 shows clearly the overall variations of A_{P4C2} with its RCs, which are represented by RS of the reference and the RS of the test on the x-axis and y-axis respectively. The heights of the conical bars on the z-axis represent the A_{P4C2} values, where one division is scaled at 1 ppm, relative to the averaged value. These values distributed on the x-y plane, form four small groups, with the averaged value, $A_{(P4C2)E}$ represented by a conical bar which is located on the (0,0) coordinate (in the centre of the figure). The RDs in CW directions are denoted by positive figures, and negative figures for CCW directions.

Since the differences were small, the nature of this 3-Dimensional figure is unable to show any significant dependency between the four RCs, hence another figure has been plotted 2-dimensionally to visualise these results in an alternative way i.e. singly based on the RSs of the individual PCAs involved (regardless of their SEQ). A graph based on the fourth column against the sixth and eighth columns of Table 7.2 has been plotted (see Figure 7.2), where two separate trend lines can be seen. The RS and A_{P4C2} are represented by x-axis and y-axis respectively. Figure 7.2 still shows that there is no significant evidence of A_{P4C2} dependency on the RS since both lines show similar random fluctuation of variations.

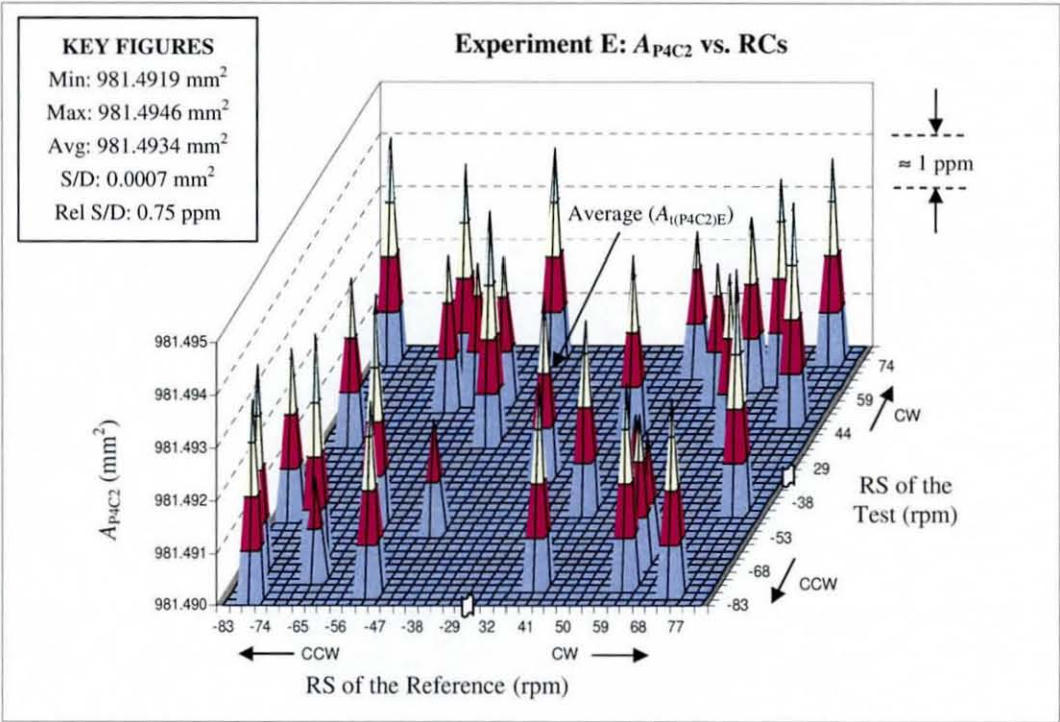


FIGURE 7.1 Variation of the overall effective areas of the P_4C_2 at 100 kPa and 20°C (A_{P4C2}) with respect to the RSs of the reference and the test PCAs

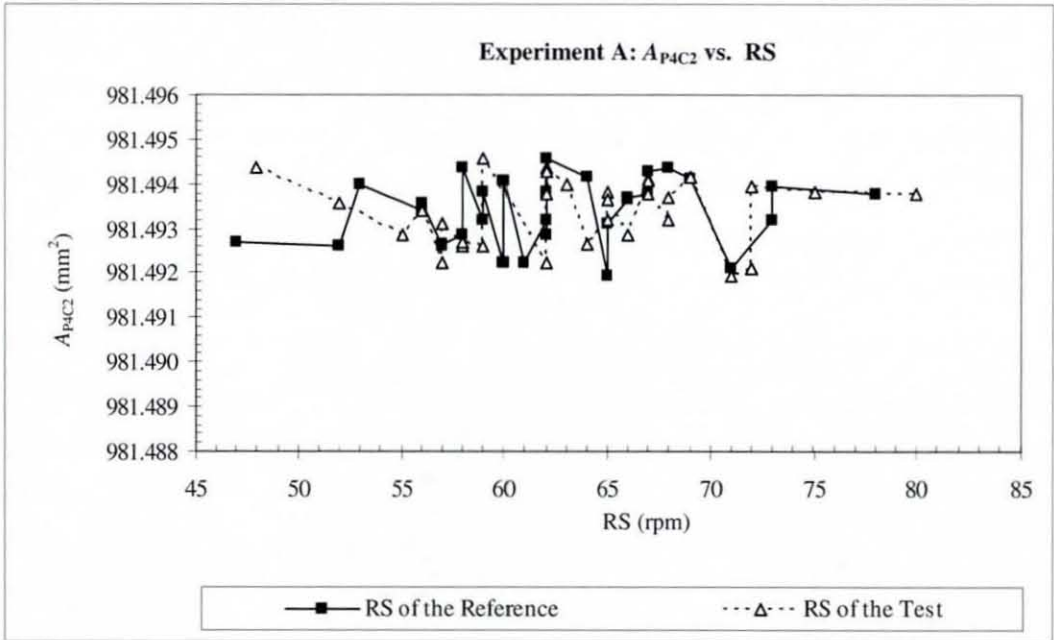


FIGURE 7.2 Variation of the A_{P4C2} based on the RS (regardless of RD) of the individual PCA

Therefore, the way in which these A_{P4C2} results were examined was once again reviewed. This was completed by rearranging the A_{P4C2} results which are tabulated in Table 7.2 in a different manner. The results were segregated based on their RCs, hence forming four smaller groups of results. The key figures from the basic statistical analysis are also included in the last five rows of this table. These key figures are the minimum (Min.), maximum (Max.), average (Avg.), standard deviation (Std. Dev.) and relative standard deviation (Rel. Std.Dev.). The relative standard deviations of the determined effective areas based on RC i.e. CW-CW, CW-CCW, CCW-CW and CCW-CCW are 0.55, 0.86, 0.95 and 0.75 ppm respectively.

TABLE 7.3 A_{P4C2} (mm²), tabulated in accordance to the four rotational combinations

CYL	Rotational Combination (RC)							
	CW-CW		CW-CCW		CCW-CW		CCW-CCW	
	SEQ	A_{P4C2} (mm ²)	SEQ	A_{P4C2} (mm ²)	SEQ	A_{P4C2} (mm ²)	SEQ	A_{P4C2} (mm ²)
1	1	981.4932	2	981.4922	3	981.4932	4	981.4927
2	5	981.4926	6	981.4929	7	981.4919	8	981.4931
3	9	981.4927	10	981.4922	11	981.4921	12	981.4926
4	13	981.4932	14	981.4938	15	981.4939	16	981.4927
5	17	981.4934	18	981.4938	19	981.4936	20	981.4944
6	21	981.4938	22	981.4937	23	981.4938	24	981.4942
7	25	981.4941	26	981.4946	27	981.4944	28	981.4941
8	29	981.4938	30	981.4936	31	981.4943	32	981.4940
Min.	981.4926 (mm ²)		981.4922 (mm ²)		981.4919 (mm ²)		981.4926 (mm ²)	
Max.	981.4941 (mm ²)		981.4946 (mm ²)		981.4944 (mm ²)		981.4944 (mm ²)	
Avg.	981.4933 (mm ²)		981.4934 (mm ²)		981.4934 (mm ²)		981.49350 (mm ²)	
Std. Dev.	0.0005 (mm ²)		0.0008 (mm ²)		0.0009 (mm ²)		0.0007 (mm ²)	
Rel. Std. Dev.	0.55 (ppm)		0.86 (ppm)		0.95 (ppm)		0.75 (ppm)	

These four groups of the A_{P4C2} values were plotted individually against their corresponding SEQ (see Figure 7.3) to visually investigate whether the RCs had significant influence on effective area variations. The x-axis represents the RS and the y-axis represents A_{P4C2} . A supplementary trend line of the overall A_{P4C2} has been included in this figure for comparison purposes, however this line has been shifted 0.003 mm² (approximately 3 ppm) downwards for the clarity of presentation.

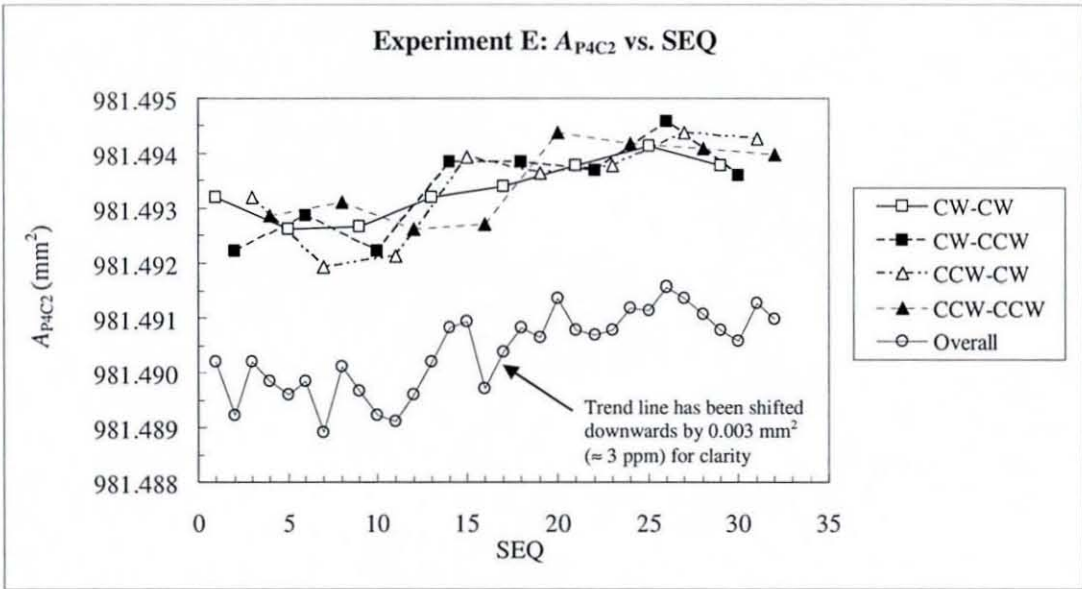


FIGURE 7.3 Variations of A_{P4C2} with SEQs based on four individual RCs. The overall results (regardless of the RCs) are represented by a shifted trend line, plotted for comparison purposes

Figure 7.3 clearly shows that A_{P4C2} increased gradually with SEQ, especially from cycle 4 onwards. The total increment of A_{P4C2} for all RCs was approximately 1.5 ppm over the 32 SEQ. These incremental changes indicated that the A_{P4C2} varied only with SEQ but not with RCs. In this case, the changes of A_{P4C2} with SEQ were believed to be due to the lack of sensitivity in the PCAs' temperature measurements. A dual-channel thermometer (of 0.1 °C resolution) used in this experiment was believed to be delayed in its response times (due to resolution limit), hence delayed in updating the current measured temperatures on both PCAs. The delay of 0.1 °C (causes an error of temperature measurement of the same amount) corresponded to approximately 1 ppm difference in A_{P4C2} value (see Tables 7.7 and 7.8 for uncertainty estimations).

The above reasoning was supported by the evidence that a sudden change of A_{P4C2} occurred between cycles 3 and 4 (at SEQ 13), where the measurements for cycles 1 to 3 and, cycles 4 to 8 were taken on two different days. Ambient temperature changes that affected both PCAs' expansion might cancel each other since both of the systems (pressure balances and PCAs) are identical in size, shape and materials. However, very small frictional components between the pistons and their respective cylinders (in both

PCAs) might have generated different levels of temperature variations (due the difference in their clearances, and possibly surface structure of the rubbing surfaces) when the pistons were rotated. The delays in detecting these small variations were believed be one of the contributing factors towards these $A_{P_4C_2}$ changes.

7.3.2 Results of Experiment F: P_4C_4 vs. P_2C_3

The same representation of the analysis work carried out in Experiment E is presented for Experiment F. Table 7.4 contains the overall results obtained in this experiment. The calculated effective areas of the P_4C_4 in mm^2 , denoted by $A_{P_4C_4}$ are given in the fourth column, whilst the RDs and RSs are given in the fifth to eighth columns. The minimum, maximum, average ($A_{t(P_4C_4)F}$), standard deviation and relative standard deviation were 981.4820 mm^2 , 981.4851 mm^2 , 981.4840 mm^2 , 0.0009 mm^2 and 0.87 ppm respectively. The maximum difference between these overall results was 0.0031 mm^2 which is equivalent to 3.2 ppm .

The results tabulated in Table 7.4 were converted into a 3-Dimensional illustration as shown in Figure 7.4. From this figure, the overall $A_{P_4C_4}$ results corresponding to their related RDs and RSs for both PCAs can be seen, where a similar pattern as demonstrated in Experiment E was obtained. No obvious RC dependency can be seen in this figure.

TABLE 7.4 Measurement results of the P_4C_4 , tabulated in accordance to their sequences

CYL	SEQ	Effective Area of P_4C_4 at 100kPa, 20°C		Rotational Combination (RC)			
		$A_{P_4C_2}$		Reference PCA (P_2C_3)		Test PCA (P_4C_4)	
		(m ²)	(mm ²)	RD	RS (rpm)	RD	RS (rpm)
1	1	9.8148309E-04	981.4831	CW	57	CW	53
	2	9.8148211E-04	981.4821	CW	48	CCW	58
	3	9.8148196E-04	981.4820	CCW	65	CCW	60
	4	9.8148358E-04	981.4836	CCW	68	CW	65
2	5	9.8148241E-04	981.4824	CW	67	CW	49
	6	9.8148437E-04	981.4844	CW	41	CCW	74
	7	9.8148309E-04	981.4831	CCW	70	CCW	50
	8	9.8148486E-04	981.4847	CCW	47	CW	65
3	9	9.8148417E-04	981.4842	CW	47	CW	42
	10	9.8148437E-04	981.4844	CW	82	CCW	58
	11	9.8148383E-04	981.4838	CCW	49	CCW	70
	12	9.8148388E-04	981.4839	CCW	63	CW	45
4	13	9.8148490E-04	981.4849	CW	59	CW	59
	14	9.8148343E-04	981.4834	CW	59	CCW	74
	15	9.8148338E-04	981.4834	CCW	79	CCW	76
	16	9.8148294E-04	981.4829	CCW	80	CW	83
5	17	9.8148392E-04	981.4839	CW	70	CW	65
	18	9.8148339E-04	981.4834	CW	59	CCW	61
	19	9.8148490E-04	981.4849	CCW	78	CCW	82
	20	9.8148441E-04	981.4844	CCW	74	CW	73
6	21	9.8148437E-04	981.4844	CW	41	CW	58
	22	9.8148486E-04	981.4847	CW	71	CCW	41
	23	9.8148431E-04	981.4843	CCW	74	CCW	58
	24	9.8148510E-04	981.4851	CCW	68	CW	56
7	25	9.8148397E-04	981.4840	CW	67	CW	80
	26	9.8148490E-04	981.4849	CW	45	CCW	42
	27	9.8148451E-04	981.4845	CCW	53	CCW	41
	28	9.8148466E-04	981.4847	CCW	46	CW	49
8	29	9.8148441E-04	981.4844	CW	44	CW	76
	30	9.8148387E-04	981.4839	CW	64	CCW	72
	31	9.8148471E-04	981.4847	CCW	44	CCW	59
	32	9.8148505E-04	981.4851	CCW	74	CW	41
Minimum Value		981.4820	mm ²	41	rpm	41	rpm
Maximum Value		981.4851	mm ²	82	rpm	83	rpm
Average Value ($A_{t(P_4C_4)F}$)		981.4840	mm ²	61	rpm	60	rpm
Standard Deviation		0.0009	mm ²	13	rpm	13	rpm
Relative Standard Deviation		0.87	ppm	21	%	21	%

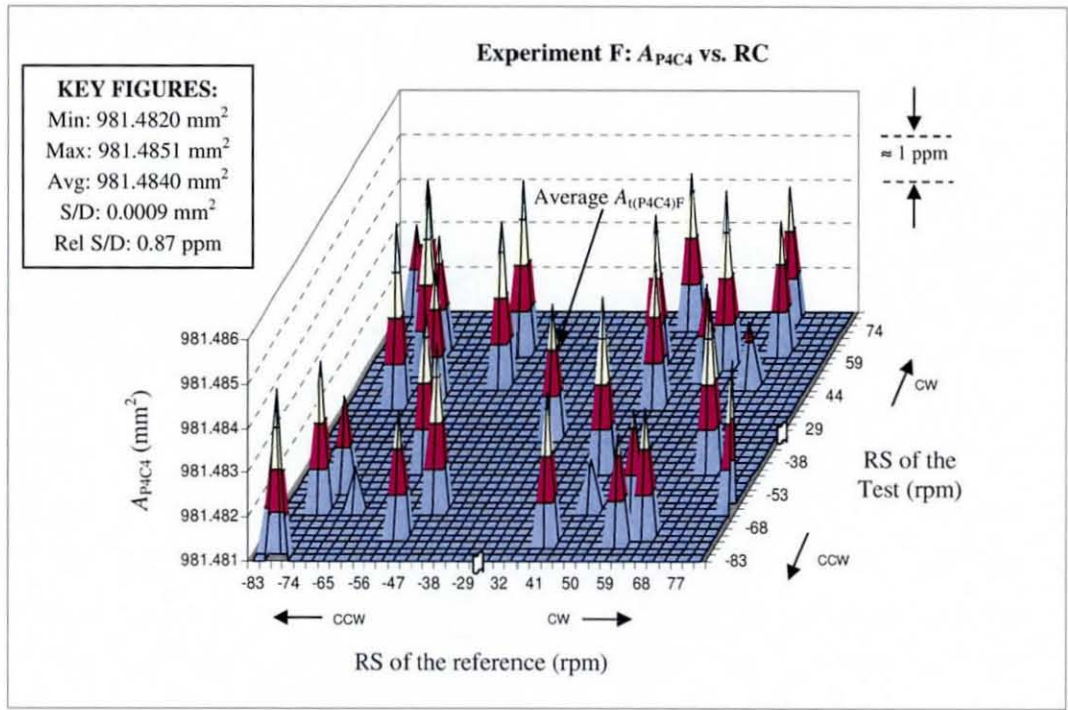


FIGURE 7.4 Variation of the overall effective areas of the P_4C_4 at 100 kPa and 20°C (A_{P4C4}) with respect to the RSs of the reference and the test PCAs

A graph showing the relationship between A_{P4C4} (y-axis) against RS (x-axis), regardless of their SEQ was plotted (see Figure 7.5) i.e. one trend line is based on RS of the reference and the other one based on the RS of the test. Figure 7.5 shows that the trend lines plotted again do not reveal any significant difference between two.

Subsequently the same rearrangement work completed on Table 7.2 has been carried out on Table 7.4. Hence a new RC-based table was produced (see Table 7.5), showing that the dispersion of A_{P4C4} values based on four types of their RCs were not significantly different, where the CW-CW, CW-CCW, CCW-CW and CCW-CCW give the relative standard deviations of 0.81, 0.95, 1.01 and 0.79 ppm respectively. This table was subsequently translated into a 2-Dimensional graphical illustration, (similar representation to Figure 7.3). Figure 7.6 demonstrates incremental changes of A_{P4C4} values over the SEQ, where the overall increments of A_{P4C4} values for all the RCs are approximately 1.5 ppm over 32 SEQs. However, this figure shows that the increment of A_{P4C4} values mainly occurred within the first three cycles, whereby their values show

better consistency in the fluctuations from cycle four to eight. The same phenomena as Experiment E was believed to take place during this transition sequence, i.e. limitations in thermometer resolution which leads to a delay in response time of temperature measurement.

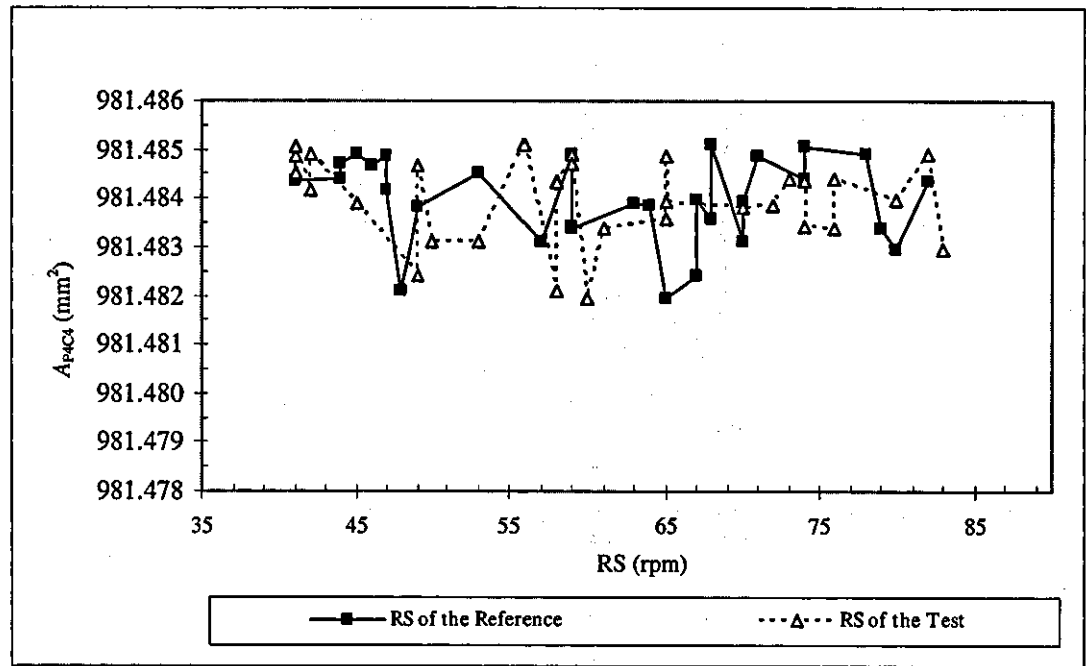


FIGURE 7.5 Variation of the A_{P4C4} based on the RS (regardless of RD) of the individual PCA

TABLE 7.5 A_{P4C4} (mm²), tabulated in accordance to their four rotational combinations

Cycle	Rotational Combination (RC)							
	CW-CW		CW-CCW		CCW-CW		CCW-CCW	
	SEQ	A_{P4C4} (mm ²)	SEQ	A_{P4C4} (mm ²)	SEQ	A_{P4C4} (mm ²)	SEQ	A_{P4C4} (mm ²)
1	1	981.4831	2	981.4821	3	981.4820	4	981.4836
2	5	981.4824	6	981.4844	7	981.4831	8	981.4849
3	9	981.4842	10	981.4844	11	981.4838	12	981.4839
4	13	981.4849	14	981.4834	15	981.4834	16	981.4829
5	17	981.4839	18	981.4834	19	981.4849	20	981.4844
6	21	981.4844	22	981.4849	23	981.4843	24	981.4851
7	25	981.4840	26	981.4849	27	981.4845	28	981.4847
8	29	981.4844	30	981.4839	31	981.4847	32	981.4851
Min.	981.4824 (mm ²)		981.4821 (mm ²)		981.4820 (mm ²)		981.4829 (mm ²)	
Max.	981.4849 (mm ²)		981.4849 (mm ²)		981.4849 (mm ²)		981.4851 (mm ²)	
Avg.	981.4839 (mm ²)		981.4839 (mm ²)		981.4838 (mm ²)		981.4843 (mm ²)	
Std. Dev.	0.0008 (mm ²)		0.0009 (mm ²)		0.0010 (mm ²)		0.0008 (mm ²)	
Rel. Std. Dev.	0.81 (ppm)		0.95 (ppm)		1.01 (ppm)		0.79 (ppm)	

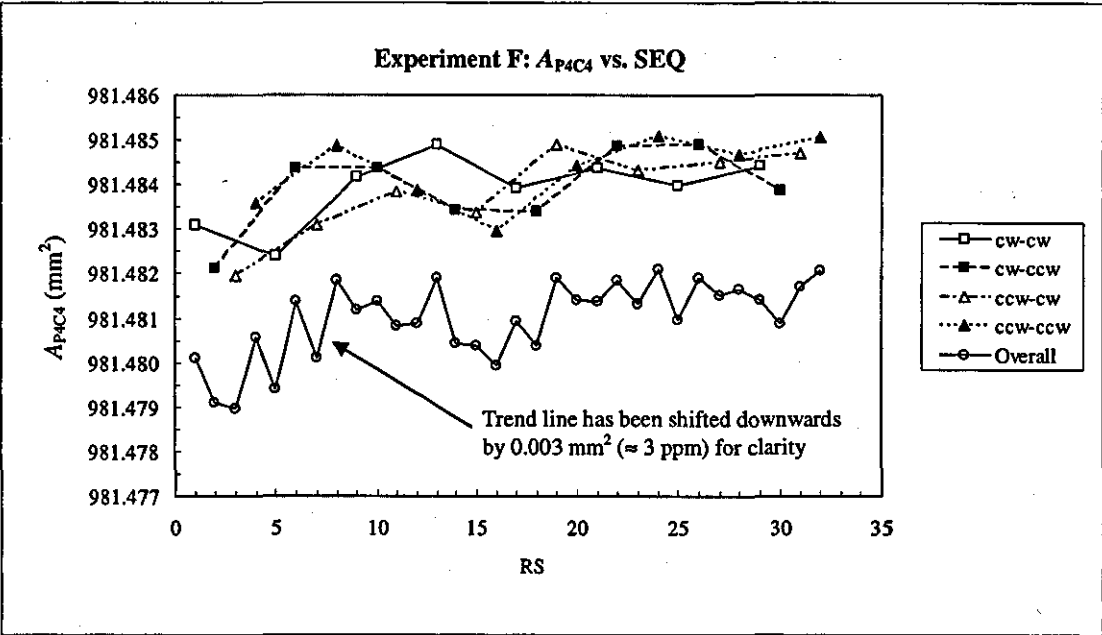


FIGURE 7.6 Variations of A_{P4C4} with SEQs based on four individual RCs. The overall results (regardless of the RCs) are represented by a shifted trend line, plotted for comparison purposes

7.4 UNCERTAINTY ANALYSIS

All uncertainty analysis in this thesis was calculated using the methods described in the ISO Guide to the Expression of Uncertainty in Measurement [ISO/TAG 4 1993]. The Type A component was obtained based on the standard deviation of the 32 measurement results, as given in Equation (6.8). Whereas for Type B components, input quantities were assumed based on their typical value e.g. the thermal expansion coefficients of the piston and cylinder were assumed to be $4.55 \times 10^{-6} \text{ }^{\circ}\text{C}^{-1}$ respectively, and the average density of a combination of weights and other floating components was assumed to be 7800 kgm^{-3} , which is a typical value for the stainless steel weights (as the dominated material) [Bair and Delajoud 2002].

Other assumptions and their justification are as follows:

- Since both of the pressure balances were designed in an identical manner (including floating elements), in terms of their dimensions, shape, materials and masses: the assumption that negligible relative errors contributed from the aerodynamic effects (due to differences in RDs and RSs) was justified.
- The average of the air density that has been used in effective area calculations (on each day the measurements carried out) was estimated to vary by 0.01 kgm^{-3} , with a rectangular type distribution. This was justified with the environmental conditions in the laboratory that were well controlled on a 24-hour basis.
- The error due to downward gravitational acceleration was considered negligible since this was always nullified between two PCAs.
- The errors due to the verticality of both pistons was considered negligible since both of them were adjusted to within 40 arcsecond level conditions, which corresponded to a relative uncertainty of 0.02 ppm.

In order to proceed with the uncertainty calculations, the relative expanded uncertainties (Rel. Exp. Uncertainty) of the individual input parameters were estimated. The estimated values used in these experiments are shown in the Table 7.6 below.

TABLE 7.6 Estimated values of the relative expanded uncertainties of input parameters

No.	Parameter Description	Rel. Exp. Uncertainty	Prob. Dist.	DOF
1	Density of the weights loaded	50 kgm ⁻³	Rect.	∞
2	Density of the ambient air	0.01 kgm ⁻³	Rect.	∞
3	Thermal exp. coeff. of the PCA	1.0 x 10 ⁻⁷ °C ⁻¹	Rect.	∞
4	Temperature of the PCA	0.1 °C	Rect.	∞
5	Effective area of the ref., A _{r(P2C3)}	0	N/A	N/A
6	Pressure Distortion Coefficient	0	N/A	N/A

Note:

Prob. Dist.: Probability distribution type
DOF: Degrees of freedom
Rect: Rectangular

Consequently all of these estimated figures were keyed into the excel uncertainty spreadsheet to calculate the standard uncertainties of the A_{1(P4C2)E} and A_{1(P4C4)F} (see Tables 7.7 and 7.8). Subsequently these values were multiplied with a coverage factor (*k* = 2) for their respective relative expanded uncertainties which gives approximately a 95% level of confidence. As a result, the effective areas and their associated relative expanded uncertainties for each of the test PCA were obtained as follows:

- A_{1(P4C2)E} = 981.4934 mm² ± 3.4 ppm
- A_{1(P4C4)F} = 981.4840 mm² ± 3.5 ppm

Note: The above identified values are relative values, calculated based on experiments carried out at LU (comparison purposes only). They do not indicate a statement of traceable uncertainty. Refer to Table 9.3 for the actual uncertainty calculation, which is traceable to the Primary Pressure Standard.

TABLE 7.7 Relative uncertainty calculation of the determined effective area, $A_{t(P4C2)E}$

Input parameters							Measurand			
x_i			Prob. Dist.	Limits (2σ or ± a)	Std. Uncertainty $u(x_i)$	DOF ν_i	Sensitivity Coefficient		Standard Uncertainty $ \partial A_t / x_i u(x_i)$	
Parameter Description	Approx. Value	Unit					$ \partial A_t / x_i $	Value	m ²	ppm
<Test Pressure Balance>										
Total mass loaded, m_{wt}	10.00	kg	Norm.	6.0E-06	3.0E-06	∞	A_t/m_{wt}	9.81E-05	2.943E-10	3.0E-01
Density of the weights loaded, ρ_{wt}	7800	kg/m ³	Rect.	5.0E+01	2.9E+01	∞	$A_t(\rho_d/\rho_{wt}^2)/(1-\rho_d/\rho_{wt})$	1.94E-11	5.602E-10	4.6E-01
Density of the ambient air, ρ_{at}	1.20	kg/m ³	Rect.	1.0E-02	5.8E-03	∞	$A_t/(\rho_{wt}(1-\rho_d/\rho_{wt}))$	1.26E-07	7.266E-10	7.4E-01
Thermal exp. coeff. of the PCA, ($\alpha_{pt} + \alpha_{cp}$)	9.10E-06	°C ⁻¹	Rect.	1.0E-07	5.8E-08	∞	$2A_t(t_r - 20)$	1.96E-04	1.133E-11	1.2E-02
Temperature of the PCA, t_r	20.1	°C	Rect.	1.0E-01	5.8E-02	∞	$A_t(\alpha_{pt} + \alpha_{cp})$	8.93E-09	5.157E-10	5.3E-01
<Reference Pressure Balance>										
Total mass loaded, m_{wr}	10.00	kg	Norm.	6.0E-06	3.0E-06	∞	A_t/m_{wr}	9.81E-05	2.943E-10	3.0E-01
Density of the weights loaded, ρ_{wr}	7800	kg/m ³	Rect.	5.0E+01	2.9E+01	∞	$A_t(\rho_d/\rho_{wr}^2)/(1-\rho_d/\rho_{wr})$	1.94E-11	5.602E-10	4.6E-01
Density of the ambient air, ρ_{ar}	1.20	kg/m ³	Rect.	1.0E-02	5.8E-03	∞	$A_t/(\rho_{wr}(1-\rho_d/\rho_{wr}))$	1.259E-07	7.266E-10	7.4E-01
Thermal exp. coeff. of the PCA, ($\alpha_{pr} + \alpha_{cr}$)	9.10E-06	°C ⁻¹	Rect.	1.0E-07	5.8E-08	∞	$2A_t(t_r - 20)$	1.963E-04	1.133E-11	1.2E-02
Temperature of the PCA, t_r	19.9	°C	Rect.	1.0E-01	5.8E-02	∞	$A_t(\alpha_{pr} + \alpha_{cr})$	8.932E-09	5.157E-10	5.3E-01
Effective area at 100 kPa, 20°C, A_{t0}	9.815E-04	m ²	N/A	N/A	N/A	N/A	A_t/A_{t0}	N/A		
Pressure distortion coefficient, λ_r	0	Pa ⁻¹	N/A	N/A	N/A	N/A	$A_t p_r$	N/A		
<Head Correction>										
Density of pressure-transmitting fluid, ρ_f	2.23	kg/m ³	Rect.	1.0E-02	5.8E-03	∞	$(A_t/p_r) g \Delta h$	1.11E-10	6.419E-13	6.5E-04
Density of ambient air, ρ_a	1.20	kg/m ³	Rect.	1.0E-02	5.8E-03	∞	$(A_t/p_r) g \Delta h$	1.112E-10	6.419E-13	6.5E-04
Height difference in the reference levels, Δh	0	m	Rect.	2.0E-03	1.2E-03	∞	$(A_t/p_r)(\rho_f - \rho_a) g L$	2.24E-07	2.591E-10	2.6E-01
<Equilibrium Conditions>										
Sensitivity of cross-floating, m_{dis}	2.0E-06	kg	Rect.	2.0E-06	1.2E-06	∞	A_t/m_{wt}	9.81E-05	9.809E-11	1.2E-01
Repeatability, R	Std. Dev.	m ²	Norm.	1.48E-09	7.40E-10	31	1	1	7.402E-10	7.5E-01
Sum of squared = $\sum (A_t / x_i)^2 u^2(x_i) + u^2(m_{dis}) + u^2 R$							2.83 ppm ²	Note: This is not a statement of traceable uncertainty value. Refer to Table 9.3 for the actual uncertainty calculation, which is traceable to the Primary Pressure Standard.		
Relative standard uncertainty of the test effective area at 100 kPa and 20°C, $u(A_{t(P4C2)})$							1.68 ppm			
Relative expanded uncertainty at a level of confidence of approximately 95% , coverage factor of $k = 2$							3.4 ppm			

TABLE 7.8 Relative uncertainty calculation of the determined effective area, $A_{t(P4C4)F}$

Input parameters							Measurand			
x_i			Prob. Dist.	Limits (2 σ or $\pm a$)	Std. Uncertainty $u(x_i)$	DOF ν_i	Sensitivity Coefficient		Standard Uncertainty $ dA_t / x_i u(x_i)$	
Parameter Description	Approx. Value	Unit					$ dA_t / x_i $	Value	m ²	ppm
<Test Pressure Balance>										
Total mass loaded, m_{wt}	10.00	kg	Norm.	6.0E-06	3.0E-06	∞	A/m_{wt}	9.81E-05	2.943E-10	3.0E-01
Density of the weights loaded, ρ_{wt}	7800	kg/m ³	Rect.	5.0E+01	2.9E+01	∞	$A(\rho_d/\rho_{wt}^2)/(1-\rho_d/\rho_{wt})$	1.94E-11	5.602E-10	4.6E-01
Density of the ambient air, ρ_{at}	1.20	kg/m ³	Rect.	1.0E-02	5.8E-03	∞	$A/(\rho_{wt}(1-\rho_d/\rho_{wt}))$	1.26E-07	7.266E-10	7.4E-01
Thermal exp. coeff. of the PCA, ($\alpha_{pt} + \alpha_{cp}$)	9.10E-06	°C ⁻¹	Rect.	1.0E-07	5.8E-08	∞	$2A_t(t_t - 20)$	1.96E-04	1.133E-11	1.2E-02
Temperature of the PCA, t_t	20.1	°C	Rect.	1.0E-01	5.8E-02	∞	$A_t(\alpha_{pt} + \alpha_{ct})$	8.93E-09	5.157E-10	5.3E-01
<Reference Pressure Balance>										
Total mass loaded, m_{wr}	10.00	kg	Norm.	6.0E-06	3.0E-06	∞	A_t/m_{wr}	9.81E-05	2.943E-10	3.0E-01
Density of the weights loaded, ρ_{wr}	7800	kg/m ³	Rect.	5.0E+01	2.9E+01	∞	$A(\rho_d/\rho_{wr}^2)/(1-\rho_d/\rho_{wr})$	1.94E-11	5.602E-10	4.6E-01
Density of the ambient air, ρ_{ar}	1.20	kg/m ³	Rect.	1.0E-02	5.8E-03	∞	$A/(\rho_{wr}(1-\rho_d/\rho_{wr}))$	1.259E-07	7.266E-10	7.4E-01
Thermal exp. coeff. of the PCA, ($\alpha_{pr} + \alpha_{cr}$)	9.10E-06	°C ⁻¹	Rect.	1.0E-07	5.8E-08	∞	$2A_t(t_r - 20)$	1.963E-04	1.133E-11	1.2E-02
Temperature of the PCA, t_r	19.9	°C	Rect.	1.0E-01	5.8E-02	∞	$A_t(\alpha_{pr} + \alpha_{cr})$	8.932E-09	5.157E-10	5.3E-01
Effective area at 100 kPa, 20°C, A_{t0}	9.815E-04	m ²	N/A	N/A	N/A	N/A	A_t/A_{t0}	N/A		
Pressure distortion coefficient, λ_r	0	Pa ⁻¹	N/A	N/A	N/A	N/A	$A_t p_r$	N/A		
<Head Correction>										
Density of pressure-transmitting fluid, ρ_f	2.23	kg/m ³	Rect.	1.0E-02	5.8E-03	∞	$(A_t/p_r) g \Delta h$	1.11E-10	6.419E-13	6.5E-04
Density of ambient air, ρ_a	1.20	kg/m ³	Rect.	1.0E-02	5.8E-03	∞	$(A_t/p_r) g \Delta h$	1.112E-10	6.419E-13	6.5E-04
Height difference in the reference levels, Δh	0	m	Rect.	2.0E-03	1.2E-03	∞	$(A_t/p_r)(\rho_f - \rho_a)g_L$	2.24E-07	2.591E-10	2.6E-01
<Equilibrium Conditions>										
Sensitivity of cross-floating, m_{dis}	2.0E-06	kg	Rect.	2.0E-06	1.2E-06	∞	A_t/m_{wt}	9.81E-05	9.809E-11	1.2E-01
Repeatability, R	Std. Dev.	m ²	Norm.	1.71E-09	8.55E-10	31	1	1	8.552E-10	8.7E-01
Sum of squared = $\sum (A_t / x_i)^2 u^2(x_i) + u^2(m_{dis}) + u^2 R$							3.02 ppm ²	Note: This is not a statement of traceable uncertainty value. Refer to Table 9.3 for the actual uncertainty calculation, which is traceable to the Primary Pressure Standard.		
Relative standard uncertainty of the test effective area at 100 kPa and 20°C, $u(A_{t(P4C4)})$							1.74 ppm			
Relative expanded uncertainty at a level of confidence of approximately 95% , coverage factor of $k = 2$							3.5 ppm			

7.5 SUMMARY AND DISCUSSIONS

The overall goal of this experiment was to investigate if there was any evidence of pressure dependency on the RDs, RSs or RCs using 35 mm diameter PCAs. The need of this novel approach was justified due to the unavailability of published similar research work that has been carried out using very large PCAs. Two experiments have been carried out between one piston which was matched with two identical cylinders at 100 kPa. Measurements were carried out based on four types of RCs per cycle i.e. CW-CW, CW-CCW, CCW-CCW and CCW-CW. Results for A_{P4C2} and A_{P4C4} were obtained from eight cycles of comparisons, consisting of 32 SEQs where they were on relative basis to the assigned reference value, $A_{r(P2C3)}$.

The results obtained were processed statistically where all related data and additional key figures such as minimum, maximum, average, standard deviation and relative standard deviation were generated. In each experiment, the data was visualised graphically using 3-Dimensional figures to identify if there was any significant observable dependency on RCs. On top of this 3-Dimensional figure, another two supporting 2-Dimensional figures were plotted so that the overall results obtained could be viewed from different angles. The first figure was the effective area vs. RS of individual PCA, and the second figure was the effective area vs. SEQ which was plotted based on the four RCs.

Based on the plotted figures (which show that there is no significant differences), it can be concluded that there is no evidence of pressure dependency on the RDs, RSs or RCs using a 35 mm PCA. Excellent performance of the LU manufactured pressure balances were proven through the results obtained, where the average determined effective areas for A_{P4C2} and A_{P4C4} were 981.4934 and 981.4840 mm²; associated with their respective relative expanded uncertainties of ± 3.4 and 3.5 ppm. Small relative expanded uncertainties obtained for both combinations have revealed that the pressure balances and their associated PCAs are comparable (in term of performance) to commercial pressure balances (of very large PCA) available in the market nowadays. The findings extracted from these experiments are very useful and important in understanding better the characteristics of the

very large tungsten carbide PCA, and it is believed that the same characteristics will be demonstrated by commercially available pressure balances.

Besides excellent performance, very small differences between $A_{t(P4C4)E}$ and $A_{t(P4C4)F}$ (i.e. 0.00941 mm^2), which is equivalent to the diametral difference of $0.17 \text{ }\mu\text{m}$ has demonstrated that Cylinder 2 and Cylinder 4 are very much identical in inner diameter and other characteristics. In other words, this small difference demonstrated that the manufacturing methods were, and are excellent and repeatable. The technical knowledge of producing identical cylinders has been applied to the manufacture of identical pistons, but with various surface textures on them. These surface-modified pistons were used in the experiments described in Chapter 8, where investigation of the effects of surface textures to the pressure generated are discussed.

CHAPTER 8

INVESTIGATION ON THE EFFECTS OF SURFACE TEXTURE ON THE DETERMINED EFFECTIVE AREA

Detailed descriptions on the investigation of the effects of the RS and RD on the determined effective area were described in Chapter 7, consisting of Experiments E and F. The experiments described in this chapter were the continuity of the experiments carried out in Chapter 7. It presents a novel investigative approach on the effects of surface texture applied to six test pistons in the same manner as in Chapter 7, however all the surfaces of the pistons involved were characterised beforehand. The aim of these experiments was to investigate if there was evidence of pressure dependency on the pressure generated with surface textures applied, associated with RS and RD of both pistons. Six identical pistons of various surface textures were matched with two identical cylinders to form 24 cross-floating experiments (inclusive of Experiments E and F, that have been described in the Chapter 7). Twelve of them were cross-floated directly against the reference PCA (P_2C_3), which were categorised as a “direct comparisons”; whereas another twelve combinations were compared against other selected combinations, thus categorised as “indirect comparisons”.

This chapter is organised as follows: The next section highlights the rationale behind this investigation approach. Section 8.2 describes the investigation approach implemented in these experiments. Section 8.3 discusses the measurement results obtained from surface texture characterisation work, and effective area determinations. Section 8.4 concentrates on the comparison of the results obtained from various calibration routes, and lastly, Section 8.5 summarises and discusses overall experimental work in this chapter, and derives conclusions.

8.1 RATIONALE

Without considering surface texture on Piston 4 (which has formed two highly polished PCAs combinations), Chapter 7 has demonstrated that the RDs, RSs or RCs have no significant influence on the pressure generated. However, the question "How smooth is a smooth surface?" is the main issue in this experimental work. From the manufacturing point of view, whatever methods are employed to generate polished surfaces, there will always be some inseparable form of texture associated with them [Miller 1962]. From a surface metrology point of view, any surface texture can be separated into three categories of profile known as surface profile, waviness and roughness. From a tribology point of view, surface texture can influence the performance of the work piece [Whitehouse 1994]. These three reasons provide the justification for investigation of surface texture issues corresponding to the pressure generated using the modified-surface pistons of various levels of roughness; with variable RSs and RDs. These investigations have been further motivated with the detailed knowledge of the manufacturing processes of the tungsten carbide PCAs which have shown excellent performance in Chapter 7. The results from these investigations are believed to be complementary to the findings obtained in Chapter 7, so that better understanding of the very large PCAs characteristic can be obtained.

8.2 INVESTIGATIVE APPROACH

The scope of this approach was to determine the apparent dependency of the pressure generated, on the surface textures applied onto pistons (associated with RSs and RDs), using 35 mm PCAs in gauge mode operation. As described in Chapter 7, apparent dependencies would be realised with the changes of generated pressure, as a function of variations of calculated determined effective areas through the cross-floating method. A consistent reference PCA was used, i.e. a combination of Piston 2 and Cylinder 3 (designated as P_2C_3). The test PCAs comprised of combinations of Pistons 1, 3, 4, 5, 6 and 7 (of predetermined, quantified and valley dominated surface texture profiles) that were matched with 2 identical cylinders (Cylinder 2 and Cylinder 4). These have formed various PCA combinations e.g. P_1C_2 , P_1C_4 , P_3C_2 , P_3C_4 etc. Cross-floating experiments

ended with three experiments where Piston 2 and Cylinder 3 (normally acted as a reference PCA in the whole calibration chain) were matched with Cylinder 2 and Piston 3 respectively, hence forming two test combinations known as P_2C_2 and P_3C_3 . Twelve direct cross-floating experiments against a reference PCA were carried out which were assigned as Experiments “A to L” (including two experiments described in Chapter 7, i.e. Experiments E and F); complimented by another twelve indirect (to the reference) cross-floating experiments, designated as Experiments “m to x”.

Figure 8.1 shows the overall calibration chain/scheme which has been performed. The PCA combinations are represented by P_XC_Y within the ovals where $X = 1, 2, 3, 4, 5, 6, 7$ and $Y = 2, 3, 4$. These test PCAs combinations are accompanied with their respective averaged effective areas at 100 kPa and 20 °C, denoted by $A_{t(PXC)}$, whilst $A_{r(P_2C_3)}$ denotes the estimated value of the reference PCA at 100 kPa and 20 °C (please note that $A_{t(PXC)}$ is a general symbol for the average of the determined effective area of P_XC_Y combination regardless of experiment identifications or calibration routes). Cross-floating routes are represented by letters within small shaded-rectangular boxes (“A to L” and “m to x”), linking between two oval-shaped circles. The solid lines represent direct comparisons, whereas dashed lines represent indirect comparisons. The direction of the arrows symbolises the direction of the traceability chain. Two examples explaining this figure are as follows:

- Comparison between P_1C_2 against P_2C_3 is known as “Experiment A”, where the average of the determined effective area of P_1C_2 in Experiment A is denoted by $A_{t(P_1C_2)A}$. As a general rule, the average of the determined effective area for P_XC_Y in a specific Experiment Z is denoted by $A_{t(PXC)Z}$, where Z represents the experiment identification ($Z = A$ to L, m to x). However, the route of traceability for P_1C_2 is the known as the “Route A”.
- A more complicated route such as a comparison between P_3C_3 against P_2C_2 , where it was known as “Experiment x”. As shown in Figure 8.1, there were four routes to derive $A_{t(P_3C_3)}$ from a single source of the reference PCA, $A_{r(P_2C_3)}$. Three

routes went through Experiment x, however one route bypassing this experiment. The four routes available for this case were as follows:

- First route: Through the cross-floating Experiments F, q and x; thus the route of traceability is known as the "Route F-q-x". The averaged effective area is denoted by $A_{t(P_3C_3)}^{Fqx}$.
- Second route: Through cross-floating Experiments C, m, w and x; thus the route of traceability is known as the "Route C-m-w-x". The averaged effective area is denoted by $A_{t(P_3C_3)}^{Cmwx}$.
- Third route: Through cross-floating Experiments E, p, w and x; thus the route of traceability is known as the "Route E-p-w-x". The averaged effective area is denoted by $A_{t(P_3C_3)}^{Epwx}$.
- Fourth route: Through cross-floating Experiments F and r (bypassing Experiment x); thus the route of traceability is known as the "Route F-r". The averaged effective area is denoted by $A_{t(P_3C_3)}^{Fr}$.

The averaged results obtained from various routes available for each test combination were compared with each other to find any disagreements between them. Within this small group of comparisons, the average value from the shortest route to P_2C_3 has been used as a reference value (this is believed to inherit the minimum propagation errors).

The effects of the surface texture to the pressure generated were investigated through two steps, as follows:

- Step 1: Investigation on the determined effective areas from each cross-floating experiment was carried out. The trend lines of the overall results were plotted, where each RC was distinctively marked with its own symbol to differentiate the RCs. This would reveal graphically if there was pressure dependency as a function of surface texture when four RCs were applied.

- Step 2: The averaged effective areas calculated for each different route of each test PCA were compared each other, to find any disagreements between them. For example, a comparison between P_3C_3 against P_2C_2 (as described above). All the effective areas determined for this particular PCA (from various possible routes) were compared. They were comparisons between $A_{i(P3C3)}^{Fqx}$, $A_{i(P3C3)}^{Cmwx}$, $A_{i(P3C3)}^{Epwx}$ and $A_{i(P3C3)}^{Fr}$, where $A_{i(P3C3)}^{Fr}$ was treated as a reference value.

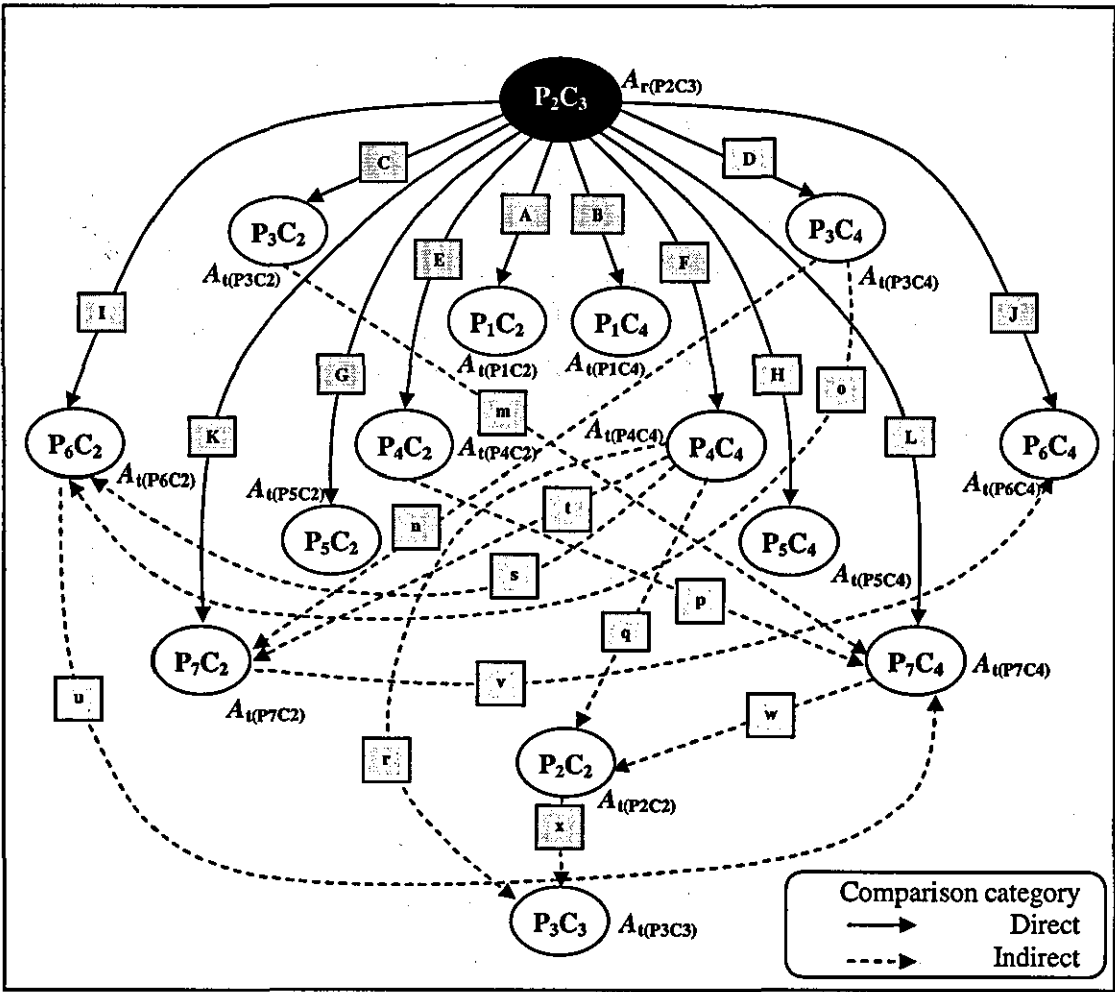


FIGURE 8.1 A schematic diagram of the calibration chain that relates the test PCAs to the reference PCA through direct and indirect cross-floating experiments

The two steps described above complemented each other since Step 2 acted as a “booster” in magnifying the scale of dependability of the pressure generated (if any).

Any trivial effects might be more significant/observable after undergoing a few series of cross-floating routes, thus this comparative method was a sensible approach to investigate any trivial or non-trivial effects. Besides investigating the effects of the surface texture, this calibration chain also acted as a “performance indicator” on how reliable the interchangeable PCAs worked, since the results obtained can always be compared at any level (after few series of cross-floating route) if necessary.

8.2.1 Comparison Procedure

All preparations as described in Section 6.2.2 and Chapter 7 have been carried out prior to the experiments. The same comparison procedures as described in Chapter 7 were applied in these experiments. The total masses loaded (including trim weights), PCAs' temperature, RDs and RSs of both pressure balances were noted as soon as equilibrium conditions were established. The environmental conditions were also taken four times, i.e. at the beginning, quarter, three quarter, and at the end of the measurement process (within the one day experiments), where an average of the four calculated air density values was used as an approximated air density in effective area calculations. The instantaneous value of each effective area was obtained from an excel spreadsheet, based on the effective areas determined at 100 kPa and corrected to 20 °C.

8.2.2 Cycle of Measurement

Three cycles of comparison consisting of 12 individual measurement sequences were applied to all of the experiments. Each cycle consisted of four different pairs (reference-test) of the rotational combination (RC), which were sequentially arranged in RD-RD terms i.e. CW-CW, CW-CCW, CCW-CCW, CCW-CW.

8.3 MEASUREMENT RESULTS

Measurement results obtained in these experiments (direct and indirect comparisons) are presented in two sections i.e. Section 8.3.1 which is dedicated to surface texture characterisation of each piston, and Section 8.3.2 is dedicated to each cross-floating experiment.

8.3.1 Results of the Surface Texture Characterisations

A powerful 3-Dimensional optical surface profiler instrument (Scanning White Light Interferometer) known as Zygo New View 5000 was used for characterising and quantifying micro structure and other topographical features of the piston surfaces with excellent precision. All measurements were nondestructive and required no sample preparation [Zygo Corporation 2006].

All seven pistons involved in these experiments were scanned at five levels i.e. 5, 15, 30, 45 and 55 mm (from the base of each piston), where two areas have been scanned for each level. Images of approximately 0.4 x 0.3 mm in dimensions were captured in every scanning process. Using the MetroPro software (dedicated software for the Zygo New View 5000), three sets of surface parameters (obtained from three equally spaced surface profiles across the image) were extracted from each scanned area. Therefore, thirty sets of surface parameter were obtained for each piston under investigation. The three types of surface parameters that were considered were as follows:

- R_t – The vertical distance between the profile peak height above the mean line (R_p) to the maximum profile valley depth below the mean line (R_v) which are taken over the evaluation length.
- R_q – The root mean square (RMS) of the arithmetic mean of the roughness profile which is taken over the entire measured length that deviates from its mean line. It represents the standard deviation of the profile heights.
- R_a – The arithmetic mean of the absolute magnitude of the roughness profile that deviates from its mean line over one sampling length.

The summarised results obtained for each piston are tabulated in their respective sections where all the tables are accompanied with a sample of their typical surface images. The surface images depicted are taken from a single scanned area, which are shown in oblique, solid and surface profile plots. A profile statistic that indicates the measurement results of this scanned area is attached next to the surface profile plot.

8.3.1.1 Surface Characterisation Results of Piston 1

Table 8.1 shows the summarised results obtained from the surface characterisation work for Piston 1 with the images shown in Figure 8.2. The average values for R_t , R_q and R_a of Piston 1 are represented by the R_{t1} , R_{q1} and R_{a1} .

TABLE 8.1 Summarised results of the surface profile characterisations for Piston 1

Piston 1 - Surface Parameters			
Statistical Description	$R_{t1} (\mu\text{m})$	$R_{q1} (\mu\text{m})$	$R_{a1} (\mu\text{m})$
Average	0.045	0.007	0.006
Standard Deviation	0.019	0.003	0.002
Standard Deviation (%)	42	44	41
Minimum	0.027	0.005	0.004
Maximum	0.085	0.014	0.009
Max. Difference (Max – Min)	0.058	0.009	0.005

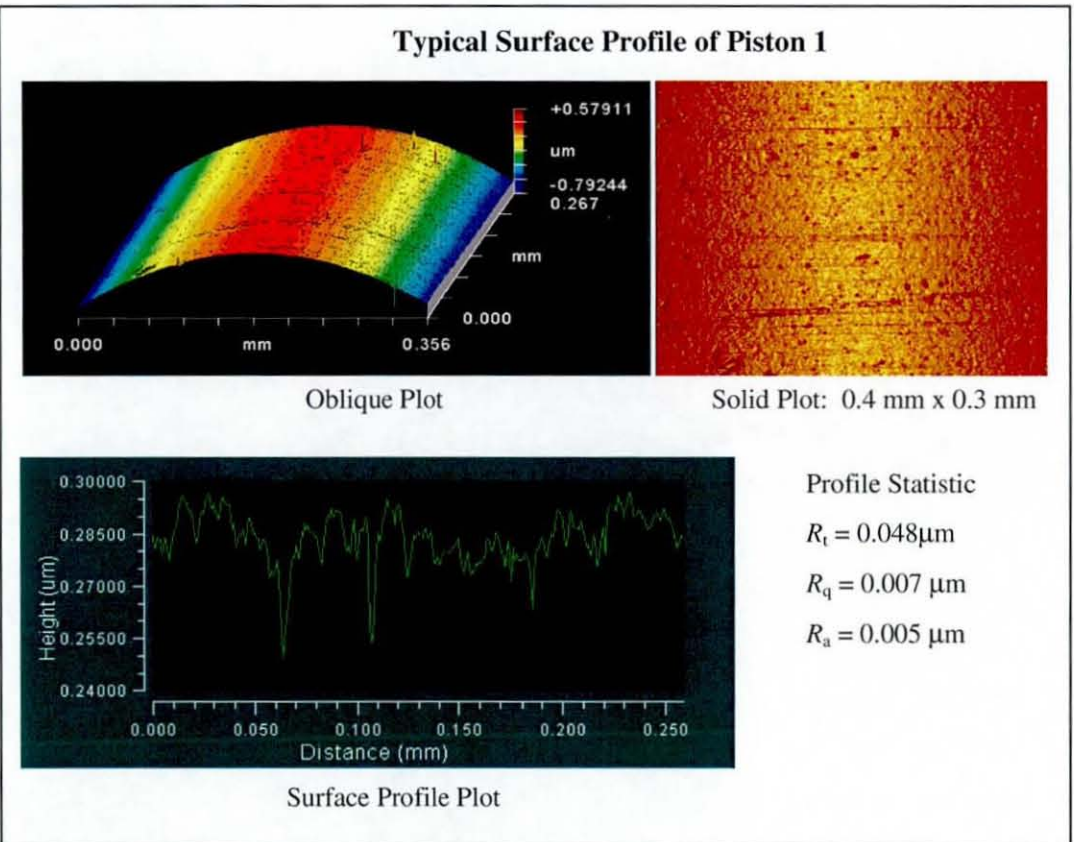


FIGURE 8.2 Typical images of Piston 1

8.3.1.2 Surface Characterisation Results of Piston 2

The summarised results obtained for Piston 2 are tabulated in Table 8.2, and Figure 8.3. The results obtained demonstrated that Piston 2 had very similar surface quality compared to Piston 1 in terms of surface profiles and microscopic surface outlook (solid plot).

TABLE 8.2 Summarised results of the surface profile characterisations for Piston 2

Piston 2 - Surface Parameters			
Statistical Description	$R_{t2} (\mu\text{m})$	$R_{q2} (\mu\text{m})$	$R_{a2} (\mu\text{m})$
Average	0.044	0.007	0.006
Standard Deviation	0.015	0.002	0.002
Standard Deviation (%)	34	33	35
Minimum	0.018	0.005	0.003
Maximum	0.065	0.013	0.008
Max. Difference (Max – Min)	0.047	0.008	0.005

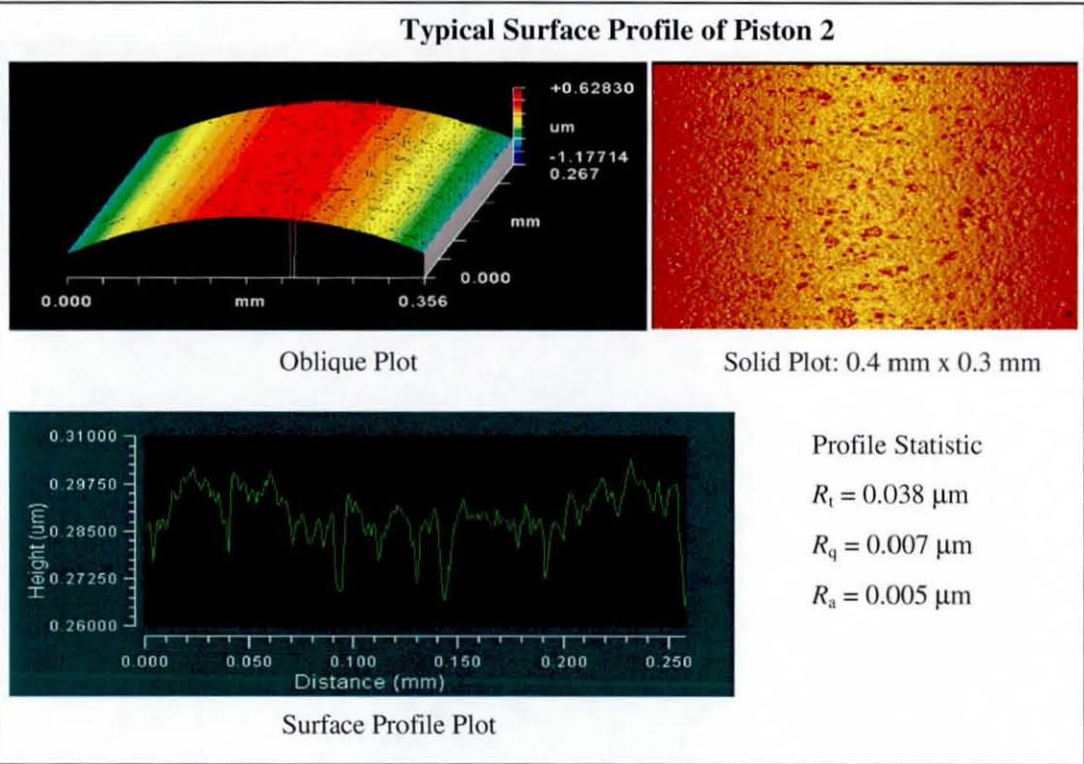


FIGURE 8.3 Typical images of Piston 2

8.3.1.3 Surface Characterisation Results of Piston 3

The summarised results obtained for Piston 3 are tabulated in Table 8.3. A set of typical images of Piston 3 is shown in Figure 8.4, where the solid plot clearly shows the porosity of Piston 3’s surface structure. Besides having a porous surface, this piston is characterised by peaks (spikes) and valleys of approximately 0.3 μm in magnitude.

TABLE 8.3 Summarised results of the surface profile characterisations for Piston 3

Piston 3 - Surface Parameters			
Statistical Description	$R_{13}(\mu\text{m})$	$R_{q3}(\mu\text{m})$	$R_{a3}(\mu\text{m})$
Average	0.702	0.066	0.029
Standard Deviation	0.347	0.030	0.014
Standard Deviation (%)	49	45	49
Minimum	0.462	0.038	0.015
Maximum	1.277	0.134	0.078
Max. Difference (Max – Min)	0.815	0.096	0.063

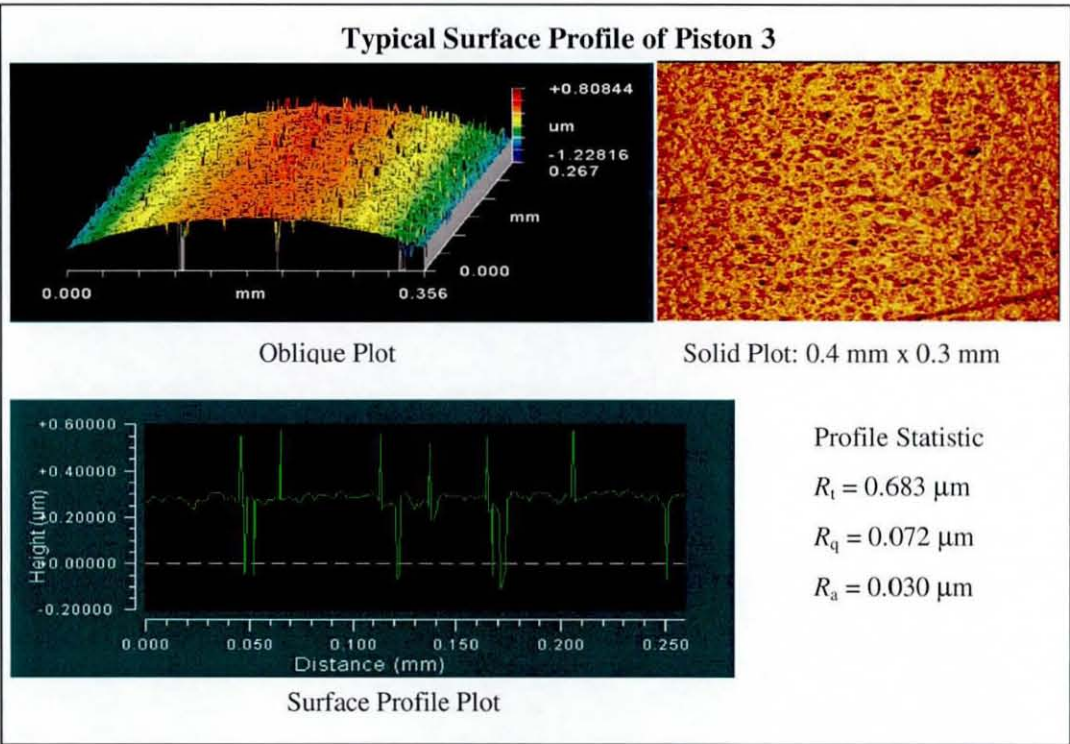


FIGURE 8.4 Typical images of Piston 3

8.3.1.4 Surface Characterisation Results of Piston 4

The results obtained for Piston 4 are tabulated in Table 8.4 with typical images shown in Figure 8.5. Piston 4 is smoother than Piston 3, but rougher than Pistons 1 and 2.

TABLE 8.4 Summarised results of the surface profile characterisations for Piston 4

Piston 4 - Surface Parameters			
Statistical Description	$R_{t4} (\mu\text{m})$	$R_{q4} (\mu\text{m})$	$R_{a4} (\mu\text{m})$
Average	0.605	0.061	0.023
Standard Deviation	0.215	0.027	0.012
Standard Deviation (%)	36	44	51
Minimum	0.445	0.048	0.014
Maximum	1.256	0.105	0.058
Max. Difference (Max – Min)	0.811	0.057	0.044

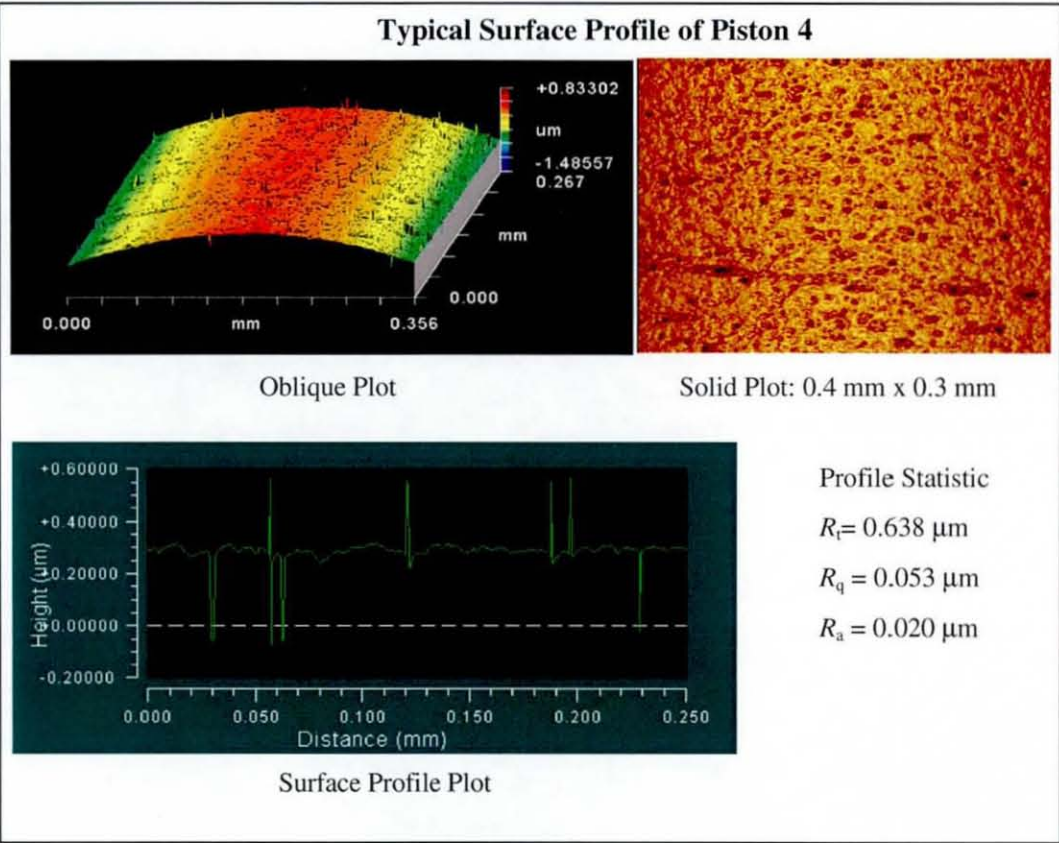


FIGURE 8.5 Typical images of Piston 4

8.3.1.5 Surface Characterisation Results of Piston 5

The overall results obtained for Piston 5 are summarised in Table 8.5 with images shown in Figure 8.6. These reveal that this piston has higher porosity and a rougher surface compared to Piston 3.

TABLE 8.5 Summarised results of the surface profile characterisations for Piston 5

Piston 5 - Surface Parameters			
Statistical Description	$R_{t5} (\mu\text{m})$	$R_{q5} (\mu\text{m})$	$R_{a5} (\mu\text{m})$
Average	1.119	0.121	0.053
Standard Deviation	0.357	0.048	0.032
Standard Deviation (%)	32	39	60
Minimum	0.562	0.058	0.023
Maximum	1.277	0.134	0.078
Max. Difference (Max – Min)	0.715	0.076	0.055

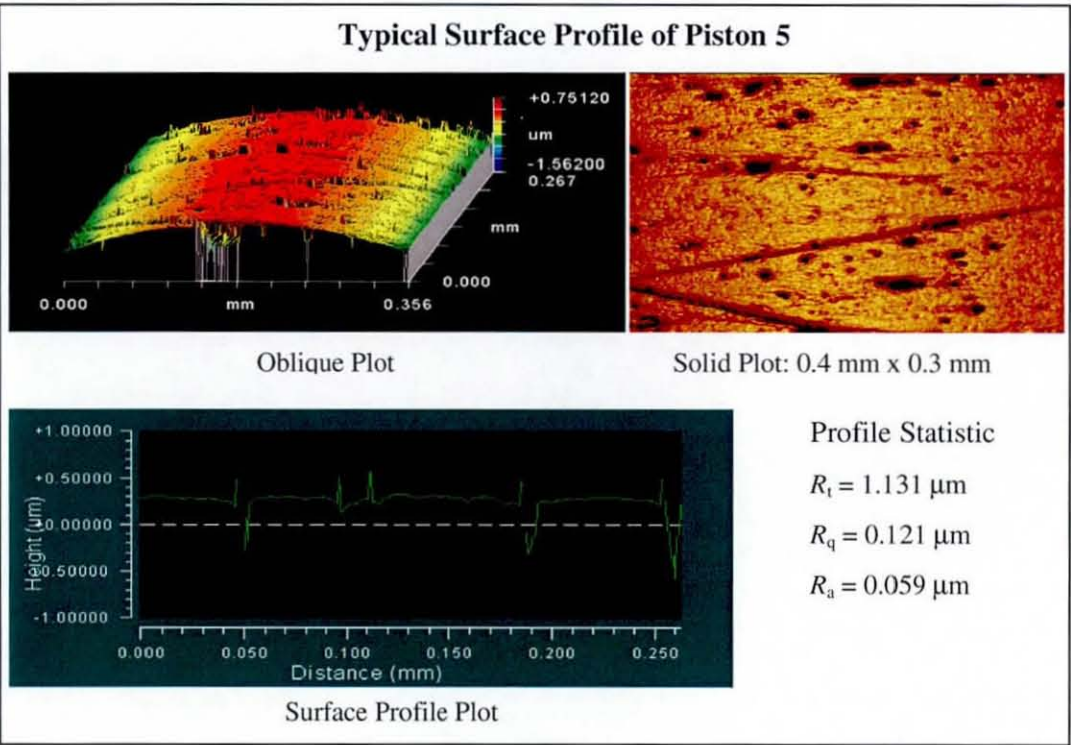


FIGURE 8.6 Typical images of Piston 5

8.3.1.6 Surface Characterisation Results of Piston 6

The summarised results obtained for Piston 6 are tabulated in Table 8.6 with images shown in Figure 8.7. They reveal that Piston 6 has the roughest surface compared to the previous 5 pistons, but has almost equivalent porosity compared to Piston 5.

TABLE 8.6 Summarised results of the surface profile characterisations for Piston 6

Piston 6 - Surface Parameters			
Statistical Description	$R_{16} (\mu\text{m})$	$R_{q6} (\mu\text{m})$	$R_{a6} (\mu\text{m})$
Average	1.470	0.153	0.073
Standard Deviation	0.857	0.046	0.032
Standard Deviation (%)	58	30	44
Minimum	0.662	0.058	0.031
Maximum	1.677	0.134	0.078
Max. Difference (Max – Min)	1.015	0.076	0.047

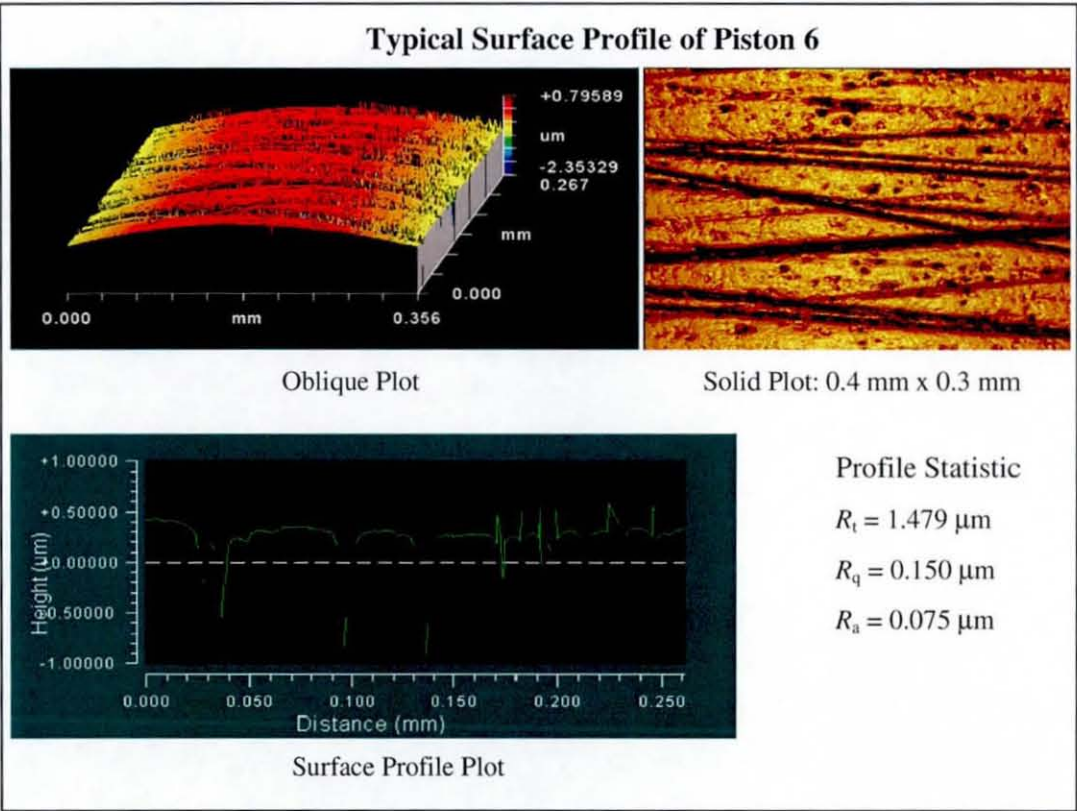


FIGURE 8.7 Typical images of Piston 6

8.3.1.7 Surface Characterisation Results of Piston 7

The summarised results obtained for Piston 7 are tabulated in Table 8.7 with images shown in Figure 8.8

TABLE 8.7 Summarised results of the surface profile characterisations for Piston 7

Piston 7 - Surface Parameters			
Statistical Description	$R_{t7} (\mu\text{m})$	$R_{q7} (\mu\text{m})$	$R_{a7} (\mu\text{m})$
Average	0.764	0.098	0.057
Standard Deviation	0.357	0.048	0.029
Standard Deviation (%)	47	49	52
Minimum	0.531	0.045	0.035
Maximum	1.137	0.126	0.078
Max. Difference (Max – Min)	0.606	0.081	0.043

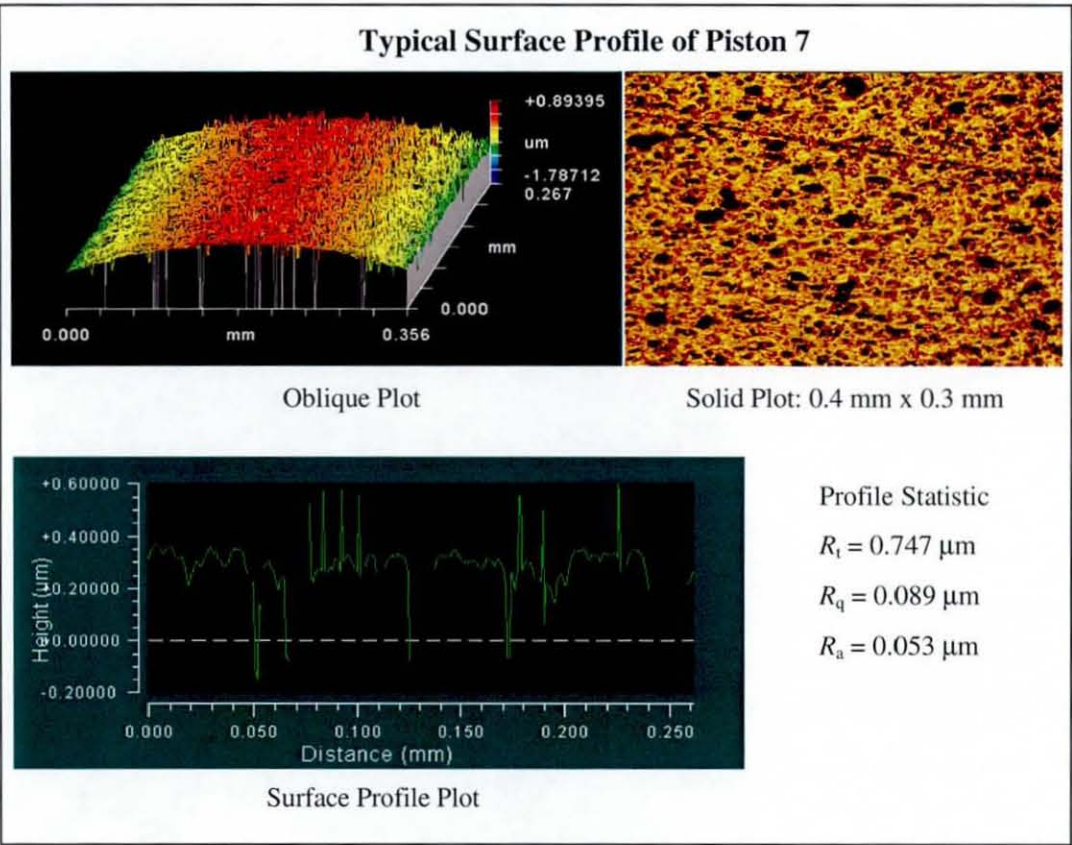


FIGURE 8.8 Typical images of Piston 7

8.3.2 Comparison of Surface Profiles Between Seven Pistons

The average values of the surface profiles are the best values to represent each surface profile of the piston under investigation. The overall results of all seven pistons are shown in Table 8.8, where the trend line of each parameter involved is plotted in the same figure (see Figure 8.9) to aid comparison. However, since the R_t values are generally ten times bigger than the values of R_q and R_a , $R_t/10$ values are used in this figure, to avoid scaling issues in the graph. The manufacturing operations of the PCAs are summarised in Figure 8.10.

TABLE 8.8 Overall results of the surface profile characterisations for the seven pistons

Piston	Surface Parameter		
	R_t (μm)	R_q (μm)	R_a (μm)
1	0.045	0.007	0.004
2	0.044	0.007	0.004
3	0.702	0.066	0.029
4	0.605	0.061	0.023
5	1.119	0.121	0.053
6	1.470	0.153	0.073
7	0.764	0.098	0.057

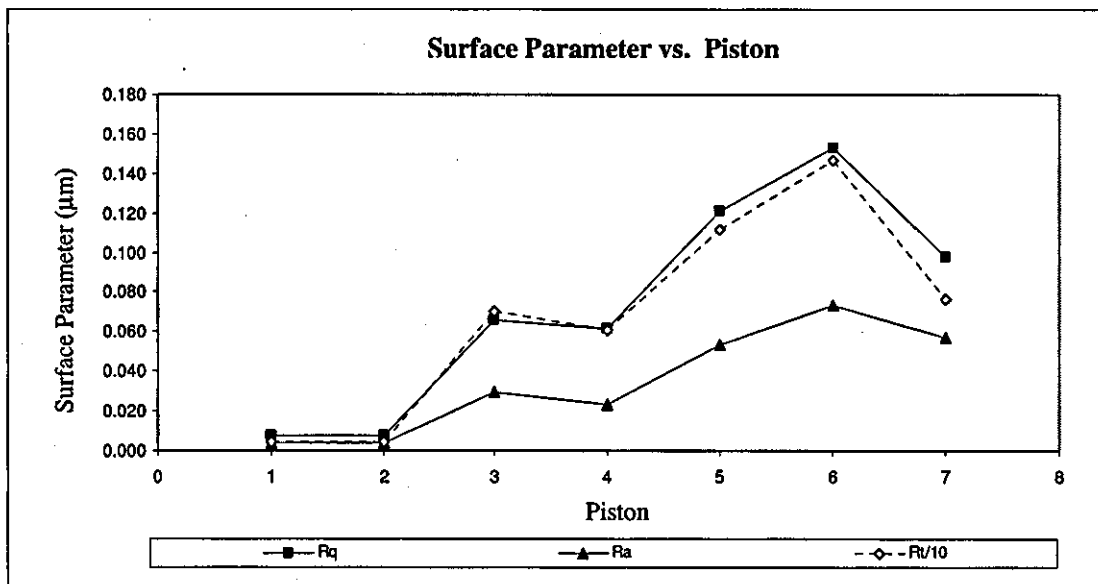


FIGURE 8.9 The trend lines of surface parameters of the seven pistons

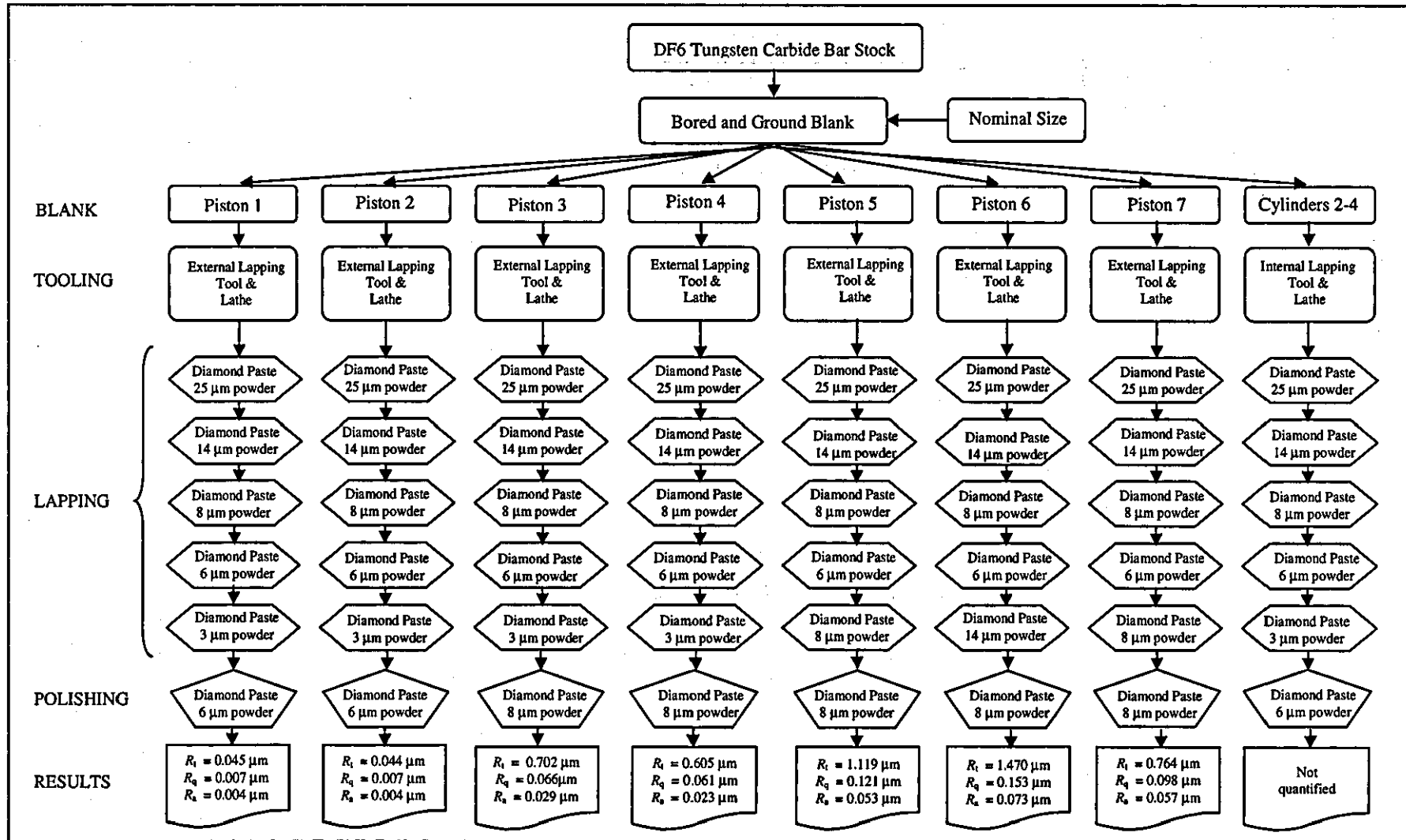


FIGURE 8.10 A summary of the manufacturing processes of the DF6 Dymet tungsten carbide PCAs

8.3.3 Results of the Effective Area Determinations

The results obtained for each cross-floating experiment are tabulated in their respective sections where each table shows the calculated effective areas obtained, accompanied with a graphical figure showing the trend line of the calculated effective areas (A_{PXY}) against the SEQ. A list of experiments that were completed is summarised in Table 8.9.

TABLE 8.9 A list of experiments for the effective area determinations

Direct Comparison		Indirect Comparison	
Experiment	Combination	Experiment	Combination
A	P_1C_2 vs. P_2C_3	m	P_7C_4 vs. P_3C_2
B	P_1C_4 vs. P_2C_3	n	P_7C_2 vs. P_3C_4
C	P_3C_2 vs. P_2C_3	o	P_6C_2 vs. P_3C_4
D	P_3C_4 vs. P_2C_3	p	P_7C_4 vs. P_4C_2
E *	P_4C_2 vs. P_2C_3	q	P_2C_2 vs. P_4C_4
F *	P_4C_4 vs. P_2C_3	r	P_3C_3 vs. P_4C_4
G	P_5C_2 vs. P_2C_3	s	P_6C_2 vs. P_4C_4
H	P_5C_4 vs. P_2C_3	t	P_7C_2 vs. P_4C_4
I	P_6C_2 vs. P_2C_3	u	P_7C_4 vs. P_6C_2
J	P_6C_4 vs. P_2C_3	v	P_6C_4 vs. P_7C_2
K	P_7C_2 vs. P_2C_3	w	P_2C_2 vs. P_7C_4
L	P_7C_4 vs. P_2C_3	x	P_3C_3 vs. P_2C_2

Note:

* Experiments that were completed and reported in Chapter 7

8.3.3.1 Experiment A: P_1C_2 vs. P_2C_3

The overall results obtained from this experiment are tabulated in Table 8.10. The first column shows the number of the experimental cycle, followed by the second column which gives the sequence of measurement (SEQ). The calculated effective areas, denoted by $A_{P_1C_2}$ are given in the third and fourth columns in m^2 and mm^2 respectively. The RDs of the reference and test are shown in the fifth and seventh columns, while the RSs of the reference and test are shown in the sixth and eighth columns. The trend of $A_{P_1C_2}$ variation against SEQ is shown in Figure 8.11 where each RC is identified with its specific marker.

TABLE 8.10 Experiment A: A_{P1C2} tabulated in accordance to its cycles and measurement sequences

CYL	SEQ	Effective Area of P_1C_2 at 100kPa, 20°C		Rotational Combination (RC)			
		A_{P1C2}		Reference PCA (P_2C_3)		Test PCA (P_1C_2)	
		(m ²)	(mm ²)	RD	RS (rpm)	RD	RS (rpm)
1	1	9.814177E-04	981.4177	CW	55	CW	56
	2	9.814165E-04	981.4165	CW	76	CCW	82
	3	9.814177E-04	981.4177	CCW	68	CCW	76
	4	9.814178E-04	981.4178	CCW	48	CW	65
2	5	9.814176E-04	981.4176	CW	37	CW	46
	6	9.814177E-04	981.4177	CW	46	CCW	59
	7	9.814176E-04	981.4176	CCW	63	CCW	51
	8	9.814172E-04	981.4172	CCW	41	CW	59
3	9	9.814178E-04	981.4178	CW	52	CW	45
	10	9.814173E-04	981.4173	CW	46	CCW	59
	11	9.814172E-04	981.4172	CCW	65	CCW	50
	12	9.814175E-04	981.4175	CCW	53	CW	64
Minimum Value		981.4165	mm ²	37	rpm	45	rpm
Maximum Value		981.4178	mm ²	76	rpm	82	rpm
Average Value ($A_{(P1C2)A}$)		981.4175	mm ²	54	rpm	59	rpm
Standard Deviation		0.0004	mm ²	12	rpm	11	rpm
Relative Standard Deviation		0.37	ppm	22	%	19	%

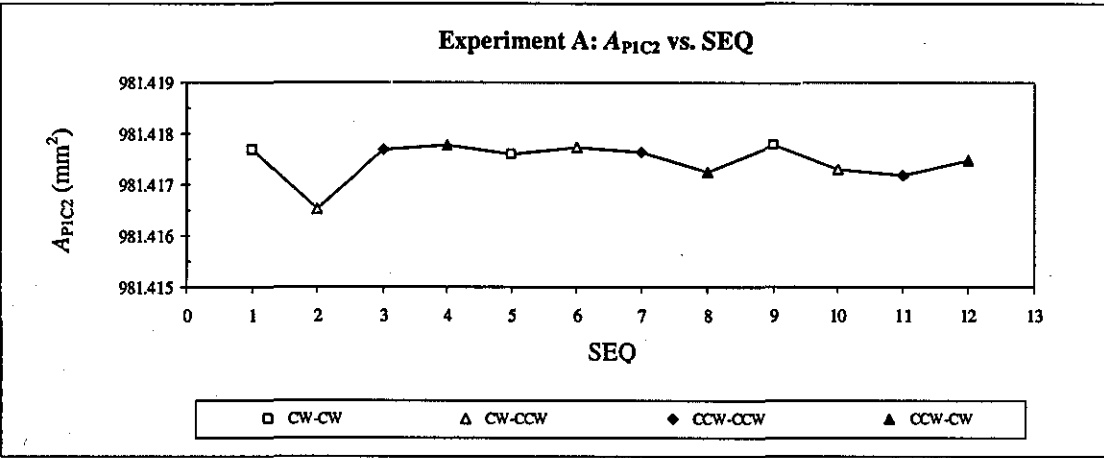


FIGURE 8.11 Experiment A: variation of A_{P1C2} with the SEQ

8.3.3.2 Experiment B: P_1C_4 vs. P_2C_3

The overall results obtained from this experiment are tabulated in Table 8.11, and graphically represented in Figure 8.12.

TABLE 8.11 Experiment B: A_{P1C4} tabulated in accordance to its cycles and measurement sequences

CYL	SEQ	Effective Area of P_1C_4 at 100kPa, 20°C		Rotational Combination (RC)			
		A_{P1C4}		Reference PCA (P_2C_3)		Test PCA (P_1C_4)	
		(m ²)	(mm ²)	RD	RS (rpm)	RD	RS (rpm)
1	1	9.814099E-04	981.4099	CW	55	CW	65
	2	9.814104E-04	981.4104	CW	63	CCW	73
	3	9.814094E-04	981.4094	CCW	71	CCW	50
	4	9.814094E-04	981.4094	CCW	65	CW	49
2	5	9.814098E-04	981.4098	CW	33	CW	36
	6	9.814100E-04	981.4100	CW	47	CCW	59
	7	9.814093E-04	981.4093	CCW	44	CCW	59
	8	9.814095E-04	981.4095	CCW	80	CW	73
3	9	9.814089E-04	981.4089	CW	37	CW	64
	10	9.814087E-04	981.4087	CW	70	CCW	50
	11	9.814098E-04	981.4098	CCW	53	CCW	60
	12	9.814093E-04	981.4093	CCW	42	CW	68
Minimum Value			981.4087 mm ²	33	rpm	36	rpm
Maximum Value			981.4104 mm ²	80	rpm	73	rpm
Average Value ($A_{(P1C4)B}$)			981.4095 mm ²	55	rpm	59	rpm
Standard Deviation			0.0005 mm ²	15	rpm	11	rpm
Relative Standard Deviation			0.47 ppm	27	%	19	%

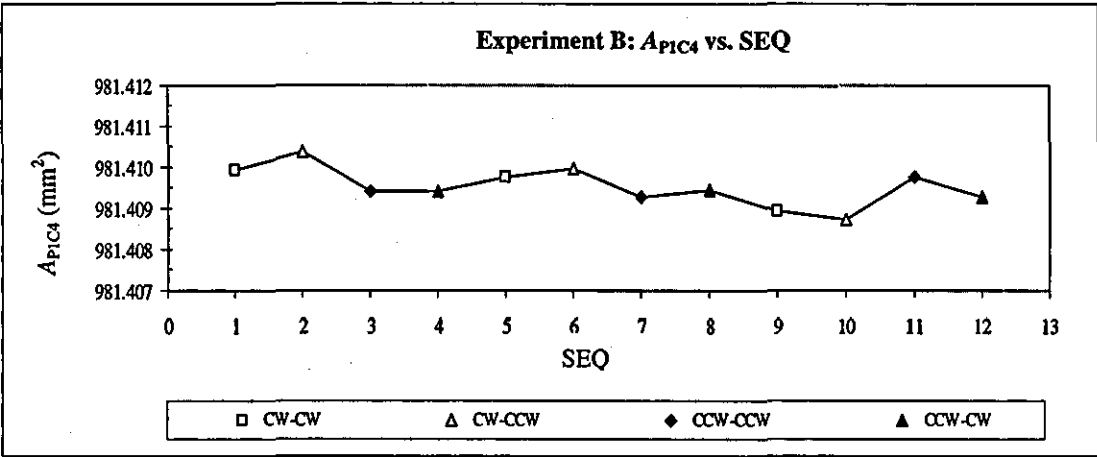


FIGURE 8.12 Experiment B: variation of A_{P1C4} with the SEQ

8.3.3.3 Experiment C: P_3C_2 vs. P_2C_3

The overall results obtained from this experiment are tabulated in Table 8.12, and graphically represented in Figure 8.13.

TABLE 8.12 Experiment C: $A_{P_3C_2}$ tabulated in accordance to its cycles and measurement sequences

CYL	SEQ	Effective Area of P_3C_2 at 100kPa, 20°C		Rotational Combination (RC)			
		$A_{P_3C_2}$		Reference PCA (P_2C_3)		Test PCA (P_3C_2)	
		(m ²)	(mm ²)	RD	RS (rpm)	RD	RS (rpm)
1	1	9.814468E-04	981.4468	CW	64	CW	64
	2	9.814457E-04	981.4457	CW	46	CCW	63
	3	9.814460E-04	981.4460	CCW	67	CCW	55
	4	9.814459E-04	981.4459	CCW	59	CW	67
2	5	9.814460E-04	981.4460	CW	60	CW	54
	6	9.814454E-04	981.4454	CW	47	CCW	59
	7	9.814457E-04	981.4457	CCW	62	CCW	54
	8	9.814452E-04	981.4452	CCW	51	CW	62
3	9	9.814460E-04	981.4460	CW	58	CW	53
	10	9.814450E-04	981.4450	CW	68	CCW	80
	11	9.814457E-04	981.4457	CCW	73	CCW	68
	12	9.814450E-04	981.4450	CCW	61	CW	69
Minimum Value			981.4450 mm ²	46	rpm	53	rpm
Maximum Value			981.4468 mm ²	73	rpm	80	rpm
Average Value ($A_{(P_3C_2)C}$)			981.4457 mm ²	60	rpm	62	rpm
Standard Deviation			0.0005 mm ²	8	rpm	8	rpm
Relative Standard Deviation			0.52 ppm	14	%	13	%

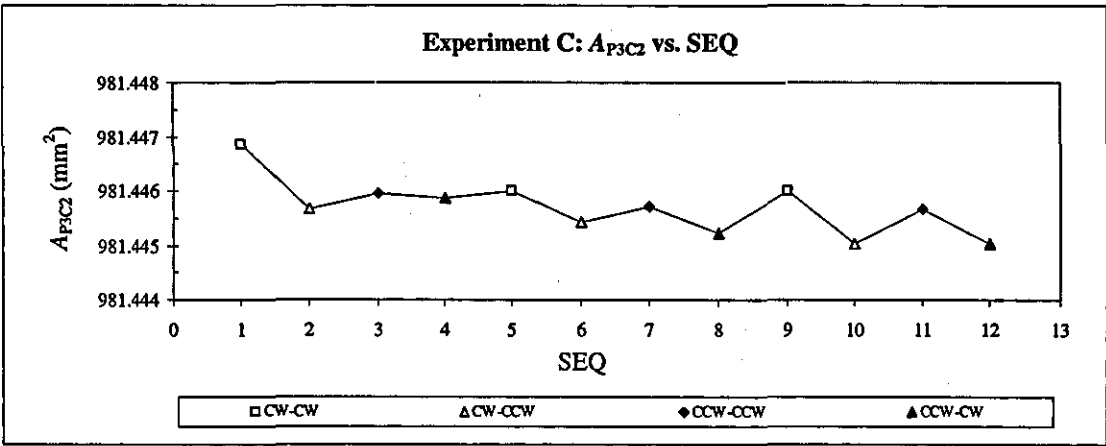


FIGURE 8.13 Experiment C: variation of $A_{P_3C_2}$ with the SEQ

8.3.3.4 Experiment D: P_3C_4 vs. P_2C_3

The overall results obtained from this experiment are tabulated in Table 8.13, and graphically represented in Figure 8.14.

TABLE 8.13 Experiment D: $A_{P_3C_4}$ tabulated in accordance to its cycles and measurement sequences

CYL	SEQ	Effective Area of P_3C_4 at 100kPa, 20°C		Rotational Combination (RC)			
		$A_{P_3C_4}$		Reference PCA (P_2C_3)		Test PCA (P_3C_4)	
		(m ²)	(mm ²)	RD	RS (rpm)	RD	RS (rpm)
1	1	9.814311E-04	981.4311	CW	41	CW	57
	2	9.814307E-04	981.4307	CW	57	CCW	74
	3	9.814308E-04	981.4308	CCW	57	CCW	68
	4	9.814304E-04	981.4304	CCW	40	CW	57
2	5	9.814304E-04	981.4304	CW	55	CW	64
	6	9.814305E-04	981.4305	CW	44	CCW	65
	7	9.814319E-04	981.4319	CCW	55	CCW	54
	8	9.814302E-04	981.4302	CCW	44	CW	59
3	9	9.814316E-04	981.4316	CW	51	CW	38
	10	9.814307E-04	981.4307	CW	55	CCW	65
	11	9.814319E-04	981.4319	CCW	58	CCW	51
	12	9.814307E-04	981.4307	CCW	44	CW	62
Minimum Value			981.4302 mm ²	40	rpm	38	rpm
Maximum Value			981.4319 mm ²	58	rpm	74	rpm
Average Value ($A_{(P_3C_4)D}$)			981.4309 mm ²	50	rpm	60	rpm
Standard Deviation			0.0006 mm ²	7	rpm	9	rpm
Relative Standard Deviation			0.62 ppm	14	%	16	%

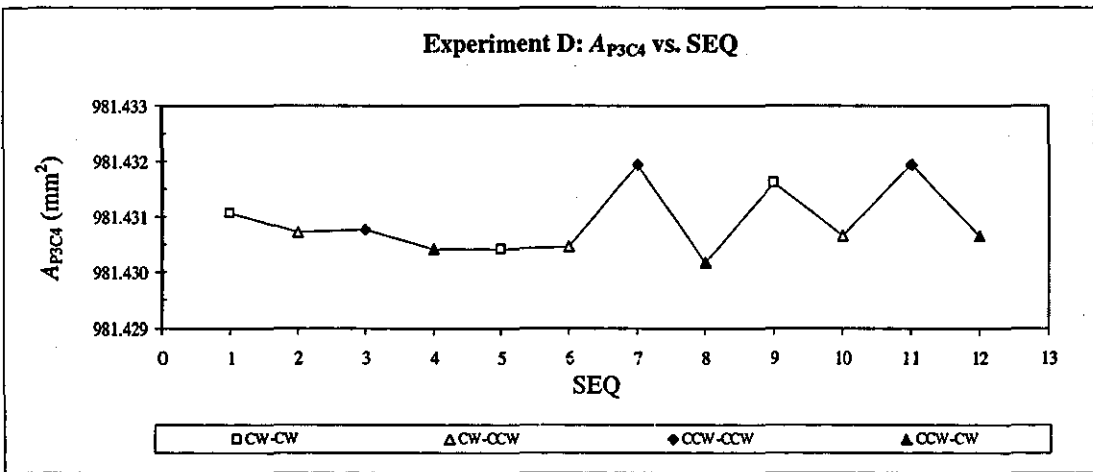


FIGURE 8.14 Experiment D: variation of $A_{P_3C_4}$ with the SEQ

8.3.3.5 Experiment G: P_5C_2 vs. P_2C_3

Experiments E and F have been explained and reported in the Chapter 7. This section explains Experiment G. The overall results obtained from this experiment are graphically represented in Figure 8.15, and the detailed data is tabulated in Table 8.14. In this experiment, eight cycles with 32 SEQ were carried out. Extra cycles were completed in order to check the consistency of the results (which were carried out on two different days) produced by the piston of modified surface, besides investigating the influences of surface textures on the pressure generated.

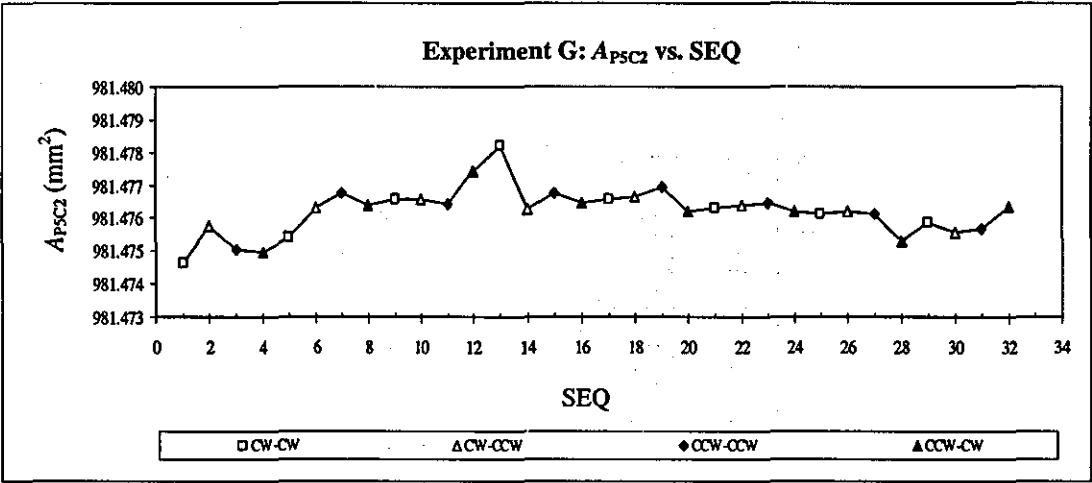


FIGURE 8.15 Experiment G: variation of A_{P5C2} with the SEQ

TABLE 8.14 Experiment G: A_{PSC2} tabulated in accordance to its cycles and measurement sequences

CYL	SEQ	Effective Area of P_5C_2 at 100kPa, 20°C		Rotational Combination (RC)			
		A_{PSC2}		Reference PCA (P_2C_3)		Test PCA (P_5C_2)	
		(m ²)	(mm ²)	RD	RS (rpm)	RD	RS (rpm)
1	1	9.814747E-04	981.4747	CW	52	CW	60
	2	9.814757E-04	981.4757	CW	47	CCW	61
	3	9.814751E-04	981.4751	CCW	63	CCW	65
	4	9.814750E-04	981.4750	CCW	58	CW	61
2	5	9.814754E-04	981.4754	CW	60	CW	59
	6	9.814763E-04	981.4763	CW	65	CCW	74
	7	9.814767E-04	981.4767	CCW	74	CCW	63
	8	9.814764E-04	981.4764	CCW	63	CW	61
3	9	9.814766E-04	981.4766	CW	67	CW	62
	10	9.814766E-04	981.4766	CW	52	CCW	70
	11	9.814764E-04	981.4764	CCW	69	CCW	80
	12	9.814774E-04	981.4774	CCW	78	CW	71
4	13	9.814782E-04	981.4782	CW	63	CW	77
	14	9.814763E-04	981.4763	CW	67	CCW	82
	15	9.814768E-04	981.4768	CCW	59	CCW	56
	16	9.814765E-04	981.4765	CCW	70	CW	67
5	17	9.814766E-04	981.4766	CW	51	CW	65
	18	9.814767E-04	981.4767	CW	65	CCW	68
	19	9.814770E-04	981.4770	CCW	71	CCW	67
	20	9.814762E-04	981.4762	CCW	63	CW	66
6	21	9.814763E-04	981.4763	CW	69	CW	60
	22	9.814764E-04	981.4764	CW	63	CCW	59
	23	9.814765E-04	981.4765	CCW	63	CCW	57
	24	9.814762E-04	981.4762	CCW	70	CW	66
7	25	9.814761E-04	981.4761	CW	55	CW	65
	26	9.814762E-04	981.4762	CW	57	CCW	58
	27	9.814761E-04	981.4761	CCW	60	CCW	58
	28	9.814753E-04	981.4753	CCW	54	CW	67
8	29	9.814759E-04	981.4759	CW	57	CW	54
	30	9.814756E-04	981.4756	CW	55	CCW	56
	31	9.814757E-04	981.4757	CCW	62	CCW	72
	32	9.814764E-04	981.4764	CCW	59	CW	56
Minimum Value		981.4747	mm ²	47	rpm	54	rpm
Maximum Value		981.4782	mm ²	78	rpm	82	rpm
Average Value ($A_{(PSC2)G}$)		981.4762	mm ²	62	rpm	64	rpm
Standard Deviation		0.0007	mm ²	7	rpm	7	rpm
Relative Standard Deviation		0.72	ppm	12	%	11	%

8.3.3.6 Experiment H: P_5C_4 vs. P_2C_3

The overall results obtained from this experiment are tabulated in Table 8.15, and graphically represented in Figure 8.16.

TABLE 8.15 Experiment H: A_{P5C4} tabulated in accordance to its cycles and measurement sequences

CYL	SEQ	Effective Area of P_5C_4 at 100kPa, 20°C		Rotational Combination (RC)			
		A_{P5C4}		Reference PCA (P_2C_3)		Test PCA (P_5C_4)	
		(m ²)	(mm ²)	RD	RS (rpm)	RD	RS (rpm)
1	1	9.814668E-04	981.4668	CW	58	CW	52
	2	9.814663E-04	981.4663	CW	60	CCW	64
	3	9.814663E-04	981.4663	CCW	75	CCW	66
	4	9.814669E-04	981.4669	CCW	54	CW	44
2	5	9.814669E-04	981.4669	CW	67	CW	65
	6	9.814658E-04	981.4658	CW	45	CCW	40
	7	9.814661E-04	981.4661	CCW	68	CCW	50
	8	9.814663E-04	981.4663	CCW	58	CW	54
3	9	9.814662E-04	981.4662	CW	74	CW	85
	10	9.814653E-04	981.4653	CW	64	CCW	77
	11	9.814655E-04	981.4655	CCW	50	CCW	45
	12	9.814653E-04	981.4653	CCW	59	CW	73
Minimum Value			981.4653 mm ²	45	rpm	40	rpm
Maximum Value			981.4669 mm ²	75	rpm	85	rpm
Average Value ($A_{(P5C4)H}$)			981.4661 mm ²	61	rpm	60	rpm
Standard Deviation			0.0006 mm ²	9	rpm	14	rpm
Relative Standard Deviation			0.59 ppm	15	%	24	%

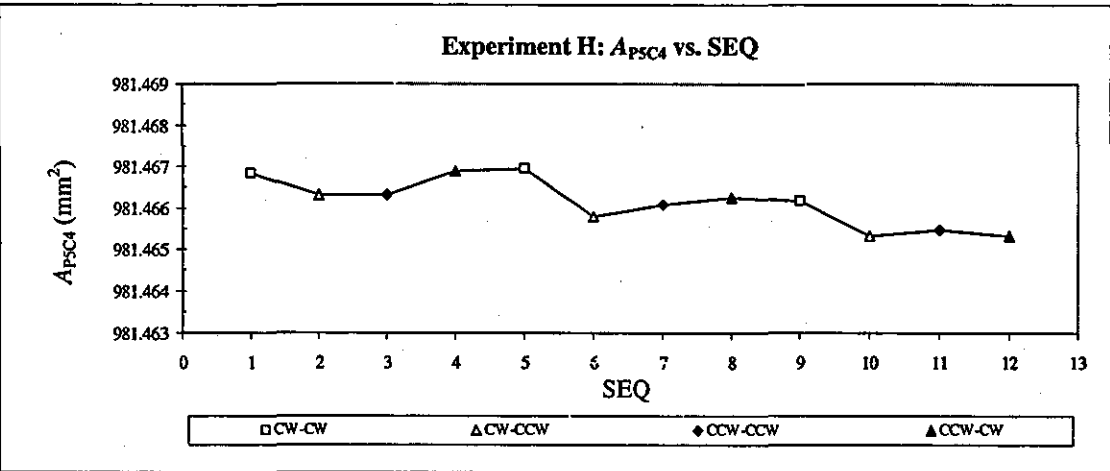


FIGURE 8.16 Experiment H: variation of A_{P5C4} with the SEQ

8.3.3.7 Experiment I: P_6C_2 vs. P_2C_3

Piston 6 is the one which has the roughest outer surface, where its average R_t is greater than $1\text{ }\mu\text{m}$. Therefore, extra numbers of cycle were completed in this experiment. The overall results obtained are graphically represented in Figure 8.17, and detailed data is tabulated in Table 8.16.

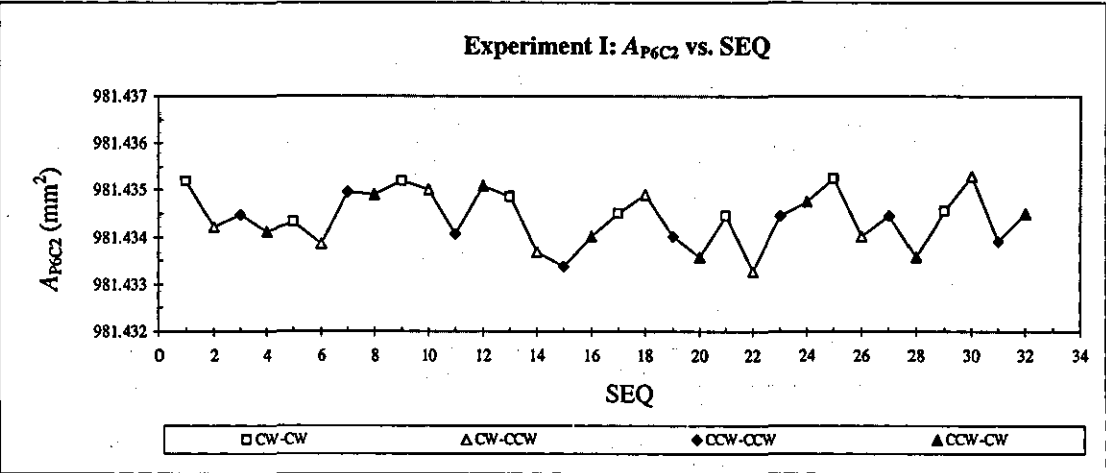


FIGURE 8.17 Experiment I: variation of $A_{P_6C_2}$ with the SEQ

TABLE 8.16 Experiment I: $A_{P_6C_2}$ tabulated in accordance to its cycles and measurement sequences

CYL	SEQ	Effective Area of P_6C_2 at 100kPa, 20°C		Rotational Combination (RC)			
		$A_{P_6C_2}$		Reference PCA (P_2C_3)		Test PCA (P_6C_2)	
		(m ²)	(mm ²)	RD	RS (rpm)	RD	RS (rpm)
1	1	9.814352E-04	981.4352	CW	46	CW	60
	2	9.814342E-04	981.4342	CW	61	CCW	61
	3	9.814345E-04	981.4345	CCW	62	CCW	73
	4	9.814341E-04	981.4341	CCW	64	CW	59
2	5	9.814343E-04	981.4343	CW	52	CW	46
	6	9.814339E-04	981.4339	CW	53	CCW	62
	7	9.814350E-04	981.4350	CCW	51	CCW	65
	8	9.814349E-04	981.4349	CCW	72	CW	71
3	9	9.814352E-04	981.4352	CW	62	CW	72
	10	9.814350E-04	981.4350	CW	60	CCW	67
	11	9.814341E-04	981.4341	CCW	69	CCW	65
	12	9.814351E-04	981.4351	CCW	67	CW	62
4	13	9.814349E-04	981.4349	CW	63	CW	67
	14	9.814337E-04	981.4337	CW	72	CCW	83
	15	9.814334E-04	981.4334	CCW	58	CCW	70
	16	9.814340E-04	981.4340	CCW	43	CW	62
5	17	9.814345E-04	981.4345	CW	54	CW	56
	18	9.814349E-04	981.4349	CW	59	CCW	65
	19	9.814340E-04	981.4340	CCW	45	CCW	73
	20	9.814336E-04	981.4336	CCW	60	CW	70
6	21	9.814345E-04	981.4345	CW	55	CW	54
	22	9.814333E-04	981.4333	CW	47	CCW	60
	23	9.814345E-04	981.4345	CCW	66	CCW	58
	24	9.814348E-04	981.4348	CCW	69	CW	67
7	25	9.814352E-04	981.4352	CW	53	CW	80
	26	9.814340E-04	981.4340	CW	44	CCW	69
	27	9.814345E-04	981.4345	CCW	66	CCW	73
	28	9.814336E-04	981.4336	CCW	56	CW	82
8	29	9.814346E-04	981.4346	CW	50	CW	74
	30	9.814353E-04	981.4353	CW	58	CCW	65
	31	9.814339E-04	981.4339	CCW	65	CCW	68
	32	9.814345E-04	981.4345	CCW	48	CW	74
Minimum Value		981.4333	mm ²	43	rpm	46	rpm
Maximum Value		981.4353	mm ²	72	rpm	83	rpm
Average Value ($A_{(P_6C_2)}$)		981.4344	mm ²	58	rpm	67	rpm
Standard Deviation		0.0006	mm ²	8	rpm	8	rpm
Relative Standard Deviation		0.58	ppm	15	%	12	%

8.3.3.8 Experiment J: P_6C_4 vs. P_2C_3

The overall results obtained from this experiment are tabulated in Table 8.17, and graphically represented in Figure 8.18.

TABLE 8.17 Experiment J: $A_{P_6C_4}$ tabulated in accordance to its cycles and measurement sequences

CYL	SEQ	Effective Area of P_6C_4 at 100kPa, 20°C		Rotational Combination (RC)			
		$A_{P_6C_4}$		Reference PCA (P_2C_3)		Test PCA (P_6C_4)	
		(m ²)	(mm ²)	RD	RS (rpm)	RD	RS (rpm)
1	1	9.814246E-04	981.4246	CW	45	CW	43
	2	9.814242E-04	981.4242	CW	57	CCW	78
	3	9.814245E-04	981.4245	CCW	65	CCW	85
	4	9.814245E-04	981.4245	CCW	58	CW	68
2	5	9.814250E-04	981.4250	CW	57	CW	62
	6	9.814243E-04	981.4243	CW	47	CCW	68
	7	9.814244E-04	981.4244	CCW	74	CCW	75
	8	9.814240E-04	981.4240	CCW	62	CW	64
3	9	9.814247E-04	981.4247	CW	58	CW	48
	10	9.814240E-04	981.4240	CW	75	CCW	67
	11	9.814242E-04	981.4242	CCW	58	CCW	76
	12	9.814250E-04	981.4250	CCW	64	CW	58
Minimum Value			981.4240 mm ²	45	rpm	43	rpm
Maximum Value			981.4250 mm ²	75	rpm	85	rpm
Average Value ($A_{I(P_6C_4)}$)			981.4244 mm ²	60	rpm	66	rpm
Standard Deviation			0.0004 mm ²	9	rpm	12	rpm
Relative Standard Deviation			0.36 ppm	15	%	18	%

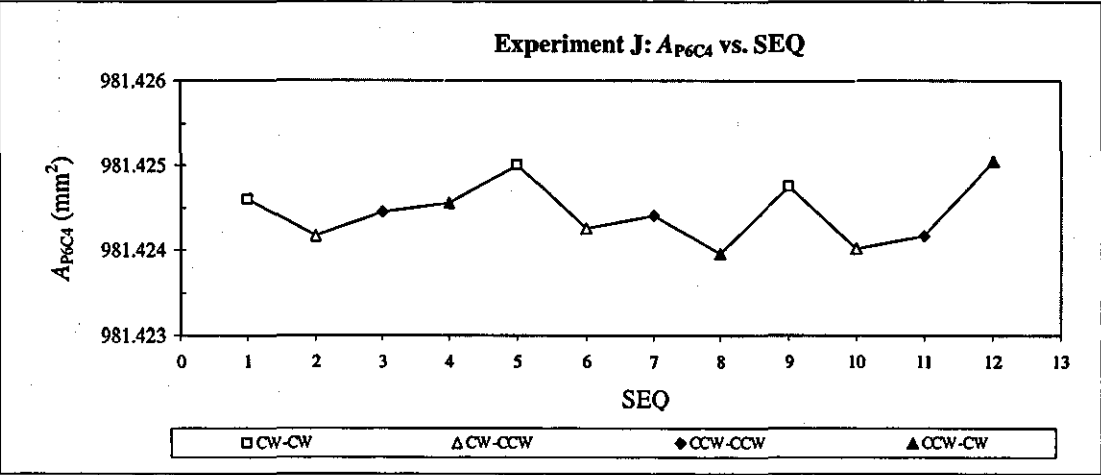


FIGURE 8.18 Experiment J: variation of $A_{P_6C_4}$ with the SEQ

8.3.3.9 Experiment K: P_7C_2 vs. P_2C_3

The overall results obtained from this experiment are tabulated in Table 8.18, and graphically represented in Figure 8.19.

TABLE 8.18 Experiment K: A_{P7C2} tabulated in accordance to its cycles and measurement sequences

CYL	SEQ	Effective Area of P_7C_2 at 100kPa, 20°C		Rotational Combination (RC)			
		A_{P7C2}		Reference PCA (P_2C_3)		Test PCA (P_7C_2)	
		(m ²)	(mm ²)	RD	RS (rpm)	RD	RS (rpm)
1	1	9.814888E-04	981.4888	CW	52	CW	69
	2	9.814882E-04	981.4882	CW	49	CCW	65
	3	9.814900E-04	981.4900	CCW	82	CCW	80
	4	9.814897E-04	981.4897	CCW	74	CW	69
2	5	9.814893E-04	981.4893	CW	64	CW	67
	6	9.814888E-04	981.4888	CW	51	CCW	74
	7	9.814893E-04	981.4893	CCW	69	CCW	68
	8	9.814907E-04	981.4907	CCW	49	CW	65
3	9	9.814908E-04	981.4908	CW	64	CW	48
	10	9.814913E-04	981.4913	CW	56	CCW	66
	11	9.814905E-04	981.4905	CCW	62	CCW	67
	12	9.814908E-04	981.4908	CCW	50	CW	55
Minimum Value			981.4882 mm ²	49	rpm	48	rpm
Maximum Value			981.4913 mm ²	82	rpm	80	rpm
Average Value ($A_{(P7C2)K}$)			981.4899 mm ²	60	rpm	66	rpm
Standard Deviation			0.0010 mm ²	11	rpm	8	rpm
Relative Standard Deviation			1.00 ppm	18	%	12	%

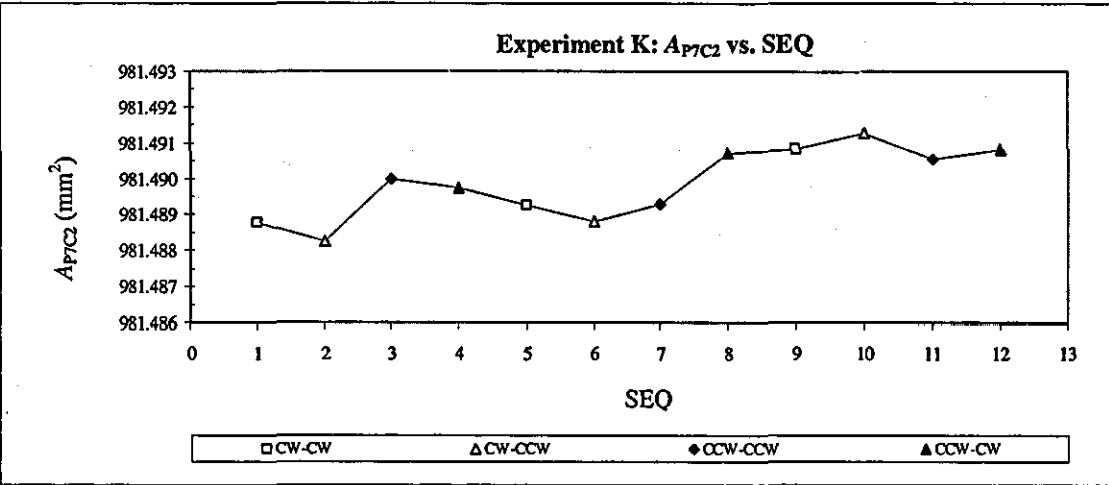


FIGURE 8.19 Experiment K: variation of A_{P7C2} with the SEQ

8.3.3.10 Experiment L: P_7C_4 vs. P_2C_3

The overall results obtained from this experiment are tabulated in Table 8.19, and graphically represented in Figure 8.20. Direct comparisons against the reference P_2C_3 ended with this experiment, followed with other twelve indirect comparisons.

TABLE 8.19 Experiment L: A_{P7C4} tabulated in accordance to its cycles and measurement sequences

CYL	SEQ	Effective Area of P_7C_4 at 100kPa, 20°C		Rotational Combination (RC)			
		A_{P7C4}		Reference PCA (P_2C_3)		Test PCA (P_7C_4)	
		(m ²)	(mm ²)	RD	RS (rpm)	RD	RS (rpm)
1	1	9.8147842E-04	981.47842	CW	65	CW	61
	2	9.8147818E-04	981.47818	CW	66	CCW	80
	3	9.8147823E-04	981.47823	CCW	58	CCW	56
	4	9.8147754E-04	981.47754	CCW	53	CW	68
2	5	9.8147862E-04	981.47862	CW	53	CW	63
	6	9.8147842E-04	981.47842	CW	79	CCW	83
	7	9.8147823E-04	981.47823	CCW	68	CCW	61
	8	9.8147872E-04	981.47872	CCW	61	CW	69
3	9	9.8147823E-04	981.47823	CW	66	CW	56
	10	9.8147675E-04	981.47675	CW	80	CCW	72
	11	9.8147842E-04	981.47842	CCW	55	CCW	58
	12	9.8147921E-04	981.47921	CCW	49	CW	65
Minimum Value		981.4768	mm ²	49	rpm	56	rpm
Maximum Value		981.4792	mm ²	80	rpm	83	rpm
Average Value ($A_{(P7C4)L}$)		981.4783	mm ²	63	rpm	66	rpm
Standard Deviation		0.0006	mm ²	10	rpm	9	rpm
Relative Standard Deviation		0.62	ppm	16	%	13	%

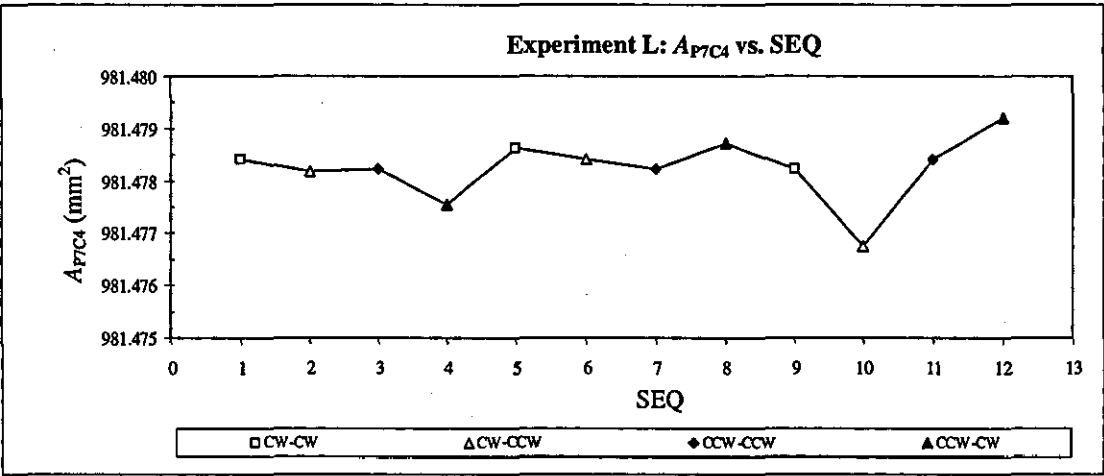


FIGURE 8.20 Experiment L: variation of A_{P7C4} with the SEQ

8.3.3.11 Experiment m: P_7C_4 vs. P_3C_2

This experiment was the first indirect comparison within the calibration chain. The overall results obtained from this experiment are tabulated in Table 8.20, and graphically represented in Figure 8.21.

TABLE 8.20 Experiment m: $A_{P_7C_4}$ tabulated in accordance to its cycles and measurement sequences

CYL	SEQ	Effective Area of P_7C_4 at 100kPa, 20°C		Rotational Combination (RC)			
		$A_{P_7C_4}$		Reference PCA (P_3C_2)		Test PCA (P_7C_4)	
		(m ²)	(mm ²)	RD	RS (rpm)	RD	RS (rpm)
1	1	9.814808E-04	981.4808	CW	54	CW	69
	2	9.814813E-04	981.4813	CW	60	CCW	65
	3	9.814821E-04	981.4821	CCW	60	CCW	67
	4	9.814808E-04	981.4808	CCW	67	CW	71
2	5	9.814812E-04	981.4812	CW	57	CW	62
	6	9.814802E-04	981.4802	CW	46	CCW	80
	7	9.814796E-04	981.4796	CCW	72	CCW	78
	8	9.814808E-04	981.4808	CCW	55	CW	79
3	9	9.814808E-04	981.4808	CW	64	CW	65
	10	9.814795E-04	981.4795	CW	58	CCW	79
	11	9.814801E-04	981.4801	CCW	45	CCW	76
	12	9.814811E-04	981.4811	CCW	56	CW	67
Minimum Value			981.4795 mm ²	45	rpm	62	rpm
Maximum Value			981.4821 mm ²	72	rpm	80	rpm
Average Value ($A_{(P_7C_4)m}$)			981.4807 mm ²	58	rpm	72	rpm
Standard Deviation			0.0007 mm ²	8	rpm	7	rpm
Relative Standard Deviation			0.75 ppm	13	%	9	%

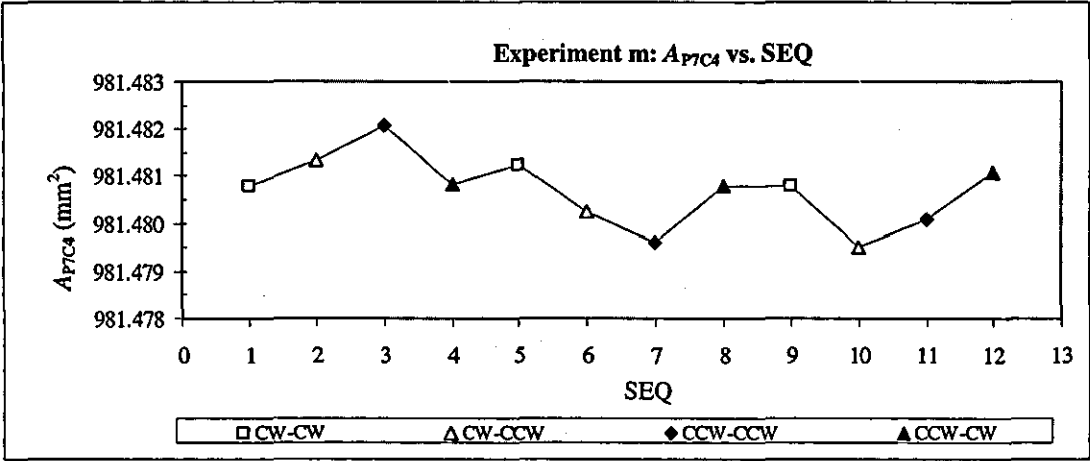


FIGURE 8.21 Experiment m: variation of $A_{P_7C_4}$ with the SEQ

8.3.3.12 Experiment n: P_7C_2 vs. P_3C_4

The overall results obtained from this experiment are tabulated in Table 8.21, and graphically represented in Figure 8.22.

TABLE 8.21 Experiment n: A_{P7C2} tabulated in accordance to its cycles and measurement sequences

CYL	SEQ	Effective Area of P_7C_2 at 100kPa, 20°C		Rotational Combination (RC)			
		A_{P7C2}		Reference PCA (P_3C_4)		Test PCA (P_7C_2)	
		(m ²)	(mm ²)	RD	RS (rpm)	RD	RS (rpm)
1	1	9.814920E-04	981.4920	CW	60	CW	50
	2	9.814895E-04	981.4895	CW	75	CCW	80
	3	9.814897E-04	981.4897	CCW	80	CCW	75
	4	9.814915E-04	981.4915	CCW	81	CW	58
2	5	9.814915E-04	981.4915	CW	62	CW	71
	6	9.814895E-04	981.4895	CW	57	CCW	70
	7	9.814900E-04	981.4900	CCW	77	CCW	53
	8	9.814898E-04	981.4898	CCW	70	CW	60
3	9	9.814897E-04	981.4897	CW	68	CW	56
	10	9.814903E-04	981.4903	CW	49	CCW	55
	11	9.814898E-04	981.4898	CCW	74	CCW	64
	12	9.814900E-04	981.4900	CCW	64	CW	72
Minimum Value		981.4895	mm ²	49	rpm	50	rpm
Maximum Value		981.4920	mm ²	81	rpm	80	rpm
Average Value ($A_{(P7C2)n}$)		981.4903	mm ²	68	rpm	64	rpm
Standard Deviation		0.0009	mm ²	10	rpm	10	rpm
Relative Standard Deviation		0.87	ppm	15	%	15	%

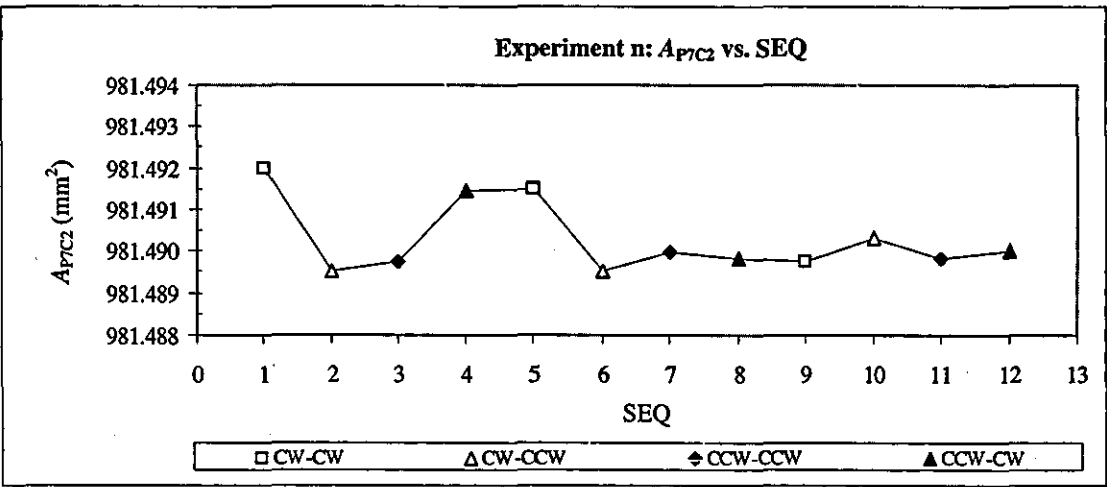


FIGURE 8.22 Experiment n: variation of A_{P7C2} with the SEQ

8.3.3.13 Experiment o: P_6C_2 vs. P_3C_4

The overall results obtained from this experiment are tabulated in Table 8.22, and graphically represented in Figure 8.23.

TABLE 8.22 Experiment o: $A_{P_6C_2}$ tabulated in accordance to its cycles and measurement sequences

CYL	SEQ	Effective Area of P_6C_2 at 100kPa, 20°C		Rotational Combination (RC)			
		$A_{P_6C_2}$		Reference PCA (P_3C_4)		Test PCA (P_6C_2)	
		(m ²)	(mm ²)	RD	RS (rpm)	RD	RS (rpm)
1	1	9.814363E-04	981.4363	CW	63	CW	69
	2	9.814344E-04	981.4344	CW	56	CCW	54
	3	9.814342E-04	981.4342	CCW	63	CCW	60
	4	9.814367E-04	981.4367	CCW	52	CW	57
2	5	9.814372E-04	981.4372	CW	59	CW	46
	6	9.814343E-04	981.4343	CW	63	CCW	64
	7	9.814363E-04	981.4363	CCW	77	CCW	81
	8	9.814354E-04	981.4354	CCW	66	CW	72
3	9	9.814357E-04	981.4357	CW	55	CW	60
	10	9.814345E-04	981.4345	CW	46	CCW	52
	11	9.814347E-04	981.4347	CCW	57	CCW	45
	12	9.814360E-04	981.4360	CCW	76	CW	65
Minimum Value			981.4342 mm ²	46	rpm	45	rpm
Maximum Value			981.4372 mm ²	77	rpm	81	rpm
Average Value ($A_{(P_6C_2)o}$)			981.4355 mm ²	61	rpm	60	rpm
Standard Deviation			0.0010 mm ²	9	rpm	11	rpm
Relative Standard Deviation			1.06 ppm	15	%	18	%

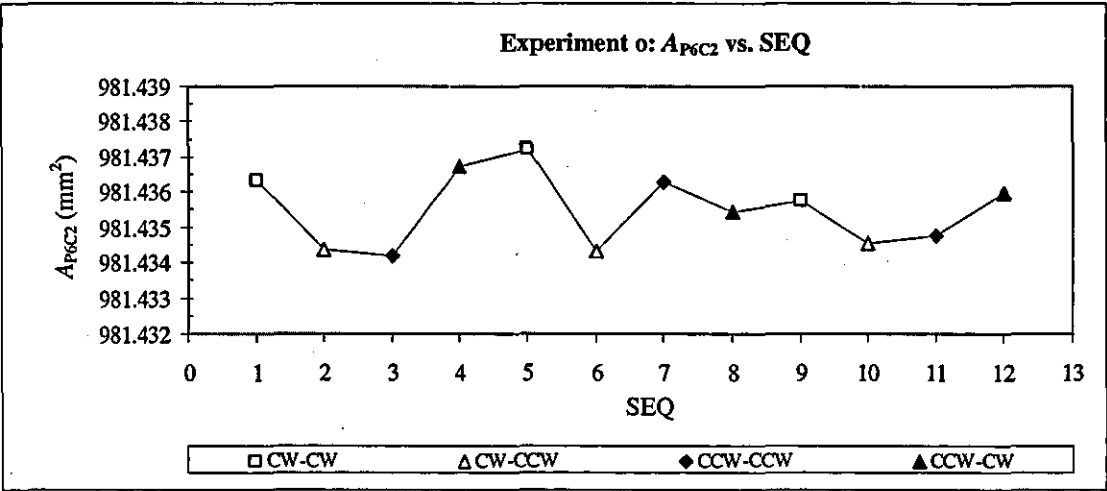


FIGURE 8.23 Experiment o: variation of $A_{P_6C_2}$ with the SEQ

8.3.3.14 Experiment p: P_7C_4 vs. P_4C_2

The overall results obtained from this experiment are tabulated in Table 8.23, and graphically represented in Figure 8.24.

TABLE 8.23 Experiment p: A_{P7C4} tabulated in accordance to its cycles and measurement sequences

CYL	SEQ	Effective Area of P_7C_4 at 100kPa, 20°C		Rotational Combination (RC)			
		A_{P7C4}		Reference PCA (P_4C_2)		Test PCA (P_7C_4)	
		(m ²)	(mm ²)	RD	RS (rpm)	RD	RS (rpm)
1	1	9.814786E-04	981.4786	CW	61	CW	51
	2	9.814771E-04	981.4771	CW	65	CCW	70
	3	9.814778E-04	981.4778	CCW	56	CCW	70
	4	9.814761E-04	981.4761	CCW	63	CW	60
2	5	9.814776E-04	981.4776	CW	76	CW	80
	6	9.814763E-04	981.4763	CW	59	CCW	59
	7	9.814764E-04	981.4764	CCW	74	CCW	67
	8	9.814766E-04	981.4766	CCW	56	CW	70
3	9	9.814768E-04	981.4768	CW	56	CW	62
	10	9.814781E-04	981.4781	CW	60	CCW	65
	11	9.814756E-04	981.4756	CCW	78	CCW	77
	12	9.814774E-04	981.4774	CCW	62	CW	83
Minimum Value		981.4756	mm ²	56	rpm	51	rpm
Maximum Value		981.4786	mm ²	78	rpm	83	rpm
Average Value ($A_{(P7C4)p}$)		981.4770	mm ²	64	rpm	68	rpm
Standard Deviation		0.0009	mm ²	8	rpm	9	rpm
Relative Standard Deviation		0.89	ppm	12	%	14	%

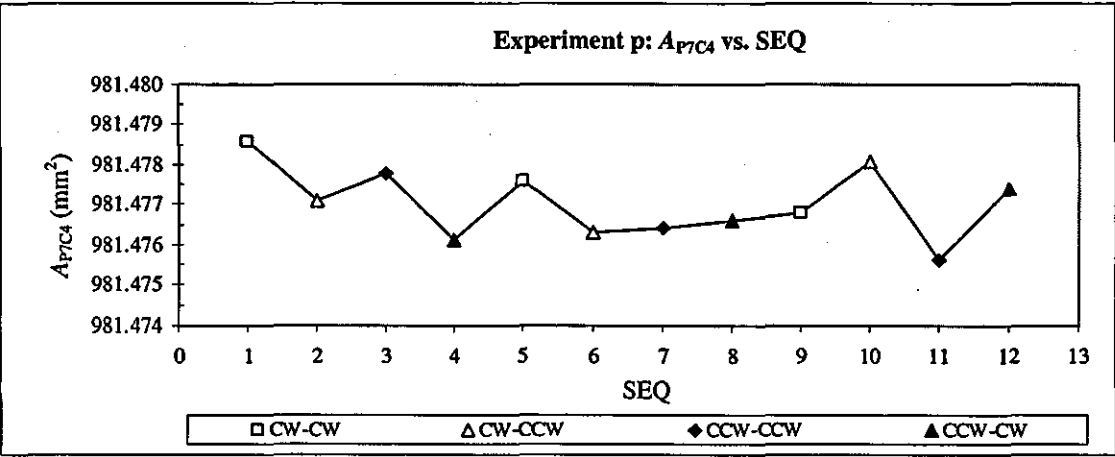


FIGURE 8.24 Experiment p: variation of A_{P7C4} with the SEQ

8.3.3.15 Experiment q: P_2C_2 vs. P_4C_4

In this experiment, the reference piston (P_2) was combined with Cylinder 2 (C_2) where this combination acted as a test PCA. The overall results obtained from this experiment are tabulated in Table 8.24, and graphically represented in Figure 8.25.

TABLE 8.24 Experiment q: $A_{P_2C_2}$ tabulated in accordance to its cycles and measurement sequences

CYL	SEQ	Effective Area of P_2C_2 at 100kPa, 20°C		Rotational Combination (RC)			
		$A_{P_2C_2}$		Reference PCA (P_4C_4)		Test PCA (P_2C_2)	
		(m ²)	(mm ²)	RD	RS (rpm)	RD	RS (rpm)
1	1	9.814794E-04	981.4794	CW	48	CW	48
	2	9.814790E-04	981.4790	CW	55	CCW	72
	3	9.814794E-04	981.4794	CCW	58	CCW	60
	4	9.814792E-04	981.4792	CCW	47	CW	63
2	5	9.814789E-04	981.4789	CW	60	CW	68
	6	9.814798E-04	981.4798	CW	48	CCW	75
	7	9.814797E-04	981.4797	CCW	74	CCW	73
	8	9.814796E-04	981.4796	CCW	48	CW	66
3	9	9.814789E-04	981.4789	CW	57	CW	56
	10	9.814798E-04	981.4798	CW	56	CCW	71
	11	9.814801E-04	981.4801	CCW	71	CCW	62
	12	9.814801E-04	981.4801	CCW	53	CW	60
Minimum Value			981.4789 mm ²	47	rpm	48	rpm
Maximum Value			981.4801 mm ²	74	rpm	75	rpm
Average Value ($A_{(P_2C_2)_q}$)			981.4795 mm ²	56	rpm	65	rpm
Standard Deviation			0.0004 mm ²	9	rpm	8	rpm
Relative Standard Deviation			0.44 ppm	16	%	12	%

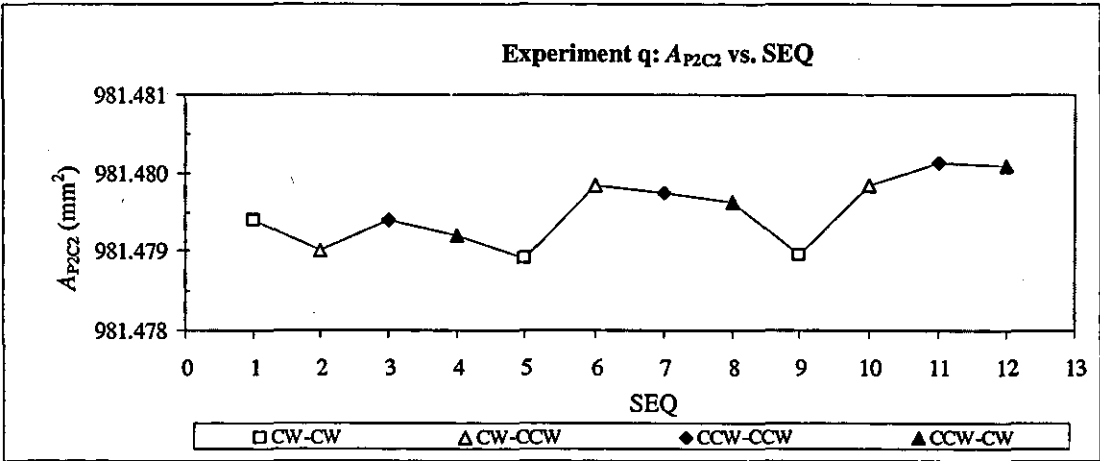


FIGURE 8.25 Experiment q: variation of $A_{P_2C_2}$ with the SEQ

8.3.3.16 Experiment r: P₃C₃ vs. P₄C₄

However, in this experiment, the reference cylinder (C₃) was combined with Piston 3 (P₃) to become a test PCA. The overall results obtained from this experiment are tabulated in Table 8.25, and graphically represented in Figure 8.26.

TABLE 8.25 Experiment r: A_{P₃C₃} tabulated in accordance to its cycles and measurement sequences

CYL	SEQ	Effective Area of P ₃ C ₃ at 100kPa, 20°C		Rotational Combination (RC)			
		A _{P₃C₃}		Reference PCA (P ₄ C ₄)		Test PCA (P ₃ C ₃)	
		(m ²)	(mm ²)	RD	RS (rpm)	RD	RS (rpm)
1	1	9.814263E-04	981.4263	CW	49	CW	59
	2	9.814269E-04	981.4269	CW	50	CCW	58
	3	9.814273E-04	981.4273	CCW	58	CCW	64
	4	9.814268E-04	981.4268	CCW	65	CW	59
2	5	9.814267E-04	981.4267	CW	57	CW	61
	6	9.814262E-04	981.4262	CW	42	CCW	57
	7	9.814268E-04	981.4268	CCW	61	CCW	60
	8	9.814267E-04	981.4267	CCW	52	CW	72
3	9	9.814259E-04	981.4259	CW	66	CW	59
	10	9.814260E-04	981.4260	CW	47	CCW	60
	11	9.814262E-04	981.4262	CCW	62	CCW	63
	12	9.814256E-04	981.4256	CCW	49	CW	65
Minimum Value			981.4261 mm ²	42	rpm	57	rpm
Maximum Value			981.4277 mm ²	66	rpm	72	rpm
Average Value (A _(P₃C₃))			981.4269 mm ²	55	rpm	61	rpm
Standard Deviation			0.0005 mm ²	8	rpm	4	rpm
Relative Standard Deviation			0.49 ppm	14	%	7	%

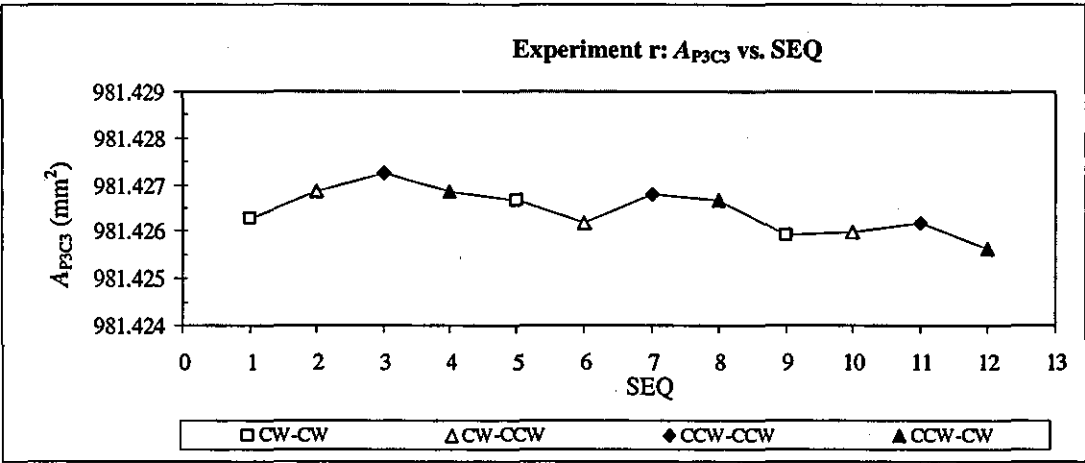


FIGURE 8.26 Experiment r: variation of A_{P₃C₃} with the SEQ

8.3.3.17 Experiment s: P_6C_2 vs. P_4C_4

The overall results obtained from this experiment are tabulated in Table 8.26, and graphically represented in Figure 8.27.

TABLE 8.26 Experiment s: $A_{P_6C_2}$ tabulated in accordance to its cycles and measurement sequences

CYL	SEQ	Effective Area of P_6C_2 at 100kPa, 20°C		Rotational Combination (RC)			
		$A_{P_6C_2}$		Reference PCA (P_4C_4)		Test PCA (P_6C_2)	
		(m ²)	(mm ²)	RD	RS (rpm)	RD	RS(rpm)
1	1	9.814353E-04	981.4353	CW	51	CW	52
	2	9.814351E-04	981.4351	CW	53	CCW	67
	3	9.814349E-04	981.4349	CCW	50	CCW	64
	4	9.814372E-04	981.4372	CCW	65	CW	66
2	5	9.814371E-04	981.4371	CW	50	CW	48
	6	9.814358E-04	981.4358	CW	55	CCW	63
	7	9.814361E-04	981.4361	CCW	58	CCW	48
	8	9.814365E-04	981.4365	CCW	72	CW	82
3	9	9.814369E-04	981.4369	CW	68	CW	68
	10	9.814364E-04	981.4364	CW	55	CCW	57
	11	9.814369E-04	981.4369	CCW	73	CCW	69
	12	9.814366E-04	981.4366	CCW	56	CW	50
Minimum Value			981.4349 mm ²	50	rpm	48	rpm
Maximum Value			981.4372 mm ²	73	rpm	82	rpm
Average Value ($A_{(P_6C_2)s}$)			981.4362 mm ²	59	rpm	61	rpm
Standard Deviation			0.0008 mm ²	8	rpm	10	rpm
Relative Standard Deviation			0.81 ppm	14	%	17	%

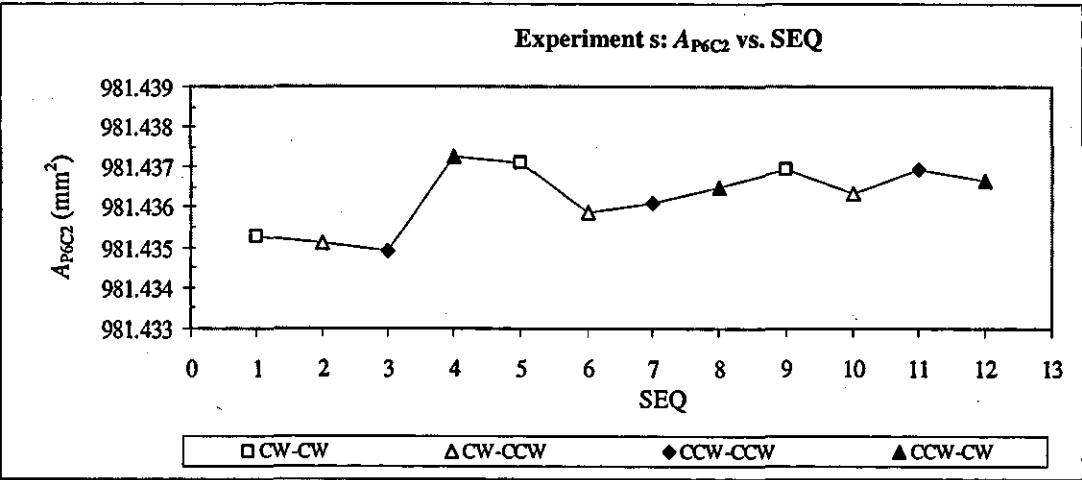


FIGURE 8.27 Experiment s: variation of $A_{P_6C_2}$ with the SEQ

8.3.3.18 Experiment t: P_7C_2 vs. P_4C_4

The overall results obtained from this experiment are tabulated in Table 8.27, and graphically represented in Figure 8.28.

TABLE 8.27 Experiment t: A_{P7C2} tabulated in accordance to its cycles and measurement sequences

CYL	SEQ	Effective Area of P_7C_2 at 100kPa, 20°C		Rotational Combination (RC)			
		A_{P7C2}		Reference PCA (P_4C_4)		Test PCA (P_7C_2)	
		(m ²)	(mm ²)	RD	RS (rpm)	RD	RS (rpm)
1	1	9.814890E-04	981.4890	CW	47	CW	34
	2	9.814888E-04	981.4888	CW	61	CCW	79
	3	9.814887E-04	981.4887	CCW	77	CCW	75
	4	9.814883E-04	981.4883	CCW	45	CW	50
2	5	9.814892E-04	981.4892	CW	61	CW	64
	6	9.814882E-04	981.4882	CW	59	CCW	60
	7	9.814892E-04	981.4892	CCW	80	CCW	78
	8	9.814888E-04	981.4888	CCW	61	CW	79
3	9	9.814898E-04	981.4898	CW	57	CW	64
	10	9.814894E-04	981.4894	CW	49	CCW	58
	11	9.814882E-04	981.4882	CCW	65	CCW	74
	12	9.814888E-04	981.4888	CCW	73	CW	56
Minimum Value			981.4882 mm ²	45	rpm	34	rpm
Maximum Value			981.4898 mm ²	80	rpm	79	rpm
Average Value ($A_{t(P7C2)}$)			981.4889 mm ²	61	rpm	64	rpm
Standard Deviation			0.0005 mm ²	11	rpm	14	rpm
Relative Standard Deviation			0.49 ppm	18	%	21	%

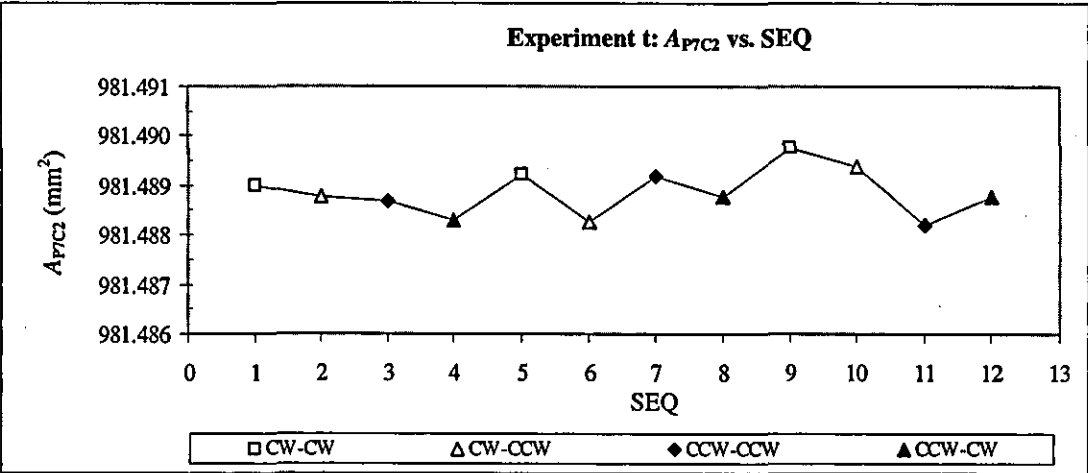


FIGURE 8.28 Experiment t: variation of A_{P7C2} with the SEQ

8.3.3.19 Experiment u: P_7C_4 vs. P_6C_2

The overall results obtained from this experiment are tabulated in Table 8.28, and graphically represented in Figure 8.29.

TABLE 8.28 Experiment u: A_{P7C4} tabulated in accordance to its cycles and measurement sequences

CYL	SEQ	Effective Area of P_7C_4 at 100kPa, 20°C		Rotational Combination (RC)			
		A_{P7C4}		Reference PCA (P_6C_2)		Test PCA (P_7C_4)	
		(m ²)	(mm ²)	RD	RS (rpm)	RD	RS (rpm)
1	1	9.814762E-04	981.4762	CW	72	CW	71
	2	9.814752E-04	981.4752	CW	68	CCW	75
	3	9.814758E-04	981.4758	CCW	75	CCW	78
	4	9.814763E-04	981.4763	CCW	61	CW	65
2	5	9.814768E-04	981.4768	CW	51	CW	62
	6	9.814759E-04	981.4759	CW	67	CCW	79
	7	9.814761E-04	981.4761	CCW	76	CCW	80
	8	9.814765E-04	981.4765	CCW	67	CW	78
3	9	9.814776E-04	981.4776	CW	62	CW	75
	10	9.814772E-04	981.4772	CW	69	CCW	68
	11	9.814778E-04	981.4778	CCW	72	CCW	79
	12	9.814759E-04	981.4759	CCW	83	CW	69
Minimum Value		981.4752	mm ²	51	rpm	62	rpm
Maximum Value		981.4778	mm ²	83	rpm	80	rpm
Average Value ($A_{(P7C4)u}$)		981.4764	mm ²	69	rpm	73	rpm
Standard Deviation		0.0008	mm ²	8	rpm	6	rpm
Relative Standard Deviation		0.79	ppm	12	%	8	%

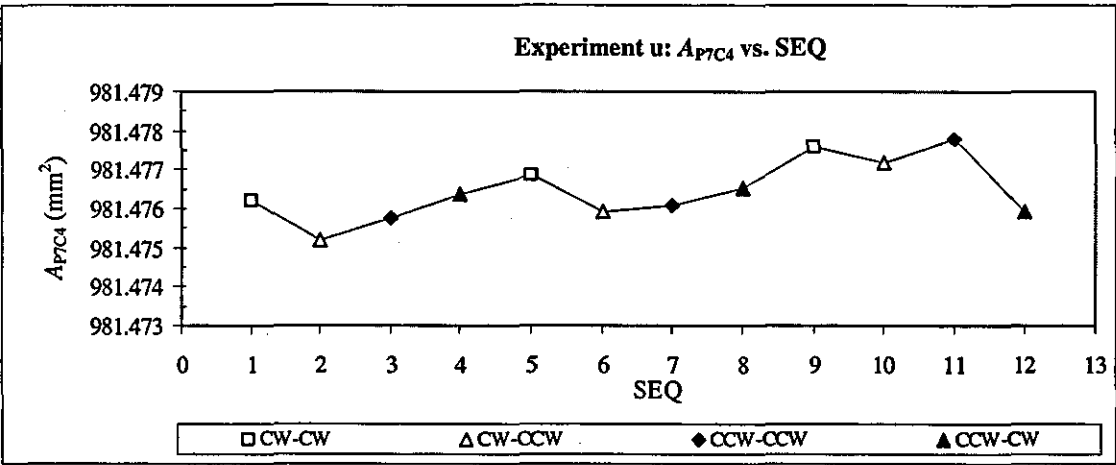


FIGURE 8.29 Experiment u: variation of A_{P7C4} with the SEQ

8.3.3.20 Experiment v: P_6C_4 vs. P_7C_2

The overall results obtained from this experiment are tabulated in Table 8.29, and graphically represented in Figure 8.30.

TABLE 8.29 Experiment v: $A_{P_6C_4}$ tabulated in accordance to its cycles and measurement sequences

CYL	SEQ	Effective Area of P_6C_4 at 100kPa, 20°C		Rotational Combination (RC)			
		$A_{P_6C_4}$		Reference PCA (P_7C_2)		Test PCA (P_6C_4)	
		(m ²)	(mm ²)	RD	RS (rpm)	RD	RS(rpm)
1	1	9.814230E-04	981.4230	CW	63	CW	61
	2	9.814237E-04	981.4237	CW	73	CCW	75
	3	9.814242E-04	981.4242	CCW	74	CCW	70
	4	9.814237E-04	981.4237	CCW	41	CW	61
2	5	9.814237E-04	981.4237	CW	63	CW	65
	6	9.814214E-04	981.4214	CW	68	CCW	85
	7	9.814220E-04	981.4220	CCW	55	CCW	86
	8	9.814217E-04	981.4217	CCW	76	CW	71
3	9	9.814215E-04	981.4215	CW	77	CW	71
	10	9.814224E-04	981.4224	CW	75	CCW	79
	11	9.814227E-04	981.4227	CCW	57	CCW	70
	12	9.814226E-04	981.4226	CCW	81	CW	72
Minimum Value			981.4214 mm ²	41	rpm	61	rpm
Maximum Value			981.4242 mm ²	81	rpm	86	rpm
Average Value ($A_{(P_6C_4)_v}$)			981.4227 mm ²	67	rpm	72	rpm
Standard Deviation			0.0009 mm ²	12	rpm	8	rpm
Relative Standard Deviation			0.95 ppm	17	%	11	%

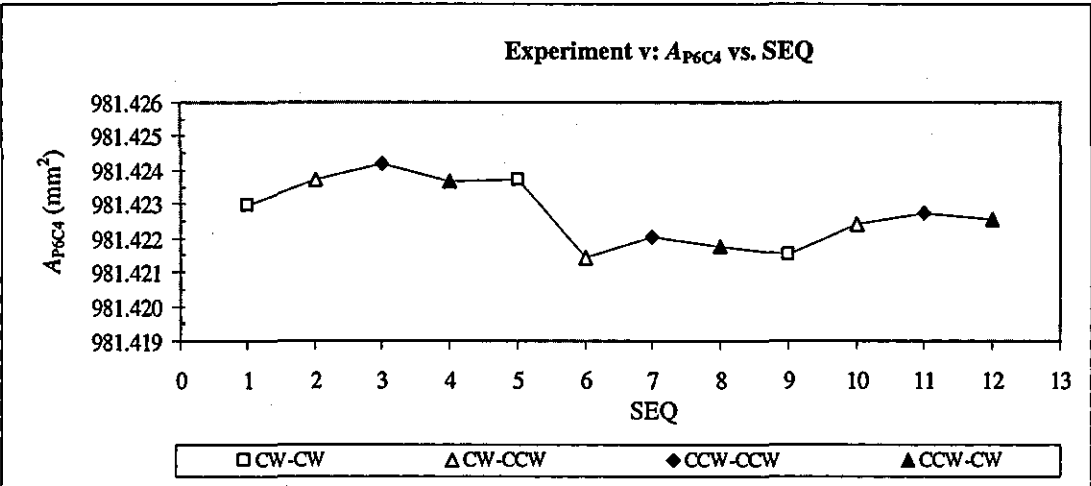


FIGURE 8.30 Experiment v: variation of $A_{P_6C_4}$ with the SEQ

8.3.3.21 Experiment w: P_2C_2 vs. P_7C_4

Once again, the combination of the P_2C_2 acted as a test PCA where the combination of P_7C_4 became a reference. The overall results obtained from this experiment are tabulated in Table 8.30, and graphically represented in Figure 8.31.

TABLE 8.30 Experiment w: $A_{P_2C_2}$ tabulated in accordance to its cycles and measurement sequences

CYL.	SEQ	Effective Area of P_2C_2 at 100kPa, 20°C		Rotational Combination (RC)			
		$A_{P_2C_2}$		Reference PCA (P_7C_4)		Test PCA (P_2C_2)	
		(m ²)	(mm ²)	RD	RS (rpm)	RD	RS (rpm)
1	1	9.814791E-04	981.4791	CW	52	CW	61
	2	9.814785E-04	981.4785	CW	53	CCW	58
	3	9.814791E-04	981.4791	CCW	56	CCW	55
	4	9.814798E-04	981.4798	CCW	55	CW	67
2	5	9.814791E-04	981.4791	CW	56	CW	53
	6	9.814789E-04	981.4789	CW	57	CCW	58
	7	9.814786E-04	981.4786	CCW	40	CCW	49
	8	9.814793E-04	981.4793	CCW	67	CW	72
3	9	9.814788E-04	981.4788	CW	58	CW	60
	10	9.814781E-04	981.4781	CW	55	CCW	75
	11	9.814791E-04	981.4791	CCW	51	CCW	65
	12	9.814786E-04	981.4786	CCW	59	CW	57
Minimum Value		981.4781	mm ²	40	rpm	49	rpm
Maximum Value		981.4798	mm ²	67	rpm	75	rpm
Average Value ($A_{(P_2C_2)w}$)		981.4789	mm ²	55	rpm	61	rpm
Standard Deviation		0.0004	mm ²	6	rpm	8	rpm
Relative Standard Deviation		0.44	ppm	11	%	13	%

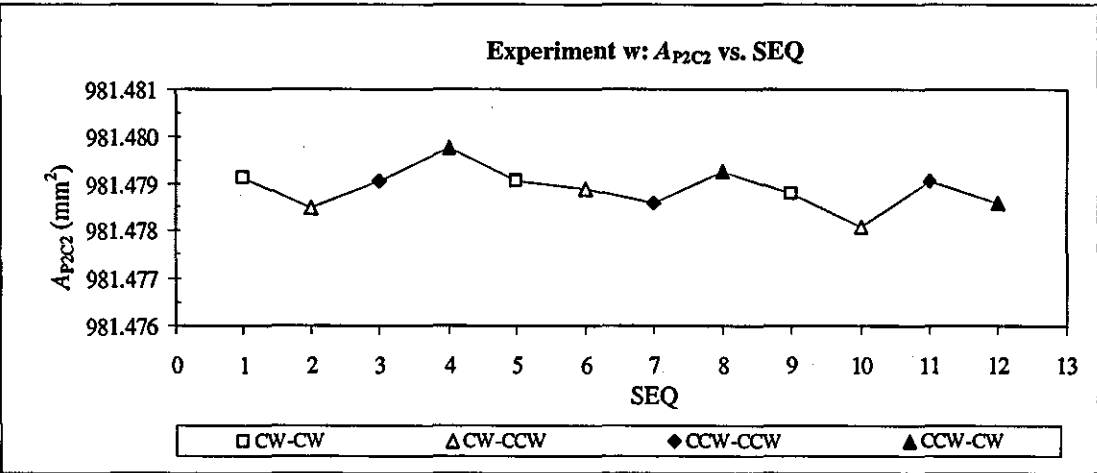


FIGURE 8.31 Experiment w: variation of $A_{P_2C_2}$ with the SEQ

8.3.3.22 Experiment x: P_3C_3 vs. P_2C_2

In this experiment, the reference piston (P_2) and the reference cylinder (C_2) formed two separate combinations were cross-floated. The overall results obtained from this experiment are tabulated in Table 8.31, and graphically represented in Figure 8.32.

TABLE 8.31 Experiment x: $A_{P_3C_3}$ tabulated in accordance to its cycles and measurement sequences

CYL	SEQ	Effective Area of P_3C_3 at 100kPa, 20°C		Rotational Combination (RC)			
		$A_{P_3C_3}$		Reference PCA (P_2C_2)		Test PCA (P_3C_3)	
		(m ²)	(mm ²)	RD	RS (rpm)	RD	RS (rpm)
1	1	9.814252E-04	981.4252	CW	62	CW	64
	2	9.814249E-04	981.4249	CW	60	CCW	70
	3	9.814247E-04	981.4247	CCW	65	CCW	69
	4	9.814246E-04	981.4246	CCW	50	CW	72
2	5	9.814244E-04	981.4244	CW	45	CW	70
	6	9.814252E-04	981.4252	CW	61	CCW	64
	7	9.814248E-04	981.4248	CCW	61	CCW	70
	8	9.814258E-04	981.4258	CCW	59	CW	56
3	9	9.814259E-04	981.4259	CW	65	CW	67
	10	9.814262E-04	981.4262	CW	56	CCW	60
	11	9.814256E-04	981.4256	CCW	71	CCW	56
	12	9.814255E-04	981.4255	CCW	60	CW	67
Minimum Value		981.4244	mm ²	45	rpm	56	rpm
Maximum Value		981.4262	mm ²	71	rpm	72	rpm
Average Value ($A_{(P_3C_3)_x}$)		981.4252	mm ²	60	rpm	65	rpm
Standard Deviation		0.0006	mm ²	7	rpm	6	rpm
Relative Standard Deviation		0.58	ppm	12	%	8	%

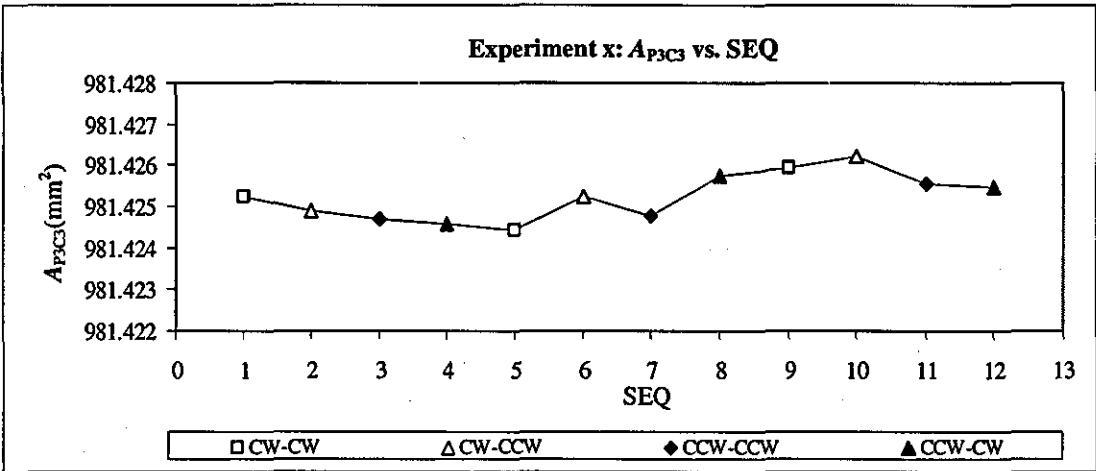


FIGURE 8.32 Experiment x: variation of $A_{P_3C_3}$ with the SEQ

A summary of the results obtained from the completed experiments is shown in Table 8.32, followed with Figures 8.33 and 8.34 showing the trend lines of the determined effective areas (first three cycles) through direct and indirect comparisons respectively.

TABLE 8.32 Summary of the results of the determined effective areas

Experiment	Average Effective Area		Standard Deviation	
	Symbol	Value (mm ²)	(mm ²)	(ppm)
A: (P ₁ C ₂ vs. P ₂ C ₃)	A _{i(P1C2)} A	981.4175	0.0004	0.37
B: (P ₁ C ₄ vs. P ₂ C ₃)	A _{i(P1C4)} B	981.4095	0.0005	0.47
C: (P ₃ C ₂ vs. P ₂ C ₃)	A _{i(P3C2)} C	981.4457	0.0005	0.52
D: (P ₃ C ₄ vs. P ₂ C ₃)	A _{i(P3C4)} D	981.4309	0.0006	0.62
E: (P ₄ C ₂ vs. P ₂ C ₃) *	A _{i(P4C2)} E	981.4934	0.0007	0.75
F: (P ₄ C ₄ vs. P ₂ C ₃) *	A _{i(P4C4)} F	981.4840	0.0009	0.87
G: (P ₅ C ₂ vs. P ₂ C ₃)	A _{i(P5C2)} G	981.4762	0.0007	0.72
H: (P ₅ C ₄ vs. P ₂ C ₃)	A _{i(P5C4)} H	981.4661	0.0006	0.59
I: (P ₆ C ₂ vs. P ₂ C ₃)	A _{i(P6C2)} I	981.4344	0.0006	0.58
J: (P ₆ C ₄ vs. P ₂ C ₃)	A _{i(P6C4)} J	981.4244	0.0004	0.36
K: (P ₇ C ₂ vs. P ₂ C ₃)	A _{i(P7C2)} K	981.4899	0.0010	1.00
L: (P ₇ C ₄ vs. P ₂ C ₃)	A _{i(P7C4)} L	981.4783	0.0006	0.62
m: (P ₇ C ₄ vs. P ₃ C ₂)	A _{i(P7C4)} m	981.4807	0.0007	0.75
n: (P ₇ C ₂ vs. P ₃ C ₄)	A _{i(P7C2)} n	981.4903	0.0009	0.87
o: (P ₆ C ₂ vs. P ₃ C ₄)	A _{i(P6C2)} o	981.4355	0.0010	1.06
p: (P ₇ C ₄ vs. P ₄ C ₂)	A _{i(P7C4)} p	981.4770	0.0009	0.89
q: (P ₂ C ₂ vs. P ₄ C ₄)	A _{i(P2C2)} q	981.4795	0.0004	0.44
r: (P ₃ C ₃ vs. P ₄ C ₄)	A _{i(P3C3)} r	981.4269	0.0005	0.49
s: (P ₆ C ₂ vs. P ₄ C ₄)	A _{i(P6C2)} s	981.4362	0.0008	0.81
t: (P ₇ C ₂ vs. P ₄ C ₄)	A _{i(P7C2)} t	981.4889	0.0005	0.49
u: (P ₇ C ₄ vs. P ₆ C ₂)	A _{i(P7C4)} u	981.4764	0.0008	0.79
v: (P ₆ C ₄ vs. P ₇ C ₂)	A _{i(P6C4)} v	981.4227	0.0009	0.95
w: (P ₂ C ₂ vs. P ₇ C ₄)	A _{i(P2C2)} w	981.4789	0.0004	0.44
x: (P ₃ C ₃ vs. P ₂ C ₂)	A _{i(P3C3)} x	981.4252	0.0006	0.58

Note: * Experiments completed and reported in Chapter 7

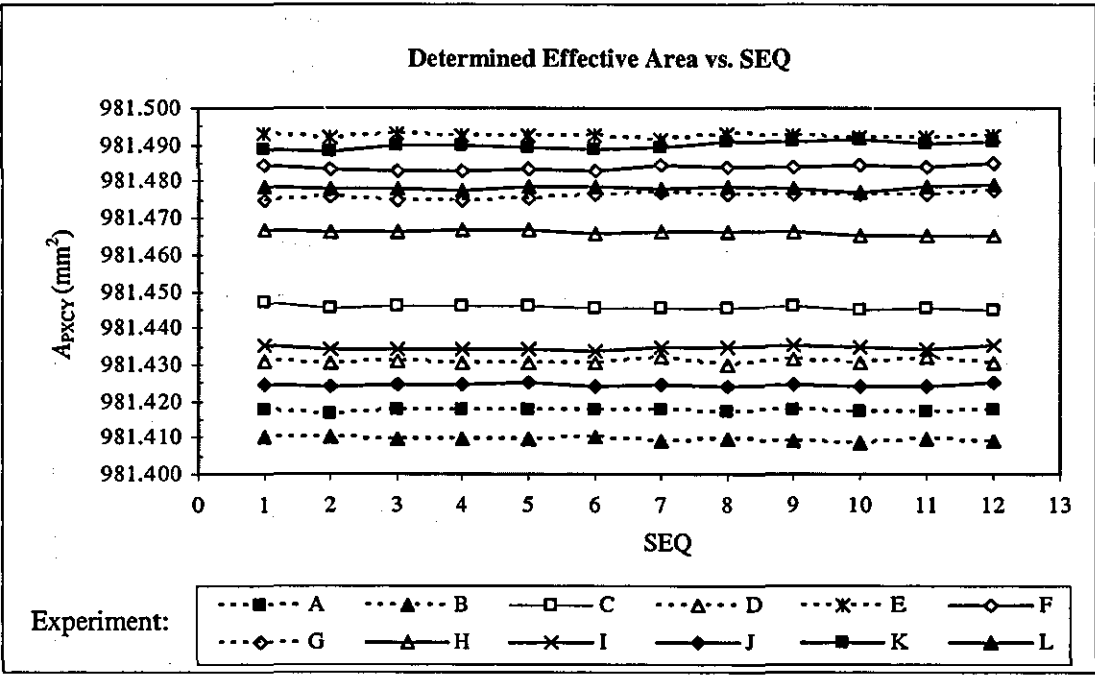


FIGURE 8.33 Trend lines of all the determined effective area through direct comparisons

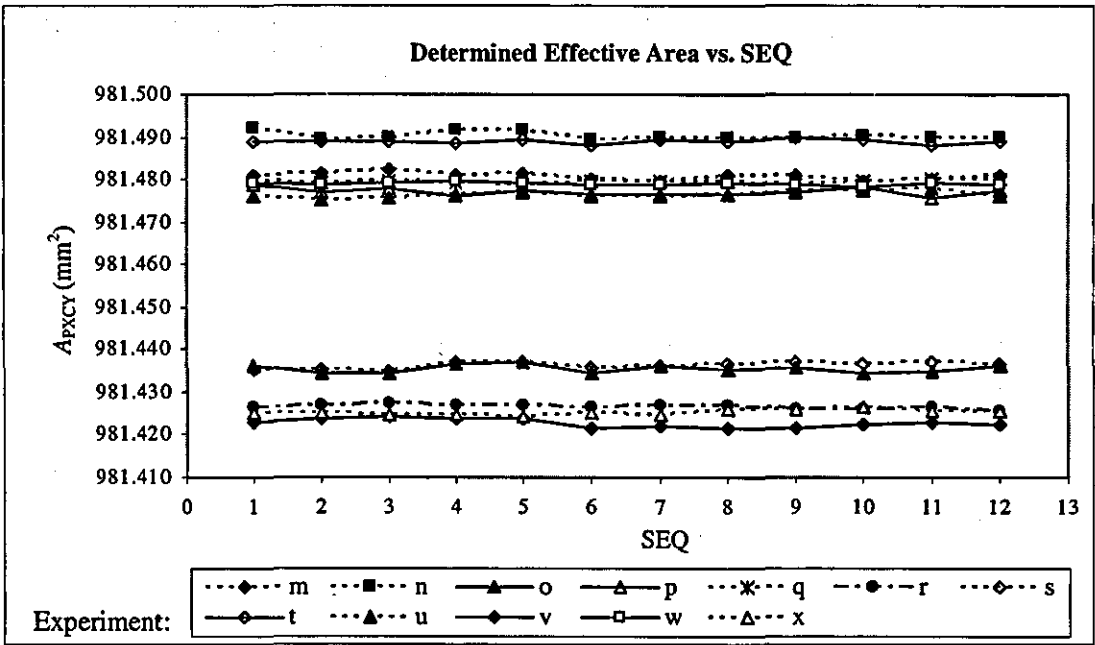


FIGURE 8.34 Trend lines of all the determined effective area through indirect comparisons

8.4 COMPARISON OF EFFECTIVE AREA DETERMINATIONS THROUGH DIFFERENT ROUTES

Experiment A to x have demonstrated that the pressures generated for the specific PCA combinations appear to be independent of the surface texture applied onto the pistons, even with different RCs. As shown in Figures 8.11 to 8.32, the effective areas determined varied randomly, where their standard deviations were within 1 ppm for any RCs applied. The effects of the surface texture may be too small with respect to the instrument repeatability and error budget, thus no significant differences in effective area determinations could be seen. However, it is noticeable that Piston 1 (the smoothest piston) produces the smallest effective area, whilst all of the rougher pistons produce larger effective area values. There again, variations of piston diameter may account for the distribution of the data.

However, any small effects that are accumulated could be significant if they keep adding together in a series of processes. For that reason, the determined effective areas based on different routes of calibration have been investigated. The effective areas of six PCA combinations, i.e. P_2C_2 , P_3C_3 , P_6C_2 , P_6C_4 , P_7C_2 and P_7C_4 which are denoted by $A_{i(P_2C_2)}$, $A_{i(P_3C_3)}$, $A_{i(P_6C_2)}$, $A_{i(P_6C_4)}$, $A_{i(P_7C_2)}$ and $A_{i(P_7C_4)}$ (see Figure 8.1) were investigated. Each of the effective area determinations are described, and compared separately in the next sections.

8.4.1 Effective Area of the P_2C_2 ($A_{i(P_2C_2)}$)

Five routes were available for this combination as tabulated in Table 8.33, where the $A_{i(P_2C_2)}^{Fq}$ value (which is the shortest route) has been used as a reference.

TABLE 8.33 Comparison of $A_{i(P_2C_2)}$ values, determined from different calibration routes

Symbol	Symbol ^{Route}	Calibration Route	Effective Area (mm ²)	Difference	
				(mm ²)	(ppm)
$A_{i(P_2C_2)}$	$A_{i(P_2C_2)}^{Fq}$	F-q	981.4795	Used as a reference	
	$A_{i(P_2C_2)}^{Lw}$	L-w	981.4789	-0.0006	-0.6
	$A_{i(P_2C_2)}^{Cmw}$	C-m-w	981.4813	0.0018	1.9
	$A_{i(P_2C_2)}^{Epw}$	E-p-w	981.4777	-0.0018	-1.9
	$A_{i(P_2C_2)}^{luw}$	I-u-w	981.4771	-0.0024	-2.5

8.4.2 Effective Area of the P_3C_3 ($A_{t(P3C3)}$)

Five possible routes were identified for this combination, where the $A_{t(P3C3)}^{Fr}$ value has been used as a reference. Comparison of the effective areas obtained from the various routes are tabulated in Table 8.34

TABLE 8.34 Comparison of $A_{t(P3C3)}$ values, determined from different calibration routes

Symbol	Symbol ^{Route}	Calibration Route	Effective Area (mm ²)	Difference	
				(mm ²)	(ppm)
$A_{t(P3C3)}$	$A_{t(P3C3)}^{Fr}$	F-r	981.4264	Used as a reference	
	$A_{t(P3C3)}^{Cmwx}$	C-m-w-x	981.4271	0.0006	0.6
	$A_{t(P3C3)}^{Epwx}$	E-p-w-x	981.4234	-0.0030	-3.1
	$A_{t(P3C3)}^{Fqx}$	F-q-x	981.4252	-0.0012	-1.2
	$A_{t(P3C3)}^{Lwx}$	L-w-x	981.4246	-0.0018	-1.9

8.4.3 Effective Area of the P_6C_2 ($A_{t(P6C2)}$)

Three possible routes were available for this combination, where the $A_{t(P6C2)}^I$ value has been used as a reference. Comparisons of the effective areas obtained from the various routes are tabulated in Table 8.35.

TABLE 8.35 Comparison of $A_{t(P6C2)}$ values, determined from different calibration routes

Symbol	Symbol ^{Route}	Calibration Route	Effective Area (mm ²)	Difference	
				(mm ²)	(ppm)
$A_{t(P6C2)}$	$A_{t(P6C2)}^I$	I	981.4344	Used as a reference	
	$A_{t(P6C2)}^{Do}$	D-o	981.4355	0.0011	1.1
	$A_{t(P6C2)}^{Fs}$	F-s	981.4362	0.0018	1.9

8.4.4 Effective Area of the P_6C_4 ($A_{t(P6C4)}$)

Four possible routes were available for this combination, where the $A_{t(P6C4)}^J$ value has been used as a reference. Comparisons of the effective areas obtained from the various routes are tabulated in Table 8.36.

TABLE 8.36 Comparison of $A_{t(P6C4)}$ values, determined from different calibration routes

Symbol	Symbol ^{Route}	Calibration Route	Effective Area (mm ²)	Difference	
				(mm ²)	(ppm)
$A_{t(P6C4)}$	$A_{t(P6C4)}^J$	J	981.4244	Used as a reference	
	$A_{t(P6C4)}^{Kv}$	K-v	981.4227	-0.0017	-1.8
	$A_{t(P6C4)}^{Dnv}$	D-n-v	981.4232	-0.0013	-1.3
	$A_{t(P6C4)}^{Ftv}$	F-t-v	981.4217	-0.0027	-2.8

8.4.5 Effective Area of the P_7C_2 ($A_{t(P7C2)}$)

There were three possible routes available for this combination, where the $A_{t(P7C2)}^K$ value has been used as a reference. Results of comparisons of the effective areas are tabulated in Table 8.37.

TABLE 8.37 Comparison of $A_{t(P7C2)}$ values, determined from different calibration routes

Symbol	Symbol ^{Route}	Calibration Route	Effective Area (mm ²)	Difference	
				(mm ²)	(ppm)
$A_{t(P7C2)}$	$A_{t(P7C2)}^K$	K	981.4899	Used as a reference	
	$A_{t(P7C2)}^{Ft}$	F-t	981.4889	-0.0010	-1.0
	$A_{t(P7C2)}^{Dn}$	D-n	981.4903	0.0004	0.4

8.4.6 Effective Area of the P_7C_4 ($A_{t(P7C4)}$)

Four possible routes were available for this combination, where the $A_{t(P7C4)}^L$ value has been used as a reference. Comparisons of the effective areas obtained from the various routes are tabulated in Table 8.38.

TABLE 8.38 Comparison of $A_{t(P7C4)}$ values, determined from different calibration routes

Symbol	Symbol ^{Route}	Calibration Route	Effective Area (mm ²)	Difference	
				(mm ²)	(ppm)
$A_{t(P7C4)}$	$A_{t(P7C4)}^L$	L	981.4782	Used as a reference	
	$A_{t(P7C4)}^{Cm}$	C-m	981.4807	0.0024	2.5
	$A_{t(P7C4)}^{Ep}$	E-p	981.4770	-0.0012	-1.2
	$A_{t(P7C4)}^{Ju}$	I-u	981.4764	-0.0018	-1.8

8.5 SUMMARY AND DISCUSSION

The overall goal of the experiments in this chapter was to investigate the effect of surface texture (applied onto pistons) to the pressure generated. The demands of this novel approach were rationalised with the fact that there will always be some inseparable form of texture associated as a function of the methods that are employed to generate polished surfaces. This rationale is supported by the surface metrology and tribological studies which revealed that any surface consists of a profile, waviness and roughness; and the performance of the work piece depends on the surface texture of the rubbing surfaces.

Twenty four experiments (including two experiments in Chapter 7) have been carried out using six test pistons which were matched with two identical test cylinders at 100 kPa. Measurements were carried out based on four types of RCs per cycle i.e. CW-CW, CW-CCW, CCW-CW and CCW-CCW. Direct comparisons against the reference P_2C_3 are denoted by Experiments A to L, and the indirect comparisons are denoted by Experiments m to x.

Prior to the cross-floating experiment, all the pistons involved were measured with a non destructive 3-Dimensional optical surface profiler instrument (Zygo New View 5000). The pistons were measured at five levels (i.e. 5, 15, 30, 45, 55 mm from the piston's base), with two areas per level. Three types of surface parameters were considered, i.e. R_t , R_q and R_a . Each captured data set has been processed using the MetroPro software, where three sets of data were produced at each scanned area. Therefore, the average values of the pistons were based on thirty sets of readings. Analysis of the piston surfaces revealed that the roughest piston was Piston 6, followed by Pistons 5, 7, 3, 4, 1 and 2.

From the cross-floating experiments, the results obtained in each experiment were plotted against their respective SEQ. The effective areas that have been produced by each RC were marked distinctly, so that the "effective area-RC" mode can clearly be observed graphically. However, all the graphs plotted have still demonstrated that the

effective area (hence pressures generated) for the specific PCA combinations appear to be independent of the surface textures applied onto pistons. The maximum standard deviation of the effective areas determined, with regards to the RCs was 1.06 ppm which occurred in the Experiment o, i.e. cross-floating experiment between P_6C_2 against P_3C_4 (see Table 8.32).

Analysis of the combined data in Figure 8.33 does support the tentative conclusion that Piston 1 (the smoothest) consistently produces the smallest effective area value, whilst all other pistons (rougher) produce larger value of the effective area.

The averaged effective areas calculated for six test PCAs (through any possible route available) have been conducted. The effective areas involved in these investigations were $A_{t(P_2C_2)}$, $A_{t(P_3C_3)}$, $A_{t(P_6C_2)}$, $A_{t(P_6C_4)}$, $A_{t(P_7C_2)}$ and $A_{t(P_7C_4)}$. The maximum difference in the $A_{t(P_2C_2)}$, $A_{t(P_3C_3)}$, $A_{t(P_6C_2)}$, $A_{t(P_6C_4)}$, $A_{t(P_7C_2)}$ and $A_{t(P_7C_4)}$ values were 2.5, 3.1, 1.9, 2.8, 1.0 and 2.5 ppm respectively, whilst the minimum differences were 0.6, 0.6, 1.1, 1.3, 0.4 and 1.2 ppm respectively. All the differences obtained were well within 3.5 ppm, which is the typical value of the relative expanded uncertainty in each cross-floating experiment carried out in this research work (as shown in Chapter 7). This has re-confirmed that the extent of the surface texture applied on the pistons has no observable effect on the pressure generated, for the specific PCAs manufactured and tested.

In order to gain a higher level of confidence on the above findings, the reference PCA (P_2C_3) and other sets of combinations have been compared against a higher level of accuracy pressure standard, which can provide traceability to the true pressure values, and simultaneously verify the calibration system within the calibration chain. Selected PCAs have been cross-floated against the UK Primary Pressure Standard, which is kept at the NPL. Verification work carried out at the NPL is described in the Chapter 9.

It is to a certain extent disappointing that a clear trend between surface texture and pressure (effective area) has not been identified at this point in time. There are few reasons why this may be so at this stage:

- The research is time and resource limited, only allowing seven pistons to be manufactured with bespoke, but random surface texture. Many more types of surface texture could be explored, and surface texture could be applied in a more controlled manner, whilst maintaining the geometric integrity of the pistons.
- Variations of effective area as a function of surface texture may fall within the uncertainty budget (noise floor) of the instrument. Hence it may not be possible to identify discrete behaviour as a function of surface texture at this point in time.
- The surface texture of the seven pistons is not of the correct type, or extensive enough to cause a measurable change of effective area or performance.
- Small variations of piston diameter, hence clearance, are causing larger changes of effective area than the surface texture contribution.

However, this novel work has successfully demonstrated all of the methodology required to extend the structure of the piston surfaces, roughness using bespoke manufacturing techniques such as laser ablation. Furthermore, it has for the first time characterised and documented the link between manufacturing of the PCAs, surface characteristics and pressure measurements.

CHAPTER 9

CALIBRATION/VERIFICATION AGAINST THE UK's NATIONAL PRIMARY PRESSURE STANDARD

Experiments carried out in Chapters 7 and 8 have identified that the extent of surface textures applied onto the piston did not significantly affect the pressure generated using the 35 mm diameter PCA, applicable to any RD and RS ranging from 30 to 90 rpm (approximately 0.5 to 1.5 Hz). However the pressure measuring systems used in these investigations were new products, with all components involved being newly designed and manufactured at LU. There was no traceability or calibration history available for all the PCAs used, and also no externally verifiable track record on the performance of the pressure balance used.

Therefore, one of the pressure balances in the system (which was consistently used as the test pressure balance in all twenty four experiments) with associated pistons and cylinders was taken to the NPL for calibration/verification purposes. This was done after the completion of all the cross-floating experiments at LU. Four combinations of PCAs were compared against the UK's Primary Pressure Standard.

This chapter is organised as follows: Section 9.1 describes the rationale behind this exercise, followed by Section 9.2 that explains the calibration/verification approach. Section 9.3 discusses the plan made for this exercise to suit the existing calibration chain. Sections 9.4 and 9.5 reveal the results obtained from the calibration work and verification processes respectively. Comparisons on the thermal stabilities of the pressure balances involved are described in Section 9.6. Finally, Section 9.7 summarises this chapter and concludes the outcome from this exercise.

9.1 RATIONALE

In order to prove that the experimental findings are trustworthy and reliable, third party verification against a superior standard is a necessity. The purpose of this calibration/verification work was to obtain a traceable pressure instrument, and establish the requirements for verifying the performance of effective area determinations at LU. Since the work carried out in this research is in the top position in the hierarchical order of pressure measurement, only verification against a pressure standard which is kept at an NMI would be valid. Therefore, verification against the UK's National Primary Standard was the only solution. The UK's Primary Pressure Standard is kept at the NPL, which is a world leading NMI in pressure metrology. The degree of agreement between the results obtained (at the NPL and LU) would indicate the validity and reliability of all the results obtained at LU, and provide confidence in the findings revealed in Chapters 7 and 8.

9.2 CALIBRATION/VERIFICATION APPROACH

In order to make the calibration work (for traceability reasons) simultaneously become a verification process, a proper approach was used. It consisted of three primary phases as described below:

- Planning – Identification of suitable PCA combinations (the reference PCA and a few additional PCA combinations) to be cross-floated against the NPL's standard within a five day period. The results obtained for the additional PCA combinations could be used as "check standards" within the designed calibration chain, hence automatically verifying the results obtained.
- Calibration – This phase involved cross-floating work against the Primary Pressure Standard where the determined effective areas were the prime concern, besides other relevant data to be noted. This was important, especially in assessing the performance of the PCAs and the pressure balance itself.
- Verification – This phase included adjustment work on all of the effective areas previously calculated, which were derived from the estimated value of $A_{r(P2C3)}$.

Comparisons of the adjusted values against the values determined by the NPL were the means of the verification. This work would not only verify the determined effective areas, but also verify the pressure measuring system as a whole.

9.3 CALIBRATION PLANS

Due to time constraints, only four PCA combinations were chosen for the calibration work against the Primary Pressure Standard. The combinations that were selected were P_2C_3 , P_3C_4 , P_4C_2 and P_4C_4 . The new traceability chain showing the linkage of the Primary Pressure Standard, (designated as PCA-602) is shown in Figure 9.1. The calibration between P_2C_3 against the PCA-602 is known as "Calibration Y1" which makes it traceable through the "Route Y1". P_3C_4 , P_4C_2 and P_4C_4 are traceable to the Primary Pressure Standard through the "Routes Y2, Y3 and Y4" respectively.

9.4 CALIBRATIONS AND THEIR RESULTS

Calibrations were carried out by the NPL staff in accordance to the NPL's procedure, so called the "Traditional Cross-floating Method" [Simpson 1994]. At each point, the effective area was determined in falling and rising modes, with the test PCA being rotated in the CW and CCW directions for each mode, but not the reference. The evaluation of the effective areas of the test from these cross-floating comparisons were calculated based on the ratio of the effective area between the two PCAs involved, known as R_p [Lewis and Peggs 1992]. Therefore, the R_p of the effective areas represents the ratio of the equilibrium loads which have been corrected for fluid heads and the temperature variations in both PCAs.

9.4.1 Initial Calibrations

Two initial calibrations were performed using the Ruska 2465 gas-operated pressure balance as a reference. It uses a tungsten carbide PCA of 84 mm^2 nominal effective area, designated as C-70, which is normally used as one of the working standards at NPL. Calibrations were performed at six points i.e. 50, 75, 100, 200, 300 and 400 kPa.

Unsatisfactory results obtained in the first and the second initial calibrations are shown in Figures 9.2 and 9.3 respectively, where the determined effective areas are represented in terms of the ratio between the test and the reference PCAs.

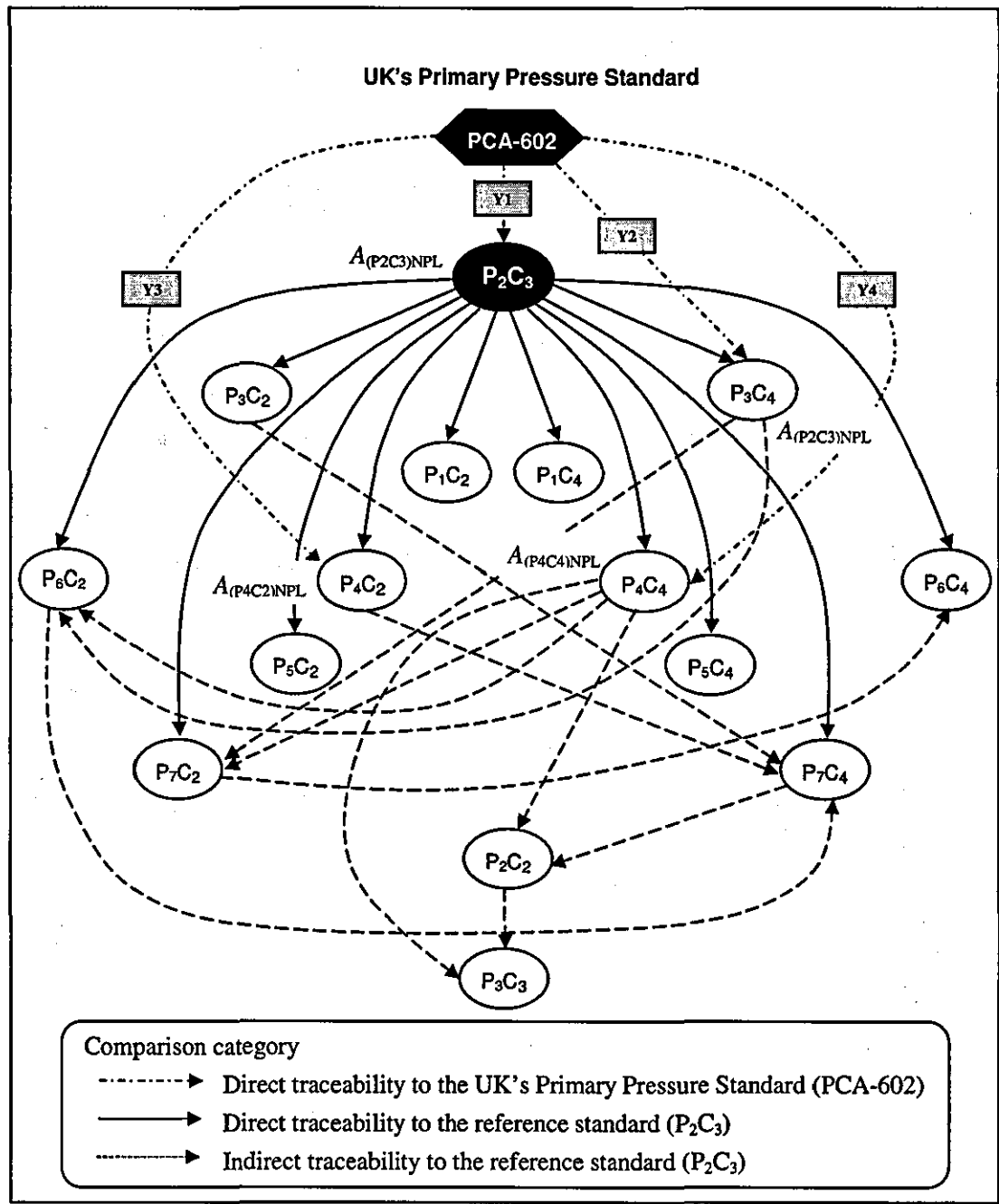


FIGURE 9.1 A complete unbroken calibration chain, with the source of traceability from the NPL. P₃C₄, P₄C₂ and P₄C₄ act as the check standards in the verification process

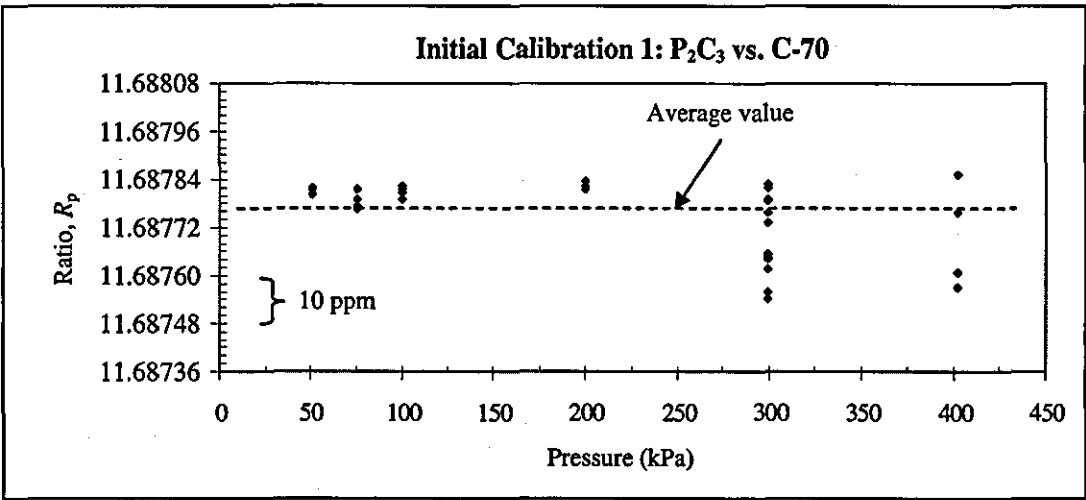


FIGURE 9.2 The first initial calibration results, which shows unsatisfactory repeatability at 300 and 400 kPa

Initial calibration resumed for the second series, but the calibration point at 75 kPa was omitted (due to time constraints). The results obtained are graphically depicted in Figure 9.3.

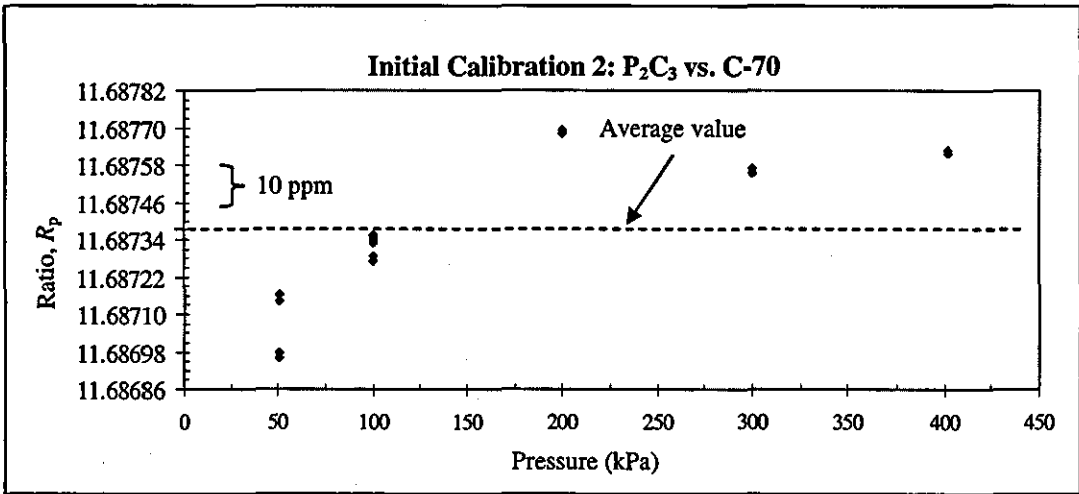


FIGURE 9.3 The second initial calibration results, which shows a deterioration of performance

As shown above, the overall results deteriorated in the second series of calibrations. Unsatisfactory results obtained using the C-70 PCA were believed to be due to the ratio of the effective areas between the test and the reference being too large, i.e. approximately 11.6. Too large a ratio makes it difficult to establish precise equilibrium conditions since both PCAs have a significant difference in sensitivity (based on the load value).

This situation persuaded the NPL to use its Primary Pressure Standard as a reference in the next calibrations. The selected reference pressure instrument was the PG7601 Primary Pressure Standard (as shown in Figure 9.4), with PCA serial number 602 (written as PCA-602 in this thesis), manufactured by DH Instruments, USA. PCA-602 has 981 mm² nominal effective area, and is manufactured from tungsten carbide. Its effective area was characterised dimensionally by the NPL, supported with extreme levels of data, extensive and unique mathematical modeling, and also comparison histories with other instruments of proven performance [NPL 2006]. Its standard uncertainty is equal to 3.51 ppm ($k = 1$) in the effective area, and 0.12 ppm/MPa ($k = 1$) in the pressure distortion coefficient, which become the Type B uncertainties in the uncertainty budget of the PCA under test.

9.4.2 Calibration Y1: P₂C₃ vs. PCA-602

In this comparison, the effective area ratio was approximately 1:1, which is the ideal ratio for calibration using the cross-floating method. The same procedures as in the first initial calibration were applied in this work. The results obtained are plotted graphically (see Figure 9.5) and shows the variation of the effective area ratios with the pressures generated.



FIGURE 9.4 Cross floating experiment against the UK's Primary Pressure Standard

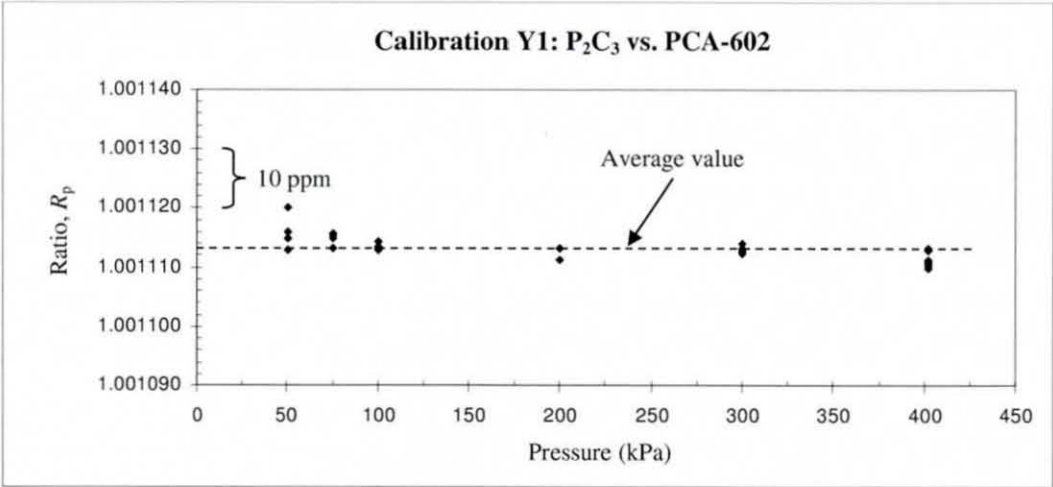


FIGURE 9.5 The results obtained from Calibration Y1, which shows excellent performance of the LU PCA and pressure balance

A summary of the calibration results produced by the NPL for P_2C_3 is as follows:

- Uncertainties of standard: $k = 1$
Area: Type B = 3.51 ppm
Type A = 0 ppm
Distortion coefficient uncertainty = 0.12 ppm/MPa
- Uncertainties of test: $k = 1$ (New method)
Type B = 6.95 ppm
Type A = 0.33 ppm
Total (added in quadrature) = 6.96 ppm
- Results calculated using $k = 2$
 $A_0 = 981.605 \text{ mm}^2 \pm 0.014 \text{ mm}^2$
 $a = 2.11 \text{ ppm/MPa} \pm 0.24 \text{ ppm/MPa}$

where A_0 is the effective area at atmospheric pressure, corrected at 20°C; and a is the pressure distortion coefficient of the PCA under test.

9.4.3 Calibration Y2: P_3C_4 vs. PCA-602

The same procedures as in the first initial calibration were applied in this work. However, due to the time constraints, calibration was carried out only at 100 kPa, repeated six times. The results obtained are plotted in a graph as shown in Figure 9.6, and the effective area determined at $k = 2$ was as follows:

$$\begin{aligned} A_0 &= 981.572 \text{ mm}^2 \pm 0.014 \text{ mm}^2 \\ a &= 2.11 \text{ ppm/MPa} \pm 0.24 \text{ ppm/MPa} \end{aligned}$$

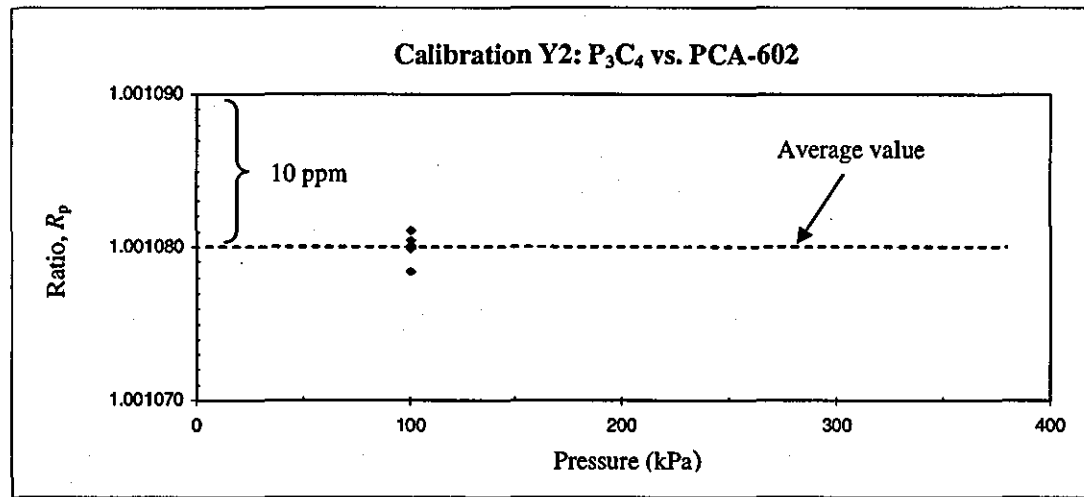


FIGURE 9.6 The results obtained from the Calibration Y2, which shows very good repeatability

9.4.4 Calibration Y3: P_4C_2 vs. PCA-602

The same procedures as described in Section 9.4.3 were applied in this work. However, the calibration was repeated ten times. The results obtained are plotted graphically in Figure 9.7, and the effective area determined at $k = 2$ was as follows:

$$A_0 = 981.635 \text{ mm}^2 \pm 0.014 \text{ mm}^2$$

$$a = 2.11 \text{ ppm/MPa} \pm 0.24 \text{ ppm/MPa}$$

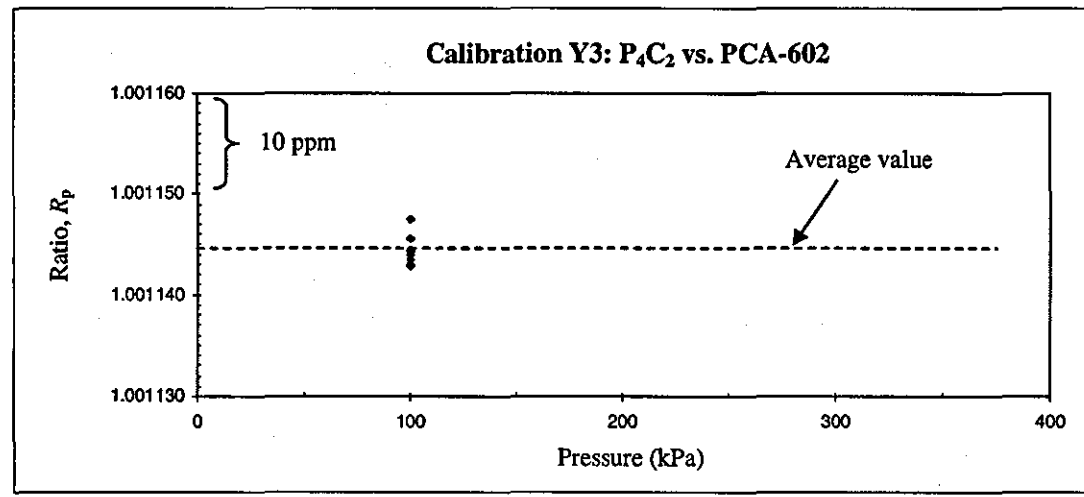


FIGURE 9.7 The results obtained from the Calibration Y3, which shows very good repeatability

9.4.5 Calibration Y4: P₄C₄ vs. PCA-602

The same procedures as described in Section 9.4.4 were applied in this work. The results obtained are plotted in Figure 9.8, and the effective area determined at $k = 2$ was as follows:

$$\begin{aligned} A_0 &= 981.625 \text{ mm}^2 \pm 0.014 \text{ mm}^2 \\ a &= 2.11 \text{ ppm/MPa} \pm 0.24 \text{ ppm/MPa} \end{aligned}$$

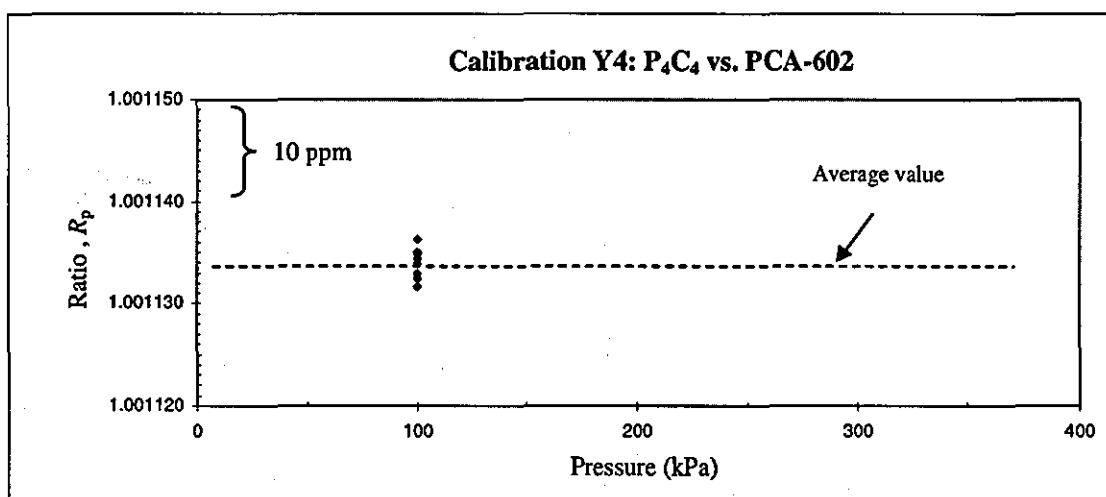


FIGURE 9.8 The results obtained from the Calibration Y4, which shows very good repeatability

In the verification work which is described in the next section, the values determined by the NPL for the P₂C₃, P₃C₄, P₄C₂ and P₄C₄ combinations were denoted by $A_{(P_2C_3)NPL}$, $A_{(P_3C_4)NPL}$, $A_{(P_4C_2)NPL}$ and $A_{(P_4C_4)NPL}$ respectively.

9.5 VERIFICATION PROCESS

Before verification work started, all the effective areas (of the check standards) that were previously obtained (based on an estimated value of the reference PCA) were adjusted accordingly, to the new value of P₂C₃ ($A_{(P_2C_3)NPL}$) which was determined by the NPL. The adjusted values of $A_{(P_3C_4)}$, $A_{(P_4C_2)}$, $A_{(P_4C_4)}$ were denoted by $A_{t0(P_3C_4)}$, $A_{t0(P_4C_2)}$ and $A_{t0(P_4C_4)}$ respectively.

A summary of the results obtained directly from the NPL is tabulated in Table 9.1, whereas the adjusted values of the check standards (recalculated based on the $A_{(P_2C_3)NPL}$) are tabulated in Table 9.2. A sample of the new uncertainty statement for all the recalculated values is shown in Table 9.3, detailing all the uncertainty components that have been taken into account.

TABLE 9.1 Effective areas of the check standards determined by the NPL

PCA Combination (P_XC_Y)	Symbol ($A_{(P_XC_Y)NPL}$)	Effective Area	
		Value (mm^2)	Uncertainty ($k = 2$)
P_2C_3	$A_{(P_2C_3)NPL}$	981.605	0.014 mm^2 (14.3 ppm)
P_3C_4	$A_{(P_3C_4)NPL}$	981.572	0.014 mm^2 (14.3 ppm)
P_4C_2	$A_{(P_4C_2)NPL}$	981.635	0.014 mm^2 (14.3 ppm)
P_4C_4	$A_{(P_4C_4)NPL}$	981.625	0.014 mm^2 (14.3 ppm)

TABLE 9.2 Effective areas of the check standards determined at LU, traceable to $A_{(P_2C_3)NPL}$

PCA Combination (P_XC_Y)	Symbol ($A_{t0(P_XC_Y)}$)	Effective Area	
		Value (mm^2)	Uncertainty ($k = 2$)
P_3C_4	$A_{t0(P_3C_4)}$	981.576	0.016 mm^2 (16.4 ppm)
P_4C_2	$A_{t0(P_4C_2)}$	981.639	0.016 mm^2 (16.4 ppm)
P_4C_4	$A_{t0(P_4C_4)}$	981.629	0.016 mm^2 (16.4 ppm)

Evaluation of the performance of the cross-floating experiments carried out at LU has been completed in two ways:

- Deviation of the LU's results from the NPL's results, so that a proper adjustment/corrective action could be carried out.
- Calculation of the Normalised Error (E_n). $|E_n| < 1$ signifies that the effective area determinations at LU are acceptable.

9.5.3 Deviation Check

The effective area values determined by the NPL were used as the references. The deviation of the LU results from the reference value (ppm) for the P_XC_Y combination is denoted by $\Delta_{P_XC_Y}$, where it was calculated using the following equation:

$$\Delta_{(PXC_Y)} = \frac{A_{i0(PXC_Y)} - A_{(PXC_Y)NPL}}{A_{(PXC_Y)NPL}} \times 10^6 \quad (9.1)$$

The calculated deviations of all the PCA combinations are as follows:

- $\Delta_{(P3C2)} = 4.1 \text{ ppm}$
- $\Delta_{(P4C2)} = 4.1 \text{ ppm}$
- $\Delta_{(P4C4)} = 4.1 \text{ ppm}$

The results indicate that there was a systematic error within the calibration system that needed to be rectified. However, this effect is relatively small, i.e. one fourth of the quoted expanded uncertainty.

9.5.4 Normalised Errors, E_n

The $E_{n(PXC_Y)}$ value measured the relative difference between the LU results and the NPL values for the $P_X C_Y$ combination, with the standard uncertainty of measurement, u ($k = 1$) being taken into account. The following equation was used:

$$E_{n(PXC_Y)} = \frac{A_{i0(PXC_Y)} - A_{(PXC_Y)NPL}}{2\sqrt{u_{i0(PXC_Y)}^2 + u_{(PXC_Y)NPL}^2}} \quad (9.2)$$

The calculated $|E_{n(PXC_Y)}|$ values of all the PCA combinations were as follows:

- $|E_{n(P3C4)}| = 0.19$
- $|E_{n(P4C2)}| = 0.19$
- $|E_{n(P4C4)}| = 0.19$

The above calculated values demonstrated that the effective areas derived at LU were acceptable, in line with the definition of the pressure unit which is in accordance with the SI system. At the same time these verification processes prove that the performance

of the LU pressure balances is comparable with the DHI PG7601, which is widely used as a Primary Pressure Standard around the world.

9.6 THERMAL STABILITY COMPARISONS

Stable ambient temperature conditions are necessary in the cross-floating experiments, especially if state-of-the-art uncertainty is the prime concern. This is to ensure that the pressure balance (especially the PCAs) remain as thermally constant as possible during the experimental work in progress. However, due to the complexity of pressure balance designs that are available in the market nowadays, stable ambient temperature conditions cannot necessarily be guaranteed in these instruments due to internal heat sources within the systems.

One should bear in mind that stability is the key aspect to be considered, rather than control of the temperature at a specific level (i.e. within a tolerable range). The higher the stability, the more accurate the thermal corrections can be made, thus reducing the uncertainty of measurement invoked from the thermal expansion coefficient of the PCA. Therefore, analysis of the thermal stability performance of the LU pressure balance (denoted as Lufbra 1) was carried out. Comparisons against two well known pressure balances (NPL) were completed as a function time of measurement taken. The data were extracted from the actual data taken during calibration work at NPL.

Temperature measurements were completed using a multi-channel thermometer (Edale Instruments, resolution 0.01 °C and uncertainty less than 0.02 °C). The first thermistor probe was placed in between the two pressure balances, exposed directly to the ambient room temperature. The second and the third thermistor probes were inserted into the access holes in the pressure balances, close to the respective PCAs.

TABLE 9.3 Uncertainty calculation of the effective area of P_4C_2 , $A_{100(P4C2)}$

Input parameters							Measurand			
x_i			Prob. Dist.	Limits (2σ or ± a)	Std. Uncertainty $u(x_i)$	DOF ν_i	Sensitivity Coefficient		Standard Uncertainty $ \partial A_i / x_i u(x_i)$	
Parameter Description	Approx. Value	Unit					$ \partial A_i / x_i $	Value	m ²	ppm
<Test Pressure Balance>										
Total mass loaded, m_{wt}	10.00	kg	Norm.	5.0E-05	2.5E-05	∞	A/m_{wt}	9.81E-05	2.452E-09	2.5E+00
Density of the weights loaded, ρ_{wr}	7800	kg/m ³	Rect.	5.0E+01	2.9E+01	∞	$A(\rho_d/\rho_{wr}^2)/(1-\rho_d/\rho_{wr})$	1.94E-11	5.602E-10	5.7E-01
Density of the ambient air, ρ_{ar}	1.20	kg/m ³	Rect.	1.0E-02	5.8E-03	∞	$A/(\rho_{wr}(1-\rho_d/\rho_{wr}))$	1.26E-07	7.266E-10	7.4E-01
Thermal exp. coeff. of the PCA, ($\alpha_{pt} + \alpha_{ct}$)	9.10E-06	°C ⁻¹	Rect.	5.0E-07	2.9E-07	∞	$2A_i(t_t - 20)$	1.96E-04	5.667E-11	5.8E-02
Temperature of the PCA, t_t	20.1	°C	Rect.	2.0E-01	1.2E-01	∞	$A(\alpha_{pt} + \alpha_{ct})$	8.93E-09	1.031E-09	1.1E+00
<Reference Pressure Balance>										
Total mass loaded, m_{wr}	10.00	kg	Norm.	5.0E-05	2.5E-05	∞	A/m_{wr}	9.81E-05	2.452E-09	2.5E+00
Density of the weights loaded, ρ_{wr}	7800	kg/m ³	Rect.	5.0E+01	2.9E+01	∞	$A(\rho_d/\rho_{wr}^2)/(1-\rho_d/\rho_{wr})$	1.94E-11	5.602E-10	5.7E-01
Density of the ambient air, ρ_{ar}	1.20	kg/m ³	Rect.	1.0E-02	5.8E-03	∞	$A/(\rho_{wr}(1-\rho_d/\rho_{wr}))$	1.259E-07	7.266E-10	7.4E-01
Thermal exp. coeff. of the PCA, ($\alpha_{pr} + \alpha_{cr}$)	9.10E-06	°C ⁻¹	Rect.	5.0E-07	2.9E-07	∞	$2A_i(t_r - 20)$	1.963E-04	5.667E-11	5.8E-02
Temperature of the PCA, t_r	19.9	°C	Rect.	2.0E-01	1.2E-01	∞	$A(\alpha_{pr} + \alpha_{cr})$	8.932E-09	1.031E-09	1.1E+00
Effective area at 100 kPa, 20°C, A_{r0}	9.815E-04	m ²	N/A	1.40E-08	7.00E-09	∞	A/A_{r0}	1.000E+00	7.000E-09	7.1E+00
Pressure distortion coefficient, λ_r	0	Pa ⁻¹	N/A	2.11	1.06	∞	$A_i p_r$	9.816E+01	1.036E-04	1.1E-01
<Head Correction>										
Density of pressure-transmitting fluid, ρ_f	2.23	kg/m ³	Rect.	1.0E-02	5.8E-03	∞	$(A/p_r) g \Delta h$	1.11E-10	6.419E-13	6.5E-04
Density of ambient air, ρ_a	1.20	kg/m ³	Rect.	1.0E-02	5.8E-03	∞	$(A/p_r) g \Delta h$	1.112E-10	6.419E-13	6.5E-04
Height difference in the reference levels, Δh	0	m	Rect.	2.0E-03	1.2E-03	∞	$(A/p_r)(\rho_f - \rho_a) g_L$	2.24E-07	2.591E-10	2.6E-01
<Equilibrium Conditions>										
Sensitivity of cross-floating, m_{dis}	2.0E-06	kg	Rect.	2.0E-06	1.0E-06	∞	A/m_{wr}	9.81E-05	9.809E-11	1.0E-01
Repeatability, R	Std. Dev.	m ²	Norm.	2.60E-10	1.30E-10	31	1	1	1.300E-10	1.3E-01
Sum of squared = $\sum (A_i / x_i)^2 u^2(x_i) + u^2(m_{dis}) + u^2 R$							67.39 ppm ²			
Standard uncertainty of the test effective area at 100 kPa and 20°C, $u(A_{100kPa, 20^\circ C})$							8.21 ppm			
Expanded uncertainty at a level of confidence of approximately 95% , coverage factor of $k = 2$							16.4 ppm			

9.6.1 Lufbra 1 vs. Ruska 2465

The first comparison was between the Lufbra 1 and the Ruska 2465 (see Section 9.4.1). The data were extracted from one day of observations of the first initial experiment which ended with unsatisfactory results. Table 9.4 shows a detailed description of the data taken, followed by Figure 9.9 that illustrates graphically the temperature variations with time for the three sensors.

TABLE 9.4 Temperatures of the room, Ruska 2465 and Lufbra 1, extracted from the first initial calibration

Cross-floating Experiment at NPL : P ₂ C ₃ vs. C-70					
No.	Date and Time		Temperature (°C)		
	Date	Time (hh.mm)	Room	Ruska 2465	Lufbra 1
1	15-Nov-05	09.38	19.70	19.91	19.55
2	15-Nov-05	09.38	19.70	19.91	19.55
3	15-Nov-05	09.55	19.53	20.03	19.57
4	15-Nov-05	09.55	19.53	20.03	19.57
5	15-Nov-05	10.12	19.67	20.16	19.59
6	15-Nov-05	10.12	19.67	20.16	19.59
7	15-Nov-05	10.46	19.62	20.45	19.64
8	15-Nov-05	10.46	19.62	20.45	19.64
9	15-Nov-05	11.10	19.74	20.53	19.67
10	15-Nov-05	11.10	19.74	20.53	19.67
11	15-Nov-05	11.50	19.64	20.65	19.72
12	15-Nov-05	11.50	19.64	20.65	19.72
13	15-Nov-05	12.01	19.61	20.69	19.74
14	15-Nov-05	12.01	19.61	20.69	19.74
15	15-Nov-05	14.13	19.48	20.40	19.77
16	15-Nov-05	14.13	19.48	20.40	19.77
17	15-Nov-05	14.57	19.82	20.46	19.77
18	15-Nov-05	14.57	19.82	20.46	19.77
19	15-Nov-05	15.47	19.84	20.54	19.80
20	15-Nov-05	15.47	19.84	20.54	19.80
21	15-Nov-05	16.46	19.80	20.69	19.85
22	15-Nov-05	16.46	19.80	20.69	19.85
Average			19.68	20.41	19.70
Standard Deviation			0.11	0.26	0.10
Minimum			19.48	19.91	19.55
Maximum			19.84	20.69	19.85
Difference (Maximum – Minimum)			0.36	0.78	0.30

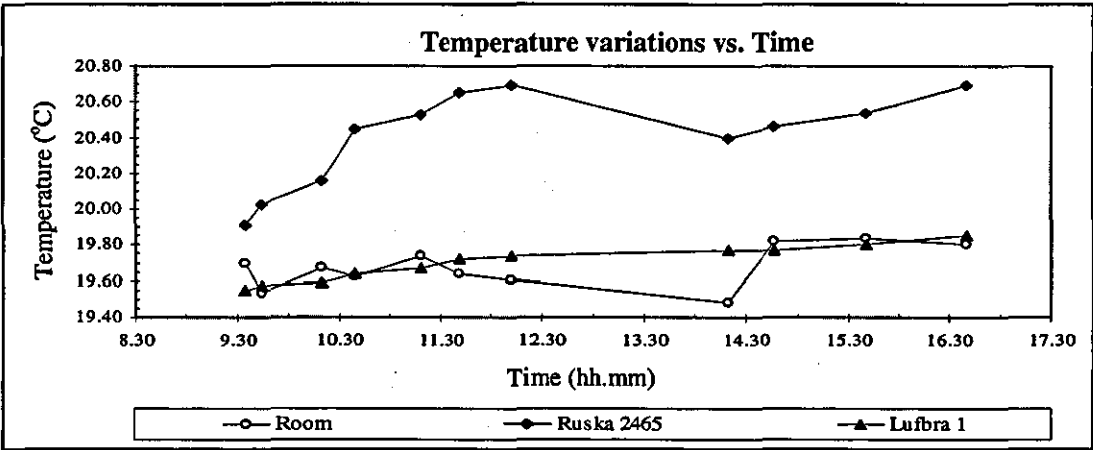


FIGURE 9.9 Temperature variations of the room with time, Ruska 2465 and Lufbra 1

9.6.2 Lufbra 1 vs. DHI PG7601

The second comparison was between the Lufbra 1 and the DHI PG7601 (see Section 9.4.2). The data were extracted from the Calibration Y1. The graphical illustration shown in Figure 9.10, followed with Table 9.5 which shows a detailed description of the data taken.

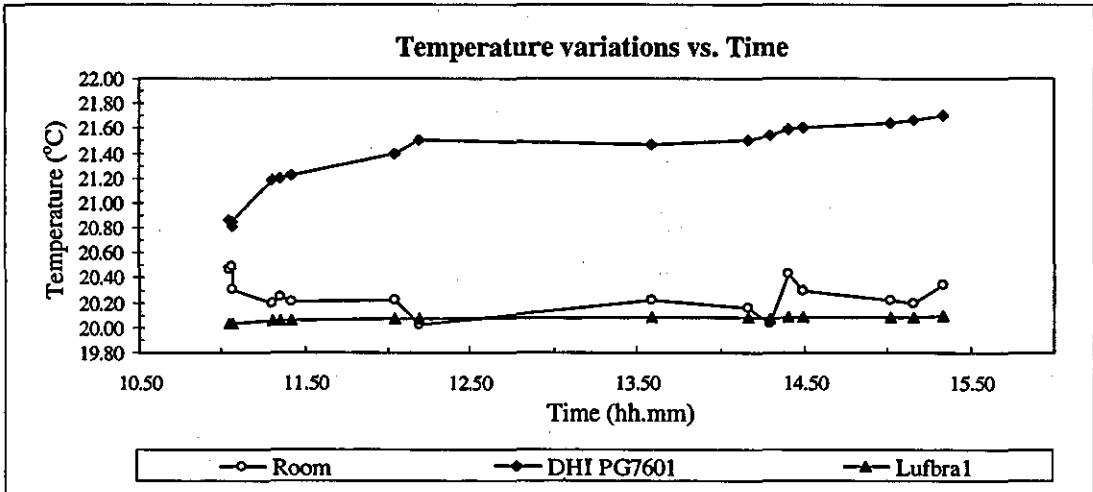


FIGURE 9.10 Temperature variations of the room with time, DHI PG7601 and Lufbra 1

TABLE 9.5 Temperatures of the room, DHI PG7601 and Lufbra 1, extracted from the Y1 Calibration

Cross-floating Experiment at NPL : P ₂ C ₃ vs. C-70					
No.	Date and Time		Temperature (°C)		
	Date	Time (hh.mm)	Room	DHI PG7601	Lufbra 1
1	17-Nov-05	11.05	20.47	20.86	20.03
2	17-Nov-05	11.05	20.47	20.86	20.03
3	17-Nov-05	11.07	20.49	20.81	20.03
4	17-Nov-05	11.07	20.31	20.85	20.03
5	17-Nov-05	11.30	20.19	21.18	20.06
6	17-Nov-05	11.35	20.24	21.20	20.06
7	17-Nov-05	11.42	20.21	21.22	20.06
8	17-Nov-05	11.42	20.21	21.22	20.06
9	17-Nov-05	12.04	20.22	21.39	20.07
10	17-Nov-05	12.04	20.22	21.39	20.07
11	17-Nov-05	12.19	20.02	21.50	20.07
12	17-Nov-05	12.19	20.02	21.50	20.07
13	17-Nov-05	13.59	20.22	21.47	20.08
14	17-Nov-05	13.59	20.22	21.47	20.08
15	17-Nov-05	14.16	20.16	21.50	20.08
16	17-Nov-05	14.16	20.16	21.50	20.08
17	17-Nov-05	14.29	20.03	21.54	20.07
18	17-Nov-05	14.29	20.03	21.54	20.07
19	17-Nov-05	14.40	20.43	21.59	20.08
20	17-Nov-05	14.40	20.43	21.59	20.08
21	17-Nov-05	14.49	20.30	21.61	20.09
22	17-Nov-05	14.49	20.30	21.61	20.09
23	17-Nov-05	15.02	20.22	21.64	20.09
24	17-Nov-05	15.02	20.22	21.64	20.09
25	17-Nov-05	15.16	20.19	21.67	20.09
26	15-Nov-05	15.16	20.19	21.67	20.09
27	15-Nov-05	15.33	20.34	21.70	20.10
28	15-Nov-05	15.33	20.34	21.70	20.10
Average			20.24	21.41	20.07
Standard Deviation			0.13	0.28	0.02
Minimum			20.02	20.81	20.03
Maximum			20.49	21.70	20.10
Difference (Maximum – Minimum)			0.47	0.89	0.07

Figures 9.9 and 9.10 clearly demonstrated that the Lufbra 1 is more stable in terms of temperature stability compared to the Ruska 2465 and DHI PG7601, which have more complicated design. Its simple (fully-mechanical) and special construction (large volume) have made the Lufbra 1 thermally extremely stable and able to represent the room temperature variations in an excellent manner (gradual change). However,

outstanding performance of the Ruska 2465 and DHI PG7601 is reduced, simply due to their thermal stability, which is due to the motor and electronic circuitry associated with them.

9.7 SUMMARY AND DISCUSSIONS

The overall goal of this exercise was to get the pressure system developed/used at the LU traceable to the National Primary Pressure Standard. Besides traceability reasons, this exercise was planned so that it simultaneously acted as a mechanism for verification on the performance of the work completed at LU. The performances of the LU pressure balance and PCAs have been assessed internally from the data given by the NPL. Successfulness of this exercise has automatically provided confidence in the LU data.

Four PCA combinations were calibrated by the NPL, where particular attention was given to P_2C_3 which acted as a reference PCA in the calibration chain. P_2C_3 was calibrated at six points, ranging from 50 to 400 kPa. Three other combinations, i.e. P_3C_4 , P_4C_2 and P_4C_4 which acted as check standards, were calibrated at 100 kPa only. Comparison against a working standard pressure balance of relatively very small effective area (approximately 11.6 times smaller) demonstrated unsatisfactory results. Therefore, the UK Primary Pressure Standard of the same effective area ratio as the LU pressure balance was used to calibrate all of the PCAs. The pressure balance (Lufbra 1) and all PCAs performed very well during the calibration processes. All of the combinations have been determined for their respective effective areas, with expanded uncertainty of 14.3 ppm ($k = 2$).

After completion of the calibration work at the NPL, internal verification process started with adjustment of the effective areas of the check standards P_3C_4 , P_4C_2 and P_4C_4 which were previously traceable to the estimated value of the P_2C_3 . The new values of the check standards (which are traceable to the Primary Pressure Standard via NPL's calibrated P_2C_3) were subsequently determined, completed with a revised statement of measurement uncertainty. The expanded uncertainty of measurement was estimated to

be 16.4 ppm ($k = 2$), applicable to all the check standards. These values were then compared against the values determined by the NPL (direct traceable to the Primary Pressure Standard). The deviation checks performed have demonstrated that all the deviations were 4.1 ppm (larger), i.e. one fourth of the estimated uncertainty quoted. The overall performance of the work completed at LU was tested out through a normalised error (E_n) check. The test results demonstrated that all values determined (inclusive of uncertainty of measurement) met the necessary requirements.

Additional performance checks have also been carried out on one of the critical elements in the high precision pressure measurement, i.e. thermal stability of the pressure balance. The thermal stability of the LU pressure balance was compared against the NPL working standard and Primary Pressure Standard, with variations of the room temperatures also included. All data were extracted from the actual calibrations performed. Comparison results demonstrated that the LU pressure balance (see Section 5.2) was extremely stable compared to the others.

This successful calibration/verification process has proven that the whole calibration system, i.e. pressure balances, PCAs, cross-floating methods, effective area determinations and uncertainty estimations are trustworthy, reliable, competent and traceable. Hence this has confirmed the validity of the findings on “the effects of the surface texture on the pressure balance” as described in Chapters 7 and 8.

CHAPTER 10

CONCLUSIONS

There were eight objectives of the research presented in this thesis, which are summarised in Section 10.1. The novel and unique engineering and scientific contributions are highlighted in Section 10.2, and future work that would be undertaken is outlined in Section 10.3. Finally, Section 10.4 lists the dissemination effort completed so far as a consequence of this research work.

10.1 RESEARCH OBJECTIVES SUMMARY

The main objective of this research work was to investigate the effects of surface texture on the pressure balances. However, in order to achieve this main objective, six other investigations and one subsequent investigation have been completed. Each additional investigation has carried along its own objective. Therefore, the overall research objectives and their achievements are described as follows:

- **Manufacturing of two identical pressure balance units for cross-floating experiments:** Two identical pressure balances have been successfully designed and manufactured using the 316 stainless steel, with aluminium bases. The overall combination of elements in the design of the pressure balances is unique, although individual elements can be found in research and commercial equipment. They have performed very well throughout all experimental work, with a maximum value of repeatability of 1.06 ppm at 100 kPa. The design and construction of these pressure balances have provided extreme thermal stability of the PCAs, which is better than other similar capacity of pressure balances available in the market nowadays.

- **Manufacturing of identical pistons (of various surface texture) and identical cylinders, which are interchangeable:** Seven identical pistons (of various surface texture applied onto their outer surfaces) and three identical cylinders have been successfully manufactured. They are interchangeable with each other, and have performed very well in all of the cross-floating experiments. Different types of material have been experimented with, including 316 stainless steel. However, due to the softness and high coefficient of friction of these materials, galling effects became the main problem. Galling effects caused the piston and the cylinder to easily bond together, thus leading to failure. The prominent material for the PCA has been chosen (Dymet DF6 tungsten carbide), which produced excellent performance. This element of the work has for the first time, explicitly documented the manufacturing processes for a PCA.
- **Identifying an approach to demonstrate pressure dependency on the surface texture applied onto the pistons:** A well planned calibration chain has been designed. The best PCA combination (based on fall rate and spinning time at 100 kPa) has been chosen (among the manufactured pistons and cylinders) as a reference, to which all other combinations were traceable (P_2C_3 – fall rate of 100 $\mu\text{m}/\text{min}$, spin time of 45 minutes). For the sake of a statistically better analysis, direct and indirect cross-floating experiments against the reference have been completed, hence more cross-floating comparisons were possible.
- **Identifying the best method in determining the equilibrium conditions in cross-floating experiments:** Two methods have been identified in judging the equilibrium conditions of the cross-floating experiments. Two well known methods have been experimented, i.e. the flow sensing and the pressure sensing methods. Both methods which were used simultaneously in all experiments have produced a sensitivity of 0.2 ppm at 100 kPa. However, due to convenience, the equilibriums based on the pressure sensing method have been used, backed-up with the flow-sensing method.
- **Identifying the effects of rotational speed (RS) and rotational direction (RD) on the pressure generated:** Before investigation into the effects of the surface

texture could be initiated, investigation into the effect of RSs and RDs was required. These were completed on Piston 4 (P_4), matched with two Cylinders 2 and 4 (C_2 and C_4), aimed at identifying any pressure dependency as a function of RS and/or RD. Eight cycles consisting of CW-CW, CW-CCW, CCW-CCW and CCW-CW per cycle have been carried out, resulting in 32 sets of data. The results obtained were inspected graphically and numerically, and have shown that the performance of the pressure balances is independent of RS or RD.

- **Identifying the most practical method of measurement in quantifying the surface texture applied onto the pistons:** A 3-Dimensional surface profiling instrument (Zygo New View 5000) was used. The profiler scanned the piston's surface to reveal its microstructure and topographical features. The three surface parameters that have been taken into account were R_t , R_q and R_a . Average values based on ten scanned areas have been used to represent the individual surface parameters of each piston.
- **Identifying the effects of the surface texture to the pressure generated:** Cross-floating experiments have been carried out on the test PCAs, with respect to the calibration chain. However, they were performed with three cycles only. Results obtained were investigated through graphical and numerical analysis where each RC was individually identified (RC-base identification). Further investigations have been carried out on six PCAs which are traceable to the reference PCA via various routes within the calibration chain. Differences in the determined effective areas via each route were the means of checking the possibility of "summing up phenomenon" due to the surface texture effects. This work has demonstrated a tentative correlation which identifies the smoothest piston as producing the lowest effective area values, whilst all rougher pistons produce larger effective area values. However, the texture effects may be masked by variations of piston diameter and hence effective area.
- **Identifying a suitable method of verifying the findings obtained:** The reference PCA and three other PCAs (acting as check standards) were calibrated by the NPL. This work functioned as the calibration/verification of the whole

calibration system within the calibration chain. Assessment of the whole calibration system, i.e. pressure balances and PCAs, cross-floating method, effective area determinations and uncertainty estimations have been made internally using the effective areas determined by the NPL.

10.2 ENGINEERING AND SCIENTIFIC CONTRIBUTION

The uniqueness of this research work has provided original engineering and scientific contributions. At the same time, other experiments/approaches that have been completed to achieve the main objective have emerged as additional engineering and scientific contributions as well. They are identified as follows:

- A well documented procedure of the manufacture of the PCA (as describe in Sections 5.3 and 5.4) is presented. There is no such document publicly available. Therefore, this thesis contributes a significant insight into the manufacturing processes involved, which is beneficial to the pressure community, existing and potential manufactures of the pressure balance.
- An approach using interchangeable identical pistons (seven) with identical cylinders (three) of 35 mm diameter has shown successful results. This research proves that this approach (interchangeable pistons and cylinders) is a practical method to further investigate other effects that might alter the pressure generated, not necessarily restricted to the effects of the surface texture.
- The method used in the cross-floating experiments themselves is considered as a unique approach where the CW-CW, CW-CCW, CCW-CCW and CCW-CW combinations have never been explored before especially with respect to 35 mm diameter PCA's. Normally, the test PCA is the only one that is subjected to a change of direction (if any). Through this approach, a 3-Dimensional presentation of the effective area variations in relation to the RSs and RDs (of both PCAs involved) can be observed or investigated.
- For the first time in the field of pressure metrology, an analysis of surface texture (of various levels and types applied onto the pistons) affecting the pressure

generated is presented. This research initiates the study on the surface texture effects on the PCAs. Two findings have been identified from two types of experiments carried out. They are as follows:

- There is no observable effect of the pressure generated due to the RSs and RDs of the PCA using a 35 mm diameter PCA, with the nitrogen as a pressure transmitting fluid (Chapter 7), with respect to the uncertainty budget and noise floor of the pressure balances.
- There is no clear effect of the pressure generated due to the surface textures (of random pattern) on the 35 mm diameter pistons, with the nitrogen as a pressure transmitting fluid (Chapter 8), with respect to the uncertainty budget and noise floor of the pressure balances however, it is noticeable that the smoothest piston does produce consistently the lowest effective area.
- The research highlights that the surfaces of piston and cylinder are not perfectly smooth due to the nature of the manufacturing processes. PCAs are purposely being manufactured with certain levels of texture on them to make sure the performance is excellent. Without this texture, lubrication between two rubbing surfaces is insufficient, due to the lack of surface pockets, which can retain pressure transmitting fluid within them. Insufficient lubrication causes higher coefficients of friction (due to solid friction of mechanical contact) between these surfaces, thus the piston can easily get stuck to the cylinder. This phenomenon can easily be seen in the “wringing process” which is commonly used in dimensional measurement using block gauges. The majority of the people within the pressure community work on the basis that the pistons and cylinders should be manufactured with the highest possible smoothness level, without requiring texture on them.
- The research has started to investigate that surface texture on the piston and cylinder may alter effective area of the PCA due to the level of roughness in the texture (even though this research cannot at this point in time demonstrate any

consistent pressure dependency on the surface texture). Theoretically, the rougher the surface, the bigger the effective area will be. In the pressure measurement context, this assumption is based on the reason that the rougher surface will make the “effective contact” between the pressure transmitting fluid and the PCA’s wall to be increased, thus enlarge the effective area (see explanations in the future work).

- The work has identified a simple, but effective method of thermal stability comparison against well establish pressure balances, which are commonly used as a Primary Pressure Standard or Reference Pressure Standards at NMIs all over the world. These simple comparisons revealed that a fully mechanical self designed pressure balance performs better in term of the thermal stability, compared to others, which have complicated electronic circuitry and motorised.

10.3 FUTURE WORK

Whilst this thesis presents several new methodologies towards the improvement of the effective area determination (through investigating the effects of surface texture to the pressure generated) of the PCA, there are many questions that have arisen from the work. These questions are illustrated in the context of the following future work. This future work is divided into two sections, i.e. Section 10.3.1 and Section 10.3.2. The first section list all the future work to be carried out, based on the existing pressure balance and the PCAs. While the second section describes the future work which would be based on the new PCAs and a modified pressure balance.

10.3.1 Existing Facilities

The future research work that would be carried out is as follows:

- Investigation of the effects of the gas species on the PCAs of various surface textures. This type of research has been carried out by several NMIs (some are still), but with normal surface finished PCAs. Larger pressure dependency effects are anticipated through this future work, since different sizes of gas molecules

(of different species) would demonstrate different manners of interactions, which may depend on different levels of roughness of the piston surface.

- Investigation on the effects of the clearance sizes (in relation to the different gas species used) to the pressure generated. This can simply be implemented with any piston, matched with the Cylinder 2 (C_2), and subsequently with the Cylinder 4 (C_4). Previous cross-floating experiments have clearly demonstrated that these two cylinders have a diameter difference of less than $0.2\text{ }\mu\text{m}$.
- Investigation on the effects of cleaning methods used to the pressure generated. Cleaning processes using different cleaning agents would be applied to the pistons of different surface texture. This is due to residue of the cleaning agents (that may be left behind after each cleaning process) which may generate different interactions between piston and cylinder thus altering the pressure generated.

10.3.2 New PCAs and Modified Pressure Balance

The research work that would be carried out in the future using new PCAs and a modified pressure balances is as follows:

- New PCAs of fully controlled surface texture should be developed. This could be achieved through ablation method machining lasers. Having a more controllable and uniform surface texture, will give better representation of each piston's overall characteristics when average values are used. Furthermore, localised laser ablation will not affect the geometry of the piston (diameter, cylindricity etc.), unlike the current approach, where the piston is matched to the cylinder, and any further surface texture modification may reduce the piston diameter. This advancement in surface modification would develop a new perspective of research:
 - Investigation on the best design of the surface texture to be applied onto piston or cylinder (or both of them) in order to get the best performance of the PCA, especially on the fall rate and spinning time. Micro-texturing

of surfaces is believed to give impact on lubrication and hydrodynamic friction between piston and cylinder, hence the performance and effective areas of the PCA. This is beneficial to the pressure balance manufacturer who is always seeking for improvement in their products.

- Comparisons of the effective areas obtained through the cross-floating method against the dimensional measurement methods. Variations in the determined effective areas are anticipated (especially when various sizes of contact probes/stylus were used). Continuous research on this subject would be able to get a functional correlation between surface textures and the effective area of the PCA, thus improve the state-of-the-art uncertainty of pressure measurement in the primary level.
- Repetition of the existing procedure (but in a more refined manner) could be applied with various gas species.
- The construction of new mounting posts (with existing base, weights and weight loading bells) to accommodate bigger PCAs, i.e. 50 mm diameter. A bigger PCA would give better opportunities to study surface texture manipulation methods especially in the degree of roughness to be applied.
- Investigating the possibility of manufacturing a PCA of different materials, other than tungsten carbide.
- Investigating the performance of the tungsten carbide PCA using a different grade of tungsten carbide (different grain sizes and compositions).

10.4 DISSEMINATIONS

The work carried out in this research has been, and is in the process of being disseminated as follows:

- Wan Mohamed, W.A.M. and Petzing, J.N., *Investigating the influence of surface texture on the performance of gas operated Dead Weight Pressure*

Balances, Proceedings of the 4th CMM International Conference on Pressure Metrology from Ultra-High Vacuum to Very High Pressures (10^{-9} Pa to 10^9 Pa), Institute of Physics, London, UK, April 2005, pp 4-5 [Wan Mohamed and Petzing 2005].

- Wan Mohamed, W.A.M and Petzing, J.N., *Investigation into piston-cylinder performance*. A Pressmet Meeting: "High pressure measurement", DH-Budenberg, Manchester, UK. 18 April 2006 [Wan Mohamed and Petzing 2006].
- Wan Mohamed, W.A.M and Petzing, J.N., *The effect of rotational speed and rotational direction on pressure generated by gas operated pressure balances*. In-review, Measurement Science and Technology, June 2006.
- Wan Mohamed, W.A.M and Petzing, J.N., *Surface texture on the PCAs and its impacts on the gas-operated pressure balances*. In-preparation, 3rd APMP Pressure and Vacuum Workshop, NPL India, December 2006.

REFERENCES

- [Astrov et al. 1994] Astrov, D.N., Guillemot, J., Legras, J.C., and Zakharov, A.A. 1994. Intercomparison of primary manometers in the range 30 kPa to 110 kPa: Pressure balance at the LNE and mercury manometer at the VNIFTRI. *Metrologia* 30, No 6, pp 711-715.
- [Bair 2002] Bair, M., 2002. Improvements in the determination of effective area through a piston-cylinder pressure calibration chain. *Proceedings of NCSLI Conference*, Anaheim, USA.
- [Bair and Delajoud 2002] Bair, M., and Delajoud, P. 2002. *Uncertainty analysis for pressure defined by a PG7601, PG7102, PG7202 or PG7302 piston gauge*. DH Instruments, Inc., Technical Note 7920TN01B.
- [Bass 1978] Bass, A.H., 1978. Analysis of mechanical pressure generators. *J. Phys. E: Sci. Instrum.* 11, No 7, pp 682-688.
- [Bass and Green 1972] Bass, A.H., and Green, E. 1972, *ISA Transactions* 11, pp 113-120.
- [BIPM 2006a] Bureau International des Poids et Mesures, 2006. *General conference on weights and measures* [online]. Available at: <URL: <http://www.bipm.fr/en/convention/cgpm/>> [Accessed 10 June 2006].
- [BIPM 2006b] Bureau International des Poids et Mesures, 2006. *SI base units* [online]. Available at: <URL: http://www.bipm.fr/en/si/base_units/> [Accessed 10 June 2006].

- [BIPM 2006c] Bureau International des Poids et Mesures, 2006. *Pressure measurements using a manobarometer* [online]. Available at: <URL: <http://www.bipm.org/en/scientific/mass/pressure.html>> [Accessed 10 June 2006].
- [BIPM 2006d] Bureau International des Poids et Mesures, 2006. CCM: Consultative Committee for Mass and Related Quantities [online]. Available at: <URL: <http://www.bipm.fr/en/committees/cc/ccm/>> [Accessed 10 June 2006].
- [Brubach 1947] Brubach, H. F., 1947. Some laboratory applications of the low friction properties of the dry hypodermic syringe. *Rev. Sci. Instrum.*, Vol 18, No 5, pp. 363-366.
- [BS1134-1 1988] British Standards Institute, 1988. *Assessment of surface texture - Part 1: Methods and instrumentation*. London: BSI.
- [BS1134-2 1990] British Standards Institute, 1990. *Assessment of surface texture - Part 2: Guidance and general information*. London: BSI.
- [Budinski and Budinski 1999] Budinski, K.G. and Budinski, M.K., 1999. *Engineering materials: Properties and selection* (6th Edition). New Jersey: Prentice Hall.
- [Colijn 1983] Colijn, H., 1983. *Weighing and proportioning of bulk solids* (2nd edition). Ohio: Trans Tech Publications.
- [Corewire 2004] Corewire Ltd., 2004. *Tungsten carbide grade list*. [online]. Available at: <URL: <http://www.corewire.com/TungstenCarbideGradeList.asp>> [Accessed 01 April 2004].

- [Cross 2003] Cross, J.W., 2003. *Scanning probe microscopy (SPM): Imaging surfaces on a fine scale*. [online] Available at: <URL: <http://www.mobot.org/jwcross/spm/>> [Accessed 13 June 2006].
- [Dadson 1983] Dadson, R.S., 1983. The precise measurement of steady pressures. In: Peggs, G.N., (editor). *High pressure measurement techniques, Part I, Chapter 1*. London: Applied Science Publishers.
- [Dadson and Greig 1964] Dadson, R.S., and Greig, G.P., 1964. The air-operated pressure balance as a standard for sub-atmospheric pressure. *Conference on fundamental problems of low pressure measurements*. Institute of Physics, London.
- [Dadson et al. 1965] Dadson, R.S., Greig, R.G.P., and Horner, A., 1965. Developments in the accurate measurement of high pressures. *Metrologia* 1, pp 55-67.
- [Dadson et al. 1982] Dadson, R.S., Lewis, S.L., and Peggs, G.N., 1982. *The pressure balance: Theory and practice*. National Physical Laboratory, London: HMSO.
- [Dargent 1994] Dargent, L. 1994. Digital piston manometers: Are they primary or transfer standards? *Metrologia* 30, pp 659-663.
- [Dargent and Poirier 1999] Dargent, L., and Poirier, F., 1999. APX50: A novel fully automatic absolute pressure balance as a primary reference in the range 10 kPa to 1 MPa. *NCSL Workshop & Symposium*.
- [Davidson et al. 2004] Davidson, S., Perkin, M., and Buckley, M., 2004. *The measurement of mass and weight, Measurement good practice guide*, No. 71. National Physical Laboratory, London: HMSO.

- [Debler 2000] Debler, E., 2000. Chap. 3, Part 3.6: Determination of mass in practice. In: Kocksiek, M. and Glaser, M., (editors). *Comprehensive mass metrology*. Berlin: Wiley-VCH Verlag, pp 400-429.
- [Delajoud and Girard 1981] Delajoud, P.R., and Girard, M.B. 1981. The development of a digital read-out primary pressure standard. Instrument Society of America, N.C.
- [Delajoud and Girard 1988] Delajoud, P., and Girard, M., 1988. Increasing the accuracy of pressure measurements through improved piston gauge effective area determination. *ISA*, USA.
- [Delajoud et al. 1999] Delajoud, P., Girard, M., and Ehrlich, C.D., 1999. Early history of the development and characterization of a 50 mm diameter, gas-operated piston gauge as a primary pressure standard. *Metrologia* 36, No 6, pp 521-524.
- [DH-Budenberg n.d.a] DH-Budenberg SA. *Model 5111 very large area PCA primary pressure standard*. France.
- [DH-Budenberg n.d.b] DH-Budenberg SA, *APX50 automatic absolute pressure balance*. France.
- [DH-Budenberg n.d. c] DH-Budenberg. *Type 5000: 5200 series gas operated pressure balances for pressure from 0.02 to 100 MPa (3 to 16,000 psi)*. France.
- [DH Instrument 1999] DH Instrument Inc., 1999. *PG piston gauges – reference level pressure standards*. USA.
- [Douslin and Osborn 1965] Douslin, D.R., and Osborn, A. 1965. Pressure measurements in the 0.01-30 torr range with an inclined-piston gauge. *J. Sci. Instrum.*, Vol 42, pp 369-372.

- [Drab and Raposo 2002] Drab, R.S. and Raposo H.L. 2002. *New ideas for machining austenitic stainless steels* Available at: <URL: <http://crswnew.cartech.com/wnew/techarticles/TA00037.html>> [Accessed 11 June 2006].
- [Ehrlich 1994] Ehrlich, C., 1994. A review of gas-operated piston gauges. *Metrologia* 30, No 6, pp 585-590.
- [Fischer 1986] Fischer, H., 1986. Honing. In: *Handbook of modern grinding technology, Chapter 13*. London: Chapman and Hall, pp 301-336.
- [Grassam and Powell 1964] Grassam, N.S. and Powell, J.W., 1964. *Gas lubricated bearings*. London: Butterworths.
- [Hammond 1992] Hammond, E.K., 1992. *Lapping and polishing*. Leceister: TEE Publishing.
- [Helical Lap Mfg n.d.] Helical Lap Mfg. *Cylindrical lapping guidelines*. Helical Lap and Manufacturing Co., Fraser, Michigan, USA.
- [Helical Lap Mfg 2006] Helical Lap Mfg., 2006. [online]. Available at: <URL: <http://www.helicallap.com/>> [Accessed 25 March 2006].
- [Heydemann and Welch 1975] Heydemann, P.L.M., and Welch, B.E., 1975. Piston gauges. In: LeNeindre, B., and Vodar, B. (editors). *Experimental thermodynamics, Vol. II, Chapter 4, Part 3*. London: Butterworths.
- [Hutton 1959] Hutton, U.O. 1959. A tilting air-lubricated piston gauge for pressure below on-half inch of mercury. *Journal of Research of the National Bureau of Standards (USA)*, Vol 63C, No 1, pp 47-57.
- [IMC 1998] The Institute of Measurement and Control, 1998. *Guide to the measurement of pressure and vacuum*. ISBN 0 904457 29 X. London: HMSO.

- [ISO/TAG 4 1993] ISO/TAG4/WG3, 1993. *Guide to the expression of uncertainty in measurement*. ISO, Switzerland.
- [Jain et al. 1993] Jain, K., Ehrlich, C., Houck, J., and Sharma, J.K.N. 1993. Intercomparison of the effective area of a pneumatic piston gauge determined by different techniques. *Meas. Sci. Technol.* 4, No 3, pp 249-257.
- [Jain et al. 2003] Jain, K., Bowers, W.J., and Schmidt, J.W. 2003. A primary dead-weight tester for pressures (0.05-1.0) MPa. *J. Res. Natl. Inst. Stand. Technol.* 108, pp 135-145.
- [Jones 1915] Jones, F.D., 1915. Laps and lapping. In: *Modern toolmaking methods, Chapter 11*. London: The Machinery Publishing Co. Ltd.
- [Klingenberg and Legras 1994] Klingenberg, G., and Legras, J.C. 1994. Bilateral comparative pressure measurements of the LNE and the PTB using 10 cm² piston-cylinder assemblies. *Metrologia* 30, No 6, pp 603-606.
- [Legras 1994a] Legras, J.C., 1994. Stability of piston-cylinder assemblies from an experience of fifteen years. *Metrologia* 30, No 6, pp 625-629.
- [Legras 1994b] Legras, J.C., 1994. Pressure intercomparisons at lowest level of uncertainty: Transfer standards and results. *Metrologia* 30, No 6, pp 701-704.
- [Legras et al. 1999a] Legras, J.C., Guinio, J.Le., and Baron, F., 1999. Calibration chain of the BNM-LNE from 10⁻⁴ Pa to 10 kPa. *Metrologia* 36, No 6, pp 631-635.

- [Legras et al. 1999b] Legras, J.C., Sabuga, W., Molinar, G.F., and Schmidt, J.W. 1999. CCM key comparison in the pressure range 50 kPa to 1000 kPa (gas medium, gauge mode). Phase A2: Pressure measurements. *Metrologia* 36, No 6, pp 663-668.
- [Les Yelland 2004] Les Yelland, 2004. *Personal communication with the honing specialist*. Delapena Honing Limited, UK.
- [Lewis and Peggs 1992] Lewis, S.L., and Peggs, G., 1992. *The pressure balance: A practical guide to use it*. National Physical Laboratory, London: HMSO.
- [Kato and Adachi 2001] Kato, K., and Adachi, K., 2001. Metals and ceramic. In: *Bushan, B., (editor-in-chief), Modern tribology handbook, Vol. 2*. London: CRC Press.
- [Kemet n.d.] Kemet International Limited, *TP5 – Cylindrical lapping using helilaps, GL/SL/9.00*. Kemet International Limited, UK.
- [Kemet 2006a] Kemet International Limited, 2006. *Helilaps bore finishing tools* [online]. Available at: <URL: <http://www.kemet.co.uk/toolroom.html#helilaps>> [Accessed 25 March 2006].
- [Kemet 2006b] Kemet International Limited, 2006. *Kemet diamond compound / Kemet diamond paste* [online]. Available at: <URL: http://www.kemet.co.uk/diamond_compound.html> [Accessed 25 March 2006].
- [Kemet 2006c] Kemet International Limited, 2006. *Kemet lubricating fluids* [online]. Available at: <URL: http://www.kemet.co.uk/lubricating_fluid.html> [Accessed 25 March 2006].

- [Machinery Publishing n.d.] Machinery Publishing Co. *Fine grinding and lapping*. Machinery's Yellow Back Series No. 19. London: The Machinery Publishing Co., Ltd.
- [Magee 1996] Magee, J.H. 1996. *Two galling resistant stainless steels used for bridge hinge pins* [online]. Available at: <URL: <http://crswnew.cartech.com/wnew/techarticles/TA00030.html>> [Accessed 11 June 2006].
- [Maghenzani et al.1987] Maghenzani, R., Molinar, G.F., Marzola, L., and Kulshrestha, R.K. 1987. Pressure metrology up to 5 MPa in different gas media. *J. Phys. E: Sci. Instrum.* 20, pp 1173-1179.
- [Mahr 2006a] Mahr UK plc. *MarSurf surface texture measuring instruments*. [Online] Available at <URL <http://www.mahr.com/index.php?NodeID=1737&SourceID=158&LayerMenuID=3#CID274>> [Accessed 11 June 2006].
- [Mahr 2006b] Mahr UK plc. *Glossary*. [Online] Available at <URL <http://www.mahr.com/index.php?NodeID=8718&SourceID=78&LayerMenuID=3#CID2224>> [Accessed 11 June 2006].
- [Markus 1972] Markus, W. 1972. A constant volume valve. *Rev. Sci. Instrum.*, Vol 43, No 1, pp 158-159.
- [Metals Handbook 1967] Metals Handbook, 1967. Lapping,. In: *Machining, 8th Edition, Vol. 3*. Metals Park Ohio: American Society for Metals.
- [Metals Handbook 1982] Metals Handbook, 1982. Polishing and buffing In: *Surface cleaning, finishing and coating (9th Edition), Vol. 5*. Metals Park, Ohio: American Society for Metals.

- [Mettler-Toledo 1991] Mettler-Toledo AG, 1991. *Fundamental of mass determination*. Greifensee, Switzerland.
- [Meyer and Reilly 1994] Meyer, C.W., and Reilly, M.L. 1994. Measurement of the gas dependence of the effective area of a piston gauge using H₂, ³He, ⁴He, N₂, CO₂ and SF₆. *Metrologia* 30, No 6, pp 595-597.
- [Miller 1962] Miller, L., 1962. *Engineering dimensional metrology*. London: Arnold.
- [Mitutoyo 2006] Mitutoyo (UK), Ltd. *Surface measurement: Surftest SJ-201/SJ-30*. [Online] Available at <URL <http://www.mitutoyo.co.uk/Mit/DisplayResources.jsp?category=product-literature>> [Accessed 11 June 2006].
- [Molinar 1992] Molinar, G.F., 1992. Part II: Pressure measurements in the range from 10² Pa to 10⁸ Pa. In: Timmerhaus, K.D., Clark, A.F., and Rizzuto, C. (editors), *Modern gas-based temperature and pressure measurements*. New York: Plenum Press.
- [Molinar et al. 1999] Molinar, G.F., Rebaglia, B., Sacconi, A., Legras, J.C., Vailleau, G.P., Schmidt, J.W., Stoup, J.R., Flack, D.R., Sabuga, W., and Jusko, O. 1999. CCM key comparison in the pressure range 0.05 MPa to 1 MPa (gas medium, gauge mode). Phase A1: Dimensional measurements and calculation of effective area. *Metrologia* 36, No 6, pp 657-662.
- [Nagano Keiki n.d.] Nagano Keiki, n.d. Dead-weight Tester PD82 – 500 kPa. In: TY21-83A Product Manual. Nagano, Japan.
- [Neugebauer 1998] Neugebauer, M., 1998. The uncertainty of diameter calibrations with the comparator for diameter and form. *Meas. Sci. Technol.* 9, pp 1053-1058.

- [Newhall et al. 2003] Newhall, D.H., Newhall, W.C., and Malloy, B.T., 2003. Revised characterization of the controlled clearance piston gauge. *Rev. Sci. Instrum.*, Vol 74, No 5, pp 2899-2910.
- [Nishibata 1997] Nishibata, K., 1997. *Pressure measurements and standards*. SIRIM-JICA Measurement Centre Project, National Measurement Centre, SIRIM Bhd., Malaysia.
- [NMS 2002] National Measurement System, 2002. *NMS work programme for mass metrology: October 1999 – September 2002*. Department of Trade & Industry, London, UK.
- [NPL 2006] National Physical Laboratory. *Non-pressure calibration of pressure balances?* [online] Available at:
<URL:<http://www.npl.co.uk/pressure/guidance/nonpre-scal.html>> [Accessed 10 June 2006].
- [OIML R111-1 2004] OIML R111-1, 2004. *OIML R 111-1 – Weights of classes E₁, E₂, F₁, F₂, M₁, M₁₋₂, M₂, M₂₋₃ and M₃*. Edition 2004 (E). France.
- [OIML R110 1994] OIML R110, 1994. *OIML R 110 – Pressure Balances*. Edition 1994 (E). BIMP, International Recommendation. France.
- [PD 6461-4 2004] BSI, 2004. *General metrology – Part 4: Practical guide to measurement uncertainty*. London: BSI.
- [Peggs 1997] Peggs, G.N., 1997. *A method for computing the effective area of a pressure balance from diametral measurement*. National Physical Laboratory Divisional Report MOM 23, Teddington, UK.

- [Peggs and Lewis 1977] Peggs, G.N., and Lewis, S.L. 1977. The NPL primary pressure balance standard. *J. Phys. E: Sci. Instrum.* 10, No 10, pp 1028-1034.
- [Peggs et al. 1978] Peggs, G.N., Lewis, S.L., Clapham, P.B., Jäger, Bauer, H., Schoppa, G., and Schultz, W. 1978. The intercomparison of the pressure standards of the National Physical Laboratory (UK) and the Physikalisch-Technische Bundesanstalt (Germany). NPL Report MOM 32.
- [Precision Devices 2006] Precision Devices Inc, 2006. *Surface metrology guide* [online]. Available at: <URL: <http://www.predev.com/smg/standards.htm>> [Accessed 10 June 2006].
- [Prowse and Hart 1977] Prowse, D.B., and Hatt, D.J. 1977. The effect of rotation on a gas-operated free-piston pressure gauge. *J. Phys. E: Sci. Instrum.* 10, No 5, pp 450-451.
- [PTB 2006] Physikalische-Technische Bundesanstalt, 2006. *High precision 3D-calibration of cylindrical standards* [online]. Available at: <URL: http://www.ptb.de/en/org/5/_index.htm> [Accessed 14 June 2006].
- [Rantanen 1994] Rantanen, M. 1994. Experiments on the effect of torque used in mounting the cylinder on the effective area of a pressure balance. *Metrologia* 30, No 6, pp 645-647.
- [Ruska 1999] Ruska Instrument Corporation, 1999. *Model 2465A-754 User's manual: Gas lubricated piston pressure gauge*. Houston, USA.
- [Ruska 2000] Ruska Instrument Corporation, 2000. *Model 2466 – large diameter gas piston gauge*. Houston, USA.

- [Sandvik 2004] Sandvik AB, 2004. Sandvik hard materials. [online]. Available at: URL: <http://www.hardmaterials.sandvik.com> [Accessed 01 April 2004].
- [Scarr 1967] Scarr, A.J.T., 1967. Metrology and precision engineering.: McGraw-Hill.
- [Schmidt et al. 1994] Schmidt, J.W., Welch, B.E., and Ehrlich, C.D. 1994. Gas and mode, vertical and rotational effects with a three piston gauge apparatus. *Metrologia* 30, pp 599-602.
- [Schmidt et al. 1999] Schmidt, J.W., Tison, S.A., and Ehrlich, C.D. 1999. Model for drag forces in the crevice of piston gauges in the viscous-flow and molecular-flow regimes. *Metrologia* 36, No 6, pp 565-570.
- [Schmidt et al. 2000] Schmidt, J.W., Bowers, W.J., Driver, R.G., and Jain, K. 2000. *New primary pressure standard*. Technical Activities Report – FY 2000 Process Measurements Division, NIST.
- [Schmidt et al. 2005] Schmidt, J.W., May, E.F., Moldover, M.R., and Pitre, L. 2005. Progress towards a primary pressure standard to 7 MPa based on the dielectric permittivity of helium. *Proceedings of the 4th CMM International Conference on Pressure Metrology from Ultra-High Vacuum to Very High Pressures (10^{-9} Pa to 10^9 Pa)*, Institute of Physics, London, UK, pp 11-12.
- [Sharma et al. 1988] Sharma, J.K.N., Jain, K.K., and Bandyopadhyay, A.K., 1988. Characterisation of the piston gauge to assess the suitability of its use with several working fluids up to 5 MPa. *Rev. Scientific. Instrument* 59, pp 2063-2069.

- [Simpson 1994] Simpson, D. I., 1994. Computerised Techniques for Calibrating Pressure Balances, *Metrologia* 30, pp 655-658.
- [Smith 2001] Smith, T.G., 2002. *Industrial metrology: Surfaces and roundness*. London: Springer.
- [Stout and Blunt 2000] Stout, K.J., and Blunt, L., 2000. *Three-dimensional surface topography*. London: Penton.
- [Stuart 1994] Stuart, P.R. 1994. Progress report on an international intercomparison in the pressure range 10 kPa to 140 kPa. *Metrologia* 30, No 6, pp 705-709.
- [Sutton 1979] Sutton, C.M. 1979. The rotational frequency dependence of a pressure balance. *J. Phys. E: Sci. Instrum.* 12, No 6, pp 466-468.
- [Sutton 1980] Sutton, C.M. 1979. The effective area of a pressure balance at low pressure. *J. Phys. E: Sci. Instrum.* 13, No 8, pp 857-859.
- [Taylor Hobson 2006] Taylor Hobson 2006. *Surface texture parameters* [online]. Available at: <URL: <http://www.taylor-hobson.com/faqsurface.asp?headingID=6>> [Accessed 08 June 2006].
- [Taylor Hobson 2002] Taylor Hobson 2002. *A guide to surface texture parameters*. Taylor Habson Limited, UK.
- [Taylor and Kuyatt 1994] Taylor, B.N., and Kuyatt, C.E. 1994. *NIST technical note 1297 (1994 Edition) - Guidelines for evaluating and expressing the uncertainty of NIST measurement results*. NIST, USA.
- [Tesar et al. 1999] Tesar, J., Krajicek, Z., and Schultz, W. 1999. Pressure comparison measurements between the CMI and the PTB in the range 0.07 MPa to 0.4 MPa. *Metrologia* 36, No 6, pp 647-650.

References

- [Thomas 1974] Thomas, G.G., 1974. *Engineering metrology*. London: Butterworth.
- [Veeco Instruments 2003] Veeco Instruments Inc., 2003. *Surface measurement parameters for Wyko Optical Profilers*, AN505-50403, Veeco Instrument Inc., USA.
- [Veeco Instruments 2006] Veeco Instruments Inc.. *All optical application notes* [online] Available at <URL: http://www.veeco.com/html/product_bymarket_appnotes.asp?Title=OPTICAL%2FSTYLUS+PRODUCTS&ApplicationID=19&marketID=4> [Accessed 13 June 2006].
- [Wan Mohamed and Petzing 2005] Wan Mohamed, W.A.M. and Petzing, J.N., 2005. Investigating the influence of surface texture on the performance of gas operated dead weight pressure balances. *Proceedings of the 4th CMM International Conference on Pressure Metrology from Ultra-High Vacuum to Very High Pressures (10⁻⁹ Pa to 10⁹ Pa)*, Institute of Physics, London, UK, pp 4-5.
- [Wan Mohamed and Petzing 2006] Wan Mohamed, W.A.M. and Petzing, J.N., 2006. *Investigation into piston-cylinder performance*. A Pressmet Meeting: "High pressure measurement", DH-Budenberg, Manchester, UK. 18 April 2006.
- [Westbury n.d.] Westbury, E.T. *Grinding, lapping and honing*. Percival Marshall & Co. Ltd., Cordwallis Works, Maidenhead Berks.
- [Whitehouse 1994] Whitehouse, D.J., 1994. *Handbook of surface metrology*. Bristol: Institute of Physics Publishing.
- [Whitehouse 2001] Whitehouse, D.J., 2001. *Surfaces and their measurement*. London: Penton.

References

- [Wikipedia 2006a] Wikipedia 2006. [online]. *Pressure*. Available at: <URL: <http://en.wikipedia.org/wiki/Pressure>> [Accessed 10 June 2006].
- [Wikipedia 2006b] Wikipedia 2006. [online]. Available at: <<URL: http://en.wikipedia.org/wiki/Main_Page> [Accessed 10 June 2006].
- [Zygo Corporation 2005] Zygo Corporation, 2005. *Surface texture parameters*. OMP-0514A 06/2005, Zygo Corporation, USA.
- [Zygo Corporation 2006] Zygo Corporation. *Optical metrology* [online]. Available at: <URL: <http://www.zygo.com/?/products/metrology.htm>> [Accessed 13 June 2006].

